EFFECTS OF NUTRITION AND ULTRASOUND IMAGING ON THE CARDIOVASCULAR SYSTEM

BY

BRENDON WILLIS SMITH

DISSERTATION

Submitted in partial fulfillment of the requirements
for the degree of Doctor of Philosophy in Nutritional Sciences
in the Graduate College of the
University of Illinois at Urbana-Champaign, 2014

Urbana, Illinois

Doctoral Committee:

Professor Rodney W. Johnson, Chair
Professor Emeritus William D. O'Brien, Jr., Co-Director of Research
Professor Emeritus John W. Erdman, Jr., Co-Director of Research
Associate Professor Kenneth R. Wilund

Abstract

The work described in this dissertation is focused on two major areas: the biological effects of ultrasound and ultrasound contrast agents, and nutritional interventions to inhibit the development of atherosclerosis.

Ultrasound is a highly flexible and affordable imaging modality that has proven clinically useful in many diagnostic situations ranging from pregnancy to cardiovascular disease and cancer. Ultrasound imaging can be performed with concomitant intravenous administration of microbubble contrast agents to improve image clarity. While useful for imaging of the cardiovascular system, concerns have been raised regarding the safety of ultrasound contrast agents, and further research is needed to determine their biological effects. This work investigates interactions between ultrasound, microbubbles, and the vascular endothelium, the inner cellular lining of blood vessels. The goal of this research is to help define the specific conditions under which contrast ultrasound is safe so that this knowledge can be applied to clinical patient care and diagnosis. A series of four studies were conducted to evaluate the effects of ultrasound and ultrasound contrast agents (Chapters 3-6). First, ultrasound imaging was performed on rabbit arteries, and histological and biochemical analyses were used to determine any effects on the tissue being imaged. As part of this project, an ELISA was developed and validated for measurement of one of the biomarkers, von Willebrand Factor (Chapter 2). Effects of contrast ultrasound on von Willebrand Factor and atheroma thickness were observed. Next, another rabbit study was performed to assess the effect of contrast ultrasound on Hsp70, a cellular stress protein. The ultrasound procedure was hypothesized to elevate Hsp70 protein levels. Hsp70 protein levels were measured in aorta tissue at the site of ultrasound exposure by Western blot. Ultrasound with contrast agent did not affect Hsp70 levels (Chapter 4). In addition to rabbits, work with ApoE$^{-/-}$ mice and rats will be described. We did not observe any adverse effects of ultrasound in these models (Chapters 5 and 6).

We also studied the effects of tomato and soy germ on atherosclerosis in ApoE$^{-/-}$ mice (Chapter 7). We did not find that tomato and soy germ decreased atherosclerosis, but soy germ consumption favorably affected plasma and tissue lipid accumulation.

Acknowledgements

I would first like to thank my doctoral advisors, Drs. O'Brien and Erdman, for including me in their research programs. The opportunities and guidance they provided have resulted in the studies outlined in this dissertation. I would also like to thank the other members of my committee, Drs. Johnson and Wilund, for their time and intellectual input. I am grateful to all the members of the Bioacoustics Research Lab and the Erdman lab for their contributions to this work.

I would like to express my gratitude to the Division of Nutritional Sciences. I am thankful for the excellent support provided by the administration. I have benefitted from the interdisciplinary focus of the program as a nutrition student in an engineering lab. This type of experience is uncommon for a student with a nutrition background, and has given me a unique interdisciplinary skill set and perspective on science. The flexible Nutritional Sciences curriculum has given me the freedom to pursue my interests and make progress toward my degree. And finally, graduate students in the Division of Nutritional Sciences create a thriving culture that has greatly enhanced my experience and has provided me with a strong network of peer support.

I had the support of many others prior to my time here. In particular, I would like to thank Drs. Richard Baybutt and Vincent Bacote at Wheaton College for mentoring me. I would also like to thank my family for their unconditional support throughout my life.

I am grateful to the National Institutes of Health and the Arnold & Mabel Beckman Foundation for funding this work.

Table of contents

List of abbreviations

ABC	ATP-binding cassette transporter
ACAT	acyl-coenzyme A:cholesterol acyltransferase
AIN	AIN-93G purified control diet
ANOCOVA	analysis of covariance
ANOVA	analysis of variance
ARE	antioxidant response element
AS	attenuation slope
AT1R	angiotensin 1 receptor
AT2	angiotensin 2
BSA	bovine serum albumin
CE	cholesterol ester
CETP	cholesterol ester transfer protein
CI	confidence interval
CRP	C-reactive protein
CT	computed tomography
CV	coefficient of variation
CVD	cardiovascular disease
CYP7A1	cholesterol 7α hydroxylase
CYP27A1	sterol 27 hydroxylase
DGAT	diacylglycerol acyltransferase
EDTA	ethylenediaminetetraacetic acid
ELISA	enzyme-linked immunosorbent assay
ER	endoplasmic reticulum
FDA	U.S. Food & Drug Administration
FFA	free fatty acids
FPLC	fast performance/phase/protein liquid chromatography
H&E	hematoxylin and eosin
HDL	high-density lipoprotein
HIFU	high-intensity focused ultrasound
HMG-CoA	3-hydroxy-3-methylglutaryl-coenzyme A
HRP	horseradish peroxidase
Hsp70	heat shock protein
IL	interleukin
cIMT	carotid intima-media thickness
INSIG	insulin-induced gene
kcal	kilocalories
LCAT	lecithin:cholesterol acyltransferase
LDL	low-density lipoprotein
LDLR	low-density lipoprotein receptor
LPL	lipoprotein lipase
LRP	low-density lipoprotein receptor-related protein
LXR	liver X receptor
MCP-1	monocyte chemoattractant protein 1
MDC	minimum detectable concentration
MI	mechanical index

MRD	minimum required dilution
MRI	magnetic resonance imaging
mRNA	messenger ribonucleic acid
miRNA	micro ribonucleic acid
MTTP	microsomal triglyceride transfer protein
NBF	neutral buffered formalin
NCoR	nuclear receptor corepressor
NF-κB	nuclear factor κB
NLRP3	nucleotide-binding domain and leucine rich repeat containing family pyrin domain containing 3
NO	nitric oxide
NPC	Niemann-Pick C
Nrf2	nuclear factor erythroid-derived 2 related factor 2
OCT	optimum cutting temperature compound
PAF	paraformaldehyde
PBS	phosphate-buffered saline
PCSK9	proprotein convertase subtilisin kexin 9
PGC1α	peroxisome proliferator-activated receptor γ coactivator 1α
PPAR	peroxisome proliferator-activated receptor
PPIA	peptidylprolyl isomerase A/cyclophilin A
p_r	peak rarefactional pressure amplitude
PRPA	derated peak rarefactional pressure amplitude
PREDIMED	prevención con dieta mediterránea
RDL	reliable detection limit
RIPA	radioimmunoprecipitation assay
RORα	retinoid orphan receptor α
ROS	reactive oxygen species
RT	room temperature
SCAP	SREBP cleavage activating protein
SMRT	silencing mediator of retinoid and thyroid hormones
SREBP	sterol response element binding protein
TG	triglyceride
TGF-β	transforming growth factor β
TLR	toll-like receptor
TNFR1	TNF-α receptor 1
TMB	3,3',5,5'-tetramethylbenzidine
UCA	ultrasound contrast agent
US	ultrasound
VCAM-1	vascular cell adhesion molecule 1
VEGF	vascular endothelial growth factor
VLDL	very-low density lipoprotein
vWF	von Willebrand Factor
WD	Western diet
WDSG	Western diet with 2% soy germ
WDTP	Western diet with 10% tomato powder
WDTPSG	Western diet with 10% tomato powder and 2% soy germ

CHAPTER 1: Literature review

Introduction

Cardiovascular Disease (CVD) is the leading cause of death in the United States. It progresses silently throughout life and manifests itself in old age, reducing life expectancy and prematurely killing over 2000 Americans each day[1]. The economic burden is also staggering, with direct costs alone totaling $300 billion each year[1]. CVD is an umbrella term that broadly refers to several related conditions, including heart attack (myocardial infarction), strokes, peripheral arterial disease, hypertension, and heart failure. The vast majority of heart attacks, strokes, and deaths are caused by atherosclerosis. Atherosclerosis is, in large part, a disorder of lipoprotein metabolism. This review will thus begin with an overview of cholesterol and lipoprotein metabolism, and will then apply this information to an explanation of atherosclerosis. Risk factors and imaging modalities used in human clinical management of cardiovascular disease will be covered. After a description of the effects of diet on atherosclerosis and CVD, the final sections will discuss animal models and methods used in atherosclerosis research.

Cholesterol and lipoprotein metabolism

Transport of lipophilic compounds through the aqueous systemic circulation is facilitated by their inclusion in lipoproteins. Lipoproteins contain triglycerides, cholesterol esters, and other fat-soluble compounds enclosed within a phospholipid monolayer. Integral membrane proteins called apolipoproteins mediate functions related to enzymatic activity and receptor recognition. After consumption of a lipid-containing meal, triglycerides from food are hydrolyzed to free fatty acids and glycerol. These, and other lipophilic digestion products including cholesterol and fat-soluble vitamins A, D, E and K, are mixed with bile acids in the intestinal lumen to form micelles, which are then absorbed into enterocytes, the epithelial cells of the intestine. Sterol absorption is also actively regulated by transporters including ATP-binding cassette transporter (ABC) G isoforms and Niemann-Pick C1-like 1[2-5]. Production of these transporters is regulated transcriptionally by the liver x receptor (LXR)[5]. The enterocyte packages lipophilic compounds into lipoprotein particles called chylomicrons for export into the circulation[6,7]. Chylomicrons contain predominantly triglyceride enclosed within a

phospholipid monolayer, along with a small amount of cholesterol[8]. At this stage, chylomicrons contain one major apolipoprotein, ApoB48, which is a truncated form of ApoB100 produced by editing of the ApoB mRNA by Apobec-1[9-11]. ApoB48 is loaded onto the chylomicron with the assistance of the chaperone microsomal triglyceride transfer protein (MTTP)[6,7].

Chylomicrons are then absorbed from the enterocyte into the lymphatic system, and not the blood, primarily because they are too large to move past capillary endothelial cells[12]. A major purpose of the chylomicron is to deliver fatty acids to extrahepatic tissues such as heart and skeletal muscle. Transport through the lymph, which empties into the subclavian vein, allows chylomicrons to be distributed throughout the general circulation and metabolized before being managed by the liver. In addition to their initial ApoB48, chylomicrons also receive ApoA, C, and E lipoproteins in the circulation, usually donated from HDL. After removal of triglyceride in the circulation, primarily through the action of capillary endothelial lipoprotein lipase (LPL)[13], the particle is referred to as a chylomicron remnant. Remnant lipoproteins are cleared from the circulation through the action of the LDL receptor-related protein (LRP)[14].

In addition to the intestine, the liver is the second major site of lipoprotein production. Fats from the diet or circulation are taken up, processed, and incorporated into VLDL particles in the liver. In the fed state, particularly after a carbohydrate-rich meal, insulin suppresses ApoB production and VLDL formation[15,16]. Fatty acids are esterified through a series of enzymatic reactions, finishing with the formation of triglycerides by diacylglycerol acyl transferase (DGAT)[17], and the triglycerides are stored in cytosolic lipid droplets at this stage. When the suppression by insulin is relieved, ApoB and triglyceride can be incorporated into VLDL particles, with the activity of MTTP being particularly important again, and the particles are then exported to the circulation. In addition to ApoB100, human VLDL may contain ApoA5[18], multiple ApoC isoforms, and ApoE[19]. As with chylomicrons, VLDL particles primarily serve to distribute triglycerides to extrahepatic tissues. Metabolism by LPL produces the VLDL remnant.

LDL can be produced either by removal of ApoE from the VLDL remnant, or by *de novo* synthesis in the liver. LDL contains mostly cholesterol, and carries a single lipoprotein, ApoB100. Although almost all cells can synthesize cholesterol[20], LDL

assists by delivering cholesterol to extrahepatic tissues, especially steroidogenic tissues such as the adrenals and gonads[21]. The majority of LDL particles are cleared from the circulation through the use of the hepatic LDLR in a process known as receptor-mediated endocytosis[22-25]. Receptor-mediated endocytosis was discovered through studies of the LDLR, and is now recognized as a general cellular strategy for internalization of large particles and their cargo[26]. This process begins with recognition of ApoB100 by LDLRs located in clathrin-coated extracellular pits. Binding of LDL to LDLRs triggers formation of vesicles that are rapidly internalized and fuse with lysosomes. Once LDL enters the lysosome, its protein components are digested to amino acids, and its cholesterol is subject to the actions of two Niemann-Pick C (NPC) proteins, NPC1 and NPC2. Recent studies support the existence of a cooperative handoff mechanism whereby NPC2 binds cholesterol, with cholesterol's hydrophobic iso-octyl side chain buried in NPC2's binding pocket, forms a closed channel with NPC1, and hands off the cholesterol molecule[27]. NPC1 may then be able to move cholesterol through the membrane for exit from the lysosome and transport to the endoplasmic reticulum (ER), but this step is not fully understood.

Internalization of cholesterol results in three cellular regulatory responses: suppression of 3-hydroxy-3-methylglutaryl-coenzyme A (HMG-CoA) reductase, the rate-limiting step in cholesterol biosynthesis; activation of acyl-coenzyme A:cholesterol acyltransferase (ACAT) for cholesterol esterification and intracellular storage; and reduction in synthesis of LDLR, preventing excess cholesterol accumulation. In addition to the three classical regulatory mechanisms, further layers of regulation are achieved through the sterol response element binding protein (SREBP) pathway and through the use of microRNAs (miRNAs). SREBPs are master transcriptional regulators of cholesterol and lipid synthesis[28,29]. When cellular cholesterol levels are high, cholesterol binds directly to SREBP cleavage activating protein (Scap), triggering binding of Scap to insulin-induced gene (INSIG), a protein that promotes retention of Scap and SREBP at the ER. When cellular cholesterol concentrations decrease, Scap is released from INSIG. The six amino acid MELADL sequence in Scap interacts with CopII coat proteins to generate membrane vesicles that enclose Scap and SREBP for transport to the Golgi apparatus, where Site-1 and Site-2 proteases sequentially cleave SREBP to release the

mature basic helix-loop-helix transcription factor. SREBP regulates the transcription of target genes including those encoding HMG-CoA reductase and the LDL receptor. MiRNAs provide another layer of regulation. The canonical function of miRNAs is to bind complementary sequences on mRNAs to trigger their degradation[30,31]. Recent studies have uncovered miRNAs located within intronic regions of the SREBP genes. These miRNAs, miR-33 in mice and miR-33a and b in humans, are co-transcribed with SREBPs in times of low cellular cholesterol and inhibit translation of ABCA1 mRNA, decreasing cholesterol efflux[32-36]. SREBP-2 also regulates transcription of miR-96, 182, and 183, which in turn regulate levels of other proteins in the SREBP pathway[37]. These homeostatic feedback mechanisms allow close regulation of cholesterol levels within the cell.

HDL is another type of lipoprotein with unique functions and benefits. In contrast with other lipoproteins, its primary component by weight is protein. ApoA1 from the liver or intestine combines with phospholipid and cholesterol to form pre-β HDL. HDL can also be formed in plasma from chylomicron and VLDL remnants. ApoA1 is the sole apolipoprotein on pre-β and discoidal HDL; mature HDL particles may pick up other ApoA, C, D and E isoforms. ApoA1 on HDL activates lecithin:cholesterol acyltransferase (LCAT). This key enzyme esterifies cholesterol to move it from the surface to the center of the lipoprotein, allowing for continued cholesterol uptake. The production of ApoA1 is controlled transcriptionally by the retinoid orphan receptor α (RORα), which binds cholesterol as a ligand[38]. HDL particles are highly heterogeneous, and can be categorized based on their shape (spherical or discoidal), density (HDL2 and 3), electrophoretic mobility (pre-β vs. α), and apolipoproteins[39]. HDL has anti-inflammatory, antioxidant, anti-thrombotic, and vasodilatory functions, and has a central role in the process of reverse cholesterol transport[40].

Reverse cholesterol transport is the process of returning cholesterol from peripheral tissues to the liver for disposal[41]. Arterial tissue is a particularly important peripheral location in which this occurs. Cholesterol can accumulate in the arterial intima, leading to formation of atherosclerotic lesions, as will be discussed in the following section. Macrophages ingest this cholesterol in an attempt to remove it from the arterial tissue, and donate it to HDL via ABCA1 and ABCG1. The ApoA1 on HDL activates LCAT,

esterifying cholesterol to move it toward the core of the particle. Circulating HDL can then deliver cholesterol to the liver either directly, through scavenger receptor B1, or indirectly, by exchanging cholesterol and lipids with VLDL or LDL through the actions of cholesterol ester transfer protein (CETP). The liver can excrete this cholesterol through the ABCG5 and G8 transporters into the bile, or by using it to synthesize bile acids, with cholesterol 7α hydroxylase (CYP7A1) as the rate-limiting enzyme. Cholesterol and bile can then be excreted in the feces.

Nuclear receptors and miRNAs regulate reverse cholesterol transport. The nuclear receptor LXR coordinates the reverse cholesterol transport program throughout the body[5,42,43]. As a transcription factor, LXR upregulates expression of genes involved in cholesterol efflux, including ABCA1, G1, G5, and G8. This information previously led to the hypothesis that pharmacological LXR activation could reduce atherosclerosis by upregulating reverse cholesterol transport. Indeed, mice given LXR agonists display reduced atherosclerosis[44]. However, enthusiasm for this therapeutic strategy was rapidly curbed when studies of mice given LXR agonists revealed severe hepatic steatosis and hypertriglyceridemia as side effects, due to upregulation of SREBP-1c and suppression of ApoA5[5]. Reverse cholesterol transport is also regulated by miRNAs. As mentioned, miR-33 regulates cellular cholesterol efflux by inhibiting translation of ABCA1 mRNA. In the context of the cardiovascular system, pharmacological inhibition of miR-33 promotes reverse cholesterol transport[45], increases HDL[46,47], and reduces atherosclerosis[48].

It is important to note that cholesterol is essential for life. It is a critical building block for steroid hormones and bile acids, and is a major constituent of cell membranes throughout the body. LDL delivers cholesterol to tissues where it can be used, and thus should not be considered categorically bad. Cholesterol also plays an important signaling role. It is a key component of the Hedgehog signaling pathway, and depletion of cholesterol during embryonic development leads to severe birth defects[49-51].

Although cholesterol is important for normal physiology, it can also be detrimental. Aberrant cholesterol metabolism is a major contributor to atherosclerosis, the underlying pathological process that causes heart attacks and strokes. Cholesterol metabolism can be pathologically altered in several major respects. First, cholesterol metabolism can be

affected at the level of intestinal absorption and processing. This is illustrated by studies of the ABCG5 and G8 transporters. ABCG5 and G8 are involved in cholesterol efflux, including excretion from the liver into bile and from the enterocyte back into the intestine for excretion[5]. Humans with mutations in these transporters exhibit sitosterolemia, characterized by increased absorption and decreased excretion of sterols, resulting in tissue accumulation and premature atherosclerosis[52,53]. Conversely, transgene-driven overexpression of ABCG5 and G8 has been shown to reduce plasma cholesterol levels and atherosclerosis in $LDLR^{-/-}$ mice by promoting cholesterol excretion[54]. Defects in the MTTP gene cause abetalipoproteinemia, which is characterized by lack of chylomicron and VLDL synthesis[55]. In terms of cholesterol synthesis, genetic polymorphisms in the HMG-CoA Reductase gene are present in hypercholesterolemic patients and affect responsiveness to inhibition by statins[56,57]. LDL uptake is another regulatory point that is frequently disturbed. Genetic mutations in the LDLR[23] or autosomal recessive hypercholesterolemia (ARH)[58-60] genes cause familial hypercholesterolemia, with homozygous forms being more severe than heterozygous forms. Familial hypercholesterolemia can be complicated by the actions of proprotein convertase subtilisin kexin 9 (PCSK9), an LDLR-interacting protein. PCSK9 binds to the LDLR and triggers its cellular internalization[61,62]. Defective intracellular cholesterol processing also causes Niemann-Pick diseases. In patients with these diseases, after LDL is internalized, the lysosomal processing of cholesterol is disrupted by genetic mutations in the NPC genes[63]. Mutations in ABCA1 result in defective cholesterol efflux and cause Tangier disease, which is characterized by an absence of HDL, cholesterol accumulation in tissues, and premature atherosclerosis[64]. Mutations in the LPL gene also cause premature atherosclerosis by preventing removal of fatty acids from chylomicrons, resulting in familial hyperchylomicronemia[65].

The discovery of the HMG-CoA reductase regulatory step led to the development of statin drugs as a solution to the problem of dysregulated cholesterol metabolism[66]. The canonical mode of action of statins is to inhibit HMG-CoA reductase, which decreases cellular cholesterol synthesis. The reduction of cholesterol synthesis affects the entire system of cellular cholesterol homeostasis, resulting in a compensatory increase in LDLR production. Importantly, statins also have pleiotropic effects that contribute to

their efficacy, including decreased inflammation, plaque stabilization, and reversal of endothelial dysfunction[67,68]. As concrete evidence of these pleiotropic effects, statins have been shown to reverse atherosclerosis in human patients[69-73].

Although statins have been highly successful in reducing cardiovascular events, they are not adequate in all circumstances. Patients with homozygous familial hypercholesterolemia do not enjoy the full benefits of statins because they produce defective LDLR, or none at all, in response to the suppression of cellular cholesterol synthesis. Statins also increase the production of PCSK9, which may reduce their efficacy[74]. Therapies targeting PCSK9 have recently met this need. Antibodies against PCSK9 have successfully lowered circulating cholesterol levels in familial hypercholesterolemia patients[75-77], but only in patients that produce functional LDLR. Patients who lack functional LDLR have not benefitted from PCSK9 antibody therapy[78]. Many other therapies are currently under consideration[67,79,80].

Aberrant cholesterol metabolism is important in the pathogenesis of other diseases as well, including cancers and Alzheimer's disease. Recent evidence demonstrates accumulation of cholesterol esters in prostate cancer cells, prolonging activation of SREBP for lipogenesis and cell proliferation[81]. Statins display potential as anticancer therapeutics, due in large part to their ability to reduce protein prenylation[82]. The role of cholesterol metabolism in Alzheimer's disease is apparent from the effects of ApoE polymorphisms on disease risk[83]. ApoE affects amyloid β aggregation and other aspects of brain metabolism. In addition to ApoE, other aspects of lipid metabolism and signaling affect the progression of Alzheimer's[84]. HMG-CoA reductase polymorphisms may also be important determinants of Alzheimer's risk[85,86]. In summary, the evidence presented in this section highlights the central causal role of cholesterol and lipoproteins in cardiovascular disease, and illustrates the pervasive impact of cholesterol metabolism on physiology and pathology.

Pathogenesis of atherosclerosis

Atherosclerosis is a maladaptive immune response to ectopic lipoprotein deposits in the artery wall. This maladaptive immune response leads to the development of atherosclerotic plaques in the arterial system that cause heart attacks and strokes, and

is therefore responsible for more deaths than any other disease. Atherosclerosis begins early in life. There is evidence that maternal hypercholesterolemia can promote the development of atherosclerosis in the fetus in utero[87]. Autopsy studies have demonstrated fatty streaks in children at two years of age, and advanced atherosclerotic lesions in teenagers[88]. It is not exclusively a disease of Western civilization, as recent work has demonstrated atherosclerosis in mummies from ancient Egypt and other societies[89-95]. Diet, lifestyle, genetics, and geographic location varied widely among these societies, suggesting a fundamental predisposition to the development of atheromatous plaques. Infection was also common and may have contributed.

Our understanding of atherosclerosis has advanced tremendously over the last 50 years. Although inflammation had been implicated in atherosclerosis as early as 1856[96], physicians typically regarded it as a “plumbing problem”: passive deposition of lipid in the artery wall would cause it to grow inward until it was too narrow for blood to flow through. However, after intensive study of the pathogenesis, we now understand it not simply as passive lipid accumulation, but as an active process of chronic inflammation incited by arterial lipoprotein retention[97].

The key event in initiation of atherosclerosis is the entry of ApoB-containing lipoproteins into the arterial tissue. This process is still incompletely understood, but current evidence points to several key mechanisms. First, arterial sites that experience disturbed blood flow seem to be predisposed to atherosclerosis, while sites with laminar blood flow are resistant. The altered shear stress in disturbed flow regions may affect the permeability of the vascular endothelium, the cellular monolayer lining the vessel lumen.

Second, endothelial dysfunction may facilitate the development of atherosclerosis. Normally the vascular endothelium, the inner cellular lining of the blood vessels, regulates clotting, inflammation, vasodilation through production of nitric oxide (NO), and exchange of molecules between the blood and the blood vessel tissue. As blood vessels age, their inner endothelial cell lining fails to adequately perform its functions, which predisposes aged adults to CVD in a process known as endothelial dysfunction[68]. Endothelial dysfunction promotes a vasoconstrictive, inflammatory and thrombotic environment that results in progression of hypertension and atherosclerosis, leading to

its title as “the risk of the risk factors”[98] (**Figure 1.1**). It was originally thought that endothelial damage was the primary initiating event[99], but we now realize that endothelial dysfunction and inflammation, rather than physical damage, figure more prominently in the atherosclerotic process[100]. The vasoconstriction is a result of decreased NO bioavailability in the vasculature. Normally NO mediates vasodilation by diffusing from endothelial cells to vascular smooth muscle cells, causing them to relax and allow dilation of the blood vessel. In the presence of endothelial dysfunction, inactivation of NO by reactive oxygen species (ROS) leads to decreased vasodilatory ability[101]. Additionally, dysfunctional endothelial cells display adhesion molecules such as VCAM-1 that bind monocytes and permit them to enter the vascular tissue, where they initiate an inflammatory response. These are common mechanisms by which endothelial dysfunction can lead to a variety of cardiovascular disorders, including hypertension and atherosclerosis, which in turn lead to heart attacks and strokes. Abundant data demonstrate that oxidative stress in the vasculature, primarily through elevated ROS, leads to decreased NO bioavailability and gradual endothelial dysfunction[102], a prelude to hypertension and atherosclerosis. The transcription factor nuclear factor erythroid-derived 2 related factor 2 (Nrf2) plays a central role in antioxidant defense by binding to the antioxidant response element in target genes and inducing expression of detoxifying and free radical scavenging enzymes[103]. Nrf2 is normally sequestered in the cytosol by an inhibitor protein until it is needed, when it is then liberated from the inhibitor protein and translocates into the nucleus[103]. However, in aging Nrf2 has a reduced capacity both to translocate into the nucleus and to bind to the antioxidant response element[104], diminishing the cell’s capability to resist oxidative stress. There is a great deal of interplay between oxidative stress and inflammation in endothelial dysfunction. Nuclear factor κB (NF-κB), while typified as an inflammatory transcription factor, is also redox-sensitive, with oxidative stress triggering its activation[105] and Nrf2-mediated resistance to oxidative stress inhibiting its activation[106]. Conversely, NF-κB can also evoke oxidative stress in the endothelium[107]. The end result of these processes is an endothelium that cannot perform its normal functions, and vascular health declines.

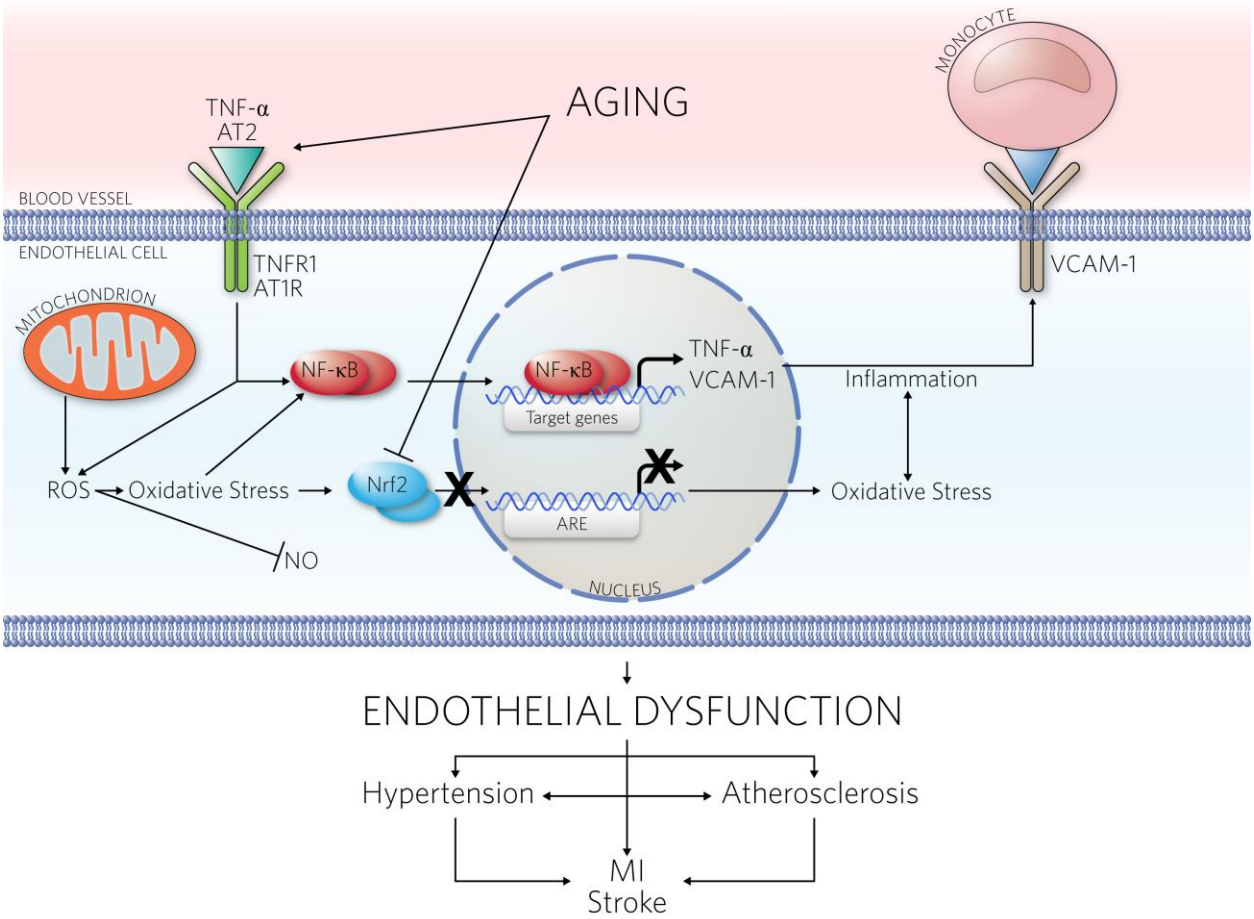

Figure 1.1. Mechanisms of endothelial dysfunction. Aging leads to endothelial dysfunction, an underlying condition characterized by oxidative stress and inflammation that leads to hypertension and atherosclerosis, which result in cardiovascular events including myocardial infarction and stroke. In aging, increased activation of key receptors, including TNFR1 and AT1R, elicits oxidative stress and inflammation within the endothelial cell. The oxidative stress would normally trigger nuclear translocation of Nrf2, but in aging Nrf2 has a reduced ability to translocate and bind to the ARE to promote oxidative stress resistance. As a result, ROS within the endothelial cell inactivate NO, reducing the ability of the blood vessel to dilate properly and leading to hypertension. Receptor activation also triggers nuclear translocation of NF-κB, which increases transcription of inflammatory genes including TNF-α and VCAM-1. VCAM-1 is an endothelial cell surface receptor that binds monocytes and promotes their extravasation into the vascular tissue, where they perpetuate the inflammatory phenotype and contribute to hypertension and formation of atherosclerotic lesions. The impaired vasodilation and inflammatory phenotype are defining features of endothelial dysfunction. ARE; Antioxidant Response Element; AT1R, Angiotensin 1 Receptor; AT2, Angiotensin 2; NO, Nitric Oxide; ROS, Reactive Oxygen Species; TNFR1, TNF-α Receptor 1.

Recent studies have demonstrated the presence of dendritic cells at atherosclerosis-prone sites of disturbed flow, and suggest their role in early arterial lipid accumulation[108]. Other risk factors like diabetes and smoking may also contribute to the dysfunctional vascular environment. It is likely that all the above mechanisms contribute

to varying degrees. The end result of these processes is the retention of ApoB-containing lipoproteins in the artery wall, which prompts the immune system to mount an inflammatory response.

Thus begins the chronic inflammatory state of atherosclerosis. Inflammation has been implicated in nearly every aspect of the atherosclerotic process. Mankind has been aware of inflammation since antiquity. The clinical signs, originally noted by Celsus in the first century AD, are *rubor* (redness), *dolor* (pain), *calor* (heat), and *tumor* (swelling). Inflammation occurs in a four-step process[109]. The first step involves inducers of inflammation, including bacterial infection or tissue damage and dysfunction, which lead to a loss of homeostasis. The “inducers” from the first step are detected in the second step by immune cells such as mast cells, dendritic cells, and macrophages. These “sensors” are both tissue-resident and circulating, and possess specialized membrane receptors, including Toll-Like Receptors (TLRs), which alert them to the problematic state. In the third step of this process, immune cells produce inflammatory mediators, such as interleukin-6 (IL-6). These molecules serve to target the immune response and appropriately prompt tissue repair and adaptation in the fourth and final stage of the immune response. Immune cells eliminate harmful bacteria and molecular debris to promote tissue healing.

The overall goal of the inflammatory state is to promote adaptation and survival of the affected tissue. Thus, this response is beneficial when performed appropriately. However, if the pathogen cannot be eliminated or the tissue repaired, the inflammatory response becomes chronic. Although the tissue may survive, its homeostatic set point has been altered and the problematic state progresses further. These principles are exhibited in the atherosclerotic process[110-113]. Dysfunctional endothelial cells respond to the problematic condition of retained lipoprotein by expressing immune cell adhesion molecules such as vascular cell adhesion molecule 1 (VCAM-1) and chemotaxis-stimulating molecules like monocyte chemoattractant protein 1 (MCP-1), inviting circulating monocytes to enter the arterial tissue for disposal of the retained lipoprotein. Monocytes respond by extravasating out of the blood and into the arterial tissue by squeezing between the endothelial cells, where they differentiate into macrophages and consume the excess cholesterol and lipid. After becoming engorged with lipid,

macrophages are referred to as foam cells based on their appearance. The condition continues with a dysregulated inflammatory response that allows for survival of the tissue but also leads to pathological alterations.

Considering the central importance of the immune system in atherosclerosis, it is not surprising that lesions contain a diverse population of immune cells. Macrophages, which result from the differentiation of monocytes, are a major constituent of the immune cell community in atherosclerotic lesions. In mice, monocytes can be subdivided into two major populations based on their expression of the surface marker Ly-6C. Ly-6C^{high} monocytes (comparable to CD16^{-} CD14^{+} cells in humans) enter lesions and participate in atherosclerosis, while Ly-6C^{low} monocytes (comparable to CD16^{+} CD14^{dim} cells in humans) roam the vasculature performing regulatory functions and typically do not enter lesions[114,115]. Lesion macrophages can be derived both from circulating Ly-6C^{high} monocytes and from local macrophage proliferation, and the relative contribution of each source varies with the stage of the lesion[116]. Circulating monocytes may enter the arterial tissue from the artery lumen, or through the vasa vasorum, the blood supply to the artery tissue itself[117]. As previously mentioned, dendritic cells are also present and may be involved in the early stages of atherogenesis. Macrophages and dendritic cells are joined in the lesion by T cells, B cells, mast cells and innate lymphoid cells. T cells can be either pro-or anti-inflammatory depending on the type. T helper 1 cells are pro-inflammatory due to interferon-γ production, whereas regulatory T cells are considered anti-inflammatory because of IL-10 and transforming growth factor β production[118]. The B cell population is not numerically prominent. It appears to generally exert a protective effect[113,119], but may also accelerate atherosclerosis depending on the type of B cell[120]. Mast cells in the lesion produce proteases and inflammatory cytokines[121,122]. Natural helper cells also enter the arterial tissue and perform protective functions complementary to those of B cells[123].

Numerous other molecular mechanisms are involved in atherosclerosis. Inflammation is important at all stages. At the transcriptional level, inflammatory cytokines initiate signaling cascades that activate the NF-κB transcription factor, which coordinates expression of genes involved in inflammation, including VCAM-1[124].

Interestingly, blockade of NF-κB in the mouse endothelium was recently shown to prevent vascular senescence and extend life span[125]. Recent studies have also focused on the role of the inflammasome, a large inflammatory protein complex. In addition to cholesterol contained within lipoproteins in the vessel wall, the formation of crystalline cholesterol deposits has been shown to promote inflammation through activation of the nucleotide-binding domain and leucine rich repeat containing family pyrin domain containing 3 (NLRP3) inflammasome, promoting plaque development in $ApoE^{-/-}$ mice and $LDLR^{-/-}$ mice[126,127]. However, another report showed that knockout of NLRP3 in $ApoE^{-/-}$ mice does not affect atherosclerosis[128,129]. More evidence is needed to delineate the role of the inflammasome in the atherosclerotic process. Oxidative stress was mentioned with regard to endothelial dysfunction. Another reported consequence of a pro-oxidative environment is the oxidation of lipoproteins, which may occur either in the circulation or arterial tissue[130-132]. Oxidative modification of ApoB100 and surface lipids prevents VLDL and LDL from being cleared by their normal receptor routes, and necessitates uptake by immune cell scavenger receptors[133]. While abundant experimental data implicate oxidized LDL in atherosclerosis, evidence for a role of oxidized LDL in human atherosclerosis is not currently compelling[118]. Nuclear receptors are also important in atherosclerosis. In addition to the functions of the nuclear receptors LXR and RORα mentioned in the section on lipoprotein metabolism, all isoforms of the peroxisome proliferator-activated receptors (PPARs)[134], as well as isoforms of nuclear receptor subfamily 4A (NR4A)[135], the peroxisome proliferator-activated receptor γ coactivator 1α (PGC1α)[136] and the corepressors silencing mediator of retinoid and thyroid hormones (SMRT) and nuclear receptor corepressor (NCoR)[137] play complex and important roles in the process, and their activation is generally beneficial and protective.

Atherosclerosis is reversible in its early stages[88], but if the risk factors and pathology are not corrected, lesions will continue to progress for decades in humans. Human plaque tissue has a slow turnover time[138], making it physiologically challenging to reverse this progression. A key feature of lesion progression is the migration of smooth muscle cells from the vascular media to the intima[96,118], where they proliferate and form a fibrous cap over the lesion, similar to a scab on the skin. Cells that appear foamy are

not only macrophages, but can also be smooth muscle cells that have migrated into the intima and adopted a foam cell phenotype[139-141]. Eventually, foam cells become overwhelmed by the accumulating lipid and die, contributing to the growing necrotic lesion core[142]. ER stress and the unfolded protein response are implicated in the process of macrophage cell death[143]. Many cellular proteins are cotranslationally translocated into the ER, where they fold into their three-dimensional conformations. During conditions of cellular stress, protein folding may be disrupted. The cell answers this dilemma by initiating an “unfolded protein response” which reduces protein synthesis, increases transcription of protein folding genes, and triggers apoptosis if homeostasis cannot be restored[144]. Excessive cholesterol accumulation in macrophages overwhelms the ER and triggers the apoptotic arm of the unfolded protein response[145]. In addition to smooth muscle cell proliferation and a necrotic core, advanced lesions may also become calcified. Calcification is performed by osteoblast-like cells that arise from pericytes or smooth muscle cells in response to high circulating phosphate levels, dysregulated calcium metabolism, oxidative stress, and other factors[146]. Accumulation of calcium in the arterial tissue reflects the presence of atherosclerotic plaques and is a predictor of cardiovascular events[147].

Chronic lesion progression occurs asymptomatically until it results in clinical cardiovascular events. These cardiovascular events, including heart attacks and strokes, occur when atherosclerotic lesions rupture, exposing the coagulatory inner components to the blood and prompting formation of a clot that occludes the vessel[148]. Many factors affect plaque rupture. Lesions that rupture are not necessarily the most occlusive. The composition of the lesion and the thickness of the lesion cap may be more important. Matrix metalloproteinase enzymes secreted by immune cells may weaken the lesion’s fibrous cap. Calcification of the plaque may influence the likelihood of its rupture, but evidence is not clear whether it promotes or inhibits rupture. Identification of plaques vulnerable to rupture is a major clinical challenge[149,150]. After plaque rupture causes a cardiovascular event, the immune system is rapidly mobilized. A reserve population of Ly-6C^{high} monocytes resides in the spleen and homes to the heart after ischemia[151]. Splenic monocytes are followed later by bone marrow-derived monocytes. Once they arrive and enter the cardiac tissue, monocytes are critical for

remodeling of the heart. Ly-6C^{high} cells predominate during the initial inflammatory response and participate in removal of necrotic debris. Ly-6C^{low} monocytes repair and stabilize the cardiac tissue later. Prior myocardial infarction increases the risk of subsequent infarction. Until recently, reasons for this were not understood. Current evidence suggests that sympathetic nervous system activation stimulates increased production of immune cells by the bone marrow and spleen, which then enter atherosclerotic lesions and contribute to their progression[114,152].

Risk factors for cardiovascular disease

The four conventional risk factors for CVD are hyperlipidemia, hypertension, diabetes, and smoking. Considering the central importance of lipoproteins in atherosclerosis, it is not surprising that they are some of the most well established cardiovascular biomarkers. Circulating cholesterol has been used as a biomarker in cardiovascular risk prediction for decades, and many studies have confirmed its predictive power for myocardial infarction, though interestingly not for stroke[153]. The most useful circulating lipid measurements have been total and HDL cholesterol, which can be reported separately or compared in a ratio. Although LDL is clearly a driver of atherosclerosis, measurement of LDL alone has not always proven effective. The utility of circulating triglycerides as a cardiovascular biomarker is also not clear[154]. While it is one of the key markers of metabolic syndrome, it has been difficult to establish elevated triglycerides as an independent risk factor because of its frequent co-occurrence with other risk factors. Other novel approaches to lipoprotein measurement have been considered, such as lipoprotein particle size. Evidence from animal[155-157], clinical[158,159], and epidemiological[160] studies suggests that lipoprotein particles with a smaller diameter are more likely to enter the artery wall. This experimental evidence has not yet been translated into routine clinical practice. HDL is another lipoprotein fraction being re-examined. A recent study evaluated myocardial infarction risk in people with genetic variants associated with elevated HDL levels. Contrary to many headlines, this study does not disprove a protective effect for HDL in the cardiovascular system. The beneficial effects of HDL are numerous, and were summarized in the section on cholesterol and lipoprotein metabolism. This study simply suggests that having

genetically elevated HDL is not protective, and possibly that raising total HDL levels may not be an appropriate therapeutic strategy. Interest has shifted to other atheroprotective properties of HDL that could be potentially measured, particularly cholesterol efflux. A recent study demonstrated a strong inverse association between serum cholesterol efflux capacity and both carotid intima-media thickness and coronary atherosclerosis[161,162]. While interesting, the measurement methods appear complicated and would be challenging to perform in clinical practice.

Blood pressure is another biomarker linearly and independently associated with cardiovascular risk. While many factors can affect blood pressure, clinical data have been remarkably consistent. Beginning at 115/75 mmHg, each increase of 20 mmHg in systolic blood pressure, or 10 mmHg diastolic, doubles mortality from myocardial infarction and stroke[163]. High blood pressure has traditionally been defined as 140/90 mmHg. A previous revision of the blood pressure guidelines[164] also recommended inclusion of a 'prehypertensive' category for those with blood pressure of 120-139/80-89 for whom lifestyle changes are encouraged. The latest guidelines were recently released, and represent a more systematic and rigorous assessment of the evidence[165-168]. Evidence strongly supports a recommendation to reduce blood pressure below 150/90 with medication for those over 60 years old. Other blood pressure cutoff points are less clear, and usually require invoking expert clinical opinion. Surprisingly, the mechanisms causing hypertension are still not well understood, and basic research is needed[169,170].

Diabetic patients have a risk of myocardial infarction equivalent to non-diabetic patients who have already experienced a myocardial infarction[171]. The mechanisms by which diabetes accelerates CVD are being actively investigated, and may involve immune mechanisms[143], altered metabolic signaling[172] and formation of advanced glycation end-products[173]. Smoking is the single behavior choice most strongly associated with cardiovascular events, with most studies showing a 30-60% increased risk[174]. It accelerates atherosclerotic cardiovascular disease by pleiotropic mechanisms including oxidative stress and endothelial dysfunction[175]. In a meta-analysis, smoking cessation was associated with a 36% reduction in all-cause mortality in heart disease patients[176].

As usual, biology is more complicated than was first realized, and shortcomings of biomarkers eventually become apparent. Conventional risk factors have been criticized because up to 50% of patients who experience cardiovascular events supposedly do not have conventional risk factors. This notion has been disproven, particularly by a set of papers published in *JAMA* in 2003[177-180]. These papers demonstrated the presence of conventional risk factors in nearly all patients who had cardiovascular events, and also questioned the value of adding novel biomarkers. A 2012 *New England Journal of Medicine* meta-analysis confirmed the predictive power of traditional risk factors on lifetime CVD risk[181]. No biomarker predicts disease with perfect accuracy, but traditional risk factors remain some of the best predictors of cardiovascular events. Additionally, what we consider "normal" cholesterol levels in our industrialized Western society may actually represent an elevation beyond what is physiologically necessary[97,182]. LDL <100 mg/dL has been considered optimal and <40 mg/dL nonpermissive[88] for development of atherosclerosis.

Traditional risk factors are usually aggregated into a scoring system[183,184]. There are several scoring systems available. The most widely used in the past has been the Framingham risk score[185]. This scoring system has proven valuable, but the Framingham cohort was not ethnically diverse, so the scoring system may not be valid for all population groups. The most recent scoring system and set of guidelines were released last year by the American Heart Association and American College of Cardiology[186-189]. This scoring system includes data from multiple cohorts in a dataset that is considered nationally representative. The updated guidelines suggest a move away from using target numbers and cutoff points as the determinants of treatment, and instead toward an approach in which all risk factors are considered holistically by the clinician, focusing on specific groups of high-risk patients. Contrary to headlines in the popular media, these guidelines are not designed to dramatically expand the population of patients treated with cholesterol-lowering statin drugs. The new guidelines are a more integrative and evidence-based approach to treatment. Instead of automatically prescribing a statin when a patient has risk factors above the target number, the clinician is instructed to carefully weigh the balance of the patient's characteristics before making a decision. Workflows are provided to assist with this.

Other novel biomarkers have been sought because of the inability of lipoprotein risk factors to perfectly predict cardiovascular risk in all cases. Two such novel biomarkers, endothelial dysfunction and C-reactive protein (CRP) will be the focus.

Endothelial dysfunction is an emerging risk factor that may also play a causal role in the pathogenesis of atherosclerosis. As mentioned previously, it is defined as an inability of vascular endothelial cells to properly mediate dilation and constriction of the blood vessels through reductions in nitric oxide bioavailability. In addition to propagating the development of major risk factors, endothelial dysfunction is an independent predictor of cardiovascular events including myocardial infarction, stroke and sudden cardiac death[190-192]. Endothelial dysfunction is usually determined through the use of brachial artery flow-mediated dilation, the compensatory response of the artery to restoration of blood flow after occlusion[193,194]. However, standardization of methods and stronger evidence for risk reclassification are needed, and the American Heart Association does not currently recommend its use in clinical risk prediction[184].

The critical role of inflammation in CVD has led to investigation of many cytokines and related molecules that are produced in response to this inflammation. One such molecule is C-Reactive Protein (CRP). This protein was first identified in 1930[195] and its pentameric structure was subsequently determined[196]. CRP is produced by the liver[197] and represents the systemic acute phase response[198]. It has a half-life less than 24 hours and a constant clearance rate, so an increase in serum levels indicates increased production[199]. Inflammatory mediators induce the production of acute phase proteins, and the acute phase protein CRP is produced in response to the inflammatory mediator IL-6. If there is a prevailing inflammatory state in the body, this could lead to development of atherosclerosis and incidence of resultant cardiovascular events. Clinical researchers thus became interested in measurement of CRP as a cardiovascular biomarker. A series of epidemiological studies and clinical trials, run mostly out of Harvard Medical School, have generated data in support of the use of CRP in clinical risk prediction. While CRP is clearly associated with cardiovascular events and has improved risk stratification in clinical trials[200,201], it has not proven itself in routine clinical use. Of particular note is a large individual-participant meta-analysis, which showed, after obtaining individual patient data for over 160,000 participants in

various CRP trials, adjustment for traditional risk factors substantially weakened the association between CRP and CVD[202]. The Harvard investigators have also been criticized for having significant financial conflicts of interest. A re-analysis of the JUPITER trial revealed troubling biases in the data that may reflect the influence of corporate sponsors[203].

An interesting question has arisen from these investigations: is CRP simply a biomarker, or does it actively mediate the development of atherosclerosis? Interest in this area was generated by a report that CRP itself had direct proinflammatory effects on human endothelial cells in culture[204]. Another cell culture study demonstrated that CRP can attenuate endothelial progenitor cells[205], a population of putative circulating stem cells that may contribute to vascular repair and angiogenesis. However, these effects were later shown to merely be an artifact of LPS and azide contaminants of the commercial CRP preparation[206] and not properties of CRP itself.

Animal studies have been equally inconclusive. One mouse study demonstrated acceleration of atherosclerosis in CRP transgenic ApoE$^{-/-}$ mice as compared with regular ApoE$^{-/-}$ mice[207]. Subsequent studies have shown no effect in mice[208,209] and CRP transgenic rabbits[210], and even a protective effect of CRP on atherosclerosis in mice[211]. Attempts to reconcile these results have led to further investigation of CRP's molecular properties. After extensive investigation, one research group reported that the proatherogenic effects of CRP are dependent on a conformational rearrangement from its native pentameric structure to a monomer in endothelial cell culture[212]. A model[213] was proposed in which CRP binds to cell membranes (it can bind phosphocholine), undergoes dissociation of its subunits there, and proceeds to exert its proatherogenic effects. Monomeric CRP has recently been detected in human plaques but not in the circulation[214] and monomeric CRP was also shown in that study to form on activated platelets. The activated platelets may tether to the vessel wall and attract monocytes, suggesting a possible mechanism of action for CRP. Furthermore, blocking the dissociation of CRP prevents its proinflammatory effects[215]. However, one mouse study demonstrated that native pentameric CRP *increases* atherosclerosis, but monomeric CRP is strongly *protective* against atherosclerosis[216], findings which completely fly in the face of the proposed model of monomeric CRP's involvement in atherosclerosis.

More research is needed before sound conclusions can be drawn. It is most likely that, if CRP is actually involved in atherosclerosis, there are other indirect mechanisms at work. It is probably more complex than CRP simply promoting, or protecting against, atherosclerosis.

Numerous other biomarkers have been proposed, such as fibrinogen, Lipoprotein(a), and homocysteine. However, none of these biomarkers has been shown to substantially and consistently improve risk prediction[179,185,217]. Although these biomarkers may be associated with cardiovascular disease, they usually do not adequately meet the criterion of independent risk prediction, or reclassification of patients into different risk categories[183]. Genetics are involved in cardiovascular disease, but their role is unclear. In individuals without familial hypercholesterolemia or other monogenic disorders, the contribution of genetics to cardiovascular disease is highly complex[218-221]. Determination of family history is recommended[184], but no specific genetic markers have proven clinically useful. Genome-wide association studies have identified dozens of loci associated with cardiovascular disease, and the biological functions of many of the genes are unclear at this time. Arterial calcium is emerging as a useful measurement[147,222,223]. Finally, age is a major risk factor, yet the mechanisms by which aging contributes to cardiovascular disease progression are not well understood. Evidence suggests that aging leads to a large number of changes in the cardiovascular system, including endothelial dysfunction, that create an atherogenic environment[224-226]. Cardiovascular aging will remain an important research area in the future.

Imaging of cardiovascular disease

In addition to measurement of biomarkers, imaging is the second major strategy for early detection of cardiovascular disease[67,227]. X-ray angiography has been the gold-standard imaging modality for diagnosis of coronary and cerebral atherosclerosis. This procedure involves catheterization of the coronary artery, injection of a radio-opaque dye, and application of x-rays to the tissue. The invasiveness and use of ionizing radiation are obvious drawbacks, and it only provides a 2-dimensional extravascular image, which can limit its usefulness. Less invasive techniques have been developed, including computed tomography (CT), magnetic resonance imaging (MRI), and

ultrasound. CT scanning can be performed without invasive catheterization, but requires the use of ionizing radiation and contrast agents that may be toxic to the kidneys. MRI is emerging as a promising imaging modality. MRI utilizes non-ionizing radiation, and while it tends to deposit heat in biological tissues, its effects are generally considered less harmful than ionizing radiation. Data for multiple endpoints related to cardiac function and coronary artery stenosis can be gathered in a single imaging session, and contrast agents can be included for identification of cardiac scar tissue after myocardial infarction. It also has an emerging use in the measurement of endothelial function[228].

Ultrasound, sound waves above the 20 kHz threshold of human hearing, can be used in multiple ways for cardiovascular imaging[229]. Ultrasound transducers typically operate in the range of 1-40 MHz, and leverage the piezoelectric effect, the ability of quartz and related crystalline materials to interconvert electrical and sound energy. Pulses of electrical energy from the imaging system are received by the transducer, which then transduces that energy into sound waves. When the transducer is applied to biological tissue, sound waves are propagated through the tissue, reflected back to the transducer, and the transducer again uses the piezoelectric effect to transduce the sound waves back into electrical energy, which is returned to the imaging system for real-time processing. In terms of atherosclerosis, the key ultrasound imaging procedures are intravascular ultrasound and carotid intima-media thickness. Intravascular ultrasound imaging is another gold-standard technique that addresses some of the limitations of x-ray angiography. This invasive procedure requires insertion of an ultrasound probe into the artery[230]. The artery lumen is then imaged by slowly retracting the probe back through the artery, providing a view of the full circumference of the artery wall along the length of the artery. Measurement of carotid intima-media thickness (cIMT) is another ultrasound measurement that is simple and non-invasive. An ultrasound probe is placed on the neck, and the artery wall is visualized. The combined thickness of the intima and media is then computed, with the use of anatomical landmarks encouraged for repeatability and external validity[231]. cIMT improves cardiovascular risk prediction[232], and is considered a reasonable test according to American Heart Association expert guidelines[184]. A third method is contrast ultrasound, which involves intravenous injection of gas-filled microbubbles during non-

invasive ultrasound imaging. It is most useful in left-ventricular opacification for determination of cardiac function[233,234], and some evidence suggests it may also be useful in assessing coronary artery stenosis[235].

Other than cIMT, none of the above imaging methods are recommended for screening of asymptomatic patients[184]. It should also be noted that these imaging modalities usually only provide information on stenosis and occlusion of blood vessels, and cannot determine plaque vulnerability or other important characteristics. In order to provide additional diagnostic information, novel molecular imaging technologies are in development and evaluation. While molecular imaging has primarily been used in research, it is beginning to prove its worth in clinical practice[236]. Molecular imaging of mechanistic targets is possible for nearly every aspect of the atherosclerotic process, including endothelial cell activation, inflammation, smooth muscle cell proliferation, apoptosis, angiogenesis, thrombosis, and tissue scarring[227,237]. MRI leads in this regard with the broadest assortment of molecular contrast agents. Macrophages are a key imaging target due to their pervasive influence in the atherosclerotic process. Iron oxide nanoparticles are phagocytosed by macrophages, and the macrophages can then be visualized by MRI[238]. Ultrasound can also be used for molecular imaging, and has found experimental success in imaging endothelial adhesion molecules[239,240]. Targeted microbubbles are created by conjugating an antibody to the shell of a gas-filled microbubble, typically through the use of streptavidin-biotin chemistry. These targeted microbubbles are injected intravenously, and the antibodies lead them to bind to endothelial cell surface markers, providing enhanced contrast that is detected with ultrasound.

Challenges remain before the clinical use of molecular imaging is expanded[241]. Each new contrast agent must be FDA-approved, which requires millions of dollars and years of work. Also, the degree of expertise needed for molecular imaging typically restricts its use to specialists and research-oriented clinical centers. Imaging is also expensive, placing a burden on the Medicare system, and some argue that it should only be performed in patients at the highest risk for a cardiovascular event[242]. The feasibility of molecular imaging techniques remains to be determined.

Dietary acceleration of cardiovascular disease

Ancel Keys concluded a 1952 *Circulation* article[243] with "in summary then, we may remark that direct evidence on the effect of the diet on human atherosclerosis is very little and is likely to remain unsatisfactory for a long time." Despite decades of research into the dietary causes of cardiovascular disease, questions remain. The literature on diet and cardiovascular disease is far from conclusive, but an attempt at a brief overview will be made. This first section will discuss dietary components with potentially deleterious effects on the cardiovascular system, with a focus on two types of dietary fat: *trans* and saturated fats.

Of all the dietary factors hypothesized to be harmful to cardiovascular health, *trans* fats have received the greatest consensus. These fats both occur naturally, and are produced commercially by hydrogenation of vegetable oils for processed food products. Research on *trans* fats was summarized nicely in a review article by Mozaffarian et al[244]. Mechanisms including increased blood cholesterol, inflammation, and endothelial dysfunction lead to progression of atherosclerosis and diabetes, increasing risk of cardiovascular events. Prospective cohort studies have shown a 2% increase in energy intake from *trans* fats to be associated with a 23% increased risk of coronary heart disease. It is important to note that *trans* fats have never been shown to increase mortality in a randomized, controlled trial. However, the data from prospective cohort studies and short-term clinical trials with risk endpoints have been strong enough to mobilize our society against *trans* fats, and have prompted the widespread removal of *trans* fats from the food supply. It has also been argued that long-term trials of *trans* fats would be considered unethical given our current knowledge of their adverse health effects[244].

The role of saturated fats in cardiovascular disease remains a contentious topic. Evidence suggesting this link began with the work of Ancel Keys, whose Seven Countries study explored correlations between various aspects of diet and the occurrence of cardiovascular disease, and also provided early evidence linking circulating cholesterol levels with cardiovascular disease[245]. Findings from epidemiological studies were further explored with highly controlled "metabolic ward" studies. A 1997 quantitative meta-analysis of these studies[246] demonstrated reductions

in blood total and LDL cholesterol levels when saturated fats were replaced with polyunsaturated fats or complex carbohydrates, but not monounsaturated fats, with an additional minor benefit to reductions in dietary cholesterol. Polyunsaturated and monounsaturated fats modestly increased HDL. The authors also derived equations to predict the response of circulating cholesterol levels to dietary fats and cholesterol.

The influence of dietary fats on the development of CVD has been called into question many times. Early critics of the Seven Countries study explained that Keys actually had data for 22 countries, yet excluded 15 without good cause. One particular re-analysis of the study data[247] is frequently cited[248] as evidence that inclusion of all 22 countries invalidates Keys' conclusions from the study. However, the re-analysis supports, not refutes, the association between dietary fat and circulating cholesterol levels, with saturated fats of animal origin being particularly important in the association. Epidemiological studies, by nature, are prone to confounding variables, but Keys' studies generated a wealth of data and hypotheses that have been used to create life-saving treatments. A second, more recent example involves a highly publicized meta-analysis disputing the link between saturated fats and CVD[249]. Controversy unfolded as corrections to the article had to be rapidly published, demonstrating numerous omissions and miscalculations[250]. Many confounding variables may have led to the misleading conclusions of the study. For example, grouping all sources of monounsaturated fats together ignores the differential effects of nuts and red meat on cardiovascular risk. It is surprising that the authors did not systematically address the effects of replacing saturated fats with other types of fat or carbohydrates, as the metabolic ward studies did. Additionally, a previous meta-analysis of prospective cohort studies showed that dietary polyunsaturated fats alone, as well as replacement of saturated with polyunsaturated fats, were inversely associated with coronary heart disease[251]. The Chowdhury study[249] does not address the discrepancy between the two papers. This study is a poorly performed analysis taking the literature on fats and the heart off-course.

Studies questioning the saturated fat-CVD link conveniently overlook a prodigious experimental literature on the detrimental effects of saturated fatty acids. In addition to consistently raising blood cholesterol levels in animal models, saturated fatty acids have

been shown to induce inflammation, insulin resistance, and impairment of endothelial function. Saturated fatty acids serve as ligands for TLR4[252], inducing receptor dimerization and recruitment into cell membrane lipid rafts[253]. Receptor dimerization stimulates assembly of intracellular adapter proteins for activation of downstream signaling pathways. One of the most well characterized results of TLR4 pathway activation is nuclear translocation of NF-κB, the master inflammatory gene transcriptional regulator. The consequences of saturated fat-induced inflammation are numerous and vary depending on the tissue. In adipose tissue, TLR4 activation of NF-κB by saturated fatty acids can lead to macrophage infiltration, production of inflammatory cytokines, and insulin resistance[254-256]. In the gastrointestinal tract, dietary saturated fatty acids facilitate expansion of microbial populations that stimulate inflammation and promote development of colitis[257]. In the vascular endothelium, NF-κB activation increases the expression of proatherogenic adhesion molecules, contributing to endothelial dysfunction (**Figure 1.1**), and recent evidence suggests endothelial NF-κB signaling also contributes to insulin resistance[125,258]. A human clinical trial evaluated acute effects of either safflower oil, high in polyunsaturated fatty acids, or coconut oil, high in saturated fatty acids, on HDL and endothelial function[259]. In a crossover design, subjects consumed isocaloric meals containing either safflower or coconut oils, with the two meals separated by one month. Flow-mediated dilation, a marker of endothelial function, was measured *in vivo*, and HDL from the subjects was also isolated and used to treat human umbilical vein endothelial cells in culture. The authors found impaired flow-mediated dilation, and reduced anti-inflammatory capabilities of HDL, after coconut oil consumption. They attributed these detrimental effects to the fatty acid composition of the coconut oil, though it has also been argued that the differential vitamin E content of the two oils may have partially contributed[260]. The impairment of endothelial function and insulin action by saturated fatty acids may be prevented by concomitant consumption of omega-3 fatty acids[261,262].

The overly simplistic focus on single nutrients, such as saturated fats, belies the complexity of the human diet and has produced a confusing literature from which we can draw few conclusions. Studies also rarely account for the powerful effects of exercise, which may be a key mediator between diet and the cardiovascular system[263].

To further complicate matters, levels of circulating, not dietary, saturated fatty acids may be most important. Limited evidence from small clinical trials suggests that low-carbohydrate diets decrease circulating saturated fatty acids, which is associated with decreased circulating inflammatory markers[264,265]. Although it is difficult to draw conclusions from the collection of human studies, controlled experiments in cell and animal models have demonstrated consistently detrimental effects of saturated fatty acids. In his 1952 article, Keys recommended "restriction of all fats to the point where the total extractable fats in the diet are not over about 25 to 30 per cent of total calories." This general guideline is still in use today. However, after explaining the ability of dietary fat to increase blood cholesterol levels, Keys also commented, "there is not the slightest evidence for a difference between animal and vegetable fat in this regard." We have advanced our understanding of the effects of different types of dietary fat on blood cholesterol levels since then.

A great deal of attention has recently been focused on dietary sugar intake. Added sugars, mostly in the form of high-fructose corn syrup, have been implicated in the obesity epidemic, though most studies have failed to dissociate the effects of fructose itself from the effects of excess calories from fructose[266]. The effects of dietary sugar have also been studied with specific relation to CVD. Sugar has been acknowledged as an independent risk factor for CVD mortality[267,268], not only through its association with excess calories and weight gain. Although the link between sugar intake and diabetes, a disorder of carbohydrate metabolism, is not necessarily direct, consumption of sugar may contribute to a dysfunctional cardiometabolic state that promotes atherosclerosis. Links between diabetes and CVD were briefly discussed in the risk factors section.

Dietary reduction of cardiovascular disease

Compared with the literature on harmful dietary factors, the literature on cardioprotective dietary factors is clearer. An excellent review was recently published by Mozaffarian and colleagues[269], and this section will highlight some key characteristics of a healthful diet presented in that review. It is important to consider the outcomes examined in each study, and whether these outcomes represent occurrence of hard

cardiovascular events or simply risk of cardiovascular events. When helpful, emphasis will be placed on study designs and outcomes.

Dietary patterns

The strongest evidence on diet and CVD comes from studies on dietary patterns, or groups of foods consumed together. The study of dietary patterns instead of individual foods has the advantage of being practically applicable, though it also prevents firm conclusions from being drawn about the effects of specific foods.

One of the most widely recognized and scientifically reputable dietary patterns that promotes cardiovascular health is the Dietary Approaches to Stop Hypertension (DASH) diet[270]. This diet was developed in National Institutes of Health-funded studies as a treatment for hypertension. In the original clinical trial, patients achieved substantial blood pressure reductions by consuming a diet rich in fruits, vegetables, whole grains, low-fat dairy, nuts, fish, and poultry; red meats and added sugars were limited[271]. Interestingly, the benefits in this first trial were observed without reducing sodium intake. Further studies demonstrated a dose-response relationship between amount of dietary sodium and blood pressure, with maximum benefits observed at an intake level of 1200 mg/day[272,273]. Impressively, the low-sodium DASH diet also eliminates the usual age-related increase in blood pressure. Although no long-term trials with hard endpoints (myocardial infarction, stroke, or death) have been conducted, the DASH investigators suggest that such trials are not necessary in light of the strong benefits of the diet on established risk markers[270].

A second dietary pattern with strong scientific evidence supporting its cardiovascular benefits is the Mediterranean diet. The characteristics of this diet were first identified, again by Ancel Keys[274], through the study of populations in the Mediterranean region with low incidences of cardiovascular events. There are many cultures surrounding the Mediterranean Sea, and their diets are heterogeneous[275], but the Mediterranean diet referred to in most peer-reviewed scientific studies is similar to the DASH diet. It contains large amounts of fruits and vegetables, nuts, legumes, fish, and olive oil, with moderate consumption of wine, cheese and meats. Olive oil has traditionally contributed up to 18% of total calories in southern Italy[276]. The Mediterranean diet has been shown to reduce cardiovascular events and death in prospective cohort studies[277] and

randomized controlled trials[278]. It has also improved endothelial function and management of metabolic syndrome[279], and weight loss[280] in other trials.

In addition to the established benefits of the general Mediterranean dietary pattern, specific food components have also been studied. A recent randomized controlled trial, the Prevención con Dieta Mediterránea (PREDIMED) trial[281], evaluated a Mediterranean diet with either added olive oil or mixed nuts. The investigators reported a significantly decreased incidence of cardiovascular events in both the olive oil and nut groups. Further subgroup analyses showed regression of cIMT in the nut group[282], reduced atrial fibrillation in the olive oil group[283], and reduced blood pressure, lipids, and glucose in both intervention groups[284]. While important, the PREDIMED trial had a number of limitations. First, the control group has been criticized. The editorial[285] accompanying the 2013 clinical trial paper[281] explains that the control group was basically also consuming a Mediterranean diet, and although it was considered a “low fat” group, the participants still consumed roughly the same amount of dietary fat as the intervention groups. The decision to stop the study early was also questionable. While the olive oil and nut groups did technically experience a statistically significant benefit, the results were not dramatic. The hazard ratio confidence intervals are close to encompassing 1 (which would indicate no effect). There is also evidence that stopping clinical trials early may result in artificially high estimates of benefit[286,287]. Finally, despite the title of the article, it is important to note that the diets tested did not actually prevent CVD. They merely resulted in a relatively reduced number of cardiovascular events. The olive oil group still experienced 96 events, and the nut group 83, compared with 109 in the control group. For these people, olive oil and nuts did nothing to prevent their cardiovascular events.

A third, related dietary pattern deserves mention. Plant-based vegetarian and vegan diets have been promoted by investigators including Dean Ornish, Caldwell Esselstyn, and T. Colin Campbell. In several clinical trials, Ornish consistently demonstrated reversal of coronary atherosclerosis and reduced incidence of cardiovascular events after a plant-based diet and intensive lifestyle intervention[288-292]. This lifestyle pattern has also been beneficial in prostate cancer[293-296]. Both Esselstyn and Campbell advocate a strict, low-fat diet devoid of oils, meats and added sugars. In a small clinical

trial, Esselstyn demonstrated decreases in circulating cholesterol levels and reversal of coronary atherosclerosis after a low fat, plant-based dietary intervention[297,298]. While Esselstyn's study lacks the controls, randomization and power of larger clinical trials, the results suggest a strong benefit of the dietary intervention. These results have been complemented by epidemiological studies of rural Chinese inhabitants consuming low fat, plant-based diets, which have demonstrated low circulating cholesterol levels and nearly complete absence of CVD in this population[299]. Though the evidence in support of the low fat plant-based dietary pattern is not as strong as for the DASH and Mediterranean diets, it is worth considering for the prevention and reversal of CVD.

Specific foods and food components

Epidemiological studies have consistently observed an inverse association between intake of fruits and vegetables and cardiovascular events and risk factors[300-302], with a number of studies reporting benefits of tomato intake specifically. Benefits have been more consistently observed in women[303,304] than in men[305,306]. Human clinical trials have demonstrated increased serum antioxidant enzymes[307], reduced LDL oxidation[308] and reduced blood pressure[309] after tomato consumption, with benefits seen in as little as one week. Tomatoes are usually consumed as tomato sauce in these trials, which has higher carotenoid bioavailability than raw tomatoes[310].

Tomatoes contain a variety of essential nutrients and bioactive compounds[311], and there has been great interest in the identification of specific bioactive components of tomatoes responsible for their salutary effects. Chief among these has been lycopene, the carotenoid responsible for red pigmentation in tomatoes. Lycopene has been shown to have numerous cardiovascular benefits. Epidemiologically, it has been inversely associated with carotid intima-media thickness[312], arterial stiffness[313] and incident CVD[314], especially stroke[315]. Clinical trials have shown similar decreases in LDL oxidation with purified lycopene supplementation as with tomato consumption[308,316], suggesting that lycopene may be predominantly responsible for the cardiovascular benefits of tomato consumption. Animal and cell culture studies have corroborated this epidemiological and clinical evidence. Lycopene decreases the expression of atherogenic adhesion molecules on endothelial cells[317], reduces cholesterol synthesis in

macrophages[318], and when administered at 5 mg/kg body weight for 4 weeks, reduces total and LDL cholesterol in rabbits[319]. Similar results have been shown in rats[320].

In addition to lycopene, tomatoes contain bioactive steroidal alkaloid compounds, or "sapogenols", including tomatine, tomatidine and esculeogenin A. Tomatine was originally isolated in 1945, and noted for its antifungal and antibacterial properties[321,322]. It was later discovered that tomatine is metabolized to its aglycone form, tomatidine[323]. Tomatine and its aglycone tomatidine inhibit cancer cell growth[324-326], inflammation[327] and muscle atrophy[328]. A recent study demonstrated that tomatidine inhibits the progression of atherosclerosis by reducing the activity of acyl-coenzyme A:cholesterol acyltransferase (ACAT), In addition to its health benefits, tomatidine is used as control reagent in studies of the Hedgehog signaling pathway because it is structurally similar to cyclopamine, a teratogen from the lily *Veratrum californicum* that interferes with Hedgehog signaling[50,51,329,330]. Esculeogenin A was recently discovered as an additional steroidal alkaloid similar to tomatidine that inhibits atherosclerosis through ACAT[331]. Taken together, these results suggest that tomatoes and their bioactive components promote cardiovascular health both directly, by promoting proper vascular function, and indirectly, by influencing cholesterol metabolism.

Soy foods have also generated interest as a result of their beneficial effects on the cardiovascular system. Soybeans contain many bioactive compounds with salutary properties, including isoflavones, sterols, and the soy protein itself. Numerous studies have demonstrated the hypocholesterolemic effects of soy protein consumption[332,333]. These benefits are primarily due to incorporation of cholesterol into bile and subsequent excretion in feces[334]. Soy isoflavones also affect HMG-CoA reductase, the rate-limiting enzyme in cholesterol biosynthesis.

Soy germ is a component of whole soybeans that is separated from soy protein isolate during processing in an isoflavone-rich "hypocotyledon" fraction. It is typically 44% protein, 32% fiber and 24% fat by weight. It is currently available as a dietary supplement, and its distinct isoflavone profile may confer unique benefits. Although there is ample evidence demonstrating the cardiovascular benefits of other soy products, only two recent studies (both human clinical trials) have evaluated the effects of soy germ. The first enlisted patients with hypercholesterolemia[335] (n=31/group). An

isoflavone-rich soy germ extract was added to pasta during the manufacturing process. The pasta delivered 33 mg isoflavones, which they report as being similar to levels of intake in Asian countries, and plasma isoflavones after consumption were in the 200-250 nmol/L range. In this study, consumption of soy germ significantly reduced arterial stiffness, blood pressure, total and LDL cholesterol, and high sensitivity C-reactive protein. The authors explain that soy germ isoflavones, particularly equol, may have beneficial effects on NO production by the endothelium[336]. Importantly, this depends on equol production from daidzein by intestinal bacteria. In the second clinical trial, soy germ was shown to have beneficial cardiometabolic effects in type II diabetics[337] (n=9-11/group). Consumption of the soy germ pasta resulted in remarkable decreases in arterial stiffness, blood pressure, oxidized LDL, and homocysteine, combined with an increase in plasma GSH levels. No animal studies have tested the cardiovascular effects of soy germ.

Animal models of atherosclerosis

Animal models have been vital to advancing our understanding of the pathogenesis of atherosclerosis. The first animal model to enter widespread use was the cholesterol-fed rabbit. Studies of atherosclerosis at the beginning of the 20th century in Russia and Germany utilized the rabbit as the model of choice. Experiments typically involved feeding egg yolks or various types of meat, and then examining the aorta for deposition of plaque. A Russian scientist, Anitschkow, realized that cholesterol was the dietary factor responsible. He fed rabbits purified cholesterol and hypothesized that the atherosclerosis he observed was the result of cholesterol deposition in the artery wall, further positing a role for immune cells in the process[338]. The cholesterol-fed rabbit was a favorable model when first introduced due to their physical size, large enough to facilitate pathological observation but smaller than monkeys and pigs, and the simplicity of the method used to induce atherosclerosis. Their sensitivity to dietary cholesterol appears to be due primarily to low rates of excretion[339,340]. Cholesterol-fed rabbits also carry excess blood cholesterol primarily in LDL, similar to humans, with small amounts of HDL and variable amounts of VLDL depending on the diet[341-343]. A second rabbit model, the Watanabe heritable hyperlipidemic rabbit, was created when Dr. Watanabe

observed a single male rabbit with elevated serum cholesterol levels[344]. He then used conventional animal breeding techniques to create an inbred strain of rabbits with elevated blood cholesterol. Subsequent investigations revealed that these rabbits had genetic defects in the LDLR, providing a useful model of familial hypercholesterolemia. The Watanabe model was later refined to develop more pronounced coronary atherosclerosis and myocardial infarction.

There are disadvantages to working with rabbit models that offset their benefits. While atherosclerosis can be induced simply by feeding cholesterol, it also causes anorexia and jaundice that interfere with experiments[343]. The rabbit's size was originally seen as an advantage, but they are much larger and more difficult to handle than the rodent models that are commonly used today. Diet and housing costs are also considerably higher than those of rodents. Another important factor is the limited availability of antibodies and reagents designed for use with rabbit samples. In light of these disadvantages, and the ease of genetic modification in mice, rabbits are less commonly used today than mouse models.

Mice are naturally resistant to atherosclerosis, but genetic disruption of lipoprotein metabolism has produced useful models. The creation of ApoE$^{-/-}$[345-347] and LDLR$^{-/-}$[348-350] mice in the early 1990s enabled rapid progress in knowledge of atherosclerotic mechanisms, and they remain the two most commonly used mouse models of atherosclerosis today. Deletion of ApoE is particularly effective at preventing lipoprotein clearance in rodents due to hepatic ApoB mRNA editing by Apobec-1[351,352]. In humans, ApoB mRNA is only edited in the intestine, producing the ApoB48 that is loaded onto chylomicrons. The human liver produces full-length ApoB100 that is incorporated into LDL and VLDL. In rodents, however, ApoB mRNA editing by Apobec-1 occurs in the liver also, resulting in hepatic secretion of lipoproteins decorated with ApoB48. The lack of full-length ApoB100 in chylomicron and VLDL remnants makes them critically dependent on ApoE for receptor recognition and hepatic clearance from the circulation. ApoE is capable of binding to the LDL Receptor, as well as to the LDL receptor related protein (LRP). Genetic deletion of ApoE, coupled with the truncated ApoB48, renders the murine liver virtually incapable of clearing VLDL and chylomicron remnant lipoproteins from the circulation. As a result, circulating lipoprotein levels increase, with

VLDL and remnant lipoproteins being the predominant fractions[353]. The importance of ApoE in lipoprotein metabolism is emphasized by the finding that bone marrow transfer from wild-type mice into ApoE$^{-/-}$ mice results in production of functional ApoE, normalizing lipoprotein metabolism and preventing atherosclerosis[354]. Although their lipoprotein profiles are different from hypercholesterolemic humans, these mice are similar to humans in that dietary saturated fat influences circulating cholesterol levels more than dietary cholesterol[355]. They also share many lesion characteristics with humans, with the exception that they are not susceptible to lesion rupture[356]. In this regard, hypercholesterolemia and atherosclerosis in ApoE$^{-/-}$ and LDLR$^{-/-}$ mice are dramatically increased by consumption of a Western diet, originally developed for use with the ApoE$^{-/-}$ mouse by the Breslow group at Rockefeller University in collaboration with Harlan Teklad. The Western diet contains 21% milkfat, 34% sucrose, and 0.2% cholesterol w/w added to an AIN-76[357] or AIN-93[358] purified diet formulation. The sucrose is converted to fat through the process of *de novo* lipogenesis, contributing to cardiometabolic dysfunction in these animals[359]. Consumption of a Western diet for 2-4 weeks typically triples circulating total cholesterol levels in ApoE$^{-/-}$ mice. While ApoE$^{-/-}$ mice will develop atherosclerotic lesions on chow, LDLR$^{-/-}$ mice must be fed a Western diet to develop lesions in a typical experimental time frame due to the characteristics of murine lipoprotein metabolism described above. As with all animal models, these models are subject to certain limitations. ApoE has many other physiological roles independent from receptor recognition[360,361], so its genetic deletion may influence experimental results in unforeseen ways.

Other novel mouse models have been developed. The LDLR$^{-/-}$ apobec-1$^{-/-}$ mouse was generated to prevent hepatic ApoB mRNA editing, and carries its increased cholesterol exclusively in LDL, providing a model that is more representative of human familial hypercholesterolemia[352,362]. A similar model was also created by transgenic addition of ApoB100 onto a C57 Bl/6[363] or LDLR$^{-/-}$[364] background. ApoE3-Leiden transgenic mice, another model, have a mutated ApoE3 gene inserted into their genome. In humans, this mutated *APOE3* gene is associated with type III familial hypercholesterolemia. Their total cholesterol levels and lipoprotein profile are similar to ApoE$^{-/-}$ mice, with most cholesterol contained within VLDL[365]. This has been called a

“humanized” model[366], but incorporates a genetic variant that very few people carry and displays a different lipoprotein profile than humans, so its advantages are unclear. An interesting alternative mouse model of diet-induced atherosclerosis has been reported[367]. This model involves genetic knockout of the scavenger receptor B1, coupled with expression of a mutated “hypomorphic” form of ApoE. These mice do not display substantial atherosclerosis on a chow diet, but once they are fed an atherogenic diet, they rapidly develop extensive occlusive lesions and die in one month.

A few other animal species are used in atherosclerosis research. Rats do not naturally develop atherosclerosis, although some strains are used in hypertension research[368], and tools for genetic manipulation are beginning to become available[369]. Gerbils have been used in studies of lipoprotein metabolism because their metabolism of lipids, and lipophilic compounds like carotenoids, is similar to humans[370,371]. Gerbils do not develop appreciable atherosclerotic lesions[372], and genetic modification is not commonly performed. Another rodent model is the guinea pig. Guinea pigs are similar to rabbits in that cholesterol feeding elicits a dose-dependent increase in plasma LDL, whereas dietary fat has less of an effect. They have CETP, LCAT and LPL activity, similar rates of hepatic synthesis and catabolism of cholesterol as humans, and minimal ApoB mRNA editing in liver[373]. Disadvantages of the guinea pig model include heterogeneous and individualized responses to dietary cholesterol[374], inconsistent development of atherosclerotic lesions despite hypercholesterolemia[375], and lack of reagents or assay kits (though some mouse antibodies may show cross-reactivity[376]). The Yucatan mini-pig is an older model that is occasionally used in atherosclerosis research[377,378]. These “mini” pigs can weigh over 100 kg and require special housing facilities. Pigs do display atherosclerotic plaques that are vulnerable to rupture, and thus may fill a gap left by the more prevalent mouse models[379]. They have similar blood pressure, heart rate, vessel size and plaque morphology to humans. The size of pigs and mini pigs, while it presents considerable challenges, may be useful because human diagnostic procedures like intravascular ultrasound can be performed in a controlled experimental setting[380]. Recently, a human PCSK9 transgenic mini pig was created[381] that may become a useful translational model of familial hypercholesterolemia and atherosclerosis. Primates were frequently used in early studies[382], but due to ethical

issues and the availability of simpler models, are only used today in select instances[46,383].

Methods of atherosclerosis assessment

This section will focus on established methodologies developed for use with mouse models of atherosclerosis. The aortic root and *en face* methods of atherosclerosis assessment will be discussed, as well as methods for measurement of blood lipoproteins.

The aortic root methodology was originally developed by Paigen et al. for assessing atherosclerotic plaque development in wild-type Bl/6 mice fed diets with varying amounts of fat, cholesterol, and cholate[384]. While these mice are resistant to development of atherosclerotic lesions in other areas of the arterial tree, they do develop modest lesions in the aortic root. The technique continued to prove useful after development of genetically modified mouse models, and remains the gold-standard[385].

To perform this method, the mouse is euthanized, either with CO_2 or by exsanguination under anesthesia. Cervical dislocation is the fastest euthanasia method, but it impairs perfusion and may result in damage to the aorta because it runs along the spine. The mouse is then opened along the midline, the ribcage is cut away on either side with blunt scissors, and the heart is perfused with 20-30 mL phosphate buffered saline (PBS) through the left ventricle. This works best if the animal is perfused under anesthesia, because its heart is still beating and will circulate PBS more effectively. Mice can be perfused either with gravity or using an infusion pump. For gravity perfusion, a 50 mL syringe is typically mounted 100 cm above the bench top with extension tubing connecting it to a catheter. An infusion pump is simpler to set up, and uses mechanical force to depress the syringe plunger at a constant rate that is specified by the user. It is helpful to cut either the vena cava or right atrium to allow for fluid drainage during perfusion. While cutting at the right atrium allows for full circulation of fluid, it carries the risk of cutting through the aortic root and damaging the tissue. The vena cava is more straightforward to cut. After the perfusion is complete, the mouse can optionally be perfused with a fixative such as 10% neutral buffered formalin (NBF) or 4% paraformaldehyde (PAF). NBF and PAF both fix tissue equally, but PAF is more

difficult to work with than NBF. The formaldehyde polymers frequently precipitate, and the solution must be boiled to allow the polymers to dissolve.

Next, the heart is removed with 1 mm of the aorta attached. It is helpful to use a dissecting microscope, and to perform a brief dissection to remove the pulmonary arteries and veins, and fat on the heart. The auricles (flaps above the atria) should be retained for orientation. If further fixation is desired, the heart can be immersed in NBF or PAF overnight. Next, the bottom half of the heart is cut away with a scalpel. This step is critical. The cut must be parallel to the aortic root. If it is not, the three aortic valve leaflets will not be simultaneously visible in the cryosections and quantification may not be accurate. The cut will also be roughly parallel to the atria. After the bottom of the heart has been removed, the aorta should be standing straight up from the center of the heart, and may be pointing to the right slightly (when the heart is viewed from the front). This is easier to perform with fixed tissue than fresh tissue, because fixed tissue is more rigid, but fixing tissue may affect its ability to bind to charged microscope slides for histology (Smith BW, unpublished observations). Fixed hearts can optionally be moved to 15-30% sucrose in PBS overnight at 4ºC[386], and should sink after being infiltrated by the sucrose solution. The sucrose solution protects against freezing artifacts such as ice crystals because it has a lower freezing temperature than water. Before freezing in optimum cutting temperature compound (OCT), hearts should be washed 3 times for 3 minutes each in cold PBS.

The tissue should then be acclimated to the OCT freezing medium in a small weigh boat or cryomold for 5-10 minutes at room temperature, with attention given to removal of air from inside the aorta. Next, tissues are transferred to a fresh cryomold, covered with OCT, and frozen. If retention of lipid in the tissues is not important, they can also be paraffin embedded after fixation. Several options are available for freezing tissue. The most effective and user-friendly is dry ice-cooled isopentane (2-methylbutane). With this method, isopentane is added to a small vessel, preferably stainless steel for efficient heat transfer, and surrounded with dry ice. The tissue in OCT is then placed in the isopentane for 3 minutes. The key to even freezing is to prevent the isopentane from covering the top of the tissue block. This can be accomplished by using deeper OCT molds that will not be completely filled after addition of heart tissue, and by only adding

a small amount of isopentane to the freezing vessel. If the tissue is fully submerged in isopentane, it will freeze more quickly, but the OCT may bubble, ripple and crack. The tissue can then be wrapped in parafilm, placed in a sealed plastic bag to prevent drying, and stored at -80ºC. Tissue blocks can also be frozen with isopentane cooled in liquid nitrogen. This method results in faster freezing than dry ice-cooled isopentane, but is more difficult to perform. It is more likely that OCT blocks will expand and crack. Also, the isopentane will eventually freeze, so it is difficult to keep it at the correct temperature where it is just above freezing. Freezing directly in dry ice, liquid nitrogen, or a -80ºC freezer is simpler, but carries a risk of ice crystal formation. Storage at -80ºC is preferred long-term, but it is helpful to store tissue blocks at -20ºC overnight prior to sectioning. A block that is too cold may develop artifacts when being sectioned.

Next, serial 10 µm cryosections of the aorta are cut at the aortic valves and mounted on charged microscope slides. Ideally, all three valve leaflets will be visible. A set of 6-12 slides is typically created, with each serial section added to a different slide. Sections should be allowed to dry and adhere to the slides for 30-60 minutes. If the tissue has not previously been fixed, slides can be dipped in NBF or acetone to fix.

Once mounted on slides, a variety of stains can be applied depending on the measurements desired. The most commonly used stains are hematoxylin and eosin (H&E)[126,387-396] and Oil Red O[54,385,397]. The H&E staining procedure dissolves lipids out of the tissue, but plaque area can be estimated by examining the tissue morphology manually[394,395]. Oil Red O stains neutral lipids (cholesterol esters and triglycerides) red, and the slides are typically counterstained with hematoxylin to provide contrast. Because lesions are stained red, software can be used for automated quantification of lesion area[398]. Oil Red O does not always stain lesions effectively. It is also important to note that, although neutral lipid staining is a general marker of lesion deposition, it does not provide any mechanistic information on the atherosclerotic process such as immune cell infiltration, inflammatory cytokine production, fibrous cap development, or calcification. Because of this, immunostaining procedures can be helpful. Immunostaining of macrophages is commonly performed using Mac-2[395,399], MOMA-2[126,137,389,400-405], or F4/80[406,407] antibodies. Stains for collagen to indicate development of a fibrous lesion, such as Masson's Trichrome[137,211,390,395,408,409] or Movat's

Pentachrome[410-412], or stains for calcium to indicate lesion calcification[413,414] are also used.

For the *en face* method[385,397], the mouse is perfused as described above, first with PBS and then with fixative for 10 minutes. The aorta is delicate, and the inner endothelial layer is particularly prone to damage even when the vessel is carefully isolated. A brief *in situ* fixation helps avoid damage. Importantly, if fixation is not desired for other organs, they should be collected before perfusing the aorta. Next, the aorta should be removed with major branching vessels still attached, cut open longitudinally, pinned to a flat black wax surface, and fixed overnight in NBF or PAF. It should then be immersed in PBS to wash, and can remain in PBS for up to 12 hours. Next, the aorta is briefly rinsed in 70% ethanol and a neutral lipid stain such as Sudan IV is typically applied for 5-10 minutes. The aorta is then digitally photographed with a CCD camera and polarizing lens to avoid shine and reflections. The images can be analyzed with color thresholding as described for Oil Red O above. The aorta can then be rinsed in ethanol for destaining and storage. The *en face* method has the advantage of demonstrating total aorta surface lesion coverage, but provides no information on lesion depth or morphology. In addition to aortic root and *en face* preparations, artery cross-sections are sometimes used to examine specific sections of the coronary[367], brachiocephalic[415], or carotid[416] arteries, or the aorta[408]. If artery cross sections are used, care should be taken to preserve the circular shape for lesion quantification.

Circulating cholesterol levels are usually measured, due to the central role of lipoprotein metabolism in atherosclerosis. Two main methods are used: chromatography and colorimetric kits. The most informative and well-accepted method utilizes fast performance liquid chromatography (FPLC), which separates all lipoprotein fractions at once and is considered the most accurate measurement method[54,345,401]. Colorimetric kits are easier to use than FPLC, but only one fraction at a time can be determined.

Lipids from the diet are incorporated into lipoproteins, and it is therefore useful to fast animals before measurement of circulating lipid levels. There is a lack of information and standardization of fasting procedures in the literature, but they can be divided into two major strategies: daytime and overnight fasts (**Table 1.1**). Daytime fasts

are typically 4-6 hours, and overnight fasts are usually 12-16 hours. It is important to note that an overnight fast is metabolically stressful to mice, because they typically feed at night[417]. If possible, a daytime fast is preferred.

Fasting time	Model system	Lipids measured	Comments
10-120 minutes[418]	Cells (U2OS)	None	Effects on the Ulk1/AMPK interaction in autophagy in ≤30 min
3 hours[419]	Mouse	None	
4 hours[54,420-428]	Mouse	Liver: TG Blood: TG, LP	Referred to as daytime fast[54,425,426]
4-6 hours[370]	Gerbil	Liver: TG Blood: TG, LP	
7 hours[429]	Mouse	Liver: TG Blood: TG	Blood glucose
"Overnight"[430-436]	Mouse[430-435], rabbit[436]	Liver: TG Blood: TG, LP	Exact number of hours not given
12 hours[437-441]	Human	Blood: TG[437], various LP[437]	12 hours referred to as overnight, typical for humans
12 hours[390,442,443]	Mouse[390,443], rabbit[442]	Blood: TG, FFA, LP	12 hours referred to as overnight
12-14 hours[444]	Mouse	None	
16 hours[445-447]	Mouse	Liver: TG, cholesterol Blood: various LP, TG	16 hours referred to as overnight
16 hours[448]	Mouse	None	16 hours referred to as overnight
16 hours[449]	Mouse	Liver: TG	Fasted prior to taking blood glucose
16-20 hours[450]	Mouse	None	
18 hours[372,451]	Gerbil[372], rabbit[451]	Blood: TG, LP, CE	
20 hours[452]	Mouse	Blood: TG, LP	20 hours referred to as overnight
23 hours[453,454]	Mouse	Blood: FFA	Starvation studies
24 hours[455-458]	Mouse	Blood: TG, ketones	Fasting metabolism studies
48 hours[459-461]	Mouse	Liver: TG[459] Blood: TG, LP[459] None[460,461]	Fasting metabolism studies
2 weeks[462]	Zebrafish	Liver/whole body: TG, FFA, cholesterol, CE, ketones	

Table 1.1. Experimental fasting and starvation times. Abbreviations: CE, cholesterol esters; FFA, free fatty acids; LP, lipoproteins; TG, triglyceride

References

1. Go AS, Mozaffarian D, Roger VL, Benjamin EJ, Berry JD, Borden WB, Bravata DM, Dai S, Ford ES, Fox CS *et al.* Heart disease and stroke statistics--2013 update: a report from the American Heart Association. *Circulation* 127:e6-e245 (2013).

2. Iqbal J, Hussain MM. Intestinal lipid absorption. *Am. J. Physiol. Endocrinol. Metab.* 296:E1183-E1194 (2009).

3. Huff MW, Pollex RL, Hegele RA. NPC1L1: evolution from pharmacological target to physiological sterol transporter. *Arterioscler. Thromb. Vasc. Biol.* 26:2433-2438 (2006).

4. Jia L, Betters JL, Yu L. Niemann-pick C1-like 1 (NPC1L1) protein in intestinal and hepatic cholesterol transport. *Annu. Rev. Physiol.* 73:239-259 (2011).

5. Bonamassa B, Moschetta A. Atherosclerosis: lessons from LXR and the intestine. *Trends Endocrinol. Metab.* 24:120-128 (2013).

6. Mansbach CM, Siddiqi SA. The biogenesis of chylomicrons. *Annu. Rev. Physiol.* 72:315-333 (2010).

7. Abumrad NA, Davidson NO. Role of the gut in lipid homeostasis. *Physiol. Rev.* 92:1061-1085 (2012).

8. Gropper SS, Smith JL, Groff JL. *Advanced Nutrition and Human Metabolism*, 5th edn (Wadsworth Publishing Company, Inc., 2009).

9. Chen SH, Habib G, Yang CY, Gu ZW, Lee BR, Weng SA, Silberman SR, Cai SJ, Deslypere JP, Rosseneu M. Apolipoprotein B-48 is the product of a messenger RNA with an organ-specific in-frame stop codon. *Science* 238:363-366 (1987).

10. Powell LM, Wallis SC, Pease RJ, Edwards YH, Knott TJ, Scott J. A novel form of tissue-specific RNA processing produces apolipoprotein-B48 in intestine. *Cell* 50:831-840 (1987).

11. Davidson NO, Shelness GS. Apolipoprotein B: mRNA editing, lipoprotein assembly, and presecretory degradation. *Annu. Rev. Nutr.* 20:169-193 (2000).

12. Ross AC, Caballero B, Cousins RJ, Tucker KL, Ziegler TR. *Modern Nutrition in Health and Disease*, 11th edn (Lippincott Williams & Wilkins, 2012).

13. Wang H, Eckel RH. Lipoprotein lipase: from gene to obesity. *Am. J. Physiol. Endocrinol. Metab.* 297:E271-E288 (2009).

14. Rohlmann A, Gotthardt M, Hammer RE, Herz J. Inducible inactivation of hepatic LRP gene by cre-mediated recombination confirms role of LRP in clearance of chylomicron remnants. *J. Clin. Invest.* 101:689-695 (1998).

15. Sparks JD, Sparks CE, Adeli K. Selective hepatic insulin resistance, VLDL overproduction, and hypertriglyceridemia. *Arterioscler. Thromb. Vasc. Biol.* 32:2104-2112 (2012).

16. Haas ME, Attie AD, Biddinger SB. The regulation of ApoB metabolism by insulin. *Trends Endocrinol. Metab.* 24:391-397 (2013).

17. Yen CL, Stone SJ, Koliwad S, Harris C, Farese RV, Jr. Thematic review series: glycerolipids. DGAT enzymes and triacylglycerol biosynthesis. *J. Lipid Res.* 49:2283-2301 (2008).

18. Nilsson SK, Heeren J, Olivecrona G, Merkel M. Apolipoprotein A-V; a potent triglyceride reducer. *Atherosclerosis* 219:15-21 (2011).

19. Murray RK, Bender D, Rodwell VW, Botham KM, Kennelly PJ, Weil PA. *Harper's Illustrated Biochemistry*, 28th edn (McGraw-Hill Medical, 2009).

20. Chang TY, Chang CC, Ohgami N, Yamauchi Y. Cholesterol sensing, trafficking, and esterification. *Annu. Rev. Cell Dev. Biol.* 22:129-157 (2006).

21. Azhar S, Leers-Sucheta S, Reaven E. Cholesterol uptake in adrenal and gonadal tissues: the SR-BI and 'selective' pathway connection. *Front. Biosci.* 8:s998-1029 (2003).

22. Brown MS, Goldstein JL. Receptor-mediated endocytosis: insights from the lipoprotein receptor system. *Proc. Natl. Acad. Sci. USA* 76:3330-3337 (1979).

23. Brown MS, Goldstein JL. A receptor-mediated pathway for cholesterol homeostasis. *Science* 232:34-47 (1986).

24. Goldstein JL, Brown MS. The LDL receptor. *Arterioscler. Thromb. Vasc. Biol.* 29:431-438 (2009).

25. Brown MS, Goldstein JL. Richard G.W. Anderson (1940-2011) and the birth of receptor-mediated endocytosis. *J. Cell Biol.* 193:601-603 (2011).

26. Scita G, Di Fiore PP. The endocytic matrix. *Nature* 463:464-473 (2010).

27. Kwon HJ, Abi-Mosleh L, Wang ML, Deisenhofer J, Goldstein JL, Brown MS, Infante RE. Structure of N-terminal domain of NPC1 reveals distinct subdomains for binding and transfer of cholesterol. *Cell* 137:1213-1224 (2009).

28. Horton JD, Goldstein JL, Brown MS. SREBPs: activators of the complete program of cholesterol and fatty acid synthesis in the liver. *J. Clin. Invest.* 109:1125-1131 (2002).

29. Brown MS, Goldstein JL. Cholesterol feedback: from Schoenheimer's bottle to Scap's MELADL. *J. Lipid Res.* 50 Suppl:S15-27 (2009).

30. Bartel DP. MicroRNAs: genomics, biogenesis, mechanism, and function. *Cell* 116:281-297 (2004).

31. Small EM, Olson EN. Pervasive roles of microRNAs in cardiovascular biology. *Nature* 469:336-342 (2011).

32. Brown MS, Ye J, Goldstein JL. Medicine. HDL miR-ed down by SREBP introns. *Science* 328:1495-1496 (2010).

33. Najafi-Shoushtari SH, Kristo F, Li Y, Shioda T, Cohen DE, Gerszten RE, Näär AM. MicroRNA-33 and the SREBP host genes cooperate to control cholesterol homeostasis. *Science* 328:1566-1569 (2010).

34. Rayner KJ, Suárez Y, Dávalos A, Parathath S, Fitzgerald ML, Tamehiro N, Fisher EA, Moore KJ, Fernández-Hernando C. MiR-33 contributes to the regulation of cholesterol homeostasis. *Science* 328:1570-1573 (2010).

35. Marquart TJ, Allen RM, Ory DS, Baldán A. miR-33 links SREBP-2 induction to repression of sterol transporters. *Proc. Natl. Acad. Sci. USA* 107:12228-12232 (2010).

36. Moore KJ, Rayner KJ, Suárez Y, Fernández-Hernando C. microRNAs and cholesterol metabolism. *Trends Endocrinol. Metab.* 21:699-706 (2010).

37. Jeon TI, Esquejo RM, Roqueta-Rivera M, Phelan PE, Moon YA, Govindarajan SS, Esau CC, Osborne TF. An SREBP-responsive microRNA operon contributes to a regulatory loop for intracellular lipid homeostasis. *Cell Metab.* 18:51-61 (2013).

38. Boukhtouche F, Mariani J, Tedgui A. The "CholesteROR" protective pathway in the vascular system. *Arterioscler. Thromb. Vasc. Biol.* 24:637-643 (2004).

39. Camont L, Chapman MJ, Kontush A. Biological activities of HDL subpopulations and their relevance to cardiovascular disease. *Trends Mol. Med.* 17 (2011).

40. Navab M, Reddy ST, Van Lenten BJ, Fogelman AM. HDL and cardiovascular disease: atherogenic and atheroprotective mechanisms. *Nat. Rev. Cardiol.* 8:222-232 (2011).

41. Rosenson RS, Brewer HB, Davidson WS, Fayad ZA, Fuster V, Goldstein J, Hellerstein M, Jiang X-C, Phillips MC, Rader DJ *et al.* Cholesterol efflux and atheroprotection: advancing the concept of reverse cholesterol transport. *Circulation* 125:1905-1919 (2012).

42. Repa JJ, Mangelsdorf DJ. The liver X receptor gene team: potential new players in atherosclerosis. *Nat. Med.* 8:1243-1248 (2002).

43. Smith JD. Insight into ABCG1-mediated cholesterol efflux. *Arterioscler. Thromb. Vasc. Biol.* 26:1198-1200 (2006).

44. Calkin AC, Tontonoz P. Liver X receptor signaling pathways and atherosclerosis. *Arterioscler. Thromb. Vasc. Biol.* 30:1513-1518 (2010).

45. Rayner KJ, Sheedy FJ, Esau CC, Hussain FN, Temel RE, Parathath S, van Gils JM, Rayner AJ, Chang AN, Suarez Y *et al.* Antagonism of miR-33 in mice promotes reverse cholesterol transport and regression of atherosclerosis. *J. Clin. Invest.* 121:2921-2931 (2011).

46. Rayner KJ, Esau CC, Hussain FN, McDaniel AL, Marshall SM, van Gils JM, Ray TD, Sheedy FJ, Goedeke L, Liu X *et al.* Inhibition of miR-33a/b in non-human primates raises plasma HDL and lowers VLDL triglycerides. *Nature* 478:404-407 (2011).

47. Rayner KJ, Moore KJ. MicroRNA control of high-density lipoprotein metabolism and function. *Circ. Res.* 114:183-192 (2014).

48. Rotllan N, Ramirez CM, Aryal B, Esau CC, Fernandez-Hernando C. Therapeutic silencing of microRNA-33 inhibits the progression of atherosclerosis in Ldlr-/- mice--brief report. *Arterioscler. Thromb. Vasc. Biol.* 33:1973-1977 (2013).

49. Porter JA, Young KE, Beachy PA. Cholesterol modification of hedgehog signaling proteins in animal development. *Science* 274:255-259 (1996).

50. Cooper MK, Porter JA, Young KE, Beachy PA. Teratogen-mediated inhibition of target tissue response to Shh signaling. *Science* 280:1603-1607 (1998).

51. Strauss E. Developmental Biology: One-Eyed Animals Implicate Cholesterol in Development. *Science* 280:1528-1529 (1998).

52. Berge KE, Tian H, Graf GA, Yu L, Grishin NV, Schultz J, Kwiterovich P, Shan B, Barnes R, Hobbs HH. Accumulation of dietary cholesterol in sitosterolemia caused by mutations in adjacent ABC transporters. *Science* 290:1771-1775 (2000).

53. Allayee H, Laffitte BA, Lusis AJ. Biochemistry. An absorbing study of cholesterol. *Science* 290:1709-1711 (2000).

54. Wilund KR, Yu L, Xu F, Hobbs HH, Cohen JC. High-level expression of ABCG5 and ABCG8 attenuates diet-induced hypercholesterolemia and atherosclerosis in Ldlr-/- mice. *J. Lipid Res.* 45:1429-1436 (2004).

55. Berriot-Varoqueaux N, Aggerbeck LP, Samson-Bouma M, Wetterau JR. The role of the microsomal triglygeride transfer protein in abetalipoproteinemia. *Annu. Rev. Nutr.* 20:663-697 (2000).

56. Chasman DI, Posada D, Subrahmanyan L, Cook NR, Stanton VP, Ridker PM. Pharmacogenetic study of statin therapy and cholesterol reduction. *JAMA* 291:2821-2827 (2004).

57. Haga SB, Burke W. Using pharmacogenetics to improve drug safety and efficacy. *JAMA* 291:2869-2871 (2004).

58. Garcia CK, Wilund KR, Arca M, Zuliani G, Fellin R, Maioli M, Calandra S, Bertolini S, Cossu F, Grishin N *et al.* Autosomal recessive hypercholesterolemia caused by mutations in a putative LDL receptor adaptor protein. *Science* 292:1394-1398 (2001).

59. Goldstein JL, Brown MS. Molecular medicine. The cholesterol quartet. *Science* 292:1310-1312 (2001).

60. Arca M, Zuliani G, Wilund KR, Campagna F, Fellin R, Bertolini S, Calandra S, Ricci G, Glorioso N, Maioli M *et al.* Autosomal recessive hypercholesterolaemia in Sardinia, Italy, and mutations in ARH: a clinical and molecular genetic analysis. *Lancet* 359:841-847 (2002).

61. Tavori H, Fan D, Blakemore JL, Yancey PG, Ding L, Linton MF, Fazio S. Serum proprotein convertase subtilisin/kexin type 9 and cell surface low-density lipoprotein receptor: evidence for a reciprocal regulation. *Circulation* 127:2403-2413 (2013).

62. Stein EA, Raal FJ. Insights into PCSK9, low-density lipoprotein receptor, and low-density lipoprotein cholesterol metabolism: of mice and man. *Circulation* 127:2372-2374 (2013).

63. Schulze H, Sandhoff K. Lysosomal lipid storage diseases. *Cold Spring Harb. Perspect. Biol.* 3 (2011).

64. Young SG, Fielding CJ. The ABCs of cholesterol efflux. *Nat. Genet.* 22:316-318 (1999).

65. Benlian P, De Gennes JL, Foubert L, Zhang H, Gagne SE, Hayden M. Premature atherosclerosis in patients with familial chylomicronemia caused by mutations in the lipoprotein lipase gene. *N. Engl. J. Med.* 335:848-854 (1996).

66. Endo A. The discovery and development of HMG-CoA reductase inhibitors. *J. Lipid Res.* 33:1569-1582 (1992).

67. Charo IF, Taub R. Anti-inflammatory therapeutics for the treatment of atherosclerosis. *Nat. Rev. Drug Discov.* 10:365-376 (2011).

68. Widlansky ME, Gokce N, Keaney JF, Vita JA. The clinical implications of endothelial dysfunction. *J. Am. Coll. Cardiol.* 42:1149-1160 (2003).

69. Brown G, Albers JJ, Fisher LD, Schaefer SM, Lin JT, Kaplan C, Zhao XQ, Bisson BD, Fitzpatrick VF, Dodge HT. Regression of coronary artery disease as a result of intensive lipid-lowering therapy in men with high levels of apolipoprotein B. *N. Engl. J. Med.* 323:1289-1298 (1990).

70. Kane JP, Malloy MJ, Ports TA, Phillips NR, Diehl JC, Havel RJ. Regression of coronary atherosclerosis during treatment of familial hypercholesterolemia with combined drug regimens. *JAMA* 264:3007-3012 (1990).

71. Superko HR, Krauss RM. Coronary artery disease regression. Convincing evidence for the benefit of aggressive lipoprotein management. *Circulation* 90:1056-1069 (1994).

72. Nissen SE, Nicholls SJ, Sipahi I, Libby P, Raichlen JS, Ballantyne CM, Davignon J, Erbel R, Fruchart JC, Tardif J-C *et al.* Effect of very high-intensity statin therapy on regression of coronary atherosclerosis: the ASTEROID trial. *JAMA* 295:1556-1565 (2006).

73. Blumenthal RS, Kapur NK. Can a potent statin actually regress coronary atherosclerosis? *JAMA* 295:1583-1584 (2006).

74. Holmes D. Hopes soar as cholesterol plummets with new drug class. *Nat. Med.* 18:633-633 (2012).

75. Stein EA, Mellis S, Yancopoulos GD, Stahl N, Logan D, Smith WB, Lisbon E, Gutierrez M, Webb C, Wu R *et al.* Effect of a monoclonal antibody to PCSK9 on LDL cholesterol. *N. Engl. J. Med.* 366:1108-1118 (2012).

76. Maxwell KN, Breslow JL. Antibodies to PCSK9: a superior way to lower LDL cholesterol? *Circ. Res.* 111:274-277 (2012).

77. Desai NR, Giugliano RP, Zhou J, Kohli P, Somaratne R, Hoffman E, Liu T, Scott R, Wasserman SM, Sabatine MS. AMG 145, a monoclonal antibody against PCSK9, facilitates achievement of national cholesterol education program-adult treatment panel III low-density lipoprotein cholesterol goals among high-risk patients: an analysis from the LAPLACE-TIMI 57 trial (LDL-C assessment with PCSK9 monoclonal antibody inhibition combined with statin thErapy-thrombolysis in myocardial infarction 57). *J. Am. Coll. Cardiol.* 63:430-433 (2014).

78. Stein EA, Honarpour N, Wasserman SM, Xu F, Scott R, Raal FJ. Effect of the proprotein convertase subtilisin/kexin 9 monoclonal antibody, AMG 145, in homozygous familial hypercholesterolemia. *Circulation* 128:2113-2120 (2013).

79. Rader DJ, Daugherty A. Translating molecular discoveries into new therapies for atherosclerosis. *Nature* 451:904-913 (2008).

80. Weber C, Noels H. Atherosclerosis: current pathogenesis and therapeutic options. *Nat. Med.* 17:1410-1422 (2011).

81. Yue S, Li J, Lee SY, Lee HJ, Shao T, Song B, Cheng L, Masterson TA, Liu X, Ratliff TL *et al.* Cholesteryl ester accumulation induced by PTEN loss and PI3K/AKT activation underlies human prostate cancer aggressiveness. *Cell Metab.* 19:393-406 (2014).

82. Thurnher M, Nussbaumer O, Gruenbacher G. Novel aspects of mevalonate pathway inhibitors as antitumor agents. *Clin. Cancer Res.* 18:3524-3531 (2012).

83. Bu G. Apolipoprotein E and its receptors in Alzheimer's disease: pathways, pathogenesis and therapy. *Nat. Rev. Neurosci.* 10:333-344 (2009).

84. Di Paolo G, Kim T-W. Linking lipids to Alzheimer's disease: cholesterol and beyond. *Nat. Rev. Neurosci.* 12:284-296 (2011).

85. Porcellini E, Calabrese E, Guerini F, Govoni M, Chiappelli M, Tumini E, Morgan K, Chappell S, Kalsheker N, Franceschi M *et al.* The hydroxy-methyl-glutaryl CoA reductase promoter polymorphism is associated with Alzheimer's risk and cognitive deterioration. *Neurosci. Lett.* 416:66-70 (2007).

86. Keller L, Murphy C, Wang H-X, Fratiglioni L, Olin M, Gafvels M, Björkhem I, Graff C, Meaney S. A functional polymorphism in the HMGCR promoter affects transcriptional activity but not the risk for Alzheimer disease in Swedish populations. *Brain Res.* 1344:185-191 (2010).

87. Napoli C, Crudele V, Soricelli A, Al-Omran M, Vitale N, Infante T, Mancini FP. Primary prevention of atherosclerosis: a clinical challenge for the reversal of epigenetic mechanisms? *Circulation* 125:2363-2373 (2012).

88. Tabas I, Williams KJ, Borén J. Subendothelial lipoprotein retention as the initiating process in atherosclerosis: update and therapeutic implications. *Circulation* 116:1832-1844 (2007).

89. Allam AH, Thompson RC, Wann LS, Miyamoto MI, Thomas GS. Computed tomographic assessment of atherosclerosis in ancient Egyptian mummies. *JAMA* 302:2091-2094 (2009).

90. David AR, Kershaw A, Heagerty A. Atherosclerosis and diet in ancient Egypt. *Lancet* 375:718-719 (2010).

91. Allam AH, Thompson RC, Wann LS, Miyamoto MI, Nur El-Din AE-H, El-Maksoud GA, Al-Tohamy Soliman M, Badr I, El-Rahman Amer HA, Sutherland ML *et al.* Atherosclerosis in ancient Egyptian mummies: the Horus study. *JACC Cardiovasc. Imaging* 4:315-327 (2011).

92. Chandrashekhar Y, Narula J. Medical imaging: the new Rosetta stone. *JACC Cardiovasc. Imaging* 4:440-443 (2011).

93. Finch CE. Atherosclerosis is an old disease: Summary of the Ruffer Centenary Symposium, The Paleocardiology of Ancient Egypt, a meeting report of the Horus Study team. *Exp. Gerontol.* 46:843-846 (2011).

94. Heagerty AM. Scanning ancient history for evidence of modern diseases. *Lancet* 381:1165-1166 (2013).

95. Thompson RC, Allam AH, Lombardi GP, Wann LS, Sutherland ML, Sutherland JD, Soliman MA-T, Frohlich B, Mininberg DT, Monge JM *et al.* Atherosclerosis across 4000 years of human history: the Horus study of four ancient populations. *Lancet* 381:1211-1222 (2013).

96. Ross R, Glomset J. Atherosclerosis and the arterial smooth muscle cell: Proliferation of smooth muscle is a key event in the genesis of the lesions of atherosclerosis. *Science* 180:1332-1339 (1973).

97. Libby P. Atherosclerosis: the new view. *Sci. Am.* 286:46-55 (2002).

98. Bonetti PO. Endothelial Dysfunction: A Marker of Atherosclerotic Risk. *Arterioscler. Thromb. Vasc. Biol.* 23:168-175 (2002).

99. Ross R, Harker L. Hyperlipidemia and atherosclerosis. *Science* 193:1094-1100 (1976).

100. Ross R. Atherosclerosis--an inflammatory disease. *N. Engl. J. Med.* 340:115-126 (1999).

101. Muller-Delp JM, Gurovich AN, Christou DD, Leeuwenburgh C. Redox Balance in the Aging Microcirculation: New Friends, New Foes, and New Clinical Directions. *Microcirculation* (2011).

102. Ungvari Z, Buffenstein R, Austad SN, Podlutsky A, Kaley G, Csiszar A. Oxidative stress in vascular senescence: lessons from successfully aging species. *Front. Biosci.* 13:5056-5070 (2008).

103. Sykiotis GP, Bohmann D. Stress-activated cap'n'collar transcription factors in aging and human disease. *Sci. Signal.* 3:re3 (2010).

104. Suh JH, Shenvi SV, Dixon BM, Liu H, Jaiswal AK, Liu R-M, Hagen TM. Decline in transcriptional activity of Nrf2 causes age-related loss of glutathione synthesis, which is reversible with lipoic acid. *Proc. Natl. Acad. Sci. USA* 101:3381-3386 (2004).

105. Janssen-Heininger YM, Poynter ME, Baeuerle PA. Recent advances towards understanding redox mechanisms in the activation of nuclear factor kappaB. *Free Radic. Biol. Med.* 28:1317-1327 (2000).

106. Zakkar M, Van der Heiden K, Luong LA, Chaudhury H, Cuhlmann S, Hamdulay SS, Krams R, Edirisinghe I, Rahman I, Carlsen H *et al.* Activation of Nrf2 in endothelial cells protects arteries from exhibiting a proinflammatory state. *Arterioscler. Thromb. Vasc. Biol.* 29:1851-1857 (2009).

107. Pierce GL, Lesniewski LA, Lawson BR, Beske SD, Seals DR. Nuclear factor-{kappa}B activation contributes to vascular endothelial dysfunction via oxidative stress in overweight/obese middle-aged and older humans. *Circulation* 119:1284-1292 (2009).

108. Randolph GJ, Potteaux S. Vascular dendritic cells as gatekeepers of lipid accumulation within nascent atherosclerotic plaques. *Circ. Res.* 106:227-229 (2010).

109. Medzhitov R. Inflammation 2010: new adventures of an old flame. *Cell* 140:771-776 (2010).

110. Libby P. Inflammation in atherosclerosis. *Nature* 420:868-874 (2002).

111. Hansson GK. Inflammation, atherosclerosis, and coronary artery disease. *N. Engl. J. Med.* 352:1685-1695 (2005).

112. Hansson GK, Libby P. The immune response in atherosclerosis: a double-edged sword. *Nat. Rev. Immunol.* 6:508-519 (2006).

113. Hansson GK, Hermansson A. The immune system in atherosclerosis. *Nat. Immunol.* 12:204-212 (2011).

114. Swirski FK, Nahrendorf M. Leukocyte behavior in atherosclerosis, myocardial infarction, and heart failure. *Science* 339:161-166 (2013).

115. Libby P, Nahrendorf M, Pittet MJ, Swirski FK. Diversity of denizens of the atherosclerotic plaque: not all monocytes are created equal. *Circulation* 117:3168-3170 (2008).

116. Robbins CS, Hilgendorf I, Weber GF, Theurl I, Iwamoto Y, Figueiredo JL, Gorbatov R, Sukhova GK, Gerhardt LM, Smyth D *et al.* Local proliferation dominates lesional macrophage accumulation in atherosclerosis. *Nat. Med.* 19:1166-1172 (2013).

117. Eriksson EE. Intravital microscopy on atherosclerosis in apolipoprotein E-deficient mice establishes microvessels as major entry pathways for leukocytes to advanced lesions. *Circulation* 124:2129-2138 (2011).

118. Libby P, Ridker PM, Hansson GK. Progress and challenges in translating the biology of atherosclerosis. *Nature* 473:317-325 (2011).

119. Caligiuri G, Nicoletti A, Poirier B, Hansson GK. Protective immunity against atherosclerosis carried by B cells of hypercholesterolemic mice. *J. Clin. Invest.* 109:745-753 (2002).

120. Hilgendorf I, Theurl I, Gerhardt LMS, Robbins CS, Weber GF, Gonen A, Iwamoto Y, Degousee N, Holderried TAW, Winter C *et al.* Innate response activator B cells aggravate atherosclerosis by stimulating T helper-1 adaptive immunity. *Circulation* 129:1677-1687 (2014).

121. Sun J, Sukhova GK, Wolters PJ, Yang M, Kitamoto S, Libby P, MacFarlane LA, Mallen-St Clair J, Shi G-P. Mast cells promote atherosclerosis by releasing proinflammatory cytokines. *Nat. Med.* 13:719-724 (2007).

122. Libby P, Shi G-P. Mast cells as mediators and modulators of atherogenesis. *Circulation* 115:2471-2473 (2007).

123. Tedgui A, Ait-Oufella H. Innate lymphoid cells: new players in atherosclerosis? *Arterioscler. Thromb. Vasc. Biol.* 33:2697-2698 (2013).

124. De Martin R, Hoeth M, Hofer-Warbinek R, Schmid JA. The transcription factor NF-kappa B and the regulation of vascular cell function. *Arterioscler. Thromb. Vasc. Biol.* 20:E83-88 (2000).

125. Hasegawa Y, Saito T, Ogihara T, Ishigaki Y, Yamada T, Imai J, Uno K, Gao J, Kaneko K, Shimosawa T *et al.* Blockade of the Nuclear Factor-kappaB Pathway in the Endothelium Prevents Insulin Resistance and Prolongs Life Spans. *Circulation* 125:1122-1133 (2012).

126. Duewell P, Kono H, Rayner KJ, Sirois CM, Vladimer G, Bauernfeind FG, Abela GS, Franchi L, Nuñez G, Schnurr M *et al.* NLRP3 inflammasomes are required for atherogenesis and activated by cholesterol crystals. *Nature* 464:1357-1361 (2010).

127. Masters SL, Latz E, O'Neill LAJ. The inflammasome in atherosclerosis and type 2 diabetes. *Sci. Transl. Med.* 3:81ps17 (2011).

128. Menu P, Pellegrin M, Aubert JF, Bouzourene K, Tardivel A, Mazzolai L, Tschopp J. Atherosclerosis in ApoE-deficient mice progresses independently of the NLRP3 inflammasome. *Cell Death Dis.* 2:e137 (2011).

129. Hansson GK, Klareskog L. Pulling down the plug on atherosclerosis: Cooling down the inflammasome. *Nat. Med.* 17:790-791 (2011).

130. Madamanchi NR, Vendrov A, Runge MS. Oxidative stress and vascular disease. *Arterioscler. Thromb. Vasc. Biol.* 25:29-38 (2005).

131. Leopold JA, Loscalzo J. Oxidative risk for atherothrombotic cardiovascular disease. *Free Radic. Biol. Med.* 47:1673-1706 (2009).

132. Steinberg D, Witztum JL. Oxidized low-density lipoprotein and atherosclerosis. *Arterioscler. Thromb. Vasc. Biol.* 30:2311-2316 (2010).

133. Moore KJ, Freeman MW. Scavenger receptors in atherosclerosis: beyond lipid uptake. *Arterioscler. Thromb. Vasc. Biol.* 26:1702-1711 (2006).

134. Barish GD, Evans RM. PPARs and LXRs: atherosclerosis goes nuclear. *Trends Endocrinol. Metab.* 15:158-165 (2004).

135. Lefebvre P, Chinetti G, Staels B. Nur77turing macrophages in atherosclerosis. *Circ. Res.* 110:375-377 (2012).

136. McCarthy C, Lieggi NT, Barry D, Mooney D, de Gaetano M, James WG, McClelland S, Barry MC, Escoubet-Lozach L, Li AC *et al.* Macrophage PPAR gamma Co-activator-1 alpha participates in repressing foam cell formation and atherosclerosis in response to conjugated linoleic acid. *EMBO Mol. Med.* 5:1443-1457 (2013).

137. Barish GD, Yu RT, Karunasiri MS, Becerra D, Kim J, Tseng TW, Tai L-J, Leblanc M, Diehl C, Cerchietti L *et al.* The Bcl6-SMRT/NCoR Cistrome Represses Inflammation to Attenuate Atherosclerosis. *Cell Metab.* 15:554-562 (2012).

138. Goncalves I, Stenstrom K, Skog G, Mattsson S, Nitulescu M, Nilsson J. Short communication: Dating components of human atherosclerotic plaques. *Circ. Res.* 106:1174-1177 (2010).

139. Rong JX, Shapiro M, Trogan E, Fisher EA. Transdifferentiation of mouse aortic smooth muscle cells to a macrophage-like state after cholesterol loading. *Proc. Natl. Acad. Sci. USA* 100:13531-13536 (2003).

140. Allahverdian S, Chehroudi AC, McManus BM, Abraham T, Francis GA. Contribution of intimal smooth muscle cells to cholesterol accumulation and macrophage-like cells in human atherosclerosis. *Circulation* 129:1551-1559 (2014).

141. Gomez D, Owens GK. Smooth muscle cell phenotypic switching in atherosclerosis. *Cardiovasc. Res.* 95:156-164 (2012).

142. Tabas I. Macrophage death and defective inflammation resolution in atherosclerosis. *Nat. Rev. Immunol.* 10:36-46 (2010).

143. Hotamisligil GS. Endoplasmic reticulum stress and atherosclerosis. *Nat. Med.* 16:396-399 (2010).

144. Ron D, Walter P. Signal integration in the endoplasmic reticulum unfolded protein response. *Nat. Rev. Mol. Cell Biol.* 8:519-529 (2007).

145. Feng B, Yao PM, Li Y, Devlin CM, Zhang D, Harding HP, Sweeney M, Rong JX, Kuriakose G, Fisher EA *et al.* The endoplasmic reticulum is the site of cholesterol-induced cytotoxicity in macrophages. *Nat. Cell Biol.* 5:781-792 (2003).

146. Johnson RC, Leopold JA, Loscalzo J. Vascular calcification: pathobiological mechanisms and clinical implications. *Circ. Res.* 99:1044-1059 (2006).

147. Alexopoulos N, Raggi P. Biomarkers: Coronary artery calcium is a better risk marker than hsCRP. *Nat. Rev. Cardiol.* 8:616-618 (2011).

148. Borissoff JI, Spronk HMH, ten Cate H. The hemostatic system as a modulator of atherosclerosis. *N. Engl. J. Med.* 364:1746-1760 (2011).

149. Naghavi M, Libby P, Falk E, Casscells SW, Litovsky S, Rumberger J, Badimon JJ, Stefanadis C, Moreno P, Pasterkamp G *et al.* From vulnerable plaque to vulnerable patient: a call for new definitions and risk assessment strategies: Part I. *Circulation* 108:1664-1672 (2003).

150. Naghavi M, Libby P, Falk E, Casscells SW, Litovsky S, Rumberger J, Badimon JJ, Stefanadis C, Moreno P, Pasterkamp G *et al.* From vulnerable plaque to vulnerable patient: a call for new definitions and risk assessment strategies: Part II. *Circulation* 108:1772-1778 (2003).

151. Swirski FK, Nahrendorf M, Etzrodt M, Wildgruber M, Cortez-Retamozo V, Panizzi P, Figueiredo J-L, Kohler RH, Chudnovskiy A, Waterman P *et al.* Identification of splenic reservoir monocytes and their deployment to inflammatory sites. *Science* 325:612-616 (2009).

152. Dutta P, Courties G, Wei Y, Leuschner F, Gorbatov R, Robbins CS, Iwamoto Y, Thompson B, Carlson AL, Heidt T *et al.* Myocardial infarction accelerates atherosclerosis. *Nature* 487:325-329 (2012).

153. Prospective Studies Collaboration, Lewington S, Whitlock G, Clarke R, Sherliker P, Emberson J, Halsey J, Qizilbash N, Peto R, Collins R. Blood cholesterol and vascular mortality by age, sex, and blood pressure: a meta-analysis of individual data from 61 prospective studies with 55,000 vascular deaths. *Lancet* 370:1829-1839 (2007).

154. Goldberg IJ, Eckel RH, McPherson R. Triglycerides and heart disease: still a hypothesis? *Arterioscler. Thromb. Vasc. Biol.* 31:1716-1725 (2011).

155. Nordestgaard BG, Zilversmit DB. Large lipoproteins are excluded from the arterial wall in diabetic cholesterol-fed rabbits. *J. Lipid Res.* 29:1491-1500 (1988).

156. Véniant MM, Sullivan MA, Kim SK, Ambroziak P, Chu A, Wilson MD, Hellerstein MK, Rudel LL, Walzem RL, Young SG. Defining the atherogenicity of large and small lipoproteins containing apolipoprotein B100. *J. Clin. Invest.* 106:1501-1510 (2000).

157. Véniant MM, Withycombe S, Young SG. Lipoprotein size and atherosclerosis susceptibility in Apoe(-/-) and Ldlr(-/-) mice. *Arterioscler. Thromb. Vasc. Biol.* 21:1567-1570 (2001).

158. Neff LM, Culiner J, Cunningham-Rundles S, Seidman C, Meehan D, Maturi J, Wittkowski KM, Levine B, Breslow JL. Algal docosahexaenoic acid affects plasma lipoprotein particle size distribution in overweight and obese adults. *J. Nutr.* 141:207-213 (2011).

159. Sun C, Alkhoury K, Wang YI, Foster GA, Radecke CE, Tam K, Edwards CM, Facciotti MT, Armstrong EJ, Knowlton AA *et al.* IRF-1 and miRNA126 modulate VCAM-1 expression in response to a high-fat meal. *Circ. Res.* 111:1054-1064 (2012).

160. Barzilai N, Atzmon G, Schechter C, Schaefer EJ, Cupples AL, Lipton R, Cheng S, Shuldiner AR. Unique lipoprotein phenotype and genotype associated with exceptional longevity. *JAMA* 290:2030-2040 (2003).

161. Khera AV, Cuchel M, de la Llera-Moya M, Rodrigues A, Burke MF, Jafri K, French BC, Phillips JA, Mucksavage ML, Wilensky RL *et al.* Cholesterol efflux capacity, high-density lipoprotein function, and atherosclerosis. *N. Engl. J. Med.* 364:127-135 (2011).

162. Heinecke J. HDL and cardiovascular-disease risk--time for a new approach? *N. Engl. J. Med.* 364:170-171 (2011).

163. Lewington S, Clarke R, Qizilbash N, Peto R, Collins R, Prospective Studies C. Age-specific relevance of usual blood pressure to vascular mortality: a meta-analysis of individual data for one million adults in 61 prospective studies. *Lancet* 360:1903-1913 (2002).

164. Chobanian AV, Bakris GL, Black HR, Cushman WC, Green LA, Izzo JL, Jr., Jones DW, Materson BJ, Oparil S, Wright JT, Jr. *et al.* Seventh report of the Joint National Committee on Prevention, Detection, Evaluation, and Treatment of High Blood Pressure. *Hypertension* 42:1206-1252 (2003).

165. Sox HC. Assessing the trustworthiness of the guideline for management of high blood pressure in adults. *JAMA* 311:472-474 (2014).

166. Peterson ED, Gaziano JM, Greenland P. Recommendations for treating hypertension: what are the right goals and purposes? *JAMA* 311:474-476 (2014).

167. Bauchner H, Fontanarosa PB, Golub RM. Updated guidelines for management of high blood pressure: recommendations, review, and responsibility. *JAMA* 311:477-478 (2014).

168. James PA, Oparil S, Carter BL, Cushman WC, Dennison-Himmelfarb C, Handler J, Lackland DT, LeFevre ML, MacKenzie TD, Ogedegbe O *et al.* 2014 evidence-based guideline for the management of high blood pressure in adults: report from the panel members appointed to the Eighth Joint National Committee (JNC 8). *JAMA* 311:507-520 (2014).

169. Coffman TM. Under pressure: the search for the essential mechanisms of hypertension. *Nat. Med.* 17:1402-1409 (2011).

170. McCurley A, Pires PW, Bender SB, Aronovitz M, Zhao MJ, Metzger D, Chambon P, Hill MA, Dorrance AM, Mendelsohn ME *et al.* Direct regulation of blood pressure by smooth muscle cell mineralocorticoid receptors. *Nat. Med.* 18:1429-1433 (2012).

171. Haffner SM, Lehto S, Ronnemaa T, Pyorala K, Laakso M. Mortality from coronary heart disease in subjects with type 2 diabetes and in nondiabetic subjects with and without prior myocardial infarction. *N. Engl. J. Med.* 339:229-234 (1998).

172. Rask-Madsen C, King GL. Proatherosclerotic mechanisms involving protein kinase C in diabetes and insulin resistance. *Arterioscler. Thromb. Vasc. Biol.* 25:487-496 (2005).

173. Giacco F, Brownlee M. Oxidative stress and diabetic complications. *Circ. Res.* 107:1058-1070 (2010).

174. Suzuki T, Tomiyama H, Higashi Y. Vascular dysfunction even after 20 years in children exposed to passive smoking: alarming results and need for awareness. *Arterioscler. Thromb. Vasc. Biol.* 32:841-842 (2012).

175. Ambrose JA, Barua RS. The pathophysiology of cigarette smoking and cardiovascular disease: an update. *J. Am. Coll. Cardiol.* 43:1731-1737 (2004).

176. Critchley JA, Capewell S. Mortality risk reduction associated with smoking cessation in patients with coronary heart disease: a systematic review. *JAMA* 290:86-97 (2003).

177. Canto JG, Iskandrian AE. Major risk factors for cardiovascular disease: debunking the "only 50%" myth. *JAMA* 290:947-949 (2003).

178. Greenland P, Knoll MD, Stamler J, Neaton JD, Dyer AR, Garside DB, Wilson PW. Major risk factors as antecedents of fatal and nonfatal coronary heart disease events. *JAMA* 290:891-897 (2003).

179. Hackam DG, Anand SS. Emerging risk factors for atherosclerotic vascular disease: a critical review of the evidence. *JAMA* 290:932-940 (2003).

180. Khot UN, Khot MB, Bajzer CT, Sapp SK, Ohman EM, Brener SJ, Ellis SG, Lincoff AM, Topol EJ. Prevalence of conventional risk factors in patients with coronary heart disease. *JAMA* 290:898-904 (2003).

181. Berry JD, Dyer A, Cai X, Garside DB, Ning H, Thomas A, Greenland P, Van Horn L, Tracy RP, Lloyd-Jones DM. Lifetime risks of cardiovascular disease. *N. Engl. J. Med.* 366:321-329 (2012).

182. Goldstein JL, Brown MS. The low-density lipoprotein pathway and its relation to atherosclerosis. *Annu. Rev. Biochem.* 46:897-930 (1977).

183. Lloyd-Jones DM. Cardiovascular risk prediction: basic concepts, current status, and future directions. *Circulation* 121:1768-1777 (2010).

184. Greenland P, Alpert JS, Beller GA, Benjamin EJ, Budoff MJ, Fayad ZA, Foster E, Hlatky MA, Hodgson JM, Kushner FG *et al.* 2010 ACCF/AHA guideline for assessment of cardiovascular risk in asymptomatic adults: a report of the American College of Cardiology Foundation/American Heart Association Task Force on Practice Guidelines. *Circulation* 122:e584-e636 (2010).

185. Tzoulaki I, Liberopoulos G, Ioannidis JP. Assessment of claims of improved prediction beyond the Framingham risk score. *JAMA* 302:2345-2352 (2009).

186. Goff DC, Jr., Lloyd-Jones DM, Bennett G, Coady S, D'Agostino RB, Gibbons R, Greenland P, Lackland DT, Levy D, O'Donnell CJ *et al.* 2013 ACC/AHA guideline on the assessment of cardiovascular risk: a report of the American College of Cardiology/American Heart Association Task Force on Practice Guidelines. *Circulation* 129:S49-73 (2014).

187. Stone NJ, Robinson JG, Lichtenstein AH, Bairey Merz CN, Blum CB, Eckel RH, Goldberg AC, Gordon D, Levy D, Lloyd-Jones DM *et al.* 2013 ACC/AHA guideline on the treatment of blood cholesterol to reduce atherosclerotic cardiovascular risk in adults: a report of the American College of Cardiology/American Heart Association Task Force on Practice Guidelines. *Circulation* 129:S1-45 (2014).

188. Eckel RH, Jakicic JM, Ard JD, de Jesus JM, Houston Miller N, Hubbard VS, Lee IM, Lichtenstein AH, Loria CM, Millen BE *et al.* 2013 AHA/ACC guideline on lifestyle management to reduce cardiovascular risk: a report of the American College of Cardiology/American Heart Association Task Force on Practice Guidelines. *Circulation* 129:S76-S99 (2013).

189. Jensen MD, Ryan DH, Apovian CM, Ard JD, Comuzzie AG, Donato KA, Hu FB, Hubbard VS, Jakicic JM, Kushner RF *et al.* 2013 AHA/ACC/TOS guideline for the management of overweight and obesity in adults: a report of the American College of Cardiology/American Heart Association Task Force on Practice Guidelines and The Obesity Society. *Circulation* 129:S102-S138 (2013).

190. Halcox JPJ, Schenke WH, Zalos G, Mincemoyer R, Prasad A, Waclawiw MA, Nour KRA, Quyyumi AA. Prognostic value of coronary vascular endothelial dysfunction. *Circulation* 106:653-658 (2002).

191. Fernhall B, Agiovlasitis S. Arterial function in youth: window into cardiovascular risk. *J. Appl. Physiol.* 105:325-333 (2008).

192. Flammer AJ, Anderson T, Celermajer DS, Creager MA, Deanfield J, Ganz P, Hamburg NM, Lüscher TF, Shechter M, Taddei S *et al.* The assessment of endothelial function: from research into clinical practice. *Circulation* 126:753-767 (2012).

193. Deanfield JE, Halcox JP, Rabelink TJ. Endothelial function and dysfunction: testing and clinical relevance. *Circulation* 115:1285-1295 (2007).

194. Donald AE, Halcox JP, Charakida M, Storry C, Wallace SML, Cole TJ, Friberg P, Deanfield JE. Methodological approaches to optimize reproducibility and power in clinical studies of flow-mediated dilation. *J. Am. Coll. Cardiol.* 51:1959-1964 (2008).

195. Tillett WS, Francis T. Serological Reactions in Pneumonia with a Non-Protein Somatic Fraction of Pneumococcus. *J. Exp. Med.* 52:561-571 (1930).

196. Black S, Kushner I, Samols D. C-reactive Protein. *J. Biol. Chem.* 279:48487-48490 (2004).

197. Hurlimann J, Thorbecke GJ, Hochwald GM. The liver as the site of C-reactive protein formation. *J. Exp. Med.* 123:365-378 (1966).

198. Gabay C, Kushner I. Acute-phase proteins and other systemic responses to inflammation. *N. Engl. J. Med.* 340:448-454 (1999).

199. Armani A, Becker RC. The biology, utilization, and attenuation of C-reactive protein in cardiovascular disease: part I. *Am. Heart J.* 149:971-976 (2005).

200. Ridker PM. C-reactive protein and the prediction of cardiovascular events among those at intermediate risk: moving an inflammatory hypothesis toward consensus. *J. Am. Coll. Cardiol.* 49:2129-2138 (2007).

201. Buckley DI, Fu R, Freeman M, Rogers K, Helfand M. C-reactive protein as a risk factor for coronary heart disease: a systematic review and meta-analyses for the U.S. Preventive Services Task Force. *Ann. Intern. Med.* 151:483-495 (2009).

202. Emerging Risk Factors Collaboration, Kaptoge S, Di Angelantonio E, Lowe G, Pepys MB, Thompson SG, Collins R, Danesh J. C-reactive protein concentration and risk of coronary heart disease, stroke, and mortality: an individual participant meta-analysis. *Lancet* 375:132-140 (2010).

203. de Lorgeril M, Salen P, Abramson J, Dodin S, Hamazaki T, Kostucki W, Okuyama H, Pavy B, Rabaeus M. Cholesterol lowering, cardiovascular diseases, and the rosuvastatin-JUPITER controversy: a critical reappraisal. *Arch. Intern. Med.* 170:1032-1036 (2010).

204. Pasceri V, Willerson JT, Yeh ET. Direct proinflammatory effect of C-reactive protein on human endothelial cells. *Circulation* 102:2165-2168 (2000).

205. Verma S, Kuliszewski MA, Li SH, Szmitko PE, Zucco L, Wang CH, Badiwala MV, Mickle DA, Weisel RD, Fedak PW *et al.* C-reactive protein attenuates endothelial progenitor cell survival, differentiation, and function: further evidence of a mechanistic link between C-reactive protein and cardiovascular disease. *Circulation* 109:2058-2067 (2004).

206. Taylor KE, Giddings JC, van den Berg CW. C-reactive protein-induced in vitro endothelial cell activation is an artefact caused by azide and lipopolysaccharide. *Arterioscler. Thromb. Vasc. Biol.* 25:1225-1230 (2005).

207. Paul A, Ko KW, Li L, Yechoor V, McCrory MA, Szalai AJ, Chan L. C-reactive protein accelerates the progression of atherosclerosis in apolipoprotein E-deficient mice. *Circulation* 109:647-655 (2004).

208. Hirschfield GM, Gallimore JR, Kahan MC, Hutchinson WL, Sabin CA, Benson GM, Dhillon AP, Tennent GA, Pepys MB. Transgenic human C-reactive protein is not proatherogenic in apolipoprotein E-deficient mice. *Proc. Natl. Acad. Sci. USA* 102:8309-8314 (2005).

209. Trion A, de Maat MP, Jukema JW, van der Laarse A, Maas MC, Offerman EH, Havekes LM, Szalai AJ, Princen HM, Emeis JJ. No effect of C-reactive protein on early atherosclerosis development in apolipoprotein E*3-leiden/human C-reactive protein transgenic mice. *Arterioscler. Thromb. Vasc. Biol.* 25:1635-1640 (2005).

210. Koike T, Kitajima S, Yu Y, Li Y, Nishijima K, Liu E, Sun H, Waqar AB, Shibata N, Inoue T *et al.* Expression of human apoAII in transgenic rabbits leads to dyslipidemia: a new model for combined hyperlipidemia. *Arterioscler. Thromb. Vasc. Biol.* 29:2047-2053 (2009).

211. Kovacs A, Tornvall P, Nilsson R, Tegnér J, Hamsten A, Björkegren J. Human C-reactive protein slows atherosclerosis development in a mouse model with human-like hypercholesterolemia. *Proc. Natl. Acad. Sci. USA* 104:13768-13773 (2007).

212. Khreiss T, Jozsef L, Potempa LA, Filep JG. Conformational rearrangement in C-reactive protein is required for proinflammatory actions on human endothelial cells. *Circulation* 109:2016-2022 (2004).

213. Verma S, Szmitko PE, Yeh ET. C-reactive protein: structure affects function. *Circulation* 109:1914-1917 (2004).

214. Eisenhardt SU, Habersberger J, Murphy A, Chen YC, Woollard KJ, Bassler N, Qian H, von Zur Muhlen C, Hagemeyer CE, Ahrens I *et al.* Dissociation of pentameric to monomeric C-reactive protein on activated platelets localizes inflammation to atherosclerotic plaques. *Circ. Res.* 105:128-137 (2009).

215. Thiele JR, Habersberger J, Braig D, Schmidt Y, Goerendt K, Maurer V, Bannasch H, Scheichl A, Woollard KJ, von Dobschutz E *et al.* Dissociation of pentameric to monomeric C-reactive protein localizes and aggravates inflammation: in vivo proof of a powerful proinflammatory mechanism and a new anti-inflammatory strategy. *Circulation* 130:35-50 (2014).

216. Schwedler SB, Amann K, Wernicke K, Krebs A, Nauck M, Wanner C, Potempa LA, Galle J. Native C-reactive protein increases whereas modified C-reactive protein reduces atherosclerosis in apolipoprotein E-knockout mice. *Circulation* 112:1016-1023 (2005).

217. Emerging Risk Factors Collaboration, Di Angelantonio E, Gao P, Pennells L, Kaptoge S, Caslake M, Thompson A, Butterworth AS, Sarwar N, Wormser D *et al.* Lipid-related markers and cardiovascular disease prediction. *JAMA* 307:2499-2506 (2012).

218. O'Donnell CJ, Nabel EG. Genomics of cardiovascular disease. *N. Engl. J. Med.* 365:2098-2109 (2011).

219. Lusis AJ. Genetics of atherosclerosis. *Trends Genet.* 28:267-275 (2012).

220. Cohen JC, Hobbs HH. Genetics. Simple genetics for a complex disease. *Science* 340:689-690 (2013).

221. Lieb W, Vasan RS. Genetics of coronary artery disease. *Circulation* 128:1131-1138 (2013).

222. Polonsky TS, McClelland RL, Jorgensen NW, Bild DE, Burke GL, Guerci AD, Greenland P. Coronary artery calcium score and risk classification for coronary heart disease prediction. *JAMA* 303:1610-1616 (2010).

223. Ioannidis JP, Tzoulaki I. What makes a good predictor?: the evidence applied to coronary artery calcium score. *JAMA* 303:1646-1647 (2010).

224. Lakatta EG, Levy D. Arterial and cardiac aging: Major shareholders in cardiovascular disease enterprises Part I: Aging arteries: A "set up" for vascular disease. *Circulation* 107:139-146 (2003).

225. Lakatta EG, Levy D. Arterial and cardiac aging: major shareholders in cardiovascular disease enterprises: Part II: the aging heart in health: links to heart disease. *Circulation* 107:346-354 (2003).

226. Lakatta EG. Arterial and cardiac aging: major shareholders in cardiovascular disease enterprises: Part III: cellular and molecular clues to heart and arterial aging. *Circulation* 107:490-497 (2003).

227. Sanz J, Fayad ZA. Imaging of atherosclerotic cardiovascular disease. *Nature* 451:953-957 (2008).

228. Makowski MR, Henningsson M, Spuentrup E, Kim WY, Maintz D, Manning WJ, Botnar RM. Characterization of coronary atherosclerosis by magnetic resonance imaging. *Circulation* 128:1244-1255 (2013).

229. Moore CL, Copel JA. Point-of-care ultrasonography. *N. Engl. J. Med.* 364:749-757 (2011).

230. Bangalore S, Bhatt DL. Coronary intravascular ultrasound. *Circulation* 127:e868-e874 (2013).

231. Smilde TJ, Wollersheim H, Van Langen H, Stalenhoef AF. Reproducibility of ultrasonographic measurements of different carotid and femoral artery segments in healthy subjects and in patients with increased intima-media thickness. *Clin. Sci.* 93:317-324 (1997).

232. Nambi V, Pedroza C, Kao LS. Carotid intima-media thickness and cardiovascular events. *Lancet* 379:2028-2030 (2012).

233. Kitzman DW, Goldman ME, Gillam LD, Cohen JL, Aurigemma GP, Gottdiener JS. Efficacy and safety of the novel ultrasound contrast agent Perflutren (Definity) in patients with suboptimal baseline left ventricular echocardiographic images. *Am. J. Cardiol.* 86:669-674 (2000).

234. Senior R, Shah BN. Myocardial contrast echocardiography for simultaneous assessment of function and perfusion in real time: a technique comes of age. *Circulation* 126:1182-1184 (2012).

235. Porter T, Li S, Kilzer K, Deligonul U. Correlation between quantitative angiographic lesion severity and myocardial contrast intensity during a continuous infusion of perfluorocarbon-containing microbubbles. *J. Am. Soc. Echocardiogr.* 11:702-710 (1998).

236. Osborn EA, Jaffer FA. The advancing clinical impact of molecular imaging in CVD. *JACC Cardiovasc. Imaging* 6:1327-1341 (2013).

237. Nahrendorf M, Sosnovik DE, French BA, Swirski FK, Bengel F, Sadeghi MM, Lindner JR, Wu JC, Kraitchman DL, Fayad ZA *et al.* Multimodality cardiovascular molecular imaging, Part II. *Circ. Cardiovasc. Imaging* 2:56-70 (2009).

238. Weissleder R, Nahrendorf M, Pittet MJ. Imaging macrophages with nanoparticles. *Nat. Mater.* 13:125-138 (2014).

239. Kaufmann BA, Sanders JM, Davis C, Xie A, Aldred P, Sarembock IJ, Lindner JR. Molecular imaging of inflammation in atherosclerosis with targeted ultrasound detection of vascular cell adhesion molecule-1. *Circulation* 116:276-284 (2007).

240. Kaufmann BA, Carr CL, Belcik JT, Xie A, Yue Q, Chadderdon S, Caplan ES, Khangura J, Bullens S, Bunting S *et al.* Molecular imaging of the initial inflammatory response in atherosclerosis: implications for early detection of disease. *Arterioscler. Thromb. Vasc. Biol.* 30:54-59 (2010).

241. Buxton DB, Antman M, Danthi N, Dilsizian V, Fayad ZA, Garcia MJ, Jaff MR, Klimas M, Libby P, Nahrendorf M *et al.* Report of the National Heart, Lung, and Blood Institute working group on the translation of cardiovascular molecular imaging. *Circulation* 123:2157-2163 (2011).

242. Naylor AR. Time to rethink management strategies in asymptomatic carotid artery disease. *Nat. Rev. Cardiol.* 9:116-124 (2012).

243. Keys A. Human atherosclerosis and the diet. *Circulation* 5:115-118 (1952).

244. Mozaffarian D, Katan MB, Ascherio A, Stampfer MJ, Willett WC. Trans fatty acids and cardiovascular disease. *N. Engl. J. Med.* 354:1601-1613 (2006).

245. Keys A. *Seven countries: a multivariate analysis of death and coronary heart disease*, 1st edn (Harvard University Press, 1980).

246. Clarke R, Frost C, Collins R, Appleby P, Peto R. Dietary lipids and blood cholesterol: quantitative meta-analysis of metabolic ward studies. *BMJ* 314:112-117 (1997).

247. Yerushalmy J, Hilleboe HE. Fat in the diet and mortality from heart disease; a methodologic note. *N. Y. State J. Med.* 57:2343-2354 (1957).

248. Ravnskov U. A hypothesis out-of-date. the diet-heart idea. *J. Clin. Epidemiol.* 55:1057-1063 (2002).

249. Chowdhury R, Warnakula S, Kunutsor S, Crowe F, Ward HA, Johnson L, Franco OH, Butterworth AS, Forouhi NG, Thompson SG *et al.* Association of dietary, circulating, and supplement fatty acids with coronary risk: a systematic review and meta-analysis. *Ann. Intern. Med.* 160:398-406 (2014).

250. Correction: association of dietary, circulating, and supplement fatty acids with coronary risk. *Ann. Intern. Med.* 160:658 (2014).

251. Jakobsen MU, O'Reilly EJ, Heitmann BL, Pereira MA, Balter K, Fraser GE, Goldbourt U, Hallmans G, Knekt P, Liu S *et al.* Major types of dietary fat and risk of coronary heart disease: a pooled analysis of 11 cohort studies. *Am. J. Clin. Nutr.* 89:1425-1432 (2009).

252. Huang S, Rutkowsky JM, Snodgrass RG, Ono-Moore KD, Schneider DA, Newman JW, Adams SH, Hwang DH. Saturated fatty acids activate TLR-mediated proinflammatory signaling pathways. *J. Lipid Res.* 53:2002-2013 (2012).

253. Wong SW, Kwon M-J, Choi AMK, Kim H-P, Nakahira K, Hwang DH. Fatty acids modulate Toll-like receptor 4 activation through regulation of receptor dimerization and recruitment into lipid rafts in a reactive oxygen species-dependent manner. *J. Biol. Chem.* 284:27384-27392 (2009).

254. Shi H, Kokoeva MV, Inouye K, Tzameli I, Yin H, Flier JS. TLR4 links innate immunity and fatty acid-induced insulin resistance. *J. Clin. Invest.* 116:3015-3025 (2006).

255. Kennedy A, Martinez K, Chuang C-C, LaPoint K, McIntosh M. Saturated fatty acid-mediated inflammation and insulin resistance in adipose tissue: mechanisms of action and implications. *J. Nutr.* 139:1-4 (2009).

256. Chait A, Kim F. Saturated fatty acids and inflammation: who pays the toll? *Arterioscler. Thromb. Vasc. Biol.* 30:692-693 (2010).

257. Devkota S, Wang Y, Musch MW, Leone V, Fehlner-Peach H, Nadimpalli A, Antonopoulos DA, Jabri B, Chang EB. Dietary-fat-induced taurocholic acid promotes pathobiont expansion and colitis in Il10-/- mice. *Nature* 487:104-108 (2012).

258. Kim JK. Endothelial nuclear factor kappaB in obesity and aging: is endothelial nuclear factor kappaB a master regulator of inflammation and insulin resistance? *Circulation* 125:1081-1083 (2012).

259. Nicholls SJ, Lundman P, Harmer JA, Cutri B, Griffiths KA, Rye K-A, Barter PJ, Celermajer DS. Consumption of saturated fat impairs the anti-inflammatory properties of high-density lipoproteins and endothelial function. *J. Am. Coll. Cardiol.* 48:715-720 (2006).

260. Masterjohn C. The anti-inflammatory properties of safflower oil and coconut oil may be mediated by their respective concentrations of vitamin E. *J. Am. Coll. Cardiol.* 49:1825-1826 (2007).

261. Fahs CA, Yan H, Ranadive S, Rossow LM, Agiovlasitis S, Wilund KR, Fernhall B. The effect of acute fish-oil supplementation on endothelial function and arterial stiffness following a high-fat meal. *Appl. Physiol. Nutr. Metab.* 35:294-302 (2010).

262. Tishinsky JM, Gulli RA, Mullen KL, Dyck DJ, Robinson LE. Fish oil prevents high-saturated fat diet-induced impairments in adiponectin and insulin response in rodent soleus muscle. *Am. J. Physiol. Regul. Integr. Comp. Physiol.* 302:R598-605 (2012).

263. Gielen S, Schuler G, Adams V. Cardiovascular effects of exercise training: molecular mechanisms. *Circulation* 122:1221-1238 (2010).

264. Forsythe CE, Phinney SD, Fernandez ML, Quann EE, Wood RJ, Bibus DM, Kraemer WJ, Feinman RD, Volek JS. Comparison of low fat and low carbohydrate diets on circulating fatty acid composition and markers of inflammation. *Lipids* 43:65-77 (2008).

265. Forsythe CE, Phinney SD, Feinman RD, Volk BM, Freidenreich D, Quann E, Ballard K, Puglisi MJ, Maresh CM, Kraemer WJ *et al.* Limited effect of dietary saturated fat on plasma saturated fat in the context of a low carbohydrate diet. *Lipids* 45:947-962 (2010).

266. Sievenpiper JL, de Souza RJ, Mirrahimi A, Yu ME, Carleton AJ, Beyene J, Chiavaroli L, Di Buono M, Jenkins AL, Leiter LA *et al.* Effect of fructose on body weight in controlled feeding trials: a systematic review and meta-analysis. *Ann. Intern. Med.* 156:291-304 (2012).

267. Schmidt LA. New unsweetened truths about sugar. *JAMA Intern. Med.* 174:525-526 (2014).

268. Yang Q, Zhang Z, Gregg EW, Flanders WD, Merritt R, Hu FB. Added sugar intake and cardiovascular diseases mortality among US adults. *JAMA Intern. Med.* 174:516-524 (2014).

269. Mozaffarian D, Appel LJ, Van Horn L. Components of a cardioprotective diet: new insights. *Circulation* 123:2870-2891 (2011).

270. Sacks FM, Campos H. Dietary therapy in hypertension. *N. Engl. J. Med.* 362:2102-2112 (2010).

271. Appel LJ, Moore TJ, Obarzanek E, Vollmer WM, Svetkey LP, Sacks FM, Bray GA, Vogt TM, Cutler JA, Windhauser MM *et al.* A clinical trial of the effects of dietary patterns on blood pressure. DASH Collaborative Research Group. *N. Engl. J. Med.* 336:1117-1124 (1997).

272. Sacks FM, Svetkey LP, Vollmer WM, Appel LJ, Bray GA, Harsha D, Obarzanek E, Conlin PR, Miller ER, 3rd, Simons-Morton DG *et al.* Effects on blood pressure of reduced dietary sodium and the Dietary Approaches to Stop Hypertension (DASH) diet. DASH-Sodium Collaborative Research Group. *N. Engl. J. Med.* 344:3-10 (2001).

273. Bray GA, Vollmer WM, Sacks FM, Obarzanek E, Svetkey LP, Appel LJ, Dash Collaborative Research Group. A further subgroup analysis of the effects of the DASH diet and three dietary sodium levels on blood pressure: results of the DASH-Sodium Trial. *Am. J. Cardiol.* 94:222-227 (2004).

274. Keys A. Mediterranean diet and public health: personal reflections. *Am. J. Clin. Nutr.* 61:1321S--1323S (1995).

275. Nestle M. Mediterranean diets: historical and research overview. *Am. J. Clin. Nutr.* 61:1313S-1320S (1995).

276. Ferro-Luzzi A, Branca F. Mediterranean diet, Italian-style: prototype of a healthy diet. *Am. J. Clin. Nutr.* 61:1338S-1345S (1995).

277. Trichopoulou A, Costacou T, Bamia C, Trichopoulos D. Adherence to a Mediterranean diet and survival in a Greek population. *N. Engl. J. Med.* 348:2599-2608 (2003).

278. Renaud S, de Lorgeril M, Delaye J, Guidollet J, Jacquard F, Mamelle N, Martin JL, Monjaud I, Salen P, Toubol P. Cretan Mediterranean diet for prevention of coronary heart disease. *Am. J. Clin. Nutr.* 61:1360S-1367S (1995).

279. Esposito K, Marfella R, Ciotola M, Di Palo C, Giugliano F, Giugliano G, D'Armiento M, D'Andrea F, Giugliano D. Effect of a mediterranean-style diet on endothelial dysfunction and markers of vascular inflammation in the metabolic syndrome: a randomized trial. *JAMA* 292:1440-1446 (2004).

280. Shai I, Schwarzfuchs D, Henkin Y, Shahar DR, Witkow S, Greenberg I, Golan R, Fraser D, Bolotin A, Vardi H *et al.* Weight loss with a low-carbohydrate, Mediterranean, or low-fat diet. *N. Engl. J. Med.* 359:229-241 (2008).

281. Estruch R, Ros E, Salas-Salvado J, Covas MI, Corella D, Aros F, Gomez-Gracia E, Ruiz-Gutierrez V, Fiol M, Lapetra J *et al.* Primary prevention of cardiovascular disease with a Mediterranean diet. *N. Engl. J. Med.* 368:1279-1290 (2013).

282. Sala-Vila A, Romero-Mamani ES, Gilabert R, Nunez I, de la Torre R, Corella D, Ruiz-Gutierrez V, Lopez-Sabater MC, Pinto X, Rekondo J *et al.* Changes in ultrasound-assessed carotid intima-media thickness and plaque with a Mediterranean diet: a substudy of the PREDIMED trial. *Arterioscler. Thromb. Vasc. Biol.* 34:439-445 (2014).

283. Martinez-Gonzalez MA, Toledo E, Aros F, Fiol M, Corella D, Salas-Salvado J, Ros E, Covas MI, Fernandez-Crehuet J, Lapetra J *et al.* Extra-virgin olive oil consumption reduces risk of atrial fibrillation: the PREDIMED trial. *Circulation* (2014).

284. Domenech M, Roman P, Lapetra J, Garcia de la Corte FJ, Sala-Vila A, de la Torre R, Corella D, Salas-Salvado J, Ruiz-Gutierrez V, Lamuela-Raventos RM *et al.* Mediterranean diet reduces 24-hour ambulatory blood pressure, blood glucose, and lipids: one-year randomized, clinical trial. *Hypertension* 64:69-76 (2014).

285. Appel LJ, Van Horn L. Did the PREDIMED trial test a Mediterranean diet? *N. Engl. J. Med.* 368:1353-1354 (2013).

286. Mueller PS, Montori VM, Bassler D, Koenig BA, Guyatt GH. Ethical issues in stopping randomized trials early because of apparent benefit. *Ann. Intern. Med.* 146:878-881 (2007).

287. Bassler D, Briel M, Montori VM, Lane M, Glasziou P, Zhou Q, Heels-Ansdell D, Walter SD, Guyatt GH, Group S-S *et al.* Stopping randomized trials early for benefit and estimation of treatment effects: systematic review and meta-regression analysis. *JAMA* 303:1180-1187 (2010).

288. Ornish D, Scherwitz LW, Doody RS, Kesten D, McLanahan SM, Brown SE, DePuey E, Sonnemaker R, Haynes C, Lester J *et al.* Effects of stress management training and dietary changes in treating ischemic heart disease. *JAMA* 249:54-59 (1983).

289. Ornish D, Brown SE, Scherwitz LW, Billings JH, Armstrong WT, Ports TA, McLanahan SM, Kirkeeide RL, Brand RJ, Gould KL. Can lifestyle changes reverse coronary heart disease? The Lifestyle Heart Trial. *Lancet* 336:129-133 (1990).

290. Gould KL, Ornish D, Scherwitz L, Brown S, Edens RP, Hess MJ, Mullani N, Bolomey L, Dobbs F, Armstrong WT *et al.* Changes in myocardial perfusion abnormalities by positron emission tomography after long-term, intense risk factor modification. *JAMA* 274:894-901 (1995).

291. Ornish D, Scherwitz LW, Billings JH, Brown SE, Gould KL, Merritt TA, Sparler S, Armstrong WT, Ports TA, Kirkeeide RL *et al.* Intensive lifestyle changes for reversal of coronary heart disease. *JAMA* 280:2001-2007 (1998).

292. Ornish D. Mostly plants. *Am. J. Cardiol.* 104:957-958 (2009).

293. Ornish D, Weidner G, Fair WR, Marlin R, Pettengill EB, Raisin CJ, Dunn-Emke S, Crutchfield L, Jacobs FN, Barnard RJ *et al.* Intensive lifestyle changes may affect the progression of prostate cancer. *J. Urol.* 174:1065-1069 (2005).

294. Daubenmier JJ, Weidner G, Marlin R, Crutchfield L, Dunn-Emke S, Chi C, Gao B, Carroll P, Ornish D. Lifestyle and health-related quality of life of men with prostate cancer managed with active surveillance. *Urology* 67:125-130 (2006).

295. Ornish D, Magbanua MJ, Weidner G, Weinberg V, Kemp C, Green C, Mattie MD, Marlin R, Simko J, Shinohara K *et al.* Changes in prostate gene expression in men undergoing an intensive nutrition and lifestyle intervention. *Proc. Natl. Acad. Sci. USA* 105:8369-8374 (2008).

296. Ornish D, Lin J, Chan JM, Epel E, Kemp C, Weidner G, Marlin R, Frenda SJ, Magbanua MJ, Daubenmier J *et al.* Effect of comprehensive lifestyle changes on telomerase activity and telomere length in men with biopsy-proven low-risk prostate cancer: 5-year follow-up of a descriptive pilot study. *Lancet Oncol.* 14:1112-1120 (2013).

297. Esselstyn CB, Jr., Ellis SG, Medendorp SV, Crowe TD. A strategy to arrest and reverse coronary artery disease: a 5-year longitudinal study of a single physician's practice. *J. Fam. Pract.* 41:560-568 (1995).

298. Esselstyn CB. Updating a 12-year experience with arrest and reversal therapy for coronary heart disease (an overdue requiem for palliative cardiology). *Am. J. Cardiol.* 84:339--341, A338 (1999).

299. Campbell TC, Parpia B, Chen J. Diet, lifestyle, and the etiology of coronary artery disease: the Cornell China study. *Am. J. Cardiol.* 82:18T-21T (1998).

300. Hu FB, Rimm EB, Stampfer MJ, Ascherio A, Spiegelman D, Willett WC. Prospective study of major dietary patterns and risk of coronary heart disease in men. *Am. J. Clin. Nutr.* 72:912-921 (2000).

301. Bazzano LA, He J, Ogden LG, Loria CM, Vupputuri S, Myers L, Whelton PK. Fruit and vegetable intake and risk of cardiovascular disease in US adults: the first National Health and Nutrition Examination Survey Epidemiologic Follow-up Study. *Am. J. Clin. Nutr.* 76:93-99 (2002).

302. Djoussé L, Arnett DK, Coon H, Province MA, Moore LL, Ellison RC. Fruit and vegetable consumption and LDL cholesterol: the National Heart, Lung, and Blood Institute Family Heart Study. *Am. J. Clin. Nutr.* 79:213-217 (2004).

303. Sesso HD, Liu S, Gaziano JM, Buring JE. Dietary lycopene, tomato-based food products and cardiovascular disease in women. *J. Nutr.* 133:2336-2341 (2003).

304. Sesso HD, Wang L, Ridker PM, Buring JE. Tomato-based food products are related to clinically modest improvements in selected coronary biomarkers in women. *J. Nutr.* 142:326-333 (2012).

305. Ascherio A, Rimm EB, Hernan MA, Giovannucci E, Kawachi I, Stampfer MJ, Willett WC. Relation of consumption of vitamin E, vitamin C, and carotenoids to risk for stroke among men in the United States. *Ann. Intern. Med.* 130:963-970 (1999).

306. Hak AE, Stampfer MJ, Campos H, Sesso HD, Gaziano JM, Willett W, Ma J. Plasma carotenoids and tocopherols and risk of myocardial infarction in a low-risk population of US male physicians. *Circulation* 108:802-807 (2003).

307. Bose KS, Agrawal BK. Effect of lycopene from tomatoes (cooked) on plasma antioxidant enzymes, lipid peroxidation rate and lipid profile in grade-I hypertension. *Ann. Nutr. Metab.* 51:477-481 (2007).

308. Agarwal S, Rao AV. Tomato lycopene and low density lipoprotein oxidation: a human dietary intervention study. *Lipids* 33:981-984 (1998).

309. Engelhard YN, Gazer B, Paran E. Natural antioxidants from tomato extract reduce blood pressure in patients with grade-1 hypertension: a double-blind, placebo-controlled pilot study. *Am. Heart J.* 151:100 (2006).

310. Gartner C, Stahl W, Sies H. Lycopene is more bioavailable from tomato paste than from fresh tomatoes. *Am. J. Clin. Nutr.* 66:116-122 (1997).

311. Canene-Adams K, Campbell JK, Zaripheh S, Jeffery EH, Erdman JW. The tomato as a functional food. *J. Nutr.* 135:1226-1230 (2005).

312. Gianetti J, Pedrinelli R, Petrucci R, Lazzerini G, De Caterina M, Bellomo G, De Caterina R. Inverse association between carotid intima-media thickness and the antioxidant lycopene in atherosclerosis. *Am. Heart J.* 143:467-474 (2002).

313. Kim OY, Yoe HY, Kim HJ, Park JY, Kim JY, Lee S-H, Lee JH, Lee KP, Jang Y, Lee JH. Independent inverse relationship between serum lycopene concentration and arterial stiffness. *Atherosclerosis* 208:581-586 (2010).

314. Sesso HD, Buring JE, Norkus EP, Gaziano JM. Plasma lycopene, other carotenoids, and retinol and the risk of cardiovascular disease in men. *Am. J. Clin. Nutr.* 81:990-997 (2005).

315. Karppi J, Laukkanen JA, Sivenius J, Ronkainen K, Kurl S. Serum lycopene decreases the risk of stroke in men: a population-based follow-up study. *Neurology* 79:1540-1547 (2012).

316. Fuhrman B, Volkova N, Rosenblat M, Aviram M. Lycopene synergistically inhibits LDL oxidation in combination with vitamin E, glabridin, rosmarinic acid, carnosic acid, or garlic. *Antioxid. Redox Signal.* 2:491-506 (2000).

317. Martin KR, Wu D, Meydani M. The effect of carotenoids on the expression of cell surface adhesion molecules and binding of monocytes to human aortic endothelial cells. *Atherosclerosis* 150:265-274 (2000).

318. Fuhrman B, Elis A, Aviram M. Hypocholesterolemic effect of lycopene and beta-carotene is related to suppression of cholesterol synthesis and augmentation of LDL receptor activity in macrophages. *Biochem. Biophys. Res. Commun.* 233:658-662 (1997).

319. Lorenz M, Fechner M, Kalkowski J, Frohlich K, Trautmann A, Bohm V, Liebisch G, Lehneis S, Schmitz G, Ludwig A *et al.* Effects of lycopene on the initial state of atherosclerosis in New Zealand White (NZW) rabbits. *PloS one* 7:e30808 (2012).

320. Basuny AM, Gaafar AM, Arafat SM. Tomato lycopene is a natural antioxidant and can alleviate hypercholesterolemia. *Afr. J. Biotechnol.* 8:6627-6633 (2009).

321. Irving GW, Fontaine TD, Doolittle SP. Lycopersicin, a fungistatic agent from the tomato plant. *Science* 102:9-11 (1945).

322. Fontaine TD, Irving GW. Isolation and partial characterization of crystalline tomatine, an antibiotic agent from the tomato plant. *Arch. Biochem.* 18:467-475 (1948).

323. Friedman M. Anticarcinogenic, cardioprotective, and other health benefits of tomato compounds lycopene, alpha-tomatine, and tomatidine in pure form and in fresh and processed tomatoes. *J. Agric. Food Chem.* 61:9534-9550 (2013).

324. Lee K-R, Kozukue N, Han J-S, Park J-H, Chang E-Y, Baek E-J, Chang J-S, Friedman M. Glycoalkaloids and metabolites inhibit the growth of human colon (HT29) and liver (HepG2) cancer cells. *J. Agric. Food Chem.* 52:2832-2839 (2004).

325. Friedman M, Levin CE, Lee S-U, Kim H-J, Lee I-S, Byun J-O, Kozukue N. Tomatine-containing green tomato extracts inhibit growth of human breast, colon, liver, and stomach cancer cells. *J. Agric. Food Chem.* 57:5727-5733 (2009).

326. Choi SH, Ahn J-B, Kozukue N, Kim H-J, Nishitani Y, Zhang L, Mizuno M, Levin CE, Friedman M. Structure-activity relationships of α-, β(1)-, γ-, and δ-tomatine and tomatidine against human breast (MDA-MB-231), gastric (KATO-III), and prostate (PC3) cancer cells. *J. Agric. Food Chem.* 60:3891-3899 (2012).

327. Chiu F-L, Lin J-K. Tomatidine inhibits iNOS and COX-2 through suppression of NF-kappaB and JNK pathways in LPS-stimulated mouse macrophages. *FEBS Lett.* 582:2407-2412 (2008).

328. Dyle MC, Ebert SM, Cook DP, Kunkel SD, Fox DK, Bongers KS, Bullard SA, Dierdorff JM, Adams CM. Systems-Based Discovery of Tomatidine as a Natural Small Molecule Inhibitor of Skeletal Muscle Atrophy. *J. Biol. Chem.* (2014).

329. Chen JK, Taipale J, Cooper MK, Beachy PA. Inhibition of Hedgehog signaling by direct binding of cyclopamine to Smoothened. *Genes Dev.* 16:2743-2748 (2002).

330. Zhao C, Chen A, Jamieson CH, Fereshteh M, Abrahamsson A, Blum J, Kwon HY, Kim J, Chute JP, Rizzieri D *et al.* Hedgehog signalling is essential for maintenance of cancer stem cells in myeloid leukaemia. *Nature* 458:776-779 (2009).

331. Fujiwara Y, Kiyota N, Hori M, Matsushita S, Iijima Y, Aoki K, Shibata D, Takeya M, Ikeda T, Nohara T *et al.* Esculeogenin A, a new tomato sapogenol, ameliorates hyperlipidemia and atherosclerosis in ApoE-deficient mice by inhibiting ACAT. *Arterioscler. Thromb. Vasc. Biol.* 27:2400-2406 (2007).

332. Anderson JW, Johnstone BM, Cook-Newell ME. Meta-analysis of the effects of soy protein intake on serum lipids. *N. Engl. J. Med.* 333:276-282 (1995).

333. Erdman JW, Jr. Control of serum lipids with soy protein. *N. Engl. J. Med.* 333:313-315 (1995).

334. Potter SM. Overview of proposed mechanisms for the hypocholesterolemic effect of soy. *J. Nutr.* 125:606S-611S (1995).

335. Clerici C, Setchell KD, Battezzati PM, Pirro M, Giuliano V, Asciutti S, Castellani D, Nardi E, Sabatino G, Orlandi S *et al.* Pasta naturally enriched with isoflavone aglycons from soy germ reduces serum lipids and improves markers of cardiovascular risk. *J. Nutr.* 137:2270-2278 (2007).

336. Mahn K, Borras C, Knock GA, Taylor P, Khan IY, Sugden D, Poston L, Ward JP, Sharpe RM, Vina J *et al.* Dietary soy isoflavone induced increases in antioxidant and eNOS gene expression lead to improved endothelial function and reduced blood pressure in vivo. *FASEB J.* 19:1755-1757 (2005).

337. Clerici C, Nardi E, Battezzati PM, Asciutti S, Castellani D, Corazzi N, Giuliano V, Gizzi S, Perriello G, Di Matteo G *et al.* Novel soy germ pasta improves endothelial function, blood pressure, and oxidative stress in patients with type 2 diabetes. *Diabetes Care* 34:1946-1948 (2011).

338. Finking G, Hanke H. Nikolaj Nikolajewitsch Anitschkow (1885-1964) established the cholesterol-fed rabbit as a model for atherosclerosis research. *Atherosclerosis* 135:1-7 (1997).

339. Overturf ML, Smith SA, Gotto AM, Morrisett JD, Tewson T, Poorman J, Loose-Mitchell DS. Dietary cholesterol absorption, and sterol and bile acid excretion in hypercholesterolemia-resistant white rabbits. *J. Lipid Res.* 31:2019-2027 (1990).

340. Poorman JA, Buck RA, Smith SA, Overturf ML, Loose-Mitchell DS. Bile acid excretion and cholesterol 7 alpha-hydroxylase expression in hypercholesterolemia-resistant rabbits. *J. Lipid Res.* 34:1675-1685 (1993).

341. Bocan TM, Mueller SB, Mazur MJ, Uhlendorf PD, Brown EQ, Kieft KA. The relationship between the degree of dietary-induced hypercholesterolemia in the rabbit and atherosclerotic lesion formation. *Atherosclerosis* 102:9-22 (1993).

342. Smith BW, Simpson DG, Sarwate S, Miller RJ, Blue JP, Jr., Haak A, O'Brien WD, Jr., Erdman JW, Jr. Contrast ultrasound imaging of the aorta alters vascular morphology and circulating von Willebrand Factor in hypercholesterolemic rabbits. *J. Ultrasound Med.* 31:711-720 (2012).

343. Smith BW, King JL, Miller RJ, Blue JP, Jr., Sarwate S, O'Brien WD, Jr., Erdman JW, Jr. Optimization of a low magnesium, cholesterol-containing diet for the development of atherosclerosis in rabbits. *J. Food Res.* 2:168-178 (2013).

344. Shiomi M, Ito T. The Watanabe heritable hyperlipidemic (WHHL) rabbit, its characteristics and history of development: a tribute to the late Dr. Yoshio Watanabe. *Atherosclerosis* 207:1-7 (2009).

345. Plump AS, Smith JD, Hayek T, Aalto-Setala K, Walsh A, Verstuyft JG, Rubin EM, Breslow JL. Severe hypercholesterolemia and atherosclerosis in apolipoprotein E-deficient mice created by homologous recombination in ES cells. *Cell* 71:343-353 (1992).

346. Zhang SH, Reddick RL, Piedrahita JA, Maeda N. Spontaneous hypercholesterolemia and arterial lesions in mice lacking apolipoprotein E. *Science* 258:468-471 (1992).

347. Piedrahita JA, Zhang SH, Hagaman JR, Oliver PM, Maeda N. Generation of mice carrying a mutant apolipoprotein E gene inactivated by gene targeting in embryonic stem cells. *Proc. Natl. Acad. Sci. USA* 89:4471-4475 (1992).

348. Ishibashi S, Brown MS, Goldstein JL, Gerard RD, Hammer RE, Herz J. Hypercholesterolemia in low density lipoprotein receptor knockout mice and its reversal by adenovirus-mediated gene delivery. *J. Clin. Invest.* 92:883-893 (1993).

349. Witztum JL. Murine models for study of lipoprotein metabolism and atherosclerosis. *J. Clin. Invest.* 92:536-537 (1993).

350. Ishibashi S, Goldstein JL, Brown MS, Herz J, Burns DK. Massive xanthomatosis and atherosclerosis in cholesterol-fed low density lipoprotein receptor-negative mice. *J. Clin. Invest.* 93:1885-1893 (1994).

351. Greeve J, Altkemper I, Dieterich JH, Greten H, Windler E. Apolipoprotein B mRNA editing in 12 different mammalian species: hepatic expression is reflected in low concentrations of apoB-containing plasma lipoproteins. *J. Lipid Res.* 34:1367-1383 (1993).

352. Rader DJ, FitzGerald GA. State of the art: atherosclerosis in a limited edition. *Nat. Med.* 4:899-900 (1998).

353. Plump AS, Breslow JL. Apolipoprotein E and the apolipoprotein E-deficient mouse. *Annu. Rev. Nutr.* 15:495-518 (1995).

354. Linton MF, Atkinson JB, Fazio S. Prevention of atherosclerosis in apolipoprotein E-deficient mice by bone marrow transplantation. *Science* 267:1034-1037 (1995).

355. Getz GS, Reardon CA. Diet and murine atherosclerosis. *Arterioscler. Thromb. Vasc. Biol.* 26:242-249 (2006).

356. Smith JD. Mouse models of atherosclerosis. *Lab. Anim. Sci.* 48:573-579 (1998).

357. American Institute of Nutrition. Report of the American Institute of Nutrition ad hoc committee on standards for nutritional studies. *J. Nutr.* 107:1340-1348 (1977).

358. Reeves PG, Nielsen FH, Fahey GC. AIN-93 purified diets for laboratory rodents: final report of the American Institute of Nutrition ad hoc writing committee on the reformulation of the AIN-76A rodent diet. *J. Nutr.* 123:1939-1951 (1993).

359. Samuel VT. Fructose induced lipogenesis: from sugar to fat to insulin resistance. *Trends Endocrinol. Metab.* 22:60-65 (2011).

360. Strickland DK, Au DT, Cunfer P, Muratoglu SC. Low-density lipoprotein receptor-related protein-1: role in the regulation of vascular integrity. *Arterioscler. Thromb. Vasc. Biol.* 34:487-498 (2014).

361. Getz GS, Reardon CA. Animal Models of Atherosclerosis. *Arterioscler. Thromb. Vasc. Biol.*:1104-1115 (2012).

362. Powell-Braxton L, Veniant M, Latvala RD, Hirano KI, Won WB, Ross J, Dybdal N, Zlot CH, Young SG, Davidson NO. A mouse model of human familial hypercholesterolemia: markedly elevated low density lipoprotein cholesterol levels and severe atherosclerosis on a low-fat chow diet. *Nat. Med.* 4:934-938 (1998).

363. Purcell-Huynh DA, Farese RV, Jr., Johnson DF, Flynn LM, Pierotti V, Newland DL, Linton MF, Sanan DA, Young SG. Transgenic mice expressing high levels of human apolipoprotein B develop severe atherosclerotic lesions in response to a high-fat diet. *J. Clin. Invest.* 95:2246-2257 (1995).

364. Sanan DA, Newland DL, Tao R, Marcovina S, Wang J, Mooser V, Hammer RE, Hobbs HH. Low density lipoprotein receptor-negative mice expressing human apolipoprotein B-100 develop complex atherosclerotic lesions on a chow diet: no accentuation by apolipoprotein(a). *Proc. Natl. Acad. Sci. USA* 95:4544-4549 (1998).

365. van Vlijmen BJ, van den Maagdenberg AM, Gijbels MJ, van der Boom H, HogenEsch H, Frants RR, Hofker MH, Havekes LM. Diet-induced hyperlipoproteinemia and atherosclerosis in apolipoprotein E3-Leiden transgenic mice. *J. Clin. Invest.* 93:1403-1410 (1994).

366. Verschuren L, Wielinga PY, van Duyvenvoorde W, Tijani S, Toet K, van Ommen B, Kooistra T, Kleemann R. A dietary mixture containing fish oil, resveratrol, lycopene, catechins, and vitamins E and C reduces atherosclerosis in transgenic mice. *J. Nutr.* 141:863-869 (2011).

367. Zhang S, Picard MH, Vasile E, Zhu Y, Raffai RL, Weisgraber KH, Krieger M. Diet-induced occlusive coronary atherosclerosis, myocardial infarction, cardiac dysfunction, and premature death in scavenger receptor class B type I-deficient, hypomorphic apolipoprotein ER61 mice. *Circulation* 111:3457-3464 (2005).

368. Dillmann WH. The rat as a model for cardiovascular disease. *Drug Discov. Today* 5:173-178 (2008).

369. Jacob HJ, Lazar J, Dwinell MR, Moreno C, Geurts AM. Gene targeting in the rat: advances and opportunities. *Trends Genet.* 26:510-518 (2010).

370. Conlon LE, King RD, Moran NE, Erdman JW, Jr. Coconut oil enhances tomato carotenoid tissue accumulation compared to safflower oil in the Mongolian gerbil (Meriones unguiculatus). *J. Agric. Food Chem.* 60:8386-8394 (2012).

371. Moran NE, Clinton SK, Erdman JW, Jr. Differential bioavailability, clearance, and tissue distribution of the acyclic tomato carotenoids lycopene and phytoene in mongolian gerbils. *J. Nutr.* 143:1920-1926 (2013).

372. Nicolosi RJ, Marlett JA, Morello AM, Flanagan SA, Hegsted DM. Influence of dietary unsaturated and saturated fat on the plasma lipoproteins of Mongolian gerbils. *Atherosclerosis* 38:359-371 (1981).

373. Fernandez ML, Volek JS. Guinea pigs: a suitable animal model to study lipoprotein metabolism, atherosclerosis and inflammation. *Nutr. Metab.* 3:17 (2006).

374. Fernandez ML. Guinea pigs as models for cholesterol and lipoprotein metabolism. *J. Nutr.* 131:10-20 (2001).

375. Leite JO, DeOgburn R, Ratliff J, Su R, Smyth JA, Volek JS, McGrane MM, Dardik A, Fernandez ML. Low-carbohydrate diets reduce lipid accumulation and arterial inflammation in guinea pigs fed a high-cholesterol diet. *Atherosclerosis* 209:442-448 (2010).

376. Leite JO, Vaishnav U, Puglisi M, Fraser H, Trias J, Fernandez ML. A-002 (Varespladib), a phospholipase A2 inhibitor, reduces atherosclerosis in guinea pigs. *BMC Cardiovasc. Dis.* 9:7 (2009).

377. Reiser R, Sorrels MF, Williams MC. Influence of high levels of dietary fats and cholesterol on atherosclerosis and lipid distribution in swine. *Circ. Res.* 7:833-846 (1959).

378. Reitman JS, Mahley RW, Fry DL. Yucatan miniature swine as a model for diet-induced atherosclerosis. *Atherosclerosis* 43:119-132 (1982).

379. Shi ZS, Feng L, He X, Ishii A, Goldstine J, Vinters HV, Vinuela F. Vulnerable plaque in a swine model of carotid atherosclerosis. *Am. J. Neuroradiol.* 30:469-472 (2009).

380. Koskinas KC, Feldman CL, Chatzizisis YS, Coskun AU, Jonas M, Maynard C, Baker AB, Papafaklis MI, Edelman ER, Stone PH. Natural history of experimental coronary atherosclerosis and vascular remodeling in relation to endothelial shear stress: a serial, in vivo intravascular ultrasound study. *Circulation* 121:2092-2101 (2010).

381. Al-Mashhadi RH, Sørensen CB, Kragh PM, Christoffersen C, Mortensen MB, Tolbod LP, Thim T, Du Y, Li J, Liu Y *et al.* Familial hypercholesterolemia and atherosclerosis in cloned minipigs created by DNA transposition of a human PCSK9 gain-of-function mutant. *Sci. Transl. Med.* 5:166ra161 (2013).

382. Portman OW, Andrus SB. Comparative evaluation of three species of new world monkeys for studies of dietary factors, tissue lipids, and atherogenesis. *J. Nutr.* 87:429-438 (1965).

383. Frank-Kamenetsky M, Grefhorst A, Anderson NN, Racie TS, Bramlage B, Akinc A, Butler D, Charisse K, Dorkin R, Fan Y *et al.* Therapeutic RNAi targeting PCSK9 acutely lowers plasma cholesterol in rodents and LDL cholesterol in nonhuman primates. *Proc. Natl. Acad. Sci. USA* 105:11915-11920 (2008).

384. Paigen B, Morrow A, Holmes PA, Mitchell D, Williams RA. Quantitative assessment of atherosclerotic lesions in mice. *Atherosclerosis* 68:231-240 (1987).

385. Daugherty A, Whitman SC. in *Methods in Molecular Biology* Vol. 209 *Transgenic Mouse Methods and Protocols* (eds Marten H. Hofker & Jan Deursen) Ch. 16, 293-309 (Humana Press, 2002).

386. Combadiere C, Potteaux S, Rodero M, Simon T, Pezard A, Esposito B, Merval R, Proudfoot A, Tedgui A, Mallat Z. Combined inhibition of CCL2, CX3CR1, and CCR5 abrogates Ly6C(hi) and Ly6C(lo) monocytosis and almost abolishes atherosclerosis in hypercholesterolemic mice. *Circulation* 117:1649-1657 (2008).

387. Palinski W, Ord VA, Plump AS, Breslow JL, Steinberg D, Witztum JL. ApoE-deficient mice are a model of lipoprotein oxidation in atherogenesis. Demonstration of oxidation-specific epitopes in lesions and high titers of autoantibodies to malondialdehyde-lysine in serum. *Arterioscler. Thromb.* 14:605-616 (1994).

388. Tangirala RK, Rubin EM, Palinski W. Quantitation of atherosclerosis in murine models: correlation between lesions in the aortic origin and in the entire aorta, and differences in the extent of lesions between sexes in LDL receptor-deficient and apolipoprotein E-deficient mice. *J. Lipid Res.* 36:2320-2328 (1995).

389. Moore KJ, Kunjathoor VV, Koehn SL, Manning JJ, Tseng AA, Silver JM, McKee M, Freeman MW. Loss of receptor-mediated lipid uptake via scavenger receptor A or CD36 pathways does not ameliorate atherosclerosis in hyperlipidemic mice. *J. Clin. Invest.* 115:2192-2201 (2005).

390. Seimon TA, Wang Y, Han S, Senokuchi T, Schrijvers DM, Kuriakose G, Tall AR, Tabas IA. Macrophage deficiency of p38alpha MAPK promotes apoptosis and plaque necrosis in advanced atherosclerotic lesions in mice. *J. Clin. Invest.* 119:886-898 (2009).

391. Kassim SH, Li H, Vandenberghe LH, Hinderer C, Bell P, Marchadier D, Wilson A, Cromley D, Redon V, Yu H *et al.* Gene therapy in a humanized mouse model of familial hypercholesterolemia leads to marked regression of atherosclerosis. *PloS one* 5:e13424 (2010).

392. Qiang L, Lin HV, Kim-Muller JY, Welch CL, Gu W, Accili D. Proatherogenic abnormalities of lipid metabolism in SirT1 transgenic mice are mediated through Creb deacetylation. *Cell Metab.* 14:758-767 (2011).

393. Qu A, Shah YM, Manna SK, Gonzalez FJ. Disruption of Endothelial Peroxisome Proliferator-Activated Receptor γ Accelerates Diet-Induced Atherogenesis in LDL Receptor-Null Mice. *Arterioscler. Thromb. Vasc. Biol.* 32:65-73 (2011).

394. Liao X, Sluimer JC, Wang Y, Subramanian M, Brown K, Pattison JS, Robbins J, Martinez J, Tabas I. Macrophage Autophagy Plays a Protective Role in Advanced Atherosclerosis. *Cell Metab.* 15:545-553 (2012).

395. Rong JX, Blachford C, Feig JE, Bander I, Mayne J, Kusunoki J, Miller C, Davis M, Wilson M, Dehn S *et al.* ACAT inhibition reduces the progression of preexisting, advanced atherosclerotic mouse lesions without plaque or systemic toxicity. *Arterioscler. Thromb. Vasc. Biol.* 33:4-12 (2013).

396. Le NT, Heo KS, Takei Y, Lee H, Woo CH, Chang E, McClain C, Hurley C, Wang X, Li F *et al.* A crucial role for p90RSK-mediated reduction of ERK5 transcriptional activity in endothelial dysfunction and atherosclerosis. *Circulation* 127:486-499 (2013).

397. Daugherty A, Rateri DL. Development of experimental designs for atherosclerosis studies in mice. *Methods* 36:129-138 (2005).

398. Mehlem A, Hagberg CE, Muhl L, Eriksson U, Falkevall A. Imaging of neutral lipids by oil red O for analyzing the metabolic status in health and disease. *Nat. Protoc.* 8:1149-1154 (2013).

399. Takata Y, Liu J, Yin F, Collins AR, Lyon CJ, Lee CH, Atkins AR, Downes M, Barish GD, Evans RM *et al.* PPARdelta-mediated antiinflammatory mechanisms inhibit angiotensin II-accelerated atherosclerosis. *Proc. Natl. Acad. Sci. USA* 105:4277-4282 (2008).

400. Gu L, Okada Y, Clinton SK, Gerard C, Sukhova GK, Libby P, Rollins BJ. Absence of monocyte chemoattractant protein-1 reduces atherosclerosis in low density lipoprotein receptor-deficient mice. *Mol. Cell* 2:275-281 (1998).

401. Boring L, Gosling J, Cleary M, Charo IF. Decreased lesion formation in CCR2-/- mice reveals a role for chemokines in the initiation of atherosclerosis. *Nature* 394:894-897 (1998).

402. Dawson TC, Kuziel WA, Osahar TA, Maeda N. Absence of CC chemokine receptor-2 reduces atherosclerosis in apolipoprotein E-deficient mice. *Atherosclerosis* 143:205-211 (1999).

403. Kusunoki J, Hansoty DK, Aragane K, Fallon JT, Badimon JJ, Fisher EA. Acyl-CoA:cholesterol acyltransferase inhibition reduces atherosclerosis in apolipoprotein E-deficient mice. *Circulation* 103:2604-2609 (2001).

404. Frolova EG, Pluskota E, Krukovets I, Burke T, Drumm C, Smith JD, Blech L, Febbraio M, Bornstein P, Plow EF *et al.* Thrombospondin-4 regulates vascular inflammation and atherogenesis. *Circ. Res.* 107:1313-1325 (2010).

405. Luchtefeld M, Grothusen C, Gagalick A, Jagavelu K, Schuett H, Tietge UJ, Pabst O, Grote K, Drexler H, Forster R *et al.* Chemokine receptor 7 knockout attenuates atherosclerotic plaque development. *Circulation* 122:1621-1628 (2010).

406. Aiello RJ, Bourassa PA, Lindsey S, Weng W, Natoli E, Rollins BJ, Milos PM. Monocyte chemoattractant protein-1 accelerates atherosclerosis in apolipoprotein E-deficient mice. *Arterioscler. Thromb. Vasc. Biol.* 19:1518-1525 (1999).

407. Foo SY, Heller ER, Wykrzykowska J, Sullivan CJ, Manning-Tobin JJ, Moore KJ, Gerszten RE, Rosenzweig A. Vascular effects of a low-carbohydrate high-protein diet. *Proc. Natl. Acad. Sci. USA* 106:15418-15423 (2009).

408. Rong JX, Li J, Reis ED, Choudhury RP, Dansky HM, Elmalem VI, Fallon JT, Breslow JL, Fisher EA. Elevating high-density lipoprotein cholesterol in apolipoprotein E-deficient mice remodels advanced atherosclerotic lesions by decreasing macrophage and increasing smooth muscle cell content. *Circulation* 104:2447-2452 (2001).

409. Choudhury RP, Rong JX, Trogan E, Elmalem VI, Dansky HM, Breslow JL, Witztum JL, Fallon JT, Fisher EA. High-density lipoproteins retard the progression of atherosclerosis and favorably

remodel lesions without suppressing indices of inflammation or oxidation. *Arterioscler. Thromb. Vasc. Biol.* 24:1904-1909 (2004).

410. Accad M, Smith SJ, Newland DL, Sanan DA, King LE, Jr., Linton MF, Fazio S, Farese RV, Jr. Massive xanthomatosis and altered composition of atherosclerotic lesions in hyperlipidemic mice lacking acyl CoA:cholesterol acyltransferase 1. *J. Clin. Invest.* 105:711-719 (2000).

411. Lewis KE, Kirk EA, McDonald TO, Wang S, Wight TN, O'Brien KD, Chait A. Increase in serum amyloid A evoked by dietary cholesterol is associated with increased atherosclerosis in mice. *Circulation* 110:540-545 (2004).

412. Zhou Z, Subramanian P, Sevilmis G, Globke B, Soehnlein O, Karshovska E, Megens R, Heyll K, Chun J, Saulnier-Blache JS *et al.* Lipoprotein-derived lysophosphatidic acid promotes atherosclerosis by releasing CXCL1 from the endothelium. *Cell Metab.* 13:592-600 (2011).

413. Aikawa E, Nahrendorf M, Figueiredo J-L, Swirski FK, Shtatland T, Kohler RH, Jaffer Fa, Aikawa M, Weissleder R. Osteogenesis associates with inflammation in early-stage atherosclerosis evaluated by molecular imaging in vivo. *Circulation* 116:2841-2850 (2007).

414. Tomayko EJ, Chung HR, Wilund KR. Soy protein diet and exercise training increase relative bone volume and enhance bone microarchitecture in a mouse model of uremia. *J. Bone Miner. Metab.* 29:682-690 (2011).

415. Rask-Madsen C, Li Q, Freund B, Feather D, Abramov R, Wu IH, Chen K, Yamamoto-Hiraoka J, Goldenbogen J, Sotiropoulos KB *et al.* Loss of insulin signaling in vascular endothelial cells accelerates atherosclerosis in apolipoprotein E null mice. *Cell Metab.* 11:379-389 (2010).

416. Kastrup CJ, Nahrendorf M, Figueiredo JL, Lee H, Kambhampati S, Lee T, Cho S-W, Gorbatov R, Iwamoto Y, Dang TT *et al.* Painting blood vessels and atherosclerotic plaques with an adhesive drug depot. *Proc. Natl. Acad. Sci. USA* 109:21444-21449 (2012).

417. Ayala JE, Samuel VT, Morton GJ, Obici S, Croniger CM, Shulman GI, Wasserman DH, McGuinness OP. Standard operating procedures for describing and performing metabolic tests of glucose homeostasis in mice. *Dis. Model. Mech.* 3:525-534 (2010).

418. Shang L, Chen S, Du F, Li S, Zhao L, Wang X. Nutrient starvation elicits an acute autophagic response mediated by Ulk1 dephosphorylation and its subsequent dissociation from AMPK. *Proc. Natl. Acad. Sci. USA* 108:4788-4793 (2011).

419. Ford NA, Moran NE, Smith JW, Clinton SK, Erdman JW. An interaction between carotene-15,15'-monooxygenase expression and consumption of a tomato or lycopene-containing diet impacts serum and testicular testosterone. *Int. J. Cancer* 131:E143--148 (2012).

420. Buhman KK, Accad M, Novak S, Choi RS, Wong JS, Hamilton RL, Turley S, Farese RV. Resistance to diet-induced hypercholesterolemia and gallstone formation in ACAT2-deficient mice. *Nat. Med.* 6:1341-1347 (2000).

421. Smith SJ, Cases S, Jensen DR, Chen HC, Sande E, Tow B, Sanan DA, Raber J, Eckel RH, Farese RV. Obesity resistance and multiple mechanisms of triglyceride synthesis in mice lacking Dgat. *Nat. Genet.* 25:87-90 (2000).

422. Veniant MM, Sullivan MA, Kim SK, Ambroziak P, Chu A, Wilson MD, Hellerstein MK, Rudel LL, Walzem RL, Young SG. Defining the atherogenicity of large and small lipoproteins containing apolipoprotein B100. *J. Clin. Invest.* 106:1501-1510 (2000).

423. Fazio S, Major AS, Swift LL, Gleaves LA, Accad M, Linton MF, Farese RV. Increased atherosclerosis in LDL receptor-null mice lacking ACAT1 in macrophages. *J. Clin. Invest.* 107:163-171 (2001).

424. Buhman KK, Smith SJ, Stone SJ, Repa JJ, Wong JS, Knapp FF, Burri BJ, Hamilton RL, Abumrad NA, Farese RV. DGAT1 is not essential for intestinal triacylglycerol absorption or chylomicron synthesis. *J. Biol. Chem.* 277:25474-25479 (2002).

425. Wilund KR, Yu L, Xu F, Vega GL, Grundy SM, Cohen JC, Hobbs HH. No association between plasma levels of plant sterols and atherosclerosis in mice and men. *Arterioscler. Thromb. Vasc. Biol.* 24:2326-2332 (2004).

426. Weibel GL, Alexander ET, Joshi MR, Rader DJ, Lund-Katz S, Phillips MC, Rothblat GH. Wild-type ApoA-I and the Milano variant have similar abilities to stimulate cellular lipid mobilization and efflux. *Arterioscler. Thromb. Vasc. Biol.* 27:2022-2029 (2007).

427. Chung S, Sawyer JK, Gebre AK, Maeda N, Parks JS. Adipose tissue ATP binding cassette transporter A1 contributes to high-density lipoprotein biogenesis in vivo. *Circulation* 124:1663-1672 (2011).

428. Ford NA, Elsen AC, Erdman JW, Jr. Genetic ablation of carotene oxygenases and consumption of lycopene or tomato powder diets modulate carotenoid and lipid metabolism in mice. *Nutr. Res.* 33:733-742 (2013).

429. Bae EJ, Xu J, Oh DY, Bandyopadhyay G, Lagakos WS, Keshwani M, Olefsky JM. Liver-specific p70 S6 kinase depletion protects against hepatic steatosis and systemic insulin resistance. *J. Biol. Chem.* 287:18769-18780 (2012).

430. van den Maagdenberg AM, Hofker MH, Krimpenfort PJ, de Bruijn I, van Vlijmen B, van der Boom H, Havekes LM, Frants RR. Transgenic mice carrying the apolipoprotein E3-Leiden gene exhibit hyperlipoproteinemia. *J. Biol. Chem.* 268:10540-10545 (1993).

431. Lichtman AH, Clinton SK, Iiyama K, Connelly PW, Libby P, Cybulsky MI. Hyperlipidemia and atherosclerotic lesion development in LDL receptor-deficient mice fed defined semipurified diets with and without cholate. *Arterioscler. Thromb. Vasc. Biol.* 19:1938-1944 (1999).

432. Picard F, Kurtev M, Chung N, Topark-Ngarm A, Senawong T, Machado De Oliveira R, Leid M, McBurney MW, Guarente L. Sirt1 promotes fat mobilization in white adipocytes by repressing PPAR-gamma. *Nature* 429:771-776 (2004).

433. Gargalovic PS, Erbilgin A, Kohannim O, Pagnon J, Wang X, Castellani L, LeBoeuf R, Peterson ML, Spear BT, Lusis AJ. Quantitative trait locus mapping and identification of Zhx2 as a novel regulator of plasma lipid metabolism. *Circ. Cardiovasc. Genet.* 3:60-67 (2010).

434. Birkenfeld AL, Lee H-Y, Majumdar S, Juzcak MJ, Camporez J, Jornayvaz FR, Frederick DW, Guigni B, Kahn M, Zhang D *et al.* Influence of the hepatic eukaryotic initiation factor 2alpha (eIF2alpha) endoplasmic reticulum (ER) stress response pathway on insulin-mediated ER stress and hepatic and peripheral glucose metabolism. *J. Biol. Chem.* 286:36163-36170 (2011).

435. Li L, Hossain MA, Sadat S, Hager L, Liu L, Tam L, Schroer S, Huogen L, Fantus IG, Connelly PW *et al.* Lecithin cholesterol acyltransferase null mice are protected from diet-induced obesity and insulin resistance in a gender-specific manner through multiple pathways. *J. Biol. Chem.* 286:17809-17820 (2011).

436. Lorenz M, Fechner M, Kalkowski J, Fröhlich K, Trautmann A, Böhm V, Liebisch G, Lehneis S, Schmitz G, Ludwig A *et al.* Effects of lycopene on the initial state of atherosclerosis in New Zealand White (NZW) rabbits. *PloS one* 7:e30808 (2012).

437. Teixeira SR, Potter SM, Weigel R, Hannum S, Erdman JW, Hasler CM. Effects of feeding 4 levels of soy protein for 3 and 6 wk on blood lipids and apolipoproteins in moderately hypercholesterolemic men. *Am. J. Clin. Nutr.* 71:1077-1084 (2000).

438. Unlu NZ, Bohn T, Francis D, Clinton SK, Schwartz SJ. Carotenoid absorption in humans consuming tomato sauces obtained from tangerine or high-beta-carotene varieties of tomatoes. *J. Agric. Food Chem.* 55:1597-1603 (2007).

439. Uto-Kondo H, Ayaori M, Ogura M, Nakaya K, Ito M, Suzuki A, Takiguchi S-I, Yakushiji E, Terao Y, Ozasa H *et al.* Coffee consumption enhances high-density lipoprotein-mediated cholesterol efflux in macrophages. *Circ. Res.* 106:779-787 (2010).

440. Makris AP, Borradaile KE, Oliver TL, Cassim NG, Rosenbaum DL, Boden GH, Homko CJ, Foster GD. The individual and combined effects of glycemic index and protein on glycemic response, hunger, and energy intake. *Obesity* 19:2365-2373 (2011).

441. Yubero-Serrano EM, Delgado-Casado N, Delgado-Lista J, Perez-Martinez P, Tasset-Cuevas I, Santos-Gonzalez M, Caballero J, Garcia-Rios A, Marin C, Gutierrez-Mariscal FM *et al.* Postprandial antioxidant effect of the Mediterranean diet supplemented with coenzyme Q(10) in elderly men and women. *Age* 33:579-590 (2011).

442. Cho BHS, Park J-R, Nakamura MT, Odintsov BM, Wallig MA, Chung B-H. Synthetic dimyristoylphosphatidylcholine liposomes assimilating into high-density lipoprotein promote regression of atherosclerotic lesions in cholesterol-fed rabbits. *Exp. Biol. Med.* 235:1194-1203 (2010).

443. Seldin MM, Peterson JM, Byerly MS, Wei Z, Wong GW. Myonectin (CTRP15), a novel myokine that links skeletal muscle to systemic lipid homeostasis. *J. Biol. Chem.* 287:11968-11980 (2012).

444. Ozcan L, Wong CCL, Li G, Xu T, Pajvani U, Park SKR, Wronska A, Chen B-X, Marks AR, Fukamizu A *et al.* Calcium signaling through CaMKII regulates hepatic glucose production in fasting and obesity. *Cell Metab.* 15:739-751 (2012).

445. Tsutsumi K, Hagi A, Inoue Y. The relationship between plasma high density lipoprotein cholesterol levels and cholesteryl ester transfer protein activity in six species of healthy experimental animals. *Biol. Pharm. Bull.* 24:579-581 (2001).

446. Buhman KK, Wang LC, Tang Y, Swietlicki EA, Kennedy S, Xie Y, Liu Z-Y, Burkly LC, Levin MS, Rubin DC *et al.* Inhibition of Hedgehog signaling protects adult mice from diet-induced weight gain. *J. Nutr.* 134:2979-2984 (2004).

447. Iqbal J, Queiroz J, Li Y, Jiang X-C, Ron D, Hussain MM. Increased intestinal lipid absorption caused by Ire1β deficiency contributes to hyperlipidemia and atherosclerosis in apolipoprotein E-deficient mice. *Circ. Res.* 110:1575-1584 (2012).

448. Lu M, Wan M, Leavens KF, Chu Q, Monks BR, Fernandez S, Ahima RS, Ueki K, Kahn CR, Birnbaum MJ. Insulin regulates liver metabolism in vivo in the absence of hepatic Akt and Foxo1. *Nat. Med.* 18:388-395 (2012).

449. Kunkel SD, Elmore CJ, Bongers KS, Ebert SM, Fox DK, Dyle MC, Bullard SA, Adams CM. Ursolic acid increases skeletal muscle and brown fat and decreases diet-induced obesity, glucose intolerance and fatty liver disease. *PloS one* 7:e39332 (2012).

450. Cantó C, Jiang LQ, Deshmukh AS, Mataki C, Coste A, Lagouge M, Zierath JR, Auwerx J. Interdependence of AMPK and SIRT1 for metabolic adaptation to fasting and exercise in skeletal muscle. *Cell Metab.* 11:213-219 (2010).

451. Thompson KH, Zilversmit DB. Plasma very low density lipoprotein (VLDL) in cholesterol-fed rabbits: chylomicron remnants or liver lipoproteins? *J. Nutr.* 113:2002-2010 (1983).

452. Chattopadhyay A, Navab M, Hough G, Gao F, Meriwether D, Grijalva V, Springstead JR, Palgnachari MN, Namiri-Kalantari R, Su F *et al.* A novel approach to oral apoA-I mimetic therapy. *J. Lipid Res.* 54:995-1010 (2013).

453. Goldstein JL, Zhao TJ, Li RL, Sherbet DP, Liang G, Brown MS. Surviving starvation: essential role of the ghrelin-growth hormone axis. *Cold Spring Harb. Symp. Quant. Biol.* 76:121-127 (2011).

454. Li RL, Sherbet DP, Elsbernd BL, Goldstein JL, Brown MS, Zhao T-J. Profound hypoglycemia in starved, ghrelin-deficient mice is caused by decreased gluconeogenesis and reversed by lactate or fatty acids. *J. Biol. Chem.* 287:17942-17950 (2012).

455. Koo H-Y, Wallig MA, Chung BH, Nara TY, Cho BHS, Nakamura MT. Dietary fructose induces a wide range of genes with distinct shift in carbohydrate and lipid metabolism in fed and fasted rat liver. *Biochim. Biophys. Acta* 1782:341-348 (2008).

456. Potthoff MJ, Inagaki T, Satapati S, Ding X, He T, Goetz R, Mohammadi M, Finck BN, Mangelsdorf DJ, Kliewer SA *et al.* FGF21 induces PGC-1alpha and regulates carbohydrate and fatty acid metabolism during the adaptive starvation response. *Proc. Natl. Acad. Sci. USA* 106:10853-10858 (2009).

457. Sengupta S, Peterson TR, Laplante M, Oh S, Sabatini DM. mTORC1 controls fasting-induced ketogenesis and its modulation by ageing. *Nature* 468:1100-1104 (2010).

458. Merritt ME, Harrison C, Sherry AD, Malloy CR, Burgess SC. Flux through hepatic pyruvate carboxylase and phosphoenolpyruvate carboxykinase detected by hyperpolarized 13C magnetic resonance. *Proc. Natl. Acad. Sci. USA* 108:19084-19089 (2011).

459. Newberry EP, Xie Y, Kennedy S, Han X, Buhman KK, Luo J, Gross RW, Davidson NO. Decreased hepatic triglyceride accumulation and altered fatty acid uptake in mice with deletion of the liver fatty acid-binding protein gene. *J. Biol. Chem.* 278:51664-51672 (2003).

460. Yang H, Yang T, Baur JA, Perez E, Matsui T, Carmona JJ, Lamming DW, Souza-Pinto NC, Bohr VA, Rosenzweig A *et al.* Nutrient-sensitive mitochondrial NAD+ levels dictate cell survival. *Cell* 130:1095-1107 (2007).

461. Nakagawa T, Lomb DJ, Haigis MC, Guarente L. SIRT5 deacetylates carbamoyl phosphate synthetase 1 and regulates the urea cycle. *Cell* 137:560-570 (2009).

462. Hugo SE, Cruz-Garcia L, Karanth S, Anderson RM, Stainier DYR, Schlegel A. A monocarboxylate transporter required for hepatocyte secretion of ketone bodies during fasting. *Genes Dev.* 26:282-293 (2012).

CHAPTER 2: A validated sandwich ELISA for the quantification of von Willebrand Factor in rabbit plasma[1]

Abstract

Von Willebrand Factor (vWF) is a multimeric plasma protein important for platelet plug formation. As part of its haemostatic role, it is released from endothelial cells during vascular stress or injury and is considered an excellent biomarker of endothelial function. Currently, there are no validated kits available to measure vWF in rabbits. We developed a sensitive and reproducible sandwich enzyme-linked immunosorbent assay (ELISA) for detection of vWF in rabbit plasma using commercially available antibodies and reagents. Purified human vWF was used as a calibrator standard with a dynamic range of 1.56-100 ng/mL. The Minimum Required Dilution for rabbit plasma was 1:100. When plasma was spiked with 3.76 or 10 ng/mL vWF, recovery was 108±2% and 93±2%, respectively. Intra- and inter-assay precision for 8 rabbit plasma samples were 3% and 4%, respectively. The Minimum Detectable Concentration was 254 pg/mL for purified human vWF and 1:10,700 dilution of cholesterol-fed rabbit plasma, and the Reliable Detection Limits were 457 pg/mL and 1:5940. Three freeze-thaw cycles significantly decreased absorbance readings for purified human vWF and 2 of 3 plasma samples assayed. This ELISA provides sensitive and reproducible measurements of rabbit plasma vWF, which is an important biomarker for cardiovascular research.

[1]This chapter previously appeared in its entirety as Smith BW, Strakova J, King JL, Erdman JW, Jr., O'Brien WD, Jr. Validated sandwich ELISA for the quantification of von Willebrand factor in rabbit plasma. *Biomarker Insights* 5:119-127 (2010). The article is open access and the authors retain copyright.

Introduction

Atherosclerosis is a pathological process underlying the majority of clinical cardiovascular events[1] in which chronic inflammatory mechanisms are culpable in initiation and progression[2]. Vascular endothelial cells express adhesion molecules that promote the progression of atherosclerosis[3], and there is a great deal of interest in discovering biomarkers of endothelial status or inflammation that reflect the activity of the various mechanisms at work. These biomarkers can assist clinicians and researchers in monitoring the progression of atherosclerosis or predicting disease outcomes in research animals and human patients.

One such biomarker is the multimeric plasma protein von Willebrand Factor (vWF). In addition to its well-established haemostatic role[4], vWF is currently considered the best circulating biomarker of endothelial function[5]. A growing body of experimental, clinical and epidemiological evidence points to high plasma vWF levels as indicative of systemic vascular dysfunction[6] and predictive of acute cardiovascular events[7].

Our laboratory is interested in evaluating the biological effects of ultrasound, when used with ultrasound contrast agents to image the aorta. We developed a cholesterol-fed rabbit model[8] for this purpose. The vWF biomarker would be a useful circulating indicator of endothelial status, but there is currently no validated assay kit available to determine vWF levels in rabbit plasma. To facilitate accurate and precise measurement of this biomarker in pre-clinical studies, we have developed a sandwich enzyme-linked immunosorbent assay (ELISA) technique to measure rabbit plasma vWF using commercially available antibodies and reagents. The assay was validated by measuring parallelism, spike recovery, intra- and inter-assay precision, specificity, sensitivity, and freeze-thaw stability of plasma vWF.

Materials and Methods

Materials

The microplate reader (ELx800) was obtained from BioTek (Winooski, VT). Nunc Immulon 4HBX Flat Bottom 96-well microplates and adhesive plate seals were obtained from Fisher Scientific (Pittsburgh, PA). Tween-20, Thimerosal, Phosphate Buffered Saline (PBS), Na_2CO_3 and $NaHCO_3$ were obtained from Sigma-Aldrich (St. Louis, MO).

The vWF protein standard (Purified vWF from citrated human plasma, V2650) was obtained from US Biological (Swampscott, MA). Affinity purified goat anti-human vWF (GAVWF-AP), biotinylated affinity purified goat anti-human vWF (GAVWF-APBIO), and vWF-deficient plasma (VWF-DP) were obtained from Affinity Biologicals (Ancaster, Ontario, Canada). Streptavidin-Horseradish Peroxidase (HRP) (016-030-084) and Bovine Serum Albumin (BSA) (001-000-162) were obtained from Jackson ImmunoResearch (West Grove, PA). 3,3',5,5'-Tetramethylbenzidine (TMB) substrate solution (52-00-03) and TMB Stop Solution (50-85-05) were obtained from KPL (Gaithersburg, MD).

Reagents

Carbonate Buffer – 20 mM Na_2CO_3 and 40 mM $NaHCO_3$, pH 9.6, stored at 4ºC.

Blocking Buffer – 1% w/v BSA in PBS containing 11.9 mM Phosphates (Na_2HPO_4, KH_2PO_4), 137 mM NaCl, and 2.7 mM KCl, pH 7.4, stored at -20ºC.

PBST-BSA – 0.1% v/v Tween 20, 1% w/v BSA in PBS containing 11.9 mM Phosphates, 137 mM NaCl, and 2.7 mM KCl, pH 7.4, stored at -20ºC.

Wash Buffer – 0.05% v/v Tween 20 in PBS containing 11.9 mM Phosphates, 137 mM NaCl, and 2.7 mM KCl, pH 7.4, stored at 4ºC.

All buffers were preserved with 1 mg/L Thimerosal.

Rabbit Plasma and Protein Standard

Four-month-old male New Zealand White rabbits were acquired from Myrtle's Rabbitry (Thompson's Station, TN). Animals were housed individually in standard caging with stainless steel mesh bottom in a 20°C temperature-controlled room with 12 hour light/dark cycles, and fed either a standard chow diet containing 2% fat, 0% cholesterol and 0.4% magnesium (Harlan Teklad, Indianapolis, IN) or an atherogenic diet containing 10% fat, 1% cholesterol, and 0.11% magnesium (TestDiet, Richmond, IN). Blood samples were collected in heparinized tubes via the lateral saphenous vein while under restraint, centrifuged at 1380 x *g* for 10 minutes and plasma was aliquotted and frozen at -70°C. The Institutional Animal Care and Use Committee at the University of Illinois at Urbana-Champaign approved all procedures.

The vWF protein standard was purified from citrated human plasma negative for HIV1, HIV2 and HBsAg. The protein was supplied at a concentration of 0.2 mg/mL in buffer containing 25 mM Na Citrate, 100 mM NaCl, 100 mM glycine, pH 6.8, and determined by the manufacturer to be ≥95% pure as judged by SDS-PAGE under reducing conditions. Upon receipt, the solution was aliquotted and stored at -70ºC according to the manufacturer's instructions.

Antibody Selection and Optimization

Several commercially available antibodies were evaluated (**Table 2.1**). Affinity purified goat anti-human vWF and biotinylated affinity purified goat anti-human vWF were selected as capture and sandwich antibodies, respectively. Streptavidin-HRP was chosen as the detection reagent. Antibody dilutions were optimized using checkerboard titration procedures, and the dilutions which returned the strongest signal to noise ratio were selected.

Procedure

A schematic of the assay procedure can be found in **Figure 2.1**. Microplate wells were coated with 100 µL of affinity purified goat anti-human vWF capture antibody diluted 1:5000 in carbonate buffer for a final concentration of 1 µg/mL. Plates were covered with adhesive sealing film, placed in a plastic bag with wet paper towels, and incubated overnight (≥16h) at 4ºC. Reagents were allowed to equilibrate to room temperature (RT) overnight.

The next day, plates were washed three times with 300 µL of Wash Buffer per well on an orbital shaker with gentle agitation for 5 min. The buffer was removed by emptying into a sink and blotting on paper towels. Blocking Buffer (300 µL) was then added to each well and plates were sealed and blocked for 2 hours at RT with agitation.

During this time, rabbit plasma samples and the vWF standard were prepared for addition to the plate. A standard curve was generated by serially diluting the 0.2 mg/mL vWF stock in Blocking Buffer. Working dilutions of 100, 50, 25, 12.5, 6.25, 3.13 and 1.56 ng/mL were used in the assay. These dilutions span the concentration range of diluted plasma samples. Rabbit plasma was diluted 1:100 in Blocking Buffer. Following the blocking step, plates were washed three times with Wash Buffer as described above

and 100 µL of each standard and sample were added to the plate in duplicate. Blocking Buffer alone was used as a blank. Plates were incubated for 2 hours at RT with agitation.

Plates were then emptied into a sink and washed three times with Wash Buffer as described above. Biotinylated affinity purified goat anti-human vWF was diluted 1:40,000 in PBST-BSA to a final concentration of 25 ng/mL and 100 µL were added to each well. Plates were sealed and incubated for 1 hour at RT with agitation. After emptying the previous solution and washing, Streptavidin-HRP was diluted 1:100,000 in PBST-BSA to a final concentration of 5 ng/mL and 100 µL were added to each well. Plates were sealed, protected from light and incubated for 1 hour at RT with agitation.

After removing the Streptavidin-HRP solution and washing, 100 µL of the TMB substrate were added to each well. The reaction was stopped after 5 min by addition of 100 µL TMB Stop Solution per well and allowed to equilibrate for 5 min. The underside of the microplate was wiped with 70% ethanol and the plate was read immediately at 450 nm with wavelength correction at 550 nm using a microplate reader.

A linear standard curve was generated using the duplicate blanked readings from the serially diluted protein standard. Samples were interpolated into the standard curve to obtain concentration values. The dynamic range of the standard curve utilized in this assay is 1.56-100 ng/mL. The TMB incubation time was optimized to provide a reading of 1.5 absorbance units for the most concentrated standard.

Specificity

To test for non-specific signal, control wells containing either Blocking Buffer or human plasma rendered immunodeficient for vWF were incorporated into each assay. In other experiments, wells were also included where rabbit plasma samples were assayed in the absence of either the capture or sandwich antibody.

Minimum Required Dilution

Minimum Required Dilution (MRD) is identified when establishing parallelism and is defined as the minimum sample dilution providing optimal accuracy and precision[9]. Plasma from six cholesterol-fed rabbits was pooled, subjected to dilutions between 1:6.25 and 1:200 and assayed in quadruplicate. Parallelism was defined as dilution-

corrected analyte concentrations varying ≤20% between dilutions[10]. The minimum dilution achieving parallelism was chosen as the MRD.

Spike Recovery

Cholesterol-fed rabbit plasma was spiked with purified vWF at concentrations of 3.76 ng/mL (Low Spike) and 10 ng/mL (High Spike). Plasma, spikes, and spiked plasma were each assayed in quadruplicate on the same plate. Recovery was calculated using vWF concentration values with the equation: $\frac{[Sample+Spike]-[Sample]}{[Spike]} \times 100$. Brackets denote a concentration value in ng/mL. Standard deviation (SD) was obtained from the two sets of duplicate values. The measured concentration of the spiked sample should be within 20% of the expected value[9].

Precision

Eight plasma samples from cholesterol-fed rabbits were selected. Each sample was diluted 1:100 in Blocking Buffer and 10 replicates were plated to determine intra-assay precision. This experiment was repeated over three different days with parallel aliquots to evaluate inter-assay precision. We previously assayed parallel aliquots of the samples for plasma total cholesterol (**Table 2.4**) using an enzymatic colorimetric kit (Wako Chemicals, Richmond, VA).

Sensitivity

Eighteen serial dilutions of purified vWF were prepared beginning with 400 ng/mL and assayed in quadruplicate, along with 24 replicates of the zero concentration buffer blank. A similar procedure was followed for rabbit plasma. Plasma from six cholesterol-fed rabbits was pooled and subjected to serial dilutions from 1:6.25 to 1:102,000.

Freeze-Thaw Stability of Samples

Freeze-thaw stability was determined over three freeze-thaw cycles. Three rabbit plasma samples were selected. Separate aliquots of each sample were thawed between 1-3 times by removal from the -70ºC freezer and thawing on ice for ≤2 hours. They were then returned to the freezer and stored as before. All samples and aliquots were diluted 1:100 and assayed on the same plate, with 6 replicates per aliquot, along with 6 replicates of purified vWF at 100 ng/mL. Any significant changes in assay

response were determined using repeated-measures ANOVA followed by Bonferroni adjustment for multiple comparisons.

Calculations and analysis

Data are presented as means±SD. All standards and samples were run in duplicate unless otherwise noted. Data were analyzed using SigmaPlot 10.0 and PASW Statistics 18.0 for Windows, and mean differences were considered statistically significant at the $p<0.05$ level.

Results and Discussion

ELISA is the most widely used method of screening mammalian plasma for vWF, replacing the Laurell techniques previously used[11]. Several publications have utilized the vWF marker specifically in rabbits. De Meyer and coworkers[12] utilized immunohistochemistry to qualitatively observe deposition of vWF in the vascular intima. The group reported lack of an available measurement method for rabbit plasma vWF. An earlier publication by Benson et al.[13] reported adaptation of an ELISA for measurement of plasma vWF in rabbit and other species, but neither demonstrated quantitative data for rabbits nor used commercially available antibodies. Benson et al. did, however, highlight the important ability to construct a vWF assay without species-specific antibodies.

Two subsequent publications attempted to quantify rabbit plasma vWF by sandwich ELISA. The first[14] merely reported optical density values obtained in each assay, which is not useful to other researchers. It is commonly known that optical density values vary between assays due to many factors such as activity of the peroxidase conjugate, binding of antigen to antibodies, or temperature conditions, and thus it is critical to include a standard curve in each assay using purified analyte. A second publication[15] quantified rabbit plasma vWF, and found that the marker correlated well with development of atherosclerosis, but provided inadequate detail about the ELISA method utilized. Neither of these two assays was validated. Furthermore, cholesterol feeding elevates blood cholesterol to extremely high levels, a potential source of interference in an immunoassay. We developed and validated an ELISA to improve upon previous work.

An assay that appears precise but measures the wrong analyte would not be valid. We confirmed the specificity of the antibodies used by including positive (the purified vWF standard) and negative (vWF deficient plasma) controls. Antibodies demonstrated strong affinity for purified vWF. Omission of either the capture or sandwich antibody did not result in any signal above that of the buffer blank. Additionally, when vWF-deficient human plasma was assayed, no signal above blank was seen (data not shown).

Parallelism and spike recovery are important considerations when working with complex matrices such as blood plasma[16]. Lipids and other interfering substances in plasma can lead to assay variation, but diluting the sample matrix helps minimize these effects. Assaying an undiluted sample can also underestimate the amount of analyte present, presumably due to saturation of the antibodies. We observed this in our results. When rabbit plasma was serially diluted beginning with a 1:6.25 dilution, the MRD was 1:100 (**Table 2.2**). Dilution-corrected concentrations increased from 429 ng/mL in the 1:6.25 dilution to 2440 ng/mL at the 1:100 MRD. Spike recovery analysis is also useful in assessing accuracy and sample matrix interference. Theoretically, an identical assay response should be seen for a given amount of vWF, whether it is present in plasma or purified and diluted in a buffer. In order to demonstrate this, plasma is spiked with vWF and the concentration determined. The observed (uncorrected for dilution) vWF concentration of the cholesterol-fed rabbit plasma was 16.2 ng/mL. When plasma was spiked with 3.76 ng/mL vWF, the measured concentration was 20.3 ng/mL, which represents a recovery of 108±2%. When plasma was spiked with 10 ng/mL vWF, the measured concentration was 25.5 ng/mL, which represents a recovery of 93±2% (**Table 2.3**).

Measurement reproducibility, or precision, is a crucial aspect of any bioanalytical method. Intra-assay precision is the variability between replicates of the same sample in an assay, and inter-assay precision is the variability over multiple days. CV was used as a measure of precision and defined as (Mean/Standard Deviation)*100[17]. Recommended CV for immunoassays is ≤20%[16,18]. Our average intra-assay CV of 3% is well within this guideline (**Table 2.4**). Measurement of the same 8 plasma samples on

three different days yielded an inter-assay CV=4% (**Table 2.4**). Thus, this assay provides precise and reproducible measurements of plasma vWF.

These data also illustrate the excellent selectivity of the assay. Selectivity is commonly defined as the ability of the antibodies to bind consistent amounts of protein in the presence of other interfering agents, such as lipids and plasma matrix components. The antibodies bind both purified human vWF and rabbit vWF in plasma with equally high precision, despite potential interference from an average total cholesterol level of 935 mg/dL in the 8 rabbit plasma samples used (**Table 2.4**). It is recommended to establish and confirm selectivity of an immunoassay in disease states[16], however this is rarely done. Our assay is effective in atherosclerotic, hyperlipidemic animals.

Statistical measures used to evaluate assay sensitivity include Minimum Detectable Concentration (MDC) and Reliable Detection Limit (RDL). The MDC is the concentration at which there is a high probability of a response significantly lower than the blank. The RDL, conversely, is the lowest concentration of analyte that produces a response significantly greater than the blank[19]. A 4-parameter logistic regression curve was fit to the data[20] and 95% Confidence Intervals (CIs) of the curve were calculated. Graphically, the MDC is the intersection of the 4-parameter logistic curve with an asymptote drawn horizontally from the upper 95% CI of the 4-PL curve at zero concentration. The RDL lies at the intersection of the lower 95% CI of the 4-PL curve of the standards data with an asymptote drawn horizontally from the upper 95% CI of the 4-PL curve at zero concentration. The MDC and RDL were 254 and 457 pg/mL for the vWF standard and 1:10,700 and 1:5940 for rabbit plasma (**Figure 2.2**). This assay is versatile and could easily be adapted to assay protein levels in the single-digit picogram range simply by increasing the Streptavidin-HRP concentration.

The sensitivity of an ELISA is largely dependent on the antibodies used. High sensitivity requires two well-paired antibodies. Theoretical support for the use of these antibodies in screening rabbit plasma is provided by previous work which demonstrated 87% homology between human and rabbit vWF cDNA sequences, including 100% homology in the region corresponding to the first 116 amino acids of the N-terminal domain of the mature vWF subunit[21]. The aforementioned multispecies ELISA[13]

provided additional evidence of the high degree of homology of vWF molecules from many vertebrate species, and the resultant cross-reactivity of many anti-vWF antibodies.

Protein stability over multiple thaw cycles is an important practical consideration when handling biological specimens. Freeze-thaw cycles commonly reduce protein stability, and our results suggest that vWF is degraded after multiple freeze-thaw cycles. Decreases reached statistical significance for most samples, with mean absorbances 7-17% lower after three freeze-thaws (**Table 2.5**). Absorbance readings for Samples 2 and 3 were significantly different between 1 and 3 freeze-thaw cycles ($p<0.001$). Absorbance readings for the vWF standard at 100 ng/mL were significantly decreased after 3 freeze-thaw cycles compared with 1 ($p<0.01$) and 2 ($p<0.05$) freeze-thaw cycles. Sample 2 showed a 7% decrease in mean absorbance after 3 freeze-thaws, Sample 3 a 17% decrease, and the 100 ng/mL vWF standard a 9% decrease. While the decrease for Sample 1 was not statistically significant, the mean absorbance was 15% lower after 3 freeze-thaw cycles. It is advisable to aliquot all specimens prior to freezing for the first time to avoid these complications.

In conclusion, we have described an accurate, precise and sensitive method to analyze rabbit plasma for vWF that has been formally validated in accordance with current recommendations. To our knowledge, this is the only currently available validated ELISA for rabbit vWF and may prove useful in the ongoing search for suitable biomarkers of atherogenesis and endothelial damage.

Acknowledgements

This work was supported by NIH grant R37EB002641. The authors report no conflicts of interest. This paper is subject to the NIH public access policy. The authors declare no competing interests.

References

1. Lloyd-Jones D, Adams RJ, Brown TM, Carnethon M, Dai S, De Simone G, Ferguson TB, Ford E, Furie K, Gillespie C *et al.* Heart disease and stroke statistics-2010 update: a report from the American Heart Association. *Circulation* 121:e46-e215 (2010).

2. Libby P. Inflammation in atherosclerosis. *Nature* 420:868-874 (2002).

3. Hansson GK. Inflammation, atherosclerosis, and coronary artery disease. *N. Engl. J. Med.* 352:1685-1695 (2005).

4. Mannucci PM. Treatment of von Willebrand's Disease. *N. Engl. J. Med.* 351:683-694 (2004).

5. Constans J, Conri C. Circulating markers of endothelial function in cardiovascular disease. *Clin. Chim. Acta* 368:33-47 (2006).

6. Lip GY, Blann A. von Willebrand factor: a marker of endothelial dysfunction in vascular disorders? *Cardiovasc. Res.* 34:255-265 (1997).

7. Spiel AO, Gilbert JC, Jilma B. von Willebrand factor in cardiovascular disease: focus on acute coronary syndromes. *Circulation* 117:1449-1459 (2008).

8. King JL, Miller RJ, Blue JP, O'Brien WD, Erdman JW. Inadequate dietary magnesium intake increases atherosclerotic plaque development in rabbits. *Nutr. Res.* 29:343-349 (2009).

9. Smolec J, DeSilva B, Smith W, Weiner R, Kelly M, Lee B, Khan M, Tacey R, Hill H, Celniker A *et al.* Bioanalytical method validation for macromolecules in support of pharmacokinetic studies. *Pharm. Res.* 22:1425-1431 (2005).

10. Findlay JW, Smith WC, Lee JW, Nordblom GD, Das I, DeSilva BS, Khan MN, Bowsher RR. Validation of immunoassays for bioanalysis: a pharmaceutical industry perspective. *J. Pharm. Biomed. Anal.* 21:1249-1273 (2000).

11. Bartlett A, Dormandy KM, Hawkey CM, Stableforth P, Voller A. Factor-VIII-related antigen: measurement by enzyme immunoassay. *Br. Med. J.* 1:994-996 (1976).

12. De Meyer GR, Hoylaerts MF, Kockx MM, Yamamoto H, Herman AG, Bult H. Intimal deposition of functional von Willebrand factor in atherogenesis. *Arterioscler. Thromb. Vasc. Biol.* 19:2524-2534 (1999).

13. Benson RE, Catalfamo JL, Dodds WJ. A multispecies enzyme-linked immunosorbent assay for von Willebrand's factor. *J. Lab. Clin. Med.* 119:420-427 (1992).

14. Ghayour-Mobarhan M, Lamb DJ, Tavallaie S, Ferns GA. Relationship between plasma cholesterol, von Willebrand factor concentrations, extent of atherosclerosis and antibody titres to heat shock proteins-60, -65 and -70 in cholesterol-fed rabbits. *Int. J. Exp. Pathol.* 88:249-255 (2007).

15. Haghjooyjavanmard S, Nematbakhsh M, Monajemi A, Soleimani M. von Willebrand factor, C-reactive protein, nitric oxide, and vascular endothelial growth factor in a dietary reversal model of hypercholesterolemia in rabbit. *Biomed. Pap. Med. Fac. Univ. Palacky Olomouc Czech Repub.* 152:91-95 (2008).

16. DeSilva B, Smith W, Weiner R, Kelley M, Smolec J, Lee B, Khan M, Tacey R, Hill H, Celniker A. Recommendations for the bioanalytical method validation of ligand-binding assays to support pharmacokinetic assessments of macromolecules. *Pharm. Res.* 20:1885-1900 (2003).

17. Reed GF, Lynn F, Meade BD. Use of coefficient of variation in assessing variability of quantitative assays. *Clin. Diagn. Lab. Immunol.* 9:1235-1239 (2002).

18. FDA. *Guidance for Industry: Bioanalytical Method Validation* (Rockville, MD, 2001).

19. O'Connell MA, Belanger BA, Haaland PD. Calibration and assay development using the four-parameter logistic model. *Chemom. Intell. Lab. Syst.* 20:97-114 (1993).

20. Findlay JW, Dillard RF. Appropriate calibration curve fitting in ligand binding assays. *AAPS J.* 9:E260-267 (2007).

21. Lavergne JM, Piao YC, Ferreira V, Kerbiriou-Nabias D, Bahnak BR, Meyer D. Primary structure of the factor VIII binding domain of human, porcine and rabbit von Willebrand factor. *Biochem. Biophys. Res. Commun.* 194:1019-1024 (1993).

Figures and Tables

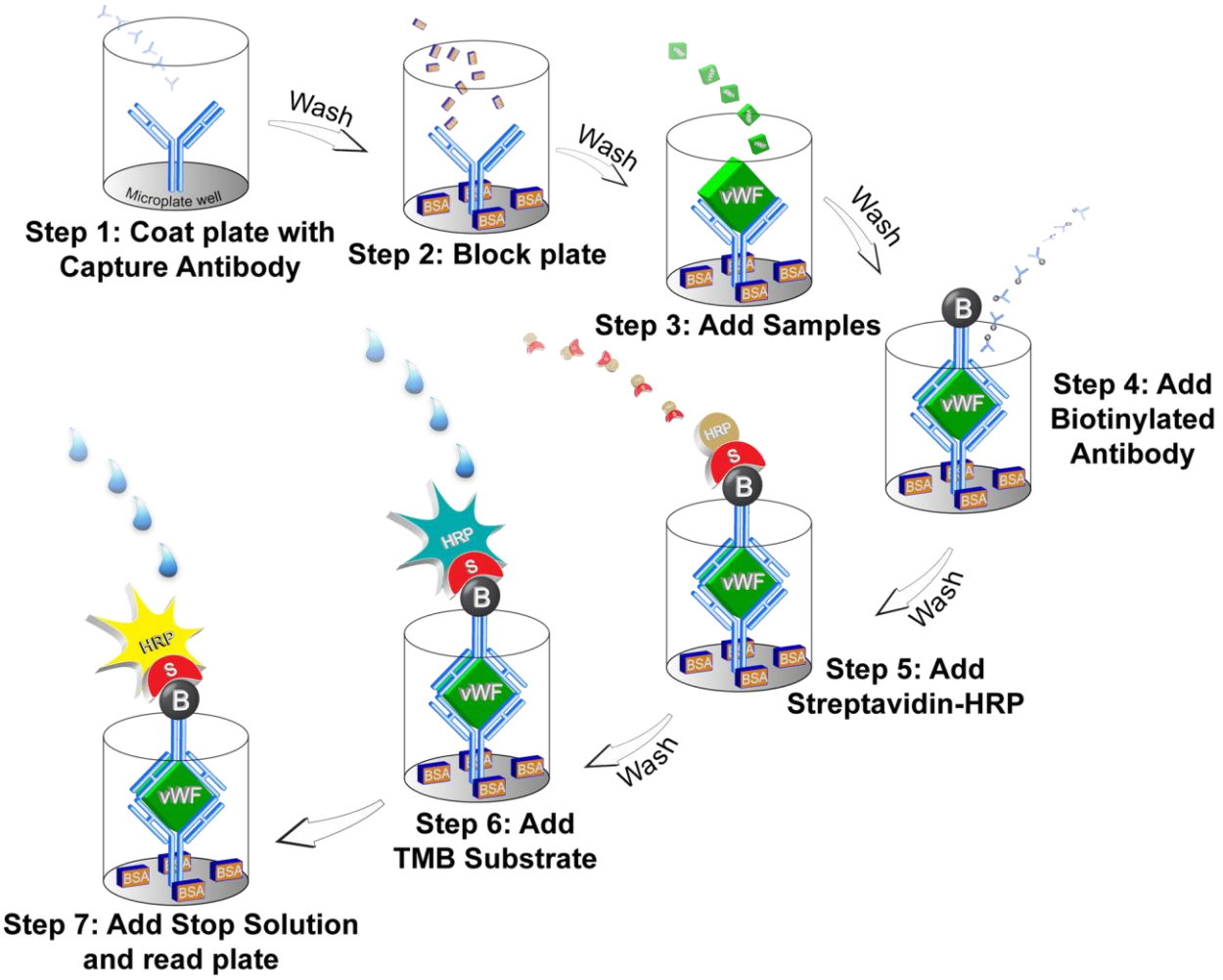

Figure 2.1. Schematic illustrating the sandwich ELISA procedure described in the *Procedure* subsection of Materials and Methods.

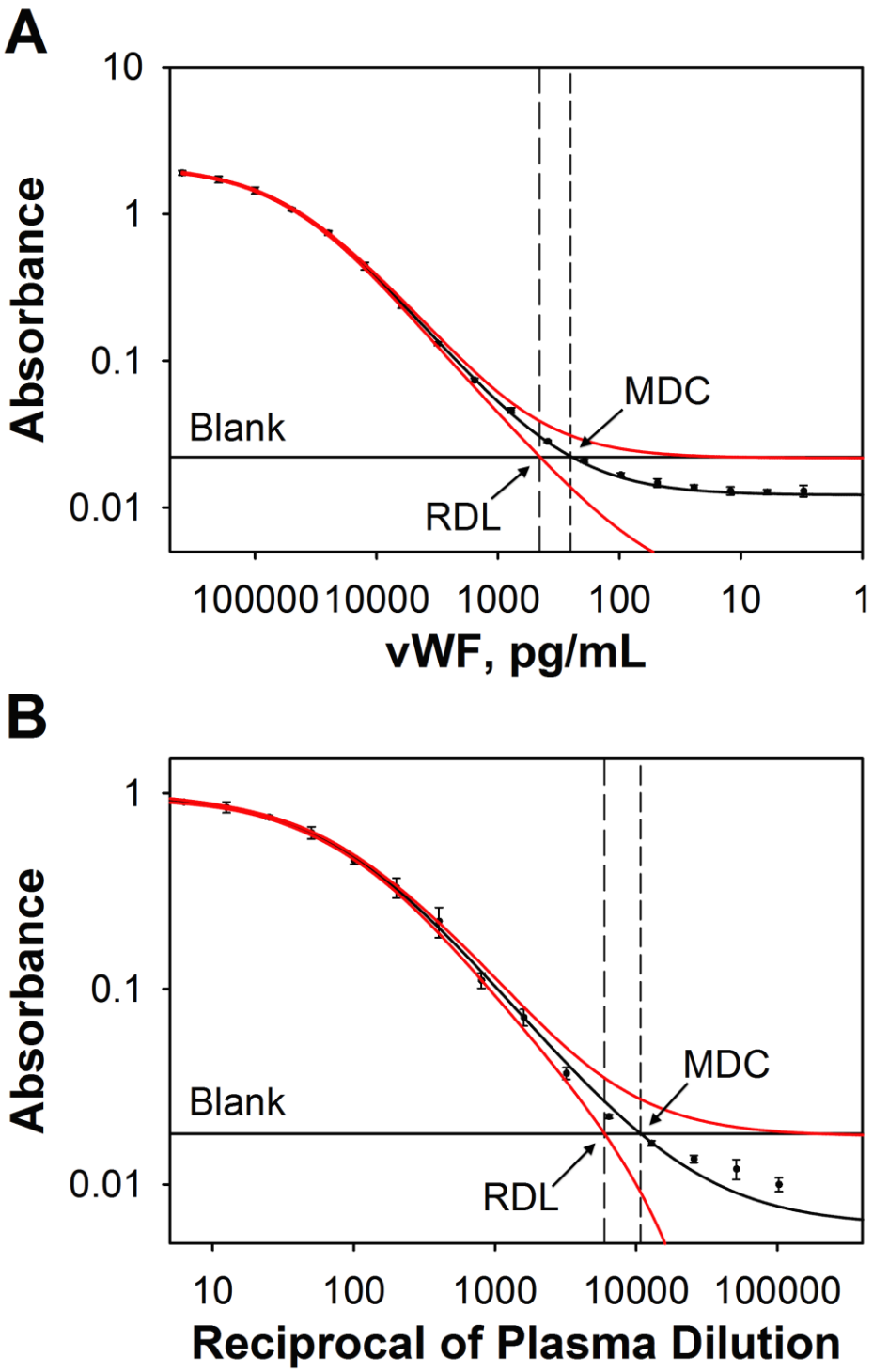

Figure 2.2. Sensitivity. (A), 18 serial dilutions of purified vWF were prepared beginning with 400 ng/mL and assayed in quadruplicate, along with 24 replicates of the zero concentration buffer blank. (B), Rabbit plasma was subjected to serial dilutions beginning at 1:6.25 and assayed in quadruplicate. 4-parameter logistic regression curves with 95% Confidence Intervals were fit to the data. Bars are SD. MDC, Minimum Detectable Concentration. RDL, Reliable Detection Limit.

Company	Catalog Number	Host	Immunogen	Type	Application	Works in Rabbit?
Abcam	ab28264	Mouse	Human vWF – N terminal region	Monoclonal IgG_{2a}	Capture	Only some lots
Takara	M025	Mouse	Human vWF – C terminal region	Monoclonal IgG_1	Capture	No
Takara	M029	Mouse	Human vWF – N terminal region	Monoclonal IgG_{2b}	Capture	No
Affinity Biologicals	GAVWF-AP	Goat	Human vWF	Polyclonal IgG	Capture	Yes
Affinity Biologicals	SACWF-IG	Sheep	Canine vWF	Polyclonal IgG	Capture	Yes
Abcam	ab19367	Goat	Human vWF	Polyclonal IgG	Sandwich	Yes
Affinity Biologicals	GAVWF-APBIO	Goat	Human vWF	Polyclonal Biotinylated IgG	Sandwich	Yes
Affinity Biologicals	GAVWF-HRP	Goat	Human vWF	Polyclonal Peroxidase Conjugated IgG	Sandwich/ Detection	Yes
Affinity Biologicals	SACWF-HRP	Sheep	Canine vWF	Polyclonal Peroxidase Conjugated IgG	Sandwich/ Detection	Yes

Table 2.1. vWF antibody selection. Several antibodies were evaluated for effectiveness in detecting rabbit vWF. Some antibodies detected neither rabbit plasma vWF nor purified human vWF (the putative antigen) in this experimental setup. When the Abcam goat anti-human vWF antibody was used in the sandwich configuration, a donkey anti-goat IgG antibody (Novus NB7357) was used as the detection reagent. When the sandwich antibody was biotinylated, Streptavidin-HRP was used as the detection reagent.

Plasma Dilution	Dilution Corrected Value, ng/mL	CV, %	% Concentration of Previous
6.25	429	2	-
12.5	794	6	185
25	1360	2	171
50	2080	7	154
100	2440	5	117
200	2420	12	99

Table 2.2. Minimum Required Dilution. Plasma from six cholesterol-fed rabbits was pooled, diluted starting at 1:6.25 and assayed in quadruplicate. The MRD is the first dilution to fall within 20% of the previous dilution's concentration.

Sample	Observed Concentration, ng/mL	Recovery, Mean±SD, %
Rabbit Plasma	16.2	
Low Spike	3.76	
Low Spike +Plasma	20.3	108±2
High Spike	10.0	
High Spike +Plasma	25.5	93±2

Table 2.3. Spike Recovery. Rabbit plasma was spiked with purified human vWF at concentrations of 3.76 ng/mL (Low Spike) and 10 ng/mL (High Spike). Plasma, spikes, and spiked plasma were each assayed in quadruplicate on the same plate. A concentration within 20% of expected was considered acceptable recovery.

Sample	Plasma Total Cholesterol, mg/dL	Mean vWF, ng/mL	Inter-assay SD, ng/mL	Intra-assay CV, %	Inter-assay CV, %
Rabbit 1	1100	1730	42	3	2
Rabbit 2	868	2430	66	4	3
Rabbit 3	897	3240	153	3	5
Rabbit 4	950	2290	153	3	7
Rabbit 5	906	3280	127	2	4
Rabbit 6	691	2600	68	2	3
Rabbit 7	1000	2200	130	2	6
Rabbit 8	1070	2720	77	4	3
Average	935	2560	102	3	4

Table 2.4. Precision. Eight plasma samples from cholesterol-fed rabbits were selected. Each sample was diluted 1:100 in Blocking Buffer and run with 10 replicates. The experiment was repeated over three different days with parallel aliquots to determine inter-assay precision. Intra-assay CV and vWF values represent means of the three experiments.

Sample	1 Freeze/Thaw cycle, ng/mL	2 Freeze/Thaw cycles, % remaining	3 Freeze/Thaw cycles, % remaining
100 ng/mL standard	100	89	83**
Rabbit 1	2350	77	59*
Rabbit 2	3030	91	83
Rabbit 3	1910	75	45*

Table 2.5. Freeze-thaw stability of vWF in rabbit plasma. Aliquots of rabbit plasma and purified vWF were frozen and thawed between 1-3 times and assayed with six replicates on the same plate. Data were analyzed by repeated-measures ANOVA followed by Bonferroni adjustment for multiple comparisons. *$p<0.001$ vs. 1 freeze-thaw cycle, **$p<0.01$ vs. 1 freeze-thaw cycle and $p<0.05$ vs. 2 freeze-thaw cycles.

CHAPTER 3: Contrast ultrasound imaging of the aorta alters vascular morphology and circulating von Willebrand Factor in hypercholesterolemic rabbits[2]

Abstract

Objective – Ultrasound contrast agents (UCAs) are intravenously infused microbubbles that add definition to ultrasonic images. UCAs continue to show clinical promise in cardiovascular imaging, but their biological effects are not known with confidence. We utilized a cholesterol-fed rabbit model to evaluate these effects when used in conjunction with ultrasound (US) to image the descending aorta.

Methods – Male New Zealand White rabbits (n=41) were weaned onto an atherogenic diet containing 1% cholesterol, 10% fat and 0.11% magnesium. At 21 days, rabbits were exposed to contrast ultrasound at one of four pressure levels using either the UCA Definity® or saline control (n=5 per group). Blood samples were collected and analyzed for lipids and von Willebrand Factor (vWF), a marker of endothelial function. Animals were euthanized at 42 days and tissues were collected for histological analysis.

Results – After adjustment for pre-exposure vWF, high-level US (*in situ* [at the aorta] peak rarefactional pressure of 1.4 or 2.1 MPa) resulted in significantly lower vWF one hour post-exposure ($p=0.0127$, $p_{adj} < 0.0762$). This difference disappeared within 24 hours. Atheroma thickness in the descending aorta was lower in animals receiving UCA as compared to animals receiving saline.

Conclusions – Contrast ultrasound affected the descending aorta as evidenced by two separate outcome measures. These results may be a first step in elucidating a previously unknown biological effect of UCAs. Further research is warranted to characterize the effects of this procedure. [Supported by NIH R37EB002641]

[2]This chapter previously appeared in its entirety as Smith BW, Simpson DG, Sarwate S, Miller RJ, Blue JP, Jr., Haak A, O'Brien WD, Jr., Erdman JW, Jr. Contrast ultrasound imaging of the aorta alters vascular morphology and circulating von Willebrand Factor in hypercholesterolemic rabbits. *Journal of Ultrasound in Medicine* 31:711-720 (2012). Reprinted with permission from the American Institute of Ultrasound in Medicine.

Introduction

Ultrasound contrast agents (UCAs) are microbubbles encapsulating inert gases that serve to enhance the echogenicity of blood for cardiovascular imaging applications[1]. The interaction of ultrasound (US) with circulating UCAs introduces the potential for unique biological effects. These bioeffects must be fully characterized and assessed before recommendations can be made regarding the appropriate uses of UCAs, and progress is urgently needed. The importance of medical imaging for early diagnosis is underscored by the fact that 2300 Americans die each day of cardiovascular disease (CVD) by current estimates[2].

Many *in vitro* and *in vivo* bioeffects of UCAs have been noted, including hemolysis[3], capillary rupture[4], endothelial cell damage[5], and elevations in Troponin T, a biomarker of cardiac damage[6]. Previous studies in our lab have demonstrated UCA-induced arterial endothelial and vascular smooth muscle injury[7] and cardiac arrhythmias[8]. These results suggest that the interactions of US with UCAs in the cardiovascular system may have important consequences, especially if exposure to contrast US hastens the onset or increases the severity of atherosclerosis in patients at risk.

To this end, we utilized a cholesterol-fed rabbit model to evaluate the biological effects of the UCA Definity® when used in conjunction with US to image the descending aorta. In order to assess these bioeffects, we chose to focus on the biomarker von Willebrand Factor (vWF). vWF is a multimeric protein produced and stored within endothelial cells, and secreted both across the basolateral endothelial membrane into the vascular intima[9] and across the apical membrane into the vessel lumen, where it circulates in the blood[10]. vWF has a physiological role in platelet plug formation during thrombosis[11]. In addition to its physiological function, elevated vWF is a biomarker of endothelial damage[12] and clinical predictor of adverse cardiovascular events[13]. vWF is positively associated with risk for CVD and cardiac death in epidemiological studies[14,15], and vWF has been shown to increase experimentally in hypercholesterolemic rabbits[16]. We hypothesized that plasma vWF would increase when rabbits consumed a cholesterol-containing diet, and that any further increase after US exposure would indicate endothelial damage due to the contrast US procedure.

Materials and Methods

Animals and Experimental Design

The experimental design is presented in **Figure 3.1**. After acclimation and consumption of a standard chow diet (2031 Teklad Global High Fiber Rabbit Diet, Harlan, Indianapolis, IN), male New Zealand White rabbits (n=41, Myrtle's Rabbitry, Thompson's Station, TN) were randomized to experimental groups and weaned onto an atherogenic diet (5TZB Test Diet®, Richmond, IN) containing 1% cholesterol, 10% fat and 0.11% magnesium over a 10-day period as previously described[17]. The diet was optimized to elevate serum cholesterol and initiate the atherosclerotic process while minimizing side effects such as jaundice and anorexia. Weight and age (±SD) of the 41 rabbits at the beginning of the study (immediately prior to initiation of the atherogenic diet) were 3.3±0.2 kg and 21.8±1.0 wk. Rabbits were exposed to ultrasound with or without UCA at day 21 and euthanized at day 42. The Institutional Animal Care and Use Committee at the University of Illinois at Urbana-Champaign approved all procedures.

Serial blood samples were collected from each rabbit at baseline (prior to initiation of the atherogenic diet), 2 weeks, 1 week, and 1 hour pre exposure, and 1 hour, 24 hours, 48 hours, 1 week, 2 weeks and 3 weeks post exposure. Blood samples were collected with heparinized syringes into heparinized tubes via the lateral saphenous vein while under restraint, centrifuged at 1380 x *g* for 10 minutes, and the plasma was aliquotted and frozen at -70°C.

Exposimetry

On day 21, 20 of the rabbits were infused with saline only and 21 were infused with saline+UCA (0.5 mL of Definity® in 19.5 mL of saline). Infusion rate was 1 mL/min. The ultrasound exposure conditions for all 41 rabbits were: 3.2 MHz, 2-min exposure duration at each of the 4 exposure sites, 10-Hz pulse repetition frequency, 1.6-μs pulse duration at four separate in situ [at the aorta] peak rarefactional pressures, $p_{r(in\ situ)}$: 0 (sham), 0.72, 1.4 and 2.1 MPa.

The exposimetry and calibration procedures have been described previously in detail[18-23]. Ultrasonic exposures were conducted using a focused f/3, 19-mm-diameter lithium niobate ultrasonic transducer (Valpey Fisher, Hopkinton, MA USA). Water-based (degassed, 22ºC) pulse-echo ultrasonic field distribution measurements were performed

according to established procedures[22,24] and yielded a center frequency of 3.2 MHz, a fractional bandwidth of 11%, a focal length of 38 mm, a -6-dB focal beamwidth of 1.6 mm, and a -6-dB depth of focus of 27 mm.

An automated procedure, based on established standards[25] was used to routinely calibrate the ultrasound fields[22]. Briefly, the source transducer's drive voltage was supplied by a high-power pulse source (RAM5000, Ritec, Inc., Warwick, RI USA). A calibrated PVDF membrane hydrophone (Marconi Model Y-34-6543, Chelmsford, UK) was mounted to the computer-controlled micropositioning system (Daedal, Inc., Harrisburg, PA USA). The hydrophone's signal was digitized with an oscilloscope (500 MS/s, LeCroy Model 9354TM, Chestnut Ridge, NY USA), the output of which was fed to the same computer (Dell Pentium II, Dell Corporation, Round Rock, TX USA) that controlled the positioning system. Off-line processing (MATLAB®, The Mathworks, Natick, MA USA) yielded the water-based peak rarefactional pressure $p_{r(\text{in vitro})}$. The Mechanical Index (MI) was also determined from the measurement procedure[25]: the $\mathrm{MI} = p_{r.3}/\sqrt{f_c}$ where $p_{r.3}$ is the derated (0.3 dB/cm-MHz) peak rarefactional pressure (in MPa) and f_c is the center frequency (in MHz). The MI is reported because it is a regulated quantity[26] of diagnostic US systems, and its value is available to system operators. Thus, there is value to provide the MI for each of our exposure settings in order to give general guidance to manufacturers and operators as to the levels we are using in this study. All four $p_{r(\text{in situ})}$ levels were below the FDA upper limit for diagnostic US of MI=1.9 (see **Table 3.1**)[26].

Independent calibrations were performed at least weekly on the 3.2-MHz focused transducer during the 7-week duration of the US exposure component of the experiment. Relative standard deviation $\left(\frac{\text{standard deviation}}{\text{mean}}\right)$ of $p_{r(\text{in vitro})}$ was 1.6% (n = 10). The pulse duration was also measured[19] at each calibration and its mean value (relative standard deviation) was 1.2 (0.6%) μs.

The calibration procedures were performed in degassed water, which minimally attenuates the US signal. In contrast, when US is used to image tissues in a live animal, the signal is attenuated as it passes through intervening tissue en route to its focus. Thus, estimation of the actual *in situ* (at the aorta) peak rarefactional pressure, $p_{r(\text{in situ})}$, requires that attenuation be taken into account. A study was conducted to estimate the

attenuation slope (AS, dB/cm-MHz) along the same *in vivo* tissue path as that of the single-element exposure path using the RF data from the Sonix RP (Ultrasonix Medical Corporation, Richmond, BC) with the reference phantom technique[27]. Three RF data sets were acquired at different locations and times. The first data set was acquired just before US exposure and UCA injection (Dataset I). Two minutes after injecting the UCA or saline the second data set was recorded (Dataset II). Then, a 1 cm section of the descending aorta near the renal artery was exposed at 4 sites, 2 above the bifurcation to the renal artery and 2 below, with 2 mm between exposure sites. At the location of the last US exposed site, a third data set was acquired (Dataset III). The *in situ* location of Dataset III was about 6 mm away from Datasets I and II. A reference dataset from a characterized physical phantom (AS = 0.67 dB/cm-MHz) was recorded using the same system settings. The AS was processed using the technique described by Yao et al.[27] and was then divided between saline-only and UCA rabbits to yield for the 3 datasets/locations (mean ± standard deviation; dB/cm-MHz): AS_{SAI} = 0.80±0.097 & AS_{UCAI} = 0.86±0.16; AS_{SAII} = 0.78±0.094 & AS_{UCAII} = 0.86±0.16; AS_{SAIII} = 0.78±0.079 & AS_{UCAIII} = 0.85±0.24. Note the AS difference in Dataset I (saline-only vs. UCA; 0.080 vs. 0.086) even though this data set was acquired under the same rabbit conditions, that is, prior to injection of either saline or UCA. Further note that AS for saline-only remains about the same for all 3 datasets (0.80, 0.78, 0.78) as does AS for UCA (0.86, 0.86, 0.85). Overall AS means were 0.79±0.089 for saline-only and 0.85±0.18 for UCA, yielding the individual $p_{r(in\ situ)}$ values listed for each exposure condition in **Table 3.1**. For practical purposes by noting how close the individual ASs are between the saline-only and UCA rabbits (relative to their individual standard deviations), an overall AS value of 0.82±0.15 dB/cm-MHz was used to estimate $p_{r(in\ situ)}$ at 3.2 MHz for a propagation distance of 4 cm, the $p_{r(in\ situ)}$. Therefore, the results reported and analyzed herein are the $p_{r(in\ situ)}$ values relative to the overall AS value of 0.82 dB/cm-MHz (**Table 3.1**).

Histology

All rabbits were anesthetized with ketamine hydrochloride and xylazine and then euthanized with CO_2. The rabbit was placed in dorsal recumbency and a ventral midline incision made to expose the abdominal and thoracic cavities. The ribs were cut along the left lateral aspect of the sternum and manually spread open to allow visualization of

the heart. A hemostat was clamped at the origin of the descending aorta. All tissues cranial to this site required to free the aorta were transected with scissors. The aorta, with heart attached, was slowly and carefully removed to the bifurcation of the aorta into common iliac arteries. Precautions were taken to gently remove the aorta in order to keep the endothelium intact. Surrounding fat was carefully removed and the aorta was opened along one lateral aspect adjacent to the renal artery bifurcation. The liver was removed en masse and weighed. A small section of the liver was immediately frozen at -20°C for analysis of lipid content. Two sections of the aorta (the entire arch and a 2 cm section surrounding the renal artery at the site of US exposure) and a representative section of the left liver lobe were then placed in 10% formalin for 24-72 hrs. for subsequent pathological evaluation.

After formalin fixation, sections of each tissue were trimmed off, placed in embedding cassettes, and subsequently processed, embedded in paraffin and cut to 3-µm thickness. Sections were stained with hematoxylin and eosin. The aortic arch was cut transversely into 3-4 sections and placed in one cassette. The 2 cm section of the aorta (1 cm on either side of the renal artery) was cut longitudinally in 3 sections. Three edges were painted with tissue ink for orientation purposes and placed in one cassette. The representative section of the liver (including the central hepatic vein) was trimmed down to 1 x 1 cm and placed in one cassette. One microscope slide was created from each cassette, resulting in 3 microscope slides per animal.

An atherosclerosis score was defined between 0 and 5 using the American Heart Association classification scheme for human atherosclerotic lesions[28]. Score 0 = Absence of atherosclerosis; Score 1 = Presence of isolated foam cells; Score 2 = Lipid accumulation mainly within the foam cells; Score 3 = Lipid accumulation within the foam cells and small pools of extracellular lipid; Score 4 = Intracellular lipid, lipid pools and core of extracellular lipid; and Score 5 = Lipid core and fibrotic layer, or multiple lipid cores and fibrotic layer, or mainly calcified or fibrotic plaque. The atheroma thickness was measured using an ocular micrometer (Olympus America Inc., Center Valley, PA). The condition of the vascular endothelium was also assessed and categorized as mostly, partially or minimally intact. The pathologist (author SS) assigned an

atherosclerosis score, measured the atheroma thickness and evaluated the endothelium for each tissue sample while blinded to exposure conditions.

Plasma von Willebrand Factor

Measurement of vWF was performed as previously described[29] with some modifications. Briefly, a mouse anti-human monoclonal antibody to the N-terminal trypsin and plasmin sensitive region of vWF (Abcam, Cambridge, MA) was diluted in carbonate buffer (pH 9.6), and 96-well microtiter plates were coated with 100 µL per well overnight at 4ºC. The next day, the coating solution was emptied and the plate was washed three times with 0.5% Tween-20 in phosphate-buffered saline (PBS). Wells were then blocked with 0.2% bovine serum albumin (BSA) in PBS for 2 hours on an orbital shaker. After removing the block solution and washing, a vWF standard from human plasma (Calbiochem, La Jolla, CA) was serially diluted and added to the plate. Rabbit plasma samples were diluted 1:100 in 0.05% BSA in PBS. The standard and all samples were plated in duplicate and incubated for 2 hours on an orbital shaker. The plate was emptied and washed again, after which a goat anti-human vWF polyclonal antibody (Abcam, Cambridge, MA) diluted in 0.05% BSA in PBS was added as the sandwich antibody for 1 hour. After emptying and washing the plate, a donkey anti-goat horseradish peroxidase-conjugated polyclonal antibody was diluted in 0.05% BSA in PBS and added to the plate for 1 hour. The chromogenic substrate o-phenylenediamine dihydrochloride (OPD) was combined with 0.05 M phosphate-citrate buffer (pH 5.0) and 30% H_2O_2. After washing, 100 µL of the OPD solution was added to the plate for 30 minutes. The reaction was stopped by addition of 0.5 N H_2SO_4 and the plate was read at 490 nm. A linear standard curve was generated using the duplicate blanked readings from the serially diluted protein standard. Sample readings were interpolated into the standard curve to obtain concentration values. Average intra- and inter-assay coefficients of variation (CV) for rabbit plasma samples were 2.9% and 18.7%. Inter-assay precision was determined by incorporating a control rabbit plasma in each assay. This control was a large amount of plasma obtained in a single blood draw from an animal on chow diet, and was separated into many aliquots to validate inter-assay precision.

Plasma and Liver Lipids

Plasma low-density lipoprotein (LDL), high-density lipoprotein (HDL) and total cholesterol were analyzed using enzymatic colorimetric kits (Wako Chemicals, Richmond, VA). Human control sera (Wako) were included in each assay for quality control. Average intra-assay CV of control sera in each assay were 12% for the LDL assay, 4.0% for HDL and 4.7% for total cholesterol. Average intra-assay CV for rabbit plasma samples were 14% for the LDL assay, 4.0% for HDL and 5.1% for total cholesterol.

Liver lipids were extracted using a modification of the Folch method[30]. A 0.5 g section of liver was placed in a 1:1 mixture of chloroform and methanol, homogenized and gravity filtered. The filtrate was immersed in 0.29% NaCl solution, vortexed briefly and centrifuged. The supernatant was then discarded and the remainder was washed with 0.29% NaCl, transferred to a weighed test tube, evaporated, placed in a desiccator for ≥48 hrs., and weighed to determine total lipids.

Statistical Analysis

Effects of UCA and $p_{r(in\ situ)}$ on vWF expression were evaluated via analysis of covariance[31] for each of the post-exposure time points, with covariate adjustment for the vWF level 1 hour prior to exposure. UCA was encoded as 0="saline only" or 1="saline + Definity®". The differences among the four levels of ultrasound were encoded as variables US_1, US_2 and US_3 according to the orthogonal contrast matrix in **Table 3.2**. US_1 is the contrast between -1=low ($p_{r(in\ situ)}$ of 0 or 0.72 MPa) and 1=high ($p_{r(in\ situ)}$ of 1.4 or 2.1 MPa) acoustic pressures, US_2 is the contrast between 0 and 0.72 MPa, and US_3 is the contrast between 1.4 and 2.1 MPa acoustic pressure. The ANOCOVA model for time point t was of the form:

$$vWF_t = b_{0t} + b_{1t}*UCA + b_{2t}*US_1 + b_{3t}*US_2 + b_{4t}*US_3 + b_{5t}*vWF_{pre} + noise$$

with the above encoding, where vWF_t is the vWF level at time t, vWF_{pre} is the pre-exposure level, b_{0t} is the regression coefficient for the intercept for time point t, b_{1t} is the coefficient for ultrasound contrast agent (UCA) at time t, b_{2t} – b_{4t} are the coefficients for US_1, US_2 and US_3, respectively, at time t, and b_{5t} is the coefficient for the effect at time t

of the pre-exposure level of vWF. The model was run for time points t = 1 hr, 24 hrs, 48 hrs, 7 days, 14 days, and 21 days post-exposure. For each of the 6 time points the coefficients were estimated by least squares multiple linear regression. The statistical computations were performed using R[32]. A conservative Bonferroni adjustment was employed to account for repeated effect testing across six time points.

Results

Plasma cholesterol levels began very low and increased rapidly after rabbits began consuming the cholesterol diet (**Figure 3.2**). At baseline, total cholesterol averaged 39 mg/dL, with approximately 27 mg/dL in LDL and 12 mg/dL in HDL. After consuming the cholesterol diet for 3 weeks, total cholesterol averaged 995 mg/dL, with 537 mg/dL in LDL and 15 mg/dL in HDL. Liver lipids for all rabbits averaged 137±32 mg lipid/g liver (mean±SD).

High-level US (1.4 or 2.1 MPa) resulted in significantly lower vWF one hour post-exposure ($p=0.0127$) than low-level US (0 or 0.72 MPa) (**Figure 3.3**). Conservative Bonferroni adjustment for multiple time points gives an upper bound of $p_{adj}< 0.0762$ for the overall significance of this difference. The other two US variables (contrasts between 0 and 0.72 MPa, and between 1.4 and 2.1 MPa) were not significant ($p>0.1$), thus supporting a reduction in the model for ultrasound effects to the contrast between low and high levels. **Figure 3.4** demonstrates the correlation between vWF levels one hour post exposure and one hour before exposure for low and high levels of ultrasound. The superimposed lines are the least squares lines for low and high levels of ultrasound, obtained from the fitted analysis of covariance model. The difference between the superimposed lines shows the US effect at one hour post-exposure. This difference disappeared within 24 hours. UCA was not a statistically significant factor in this analysis.

Animals receiving the Definity® UCA displayed lower atheroma thickness in the descending aorta as compared to animals receiving saline at the same ultrasound pressure level (**Figure 3.5**). The average atheroma thickness (mean±SEM) was 46±9 μm for Saline at 0 MPa, 55±16 μm for Definity® at 0 MPa, 86±16 μm for Saline at 0.72 MPa, 48±13 μm for Definity® at 0.72 MPa, 98±37 μm for Saline at 1.4 MPa, 45±18 μm

for Definity® at 1.4 MPa, 104±31 μm for Saline at 2.1 MPa, and 62±18 μm for Definity® at 2.1 MPa.

Atherosclerosis scores were assigned by a pathologist blinded to the exposure conditions and are represented in **Figure 3.5**. The average atherosclerosis scores (mean±SEM) were 2.8±0.20 for Saline at 0 MPa, 2.6±0.40 for Definity® at 0 MPa, 2.4±0.25 for Saline at 0.72 MPa, 2.2±0.37 for Definity® at 0.72 MPa, 3.0±0.55 for Saline at 1.4 MPa, 2.2±0.37 for Definity® at 1.4 MPa, 2.6±0.40 for Saline at 2.1 MPa, and 2.5±0.37 for Definity® at 2.1 MPa. Evaluation of the vascular endothelium is presented in **Table 3.3**.

Histological evaluation of tissues excised from the rabbits at 42 days revealed profound diet-induced atherosclerotic changes. Analysis of the abdominal aorta revealed atherosclerotic damage including atheroma, extracellular lipids, foam cells, calcification and vacuolar changes. Of the 41 animals on the study, atheroma was noted in all animals, extracellular lipids in 24 animals, foam cells were noted in all 41 animals, calcification in 1 animal and vacuolar changes in 6 animals. Analysis of the aortic arch revealed similar findings. Atheroma was noted in all 41 animals, extracellular lipids in 35 animals, foam cells in all animals, calcification in 7 animals and fibrosis in 5 animals. Damage to the liver included steatosis of hepatocytes in 40 animals, steatosis of Kupffer cells in 39 animals, steatohepatitis in 3 animals, and autolysis in 2 animals.

Discussion

Ultrasound has developed into an extremely versatile imaging modality both experimentally and diagnostically. As with any diagnostic technology, the balance of its risks and benefits must be weighed before a decision can be made regarding its safe use. While UCAs are valuable diagnostically, concerns have been raised regarding their safety. In addition to the numerous bioeffects observed experimentally, the FDA issued an advisory in 2007 indicating that cardiopulmonary complications and death have been observed in patients soon after the administration of some approved UCAs, including Definity®[1]. The further development and use of UCAs is pending additional *in vivo* data regarding their safety.

Our objective was to determine if the interaction of US with UCAs in the vasculature impacts the onset or severity of atherosclerosis. In this study, we undertook a risk-based assessment of US bioeffects in a cholesterol-fed rabbit model. Plasma cholesterol levels increased dramatically (**Figure 3.2**), rising above 1500 mg/dL in some animals. Elevated plasma cholesterol is a substantial stress on the vascular system, and we assayed for vWF to determine the extent of this stress. The vWF biomarker could also potentially provide information about any additional stress of the US+UCA interaction on the vascular system. As we expected, vWF increased as a result of the vascular stress induced by the atherogenic diet and elevated cholesterol.

However, we also observed a decrease in plasma vWF after US exposure in animals exposed to 1.4 or 2.1 MPa US as compared to those exposed to 0 or 0.72 MPa, after adjustment for pre-exposure vWF levels (**Figure 3.3**). The decrease was observed when blood was drawn after exposure, although the pre- and post-exposure time points were less than two hours apart. This raised questions about any potential effect of ultrasound exposure on plasma vWF. After 24 hours, vWF returned to levels primarily determined by consumption of the atherogenic diet and continued a gradual decrease until the completion of the study, possibly due to progressive endothelial dysfunction[33].

Interestingly, both decreased vWF and lower atheroma thickness were observed in the US+UCA groups. These results suggest an impact of US+UCA on vascular integrity. There is a substantial body of literature documenting the potential of US to damage tissue, including US-induced lesions and hemorrhage in lung tissue[34] observed in our lab. In the experiments described here, we may be seeing US-induced damage to the aorta, including the intima and endothelial monolayer. If that is so, some of the circulating vWF may be recruited to the site of damage in accordance with its coagulant role[11] to form a platelet plug before the vessel is re-endothelialized. It is unknown how plasma vWF levels change after such an event, preventing us from determining if the decrease represents an injury due to US+UCA exposure.

The post-exposure decrease in vWF is probably not due to reduced secretion by endothelial cells. Clearance time of unused plasma vWF in rabbits is 240 min[35], so a

decrease in vWF would probably not reflect reduced secretion during the time frame of US exposure.

Animals receiving UCA also displayed lower atheroma thickness in the descending aorta as compared to animals receiving saline only at three weeks post exposure. These results may suggest that at the time of US exposure the rabbits receiving UCA experienced disruption of atheromas located at the site of exposure, while the saline-only groups did not experience this. Thus, the artery walls in the UCA groups would represent only 3 weeks growth and repair following US+UCA exposure whereas the saline-only groups represent continual thickening throughout the study. The intima is the main driver of atheroma thickness[36], so US would presumably have affected the vascular intima.

We cannot rule out the possibility that less atheroma could simply be an artifact of tissue processing by the investigators or histotechnologist. However, tissue processing and histological evaluation were blinded and any changes in tissue morphology due to processing would not account for the results observed selectively in the US+UCA groups. We did not observe consistent long-term changes in the vascular endothelium across treatment groups upon pathological evaluation of the vascular endothelium at 42 days, but any damage to the endothelium would presumably have been repaired by then[37]. Ultrasonic disruption of an atheroma could potentially lead to thrombosis and myocardial infarction, and our results could be a first step in uncovering a previously unknown bioeffect of UCAs. We should also consider the alternative possibility that this is a beneficial effect. The exposure-response relationship for the US+saline animals shown in **Figure 3.5** could infer that US promotes deposition of atherogenic materials and consequent plaque growth, but coadministration of UCA protects against this effect. Atheroma thickness for 0 MPa US was very similar among animals receiving UCA or saline only, but the groups displayed a diverging trend upon introduction of US. Other beneficial therapeutic uses of UCAs have been explored, including thrombolysis in myocardial infarction[38] and gene or drug delivery[39]. Our findings may lead to additional exploration of the beneficial effects of UCAs in diagnostic and therapeutic applications. While our results are preliminary, they highlight the need for further research investigating US-UCA interactions *in vivo.*

Cholesterol, liver lipid levels and histology underscore the impact of the atherogenic diet. The rabbit is a representative model of commonly identified changes in human atherosclerotic arteries. We were able to use a human classification scheme to evaluate the pathology of atherosclerotic lesions in the rabbits, providing further justification for the model. We thus chose the rabbit as a straightforward and representative model for these experiments. We decided that all of the rabbits would be on only the atherogenic diet, allowing for an exposure-dependent effect if present, but with the largest possible number of animals per group.

In conclusion, we have described a risk-based assessment of contrast US bioeffects in a cholesterol-fed rabbit model. The contrast US procedure affected the vasculature as reflected by transient changes in plasma vWF and long-term differences in atheroma thickness. Future research is warranted to fully characterize the effects of this procedure, with the long-term goal of defining the specific conditions at which this procedure is safe for routine clinical use.

Acknowledgements

This work was supported by NIH R37EB002641. The authors do not report any conflicts of interest. We acknowledge Jennifer King, Michael Tu, Rami Abuhabsah, Matt Lee, Saurabh Kukreti, Shreyas Mathur, Michael Kurowski and Provena Covenant Medical Center for their contributions.

References

1. Miller DL, Averkiou MA, Brayman AA, Everbach EC, Holland CK, Wible JH, Wu J. Bioeffects considerations for diagnostic ultrasound contrast agents. *J. Ultrasound Med.* 27:611-616 (2008).

2. Roger VL, Go AS, Lloyd-Jones DM, Adams RJ, Berry JD, Brown TM, Carnethon MR, Dai S, de Simone G, Ford ES *et al.* Heart disease and stroke statistics-2011 update: a report from the American Heart Association. *Circulation* 123:e18-e209 (2011).

3. Dalecki D, Raeman CH, Child SZ, Cox C, Francis CW, Meltzer RS, Carstensen EL. Hemolysis in vivo from exposure to pulsed ultrasound. *Ultrasound Med. Biol.* 23:307-313 (1997).

4. Miller DL, Quddus J. Diagnostic ultrasound activation of contrast agent gas bodies induces capillary rupture in mice. *Proc. Natl. Acad. Sci. USA* 97:10179-10184 (2000).

5. Kobayashi N, Yasu T, Yamada S, Kudo N, Kuroki M, Kawakami M, Miyatake K, Saito M. Endothelial cell injury in venule and capillary induced by contrast ultrasonography. *Ultrasound Med. Biol.* 28:949-956 (2002).

6. Chen S, Kroll MH, Shohet RV, Frenkel P, Mayer SA, Grayburn PA. Bioeffects of myocardial contrast microbubble destruction by echocardiography. *Echocardiography* 19:495-500 (2002).

7. Zachary JF, Blue JP, Miller RJ, O'Brien WD. Vascular lesions and s-thrombomodulin concentrations from auricular arteries of rabbits infused with microbubble contrast agent and exposed to pulsed ultrasound. *Ultrasound Med. Biol.* 32:1781-1791 (2006).

8. Zachary JF, Hartleben SA, Frizzell LA, O'Brien WD, Jr. Arrhythmias in rat hearts exposed to pulsed ultrasound after intravenous injection of a contrast agent. *J. Ultrasound Med.* 21:1347-1356 (2002).

9. De Meyer GR, Hoylaerts MF, Kockx MM, Yamamoto H, Herman AG, Bult H. Intimal deposition of functional von Willebrand factor in atherogenesis. *Arterioscler. Thromb. Vasc. Biol.* 19:2524-2534 (1999).

10. Sadler JE. Biochemistry and genetics of von Willebrand factor. *Annu. Rev. Biochem.* 67:395-424 (1998).

11. Mannucci PM. Treatment of von Willebrand's Disease. *N. Engl. J. Med.* 351:683-694 (2004).

12. Constans J, Conri C. Circulating markers of endothelial function in cardiovascular disease. *Clin. Chim. Acta* 368:33-47 (2006).

13. Spiel AO, Gilbert JC, Jilma B. von Willebrand factor in cardiovascular disease: focus on acute coronary syndromes. *Circulation* 117:1449-1459 (2008).

14. Kucharska-Newton AM, Couper DJ, Pankow JS, Prineas RJ, Rea TD, Sotoodehnia N, Chakravarti A, Folsom AR, Siscovick DS, Rosamond WD. Hemostasis, inflammation, and fatal and nonfatal coronary heart disease: long-term follow-up of the atherosclerosis risk in communities (ARIC) cohort. *Arterioscler. Thromb. Vasc. Biol.* 29:2182-2190 (2009).

15. Frankel DS, Meigs JB, Massaro JM, Wilson PW, O'Donnell CJ, D'Agostino RB, Tofler GH. Von Willebrand factor, type 2 diabetes mellitus, and risk of cardiovascular disease: the framingham offspring study. *Circulation* 118:2533-2539 (2008).

16. Haghjooyjavanmard S, Nematbakhsh M, Monajemi A, Soleimani M. von Willebrand factor, C-reactive protein, nitric oxide, and vascular endothelial growth factor in a dietary reversal model of

hypercholesterolemia in rabbit. *Biomed. Pap. Med. Fac. Univ. Palacky Olomouc Czech Repub.* 152:91-95 (2008).

17. King JL, Miller RJ, Blue JP, O'Brien WD, Erdman JW. Inadequate dietary magnesium intake increases atherosclerotic plaque development in rabbits. *Nutr. Res.* 29:343-349 (2009).

18. O'Brien WD, Jr., Simpson DG, Frizzell LA, Zachary JF. Superthreshold behavior and threshold estimates of ultrasound-induced lung hemorrhage in adult rats: role of beamwidth. *IEEE Trans. Ultrason. Ferroelectr. Freq. Control* 48:1695-1705 (2001).

19. O'Brien WD, Jr., Simpson DG, Ho MH, Miller RJ, Frizzell LA, Zachary JF. Superthreshold behavior and threshold estimation of ultrasound-induced lung hemorrhage in pigs: role of age dependency. *IEEE Trans. Ultrason. Ferroelectr. Freq. Control* 50:153-169 (2003).

20. O'Brien WD, Jr., Simpson DG, Frizzell LA, Zachary JF. Threshold estimates and superthreshold behavior of ultrasound-induced lung hemorrhage in adult rats: role of pulse duration. *Ultrasound Med. Biol.* 29:1625-1634 (2003).

21. O'Brien WD, Jr., Simpson DG, Frizzell LA, Zachary JF. Superthreshold behavior of ultrasound-induced lung hemorrhage in adult rats: role of pulse repetition frequency and exposure duration revisited. *J. Ultrasound Med.* 24:339-348 (2005).

22. Zachary JF, Sempsrott JM, Frizzell LA, Simpson DG, O'Brien WD, Jr. Superthreshold behavior and threshold estimation of ultrasound-induced lung hemorrhage in adult mice and rats. *IEEE Trans. Ultrason. Ferroelectr. Freq. Control* 48:581-592 (2001).

23. Zachary JF, Frizzell LA, Norrell KS, Blue JP, Jr., Miller RJ, O'Brien WD, Jr. Temporal and spatial evaluation of lesion reparative responses following superthreshold exposure of rat lung to pulsed ultrasound. *Ultrasound Med. Biol.* 27:829-839 (2001).

24. Raum K, O'Brien WD, Jr. Pulse-echo field distribution measurement technique of high-frequency ultrasound sources. *IEEE Trans. Ultrason. Ferroelectr. Freq. Control* 44:810-815 (1997).

25. AIUM/NEMA (American Institute of Ultrasound in Medicine and National Electrical Manufacturers Association). *Standard for real-time display of thermal and mechanical acoustic output indices on diagnostic ultrasound equipment* Rev. 2 (Laurel, MD and Rosslyn, VA, 2004).

26. FDA (US Food and Drug Administration) Center for Devices and Radiological Health. *Information for Manufacturers Seeking Marketing Clearance of Diagnostic Ultrasound Systems and Transducers* (Rockville, MD, 1997).

27. Yao LX, Zagzebski JA, Madsen EL. Backscatter coefficient measurements using a reference phantom to extract depth-dependent instrumentation factors. *Ultrason. Imaging* 12:58-70 (1990).

28. Kumar V, Fausto N, Abbas AK. *Robbins and Cotran Pathologic Basis of Disease*, 7th edn (Saunders, 2005).

29. Smith BW, Strakova J, King JL, Erdman JW, Jr., O'Brien WD, Jr. Validated sandwich ELISA for the quantification of von Willebrand factor in rabbit plasma. *Biomark. Insights* 5:119-127 (2010).

30. Folch J, Lees M, Sloane Stanley GH. A simple method for the isolation and purification of total lipides from animal tissues. *J. Biol. Chem.* 226:497-509 (1957).

31. Faraway JJ. *Linear Models with R*, 1st edn (Chapman & Hall/CRC, 2004).

32. R Development Core Team. *R: A language and environment for statistical computing* 2.11.1 edn (2008).

33. Bonetti PO. Endothelial Dysfunction: A Marker of Atherosclerotic Risk. *Arterioscler. Thromb. Vasc. Biol.* 23:168-175 (2002).

34. Zachary JF, O'Brien WD, Jr. Lung lesions induced by continuous- and pulsed-wave (diagnostic) ultrasound in mice, rabbits, and pigs. *Vet. Pathol.* 32:43-54 (1995).

35. Sodetz JM, Pizzo SV, McKee PA. Relationship of sialic acid to function and in vivo survival of human factor VIII/von Willebrand factor protein. *J. Biol. Chem.* 252:5538-5546 (1977).

36. Tabas I, Williams KJ, Borén J. Subendothelial lipoprotein retention as the initiating process in atherosclerosis: update and therapeutic implications. *Circulation* 116:1832-1844 (2007).

37. Fadini GP, Agostini C, Sartore S, Avogaro A. Endothelial progenitor cells in the natural history of atherosclerosis. *Atherosclerosis* 194:46-54 (2007).

38. Hitchcock KE, Holland CK. Ultrasound-assisted thrombolysis for stroke therapy: better thrombus break-up with bubbles. *Stroke* 41:S50-53 (2010).

39. Suzuki J, Ogawa M, Takayama K, Taniyama Y, Morishita R, Hirata Y, Nagai R, Isobe M. Ultrasound-microbubble-mediated intercellular adhesion molecule-1 small interfering ribonucleic acid transfection attenuates neointimal formation after arterial injury in mice. *J. Am. Coll. Cardiol.* 55:904-913 (2010).

Figures and Tables

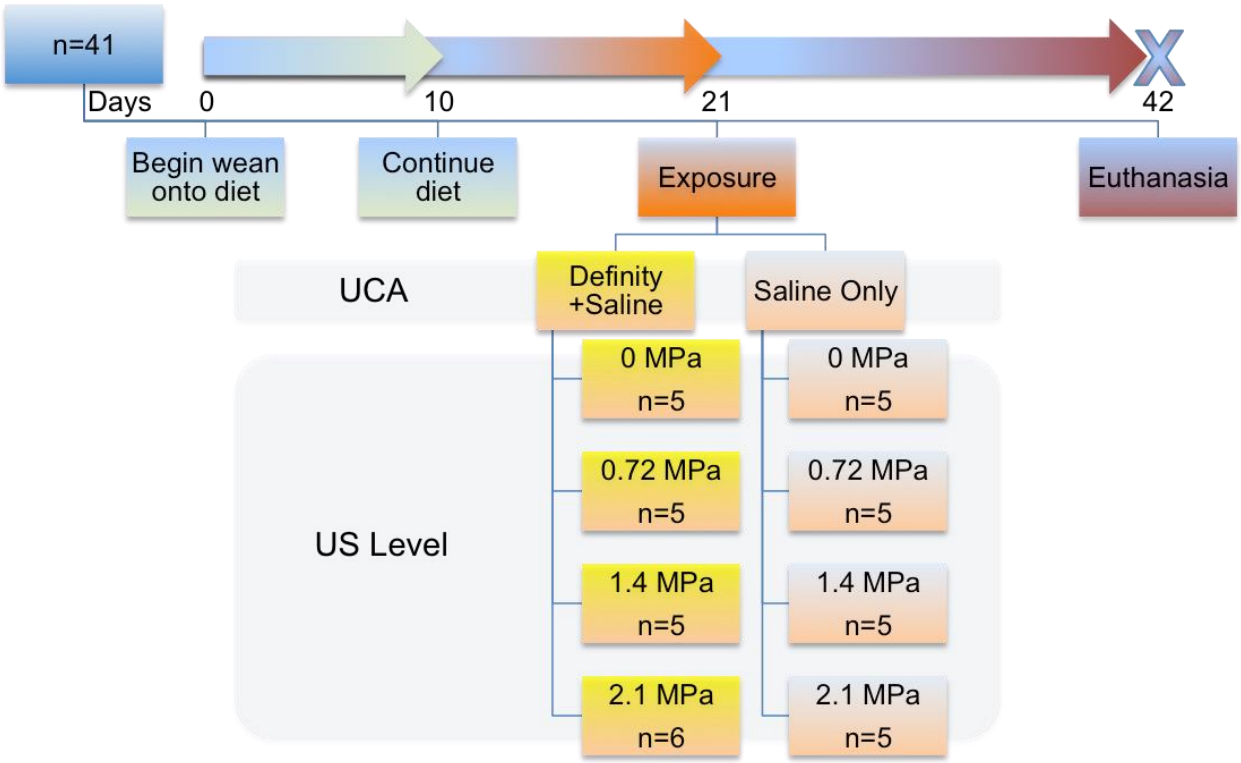

Figure 3.1. Study design with 41 four-month-old male New Zealand White rabbits. Rabbits (n=5-6 randomly assigned per group) were gradually introduced to an atherogenic diet consisting of 1% cholesterol, 10% fat, 0.11% Mg over 10 days and continued to consume the diet for 11 more days. On day 21, rabbits underwent the contrast US procedure using either the UCA Definity® in saline vehicle or saline alone at 4 different US pressure levels. Rabbits were euthanized at 42 days and tissues were collected for histology. US, ultrasound; UCA, ultrasound contrast agent.

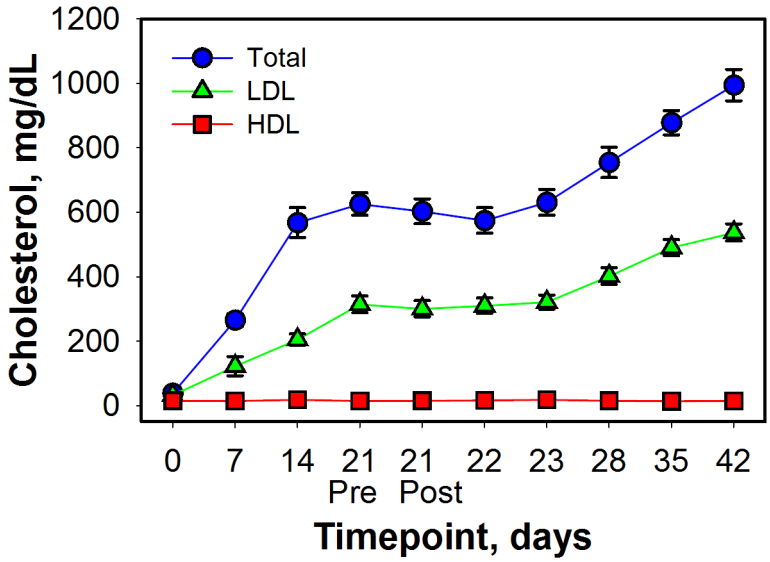

Figure 3.2. Time course plot for plasma cholesterol. Plasma LDL, HDL and total cholesterol were analyzed using enzymatic colorimetric kits (Wako Chemicals, Richmond, VA). Human control sera (Wako) were included in each assay for quality control. Serial blood samples were collected from each rabbit at the timepoints indicated. "21 pre" and "21 post" denote 1 hour pre and post exposure, respectively. Bars are SEM, n=4-41 per timepoint.

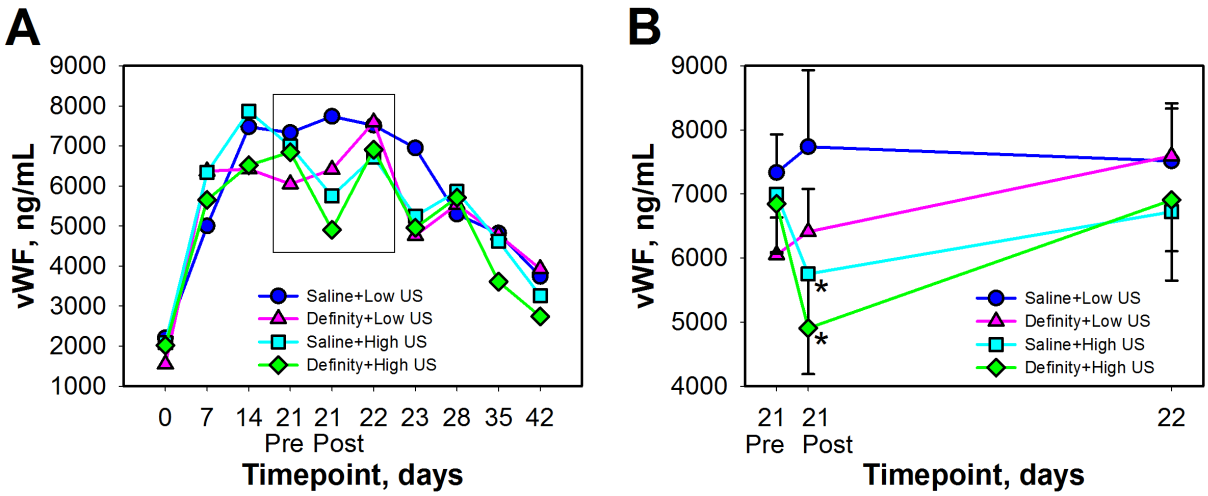

Figure 3.3. Time course plots for plasma von Willebrand Factor (vWF) over the course of the entire study (A) and near exposure time (B, enlargement of the boxed area in graph A and displaying a linear time course on the x-axis). vWF was assayed using a sandwich ELISA procedure. Serial blood samples were collected from each rabbit at the timepoints indicated. "Low" US indicates ultrasound exposure at 0 or 0.72 MPa, "High" US indicates 1.4 or 2.1 MPa. These pressure levels were combined for the purposes of statistical analysis. *significantly different from high US ($p=0.0127$, $p_{adj} < 0.0762$). Bars are SEM, n=10-11 per group. US, ultrasound; UCA, ultrasound contrast agent.

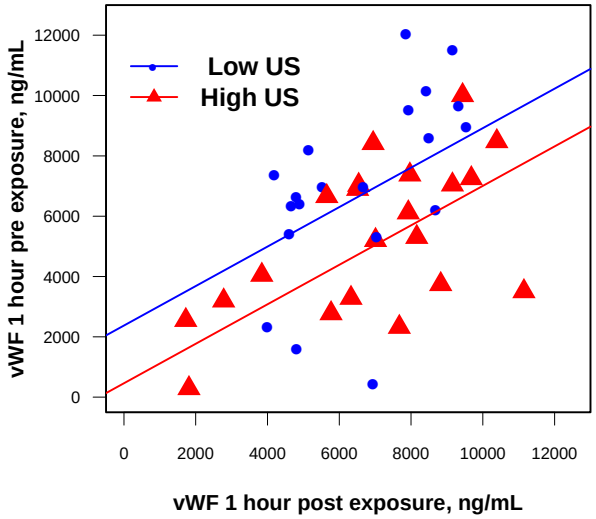

Figure 3.4. Scatter plot of vWF levels one hour post exposure versus one hour pre-exposure for low and high levels of ultrasound exposure with fitted ANOCOVA lines for each group. The difference between the superimposed lines is the US effect at one hour post exposure.

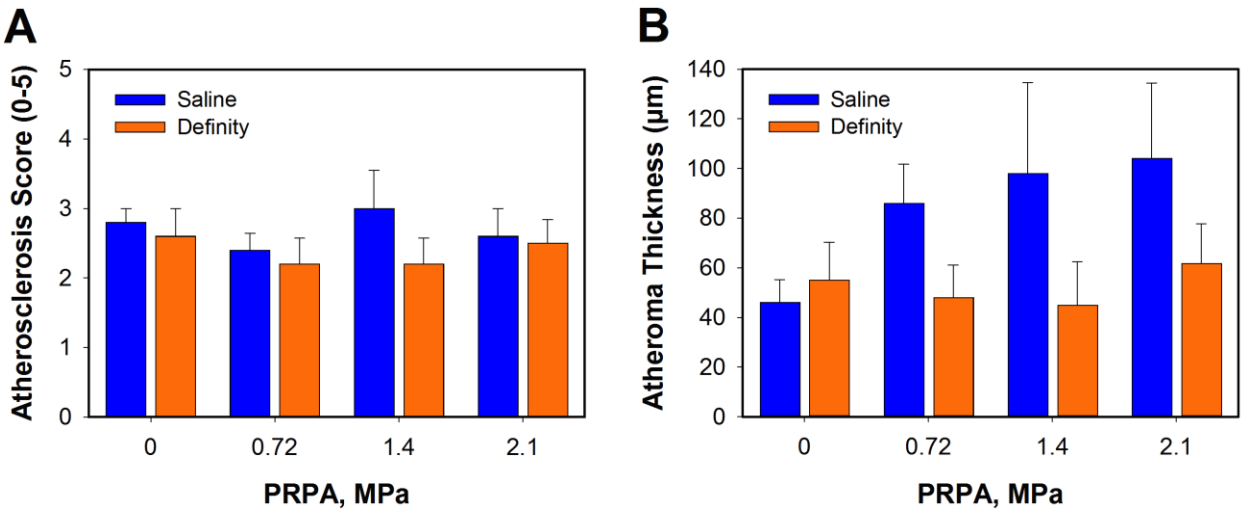

Figure 3.5. Atherosclerosis score and atheroma thickness as a function of the in situ peak rarefactional pressure amplitude (PRPA). A 2 cm section of the abdominal aorta was excised from the area surrounding the renal artery and placed in 10% formalin for 24-72 hr. An atherosclerosis score was defined between 0 and 5 using the American Heart Association classification scheme for human atherosclerotic lesions. Score 0 = Absence of atherosclerosis; Score 1 = Presence of isolated foam cells; Score 2 = Lipid accumulation mainly within the foam cells; Score 3 = Lipid accumulation within the foam cells and small pools of extracellular lipid; Score 4 = Intracellular lipid, lipid pools and core of extracellular lipid; and Score 5 = Lipid core and fibrotic layer, or multiple lipid cores and fibrotic layer, or mainly calcific or mainly fibrotic. The pathologist assigned an atherosclerosis score and measured the atheroma thickness for each tissue sample while blinded to exposure conditions. Animals are grouped based on US exposure level and UCA. Bars are SEM, n=5-6 per group. US, ultrasound; UCA, ultrasound contrast agent; PRPA, in situ peak rarefactional pressure amplitude.

Rabbit Group	$p_{r(\text{in vitro})}$ (MPa)	AS (dB/cm-MHz)	$p_{r(\text{in situ})}$ (MPa)	MI
Saline-only	0	0.79±0.089	0	
Saline-only	2.4	0.79±0.089	0.75±0.092	
Saline-only	4.7	0.79±0.089	1.5±0.18	
Saline-only	7.1	0.79±0.089	2.2±0.27	
UCA	0	0.85±0.18	0	
UCA	2.4	0.85±0.18	0.69±0.16	
UCA	4.7	0.85±0.18	1.3±0.31	
UCA	7.1	0.85±0.18	2.0±0.47	
Overall	0	0.82±0.15	0	0
Overall	2.4	0.82±0.15	0.72±0.14	0.64±0.011
Overall	4.7	0.82±0.15	1.4±0.28	1.3±0.041
Overall	7.1	0.82±0.15	2.1±0.42	1.8±0.060

Table 3.1. Ultrasound exposimetry for the four exposure groups.

$p_{r(\text{in situ})}$ (MPa)	Ultrasound Encoding Variable		
	US_1	US_2	US_3
0	-1	-1	0
0.72	-1	1	0
1.4	1	0	-1
2.1	1	0	1

Table 3.2. Orthogonal contrast matrix for encoding four levels of ultrasound acoustic pressure in the analysis of covariance model.

CHAPTER 4: Contrast ultrasound imaging does not affect Hsp70 expression in cholesterol-fed rabbit aorta

Abstract

Objective – Diagnostic ultrasound imaging is enhanced by the use of circulating microbubble contrast agents (UCAs), but the interactions between ultrasound, UCAs, and vascular tissue are not fully understood. We hypothesized that ultrasound with UCA would stress the vascular tissue and increase levels of Hsp70, a cellular stress protein.

Methods – Male New Zealand White rabbits (n=32) were fed a standard chow diet (n=4) or a 1% cholesterol, 10% fat and 0.11% magnesium diet (n=28). At 21 days, 24 rabbits on cholesterol diet were either exposed to ultrasound (3.2 MHz f/3 transducer, 2.1 MPa, Mechanical Index=1.17, 10 Hz pulse repetition frequency, 1.6 μs pulse duration, 2 min exposure duration at 4 sites along the aorta) with the UCA Definity® (1x concentration, 1 mL/min) or sham exposed with a saline vehicle injection (n=12 per group). Four rabbits on cholesterol diet and four on chow diet served as cage controls, and were not exposed to ultrasound or restrained for blood sample collection. Animals were euthanized 24 hours after exposure and aortas quickly isolated and frozen in liquid nitrogen. Aorta lysates from the area of ultrasound exposure were analyzed for Hsp70 protein level by Western blot. Blood plasma was analyzed for cholesterol, Hsp70, and von Willebrand Factor (vWF), a marker of endothelial function.

Results – Plasma total cholesterol levels increased to an average of 705 mg/dL. Ultrasound did not affect plasma vWF, plasma Hsp70, or aorta Hsp70. Restraint increased Hsp70 ($p<0.001$ by ANOVA).

Conclusions – Restraint, but not ultrasound with UCA or cholesterol feeding, significantly increased Hsp70.

Introduction

Cardiovascular disease (CVD) remains the leading cause of death in the United States and worldwide[1]. Atherosclerosis, the deposition and development of lipid-rich arterial plaques, is the pathogenic process underlying most cardiovascular events[2,3]. Evidence suggests atherosclerosis is reversible in its early stages[4], but it develops asymptomatically, and is frequently undetected until it results in heart attacks and strokes. Early detection is thus a critical frontier in reducing deaths from CVD. Ultrasound imaging is a flexible, inexpensive, widely used, and real-time imaging modality that can be used for early detection and diagnosis of CVD[5-8]. Diagnostic ultrasound imaging is improved by the use of microbubble ultrasound contrast agents (UCAs), which are injected intravenously prior to imaging. The interaction of ultrasound with UCAs in the circulation causes them to oscillate or collapse, and aids in delineation of tissue. In some cardiac imaging situations, ultrasound alone is unable to provide a clear image, but the addition of UCAs can improve images to diagnostic quality[9].

Although the clinical benefits of UCAs are established, the effects of the ultrasound-UCA interaction on cardiac and arterial tissue are not well understood. Contrast ultrasound imaging of the cardiovascular system is not typically performed in asymptomatic patients without risk factors. Rather, most patients will have some degree of pathology present[10]. Rabbits were fed a cholesterol diet to reflect this scenario, increasing the translational relevance of the model. We performed contrast ultrasound imaging of the aorta in cholesterol-fed rabbits, and hypothesized that the interaction of ultrasound with UCAs in the blood would stress the vascular tissue and increase levels of Heat shock protein 70 (Hsp70), a cellular stress protein.

Materials and Methods

Animals and Experimental Design

The University of Illinois Institutional Animal Care and Use Committee approved all live animal procedures. Twenty-eight male NZW rabbits (Myrtle's Rabbitry, Thompson's Station, TN; and Covance, Princeton, NJ) consumed a 1% cholesterol, 10% fat, 0.11% magnesium diet (5TZB; TestDiet, Richmond, IN) for three weeks as previously described[11] (**Figure 4.1**). An additional 4 rabbits consumed a chow diet (2031 Global

High Fiber Rabbit Diet; Harlan Teklad, Madison, WI), throughout the study. Animals were provided 140 g/day of feed. After three weeks, 24 animals on cholesterol diet were randomized to receive either an ultrasound exposure at 2.1 MPa with the UCA Definity® (n=12) or a sham exposure with the saline UCA vehicle (n=12). Blood samples were obtained from the lateral saphenous vein weekly, as well as 1 hour prior to, 1 hour after, and 24 hours after ultrasound exposure. Animals were then euthanized 24 hours after ultrasound exposure to allow adequate time for induction of Hsp70[12,13]. Aorta tissue from the site of ultrasound exposure (5 mm length, 10-20 mg) was rapidly isolated, rinsed with cold PBS to remove blood, frozen in liquid nitrogen, and stored at -50ºC.

Exposimetry

The ultrasound procedures have been previously described in significant detail using a calibrated polyvinylidene fluoride (PVDF) membrane hydrophone (Y-34–3598 EW295, GEC Marconi, Chelmsford, UK) with a 0.5-mm-diameter active element [11,14]. Ultrasound exposures were performed using a 3.2-MHz f/3, 19-mm-diameter lithium-niobate single-element transducer with intravenous infusion of Definity® UCA (2.6% Definity® in saline, 1 mL/min, 15-20 min total infusion time). A separate ultrasound system was used to guide and position the single-element transducer for exposures (Ultrasonix Medical Corporation, Richmond, British Columbia, Canada). The transducer was regularly calibrated in degassed water. To account for *in vivo* attenuation of the ultrasound signal, we also calculated the attenuation slope and *in situ* derated peak rarefactional pressure amplitude using the radio frequency dataset. The *in situ* peak rarefactional pressure amplitude in this study was 2.1 MPa, corresponding to a Mechanical Index of 1.17, with 10 Hz pulse repetition frequency, 1.6 μs pulse duration, and 2 minute exposure duration at each of 4 sites along the abdominal aorta (exposure 1, 2 mm cranial to the cranial edge of renal artery; exposure 2, 2 mm caudal to exposure 1; exposure 3, 2 mm caudal to exposure 2; exposure 4, 2 mm caudal to exposure 3).

Western Blotting

Aorta tissue was homogenized in 4ºC Radioimmunoprecipitation Assay (RIPA) buffer with protease inhibitor cocktail (Sigma-Aldrich, St. Louis, MO) using a glass tissue

grinder (Pyrex; Corning, Tewksbury, MA) followed by a handheld motorized homogenizer (Polytron PT1200E; Kinematica Inc., Bohemia, NY). Lysates were kept on ice with agitation for 30 min, centrifuged for 10 min at 10,000 x *g* and 4ºC, aliquotted, and frozen at -50ºC. Protein concentrations were determined in triplicate with a Bradford assay (Bio-Rad, Hercules, CA). Lysates were then diluted 1:1 in Laemmli sample buffer with 5% β-mercaptoethanol (Bio-Rad), heated at 95ºC for 5 minutes, and centrifuged at 3000 x *g* for 1 minute. Equal amounts of total protein (20 µg per sample) were loaded onto 10% Tris-Glycine gels (Mini-Protean TGX; Bio-Rad), and electrophoresis was performed for 35 minutes at 200 V (Mini-Protean Tetra Cell with PowerPac HC power supply; Bio-Rad). Proteins were then transferred onto nitrocellulose membranes with a semi-dry transfer cell (Bio-Rad) for 30 minutes at 15 V. Total protein transfer was verified by staining with 0.1% Ponceau S (Sigma-Aldrich) for 5 min, and the stain was then removed by washing membranes in 0.1 M NaOH for 30 seconds, followed by a brief rinse in deionized water. Western blotting was performed with the Fast Western kit (Pierce Biotechnology, Rockford, IL) according to the manufacturer's instructions, using a mouse monoclonal anti-Hsp70 antibody (clone C92F3A-5; Enzo Life Sciences Inc., Farmingdale, NY) with mouse monoclonal anti-β-actin (clone AC-15; Novus Biologicals, Littleton, CO) as a loading control. Purified Hsp70 and Hsc70 (Enzo) were included as positive and negative controls, respectively. Membranes were imaged using a ChemiDoc XRS system with Quantity One software (Bio-Rad). Data are expressed as density of the Hsp70 band divided by density of the β-actin band after local background subtraction.

Blood Analysis

Plasma total cholesterol, LDL, HDL, and triglyceride levels were determined in triplicate using enzymatic colorimetric kits (Wako Chemicals, Richmond, VA) with human control sera (Wako) included in each assay to evaluate precision. Coefficient of Variation (CV) was used as a measure of precision. The intra-assay CVs for control sera were 5.0% for total cholesterol, 8.1% for LDL, 5.3% for HDL, and 6.6% for triglycerides. The inter-assay CVs for control sera were 8.2% for total cholesterol, 8.0% for LDL, 23% for HDL, and 16% for triglycerides. The intra-assay CVs for rabbit plasma samples were 4.1% for total cholesterol, 5.7% for LDL, 3.7% for HDL, and 4.5% for

triglycerides. Measurement of plasma vWF was performed by ELISA as previously described[15]. The intra-assay CV for rabbit plasma vWF was 2.3%. Plasma Hsp70 was measured in duplicate by ELISA (Enzo) according to the manufacturer's instructions. Average intra-assay CV for the Hsp70 ELISA was 2.7%, and average inter-assay CV was 42%.

Statistical Analysis

Feed intakes, body weights, blood cholesterol, and Hsp70 data were evaluated with an analysis of variance (ANOVA) or analysis of covariance (ANOCOVA) approach in the general linear mixed models procedure of SAS 9.3 as previously described[16]. Plasma and aorta Hsp70 were also evaluated for correlation using simple linear regression in SAS. vWF data were analyzed in R as previously described[11]. Repeated measures analyses incorporated baseline values as a covariate random effect when the term contributed significantly to the statistical model. Datasets that did not meet the assumption of normality (Shapiro-Wilk $W>0.9$ or Spearman rank-order correlation $p<0.05$) were log-transformed. Bonferroni adjustments for multiple comparisons were made when necessary, and statistical significance was declared at $p<0.05$.

Results

Feed intake and body weights

Chow-fed animals consumed all 140 g/day they were provided throughout the study. Feed intake decreased significantly over time in cholesterol diet groups. By week 3, feed intake decreased significantly in cholesterol-fed animals to 88 g/day compared with 140 g/day for those fed chow ($p<0.05$). Body weights averaged 3.0 kg at baseline and 3.3 kg after 3 weeks, and did not differ among diet groups ($p=0.16$, adjusted for baseline body weight). Ultrasound did not affect feed intake ($p=0.35$) or body weight ($p=0.97$).

Contrast ultrasound does not affect circulating cholesterol or vWF

Plasma total cholesterol initially averaged 25 mg/dL and quickly escalated after introduction of the cholesterol diet, reaching an average of 705 mg/dL by the end of the study ($p<0.0001$, **Figure 4.2a**). No difference in plasma cholesterol levels was observed between animals receiving ultrasound with contrast agent and animals receiving the

sham treatment (p=0.57). Plasma LDL increased in parallel with total cholesterol, reaching 468 mg/dL after 3 weeks. LDL decreased after the experimental procedure at 3 weeks in both sham and ultrasound-exposed animals (p<0.001), and returned to pre-treatment levels 24 hours later. HDL levels remained unchanged throughout the study, and averaged 41 mg/dL. Plasma triglyceride levels increased from 37.2 mg/dL to 130 mg/dL after consumption of the cholesterol diet (p<0.0001), but were not altered by the ultrasound procedure. Plasma vWF levels also increased from 166 mg/dL to 2840 mg/dL during cholesterol feeding, but did not change significantly 1 hour (p=0.72) or 24 hours (p=0.27) post-ultrasound compared with animals receiving the sham treatment (**Figure 4.2b**).

Contrast ultrasound does not affect aorta or plasma Hsp70 protein levels

Rabbits that had been restrained for serial blood sample collection had significantly higher aorta Hsp70 than control rabbits that had not been restrained, regardless of diet (p<0.001, **Figure 4.3**). Ultrasound with UCA did not significantly affect aorta Hsp70 levels. Plasma Hsp70 was significantly lower at 22 days than prior to experimental procedures on day 21, regardless of ultrasound treatment group (p<0.01, **Figure 4.4a**), but was otherwise not significantly altered throughout the study. No correlation was observed between tissue and plasma Hsp70 levels 24 hours post-ultrasound exposure ($F_{0.05}$ (1,9)=0.9, r^2=0.083, p=0.36 for sham+saline; $F_{0.05}$ (1,9)=0.04, r^2=0.005, p=0.84 for ultrasound+UCA; **Figure 4.4b**). One animal had plasma Hsp70 levels an average of 10 standard deviations above the mean throughout the study (including at baseline), and was therefore excluded from the dataset during analysis.

Discussion

When exposed to ultrasound, microbubbles dynamically expand and contract[17] in response to the temporal varying acoustic pressure amplitude. Ultrasound induces oscillation of UCAs at lower pressure levels, and collapse at higher pressures. The biophysical interaction of ultrasound with circulating microbubbles increases the echogenicity of blood and results in improved contrast between blood and tissue. For this reason, UCAs have proven useful in enhancement of clinical ultrasound images. The ultrasound-UCA interaction is useful for imaging, but may cause other biological

effects. Although clinical trials and meta-analyses have recently dispelled concerns over the safety of UCAs in human patients[18-23], there is a large experimental research literature that has not been controverted. Ultrasound and UCAs have induced capillary rupture and hemorrhage[24-26], cardiac damage[27] and arrhythmias[28], and impaired vascular endothelial function[29] in animal studies. Ultrasound has been shown to mechanically disturb cell membranes, inducing temporary permeability in a phenomenon known as sonoporation[30-35]. Based on these studies, we hypothesized that the interaction of ultrasound with UCAs would stress the vasculature at the site of ultrasound exposure, resulting in increased levels of the stress protein Hsp70.

Fundamentally, proteins are chains of amino acids joined by peptide bonds. These amino acid chains (primary structures) must fold into specific three-dimensional conformations (tertiary structures) to achieve their catalytic activity. A protein's tertiary structure is determined by its primary amino acid sequence *in vitro*[36], but in the complex *in vivo* cellular environment, proteins require assistance from a quality control system of molecular chaperones to ensure proper folding[37]. These chaperones mediate not only proper initial folding of proteins, but also re-folding during times of cellular stress, including oxidative stress, exposure to ethanol and other toxins, pH or osmotic changes, UV radiation, and elevated temperatures[37,38]. All living organisms respond to elevated temperatures and other forms of cellular stress by producing a class of chaperones known as heat shock proteins[39], with Hsp70 being one of the most robustly produced in times of cellular stress. The induction of heat shock proteins is primarily controlled at the translational level[40-42]. For this reason, we chose to measure protein levels of Hsp70 instead of mRNA. Translated heat shock protein products appear within minutes of heat shock in cultured cells[43]. The reported half-life of Hsp70 varies by model system and experimental conditions[44-49], but was recently estimated to be 18 hours by quantitative proteomic profiling of U937 cells after heat shock[50]. Although Hsp70 has been detected within minutes in cell culture studies, measurable induction of the heat shock response takes longer in a physiological context. We selected our euthanasia timepoint 24 hours after ultrasound to allow for induction of Hsp70 protein expression in rabbit aorta[12,13].

Hsp70, and several other heat shock proteins, are involved in the cardiovascular system and CVD[51]. Cells in the heart and blood vessels respond to stress by increasing

production of Hsp70. Intracellular Hsp27, 70 and 90 protect against the stresses of atherosclerosis, but circulating soluble Hsp60 can activate both the innate and adaptive immune systems[52,53]. Heat shock increases the ability to withstand subsequent heat shock and environmental stress. As evidence of this thermotolerance, prior heat shock reduces myocardial infarct size in animal models[12,54,55]. Thermotolerance is most effectively induced when the animals are heat shocked 24 hours prior to infarction, providing further support for our selection of euthanasia time. Mechanical stress is another activator of the heat shock response, and the studies of sonoporation referenced above have demonstrated ultrasound-induced mechanical effects on cell membranes, providing an additional rationale for the inclusion of Hsp70 as a cellular stress marker.

Several other studies have evaluated the effects of ultrasound on heat shock proteins. Hsp70 and other heat shock proteins have been used as biomarkers in studies of high-intensity focused ultrasound (HIFU), an application that is emerging as a potential treatment for cancer. HIFU technology delivers concentrated ultrasonic energy to tumors, causing an elevation in temperature sufficient to kill the tumor cells while leaving surrounding tissue intact. Studies of cultured cancer cells[56], mice[57,58], and human breast cancer patients[59] have demonstrated increases in Hsp60 and Hsp70 after HIFU. It is important to note that HIFU uses ultrasound exposure conditions that are more intense than clinical contrast ultrasound exposures. Another study used contrast ultrasound to monitor radiofrequency thermal ablation of rabbit liver tissue[60]. They noted a qualitative increase in Hsp70 protein expression after radiofrequency ablation, and interestingly also a modest increase in Hsp70 with contrast ultrasound alone. This study used a different UCA, Sonazoid, at unknown concentration in a bolus infusion. The authors posit that this biological effect was due to the interaction of ultrasound with UCAs. The effect of ultrasound on Hsp70 has also been investigated in rat muscle. While acute ultrasound exposure did not induce Hsp70[61], a series of four exposures did result in increased production of Hsp70[62]. These two studies used a 1 MHz transducer without UCA, and measured Hsp70 by Western blot using an antibody similar to the one used in the current study. The rabbit and rat studies described above also chose a 24 hours post-exposure timepoint for collection of tissue samples. Importantly, none of

these studies have focused on the cardiovascular system, the primary target of contrast ultrasound imaging, using clinically relevant contrast ultrasound exposure conditions.

Blood collection from the lateral saphenous vein requires restraint of the animals. We included unrestrained control groups of cholesterol and chow-fed animals to account for the effect of restraint, and found that restrained animals had significantly higher aortic Hsp70 protein levels, regardless of diet (**Figure 4.3**). Previous work has shown that restraint stress can induce aortic Hsp70 protein expression in rats[63], and we have now demonstrated this effect in rabbits. However, we cannot rule out the possibility that anesthetics may have contributed to the elevated Hsp70 levels seen in these rabbits. Anesthesia has been shown to increase Hsp70 protein levels in rats[64]. We also observed a decrease in LDL after the experimental procedure at 3 weeks, independent of ultrasound treatment. Anesthetics have been shown to affect blood cholesterol levels[65,66], and it is possible that the LDL fraction was particularly affected. In addition to plasma lipids and Hsp70, we also measured plasma vWF (**Figure 4.2b**). vWF is a clotting protein produced and secreted by endothelial cells, and it serves as a marker of endothelial function[67,68]. We included vWF in order to identify any acute effects of contrast ultrasound on the vascular endothelium. The lack of effect of imaging on vWF suggests that the endothelium was not disturbed by the procedure.

In conclusion, this was an assessment of contrast ultrasound imaging focused on vascular stress, with aorta Hsp70 protein levels as the key indicator. Hsp70 was expressed in vascular tissue, but no additional vascular stress was observed as a result of the imaging procedures.

Acknowledgements

This work was supported by NIH R37EB002641. The authors do not report any conflicts of interest. We acknowledge Rami Abuhabsah, Jim Blue, Michael Kurowski, Matt Lee, Sandhya Sarwate, MD, and Presence Covenant Medical Center for their contributions.

References

1. Go AS, Mozaffarian D, Roger VL, Benjamin EJ, Berry JD, Borden WB, Bravata DM, Dai S, Ford ES, Fox CS *et al.* Heart disease and stroke statistics--2013 update: a report from the American Heart Association. *Circulation* 127:e6-e245 (2013).

2. Hansson GK, Hermansson A. The immune system in atherosclerosis. *Nat. Immunol.* 12:204-212 (2011).

3. Libby P, Ridker PM, Hansson GK. Progress and challenges in translating the biology of atherosclerosis. *Nature* 473:317-325 (2011).

4. Tabas I, Williams KJ, Borén J. Subendothelial lipoprotein retention as the initiating process in atherosclerosis: update and therapeutic implications. *Circulation* 116:1832-1844 (2007).

5. Greenland P, Alpert JS, Beller GA, Benjamin EJ, Budoff MJ, Fayad ZA, Foster E, Hlatky MA, Hodgson JM, Kushner FG *et al.* 2010 ACCF/AHA guideline for assessment of cardiovascular risk in asymptomatic adults: a report of the American College of Cardiology Foundation/American Heart Association Task Force on Practice Guidelines. *Circulation* 122:e584-e636 (2010).

6. Fuster V, Lois F, Franco M. Early identification of atherosclerotic disease by noninvasive imaging. *Nat. Rev. Cardiol.* 7:327-333 (2010).

7. Coller JM, Campbell DJ, Krum H, Prior DL. Early identification of asymptomatic subjects at increased risk of heart failure and cardiovascular events: progress and future directions. *Heart Lung Circ.* 22:171-178 (2013).

8. Cote AT, Harris KC, Panagiotopoulos C, Sandor GGS, Devlin AM. Childhood obesity and cardiovascular dysfunction. *J. Am. Coll. Cardiol.* 62:1309-1319 (2013).

9. Reilly JP, Tunick PA, Timmermans RJ, Stein B, Rosenzweig BP, Kronzon I. Contrast echocardiography clarifies uninterpretable wall motion in intensive care unit patients. *J. Am. Coll. Cardiol.* 35:485-490 (2000).

10. Mulvagh SL, Rakowski H, Vannan MA, Abdelmoneim SS, Becher H, Bierig SM, Burns PN, Castello R, Coon PD, Hagen ME *et al.* American Society of Echocardiography Consensus Statement on the Clinical Applications of Ultrasonic Contrast Agents in Echocardiography. *J. Am. Soc. Echocardiogr.* 21:1179--1201; quiz 1281 (2008).

11. Smith BW, Simpson DG, Sarwate S, Miller RJ, Blue JP, Jr., Haak A, O'Brien WD, Jr., Erdman JW, Jr. Contrast ultrasound imaging of the aorta alters vascular morphology and circulating von Willebrand Factor in hypercholesterolemic rabbits. *J. Ultrasound Med.* 31:711-720 (2012).

12. Marber MS, Latchman DS, Walker JM, Yellon DM. Cardiac stress protein elevation 24 hours after brief ischemia or heat stress is associated with resistance to myocardial infarction. *Circulation* 88:1264-1272 (1993).

13. Hauser GJ, Dayao EK, Wasserloos K, Pitt BR, Wong HR. HSP induction inhibits iNOS mRNA expression and attenuates hypotension in endotoxin-challenged rats. *Am. J. Physiol.* 271:H2529-H2535 (1996).

14. Zachary JF, Frizzell LA, Norrell KS, Blue JP, Jr., Miller RJ, O'Brien WD, Jr. Temporal and spatial evaluation of lesion reparative responses following superthreshold exposure of rat lung to pulsed ultrasound. *Ultrasound Med. Biol.* 27:829-839 (2001).

15. Smith BW, Strakova J, King JL, Erdman JW, Jr., O'Brien WD, Jr. Validated sandwich ELISA for the quantification of von Willebrand factor in rabbit plasma. *Biomark. Insights* 5:119-127 (2010).

16. Smith BW, King JL, Miller RJ, Blue JP, Jr., Sarwate S, O'Brien WD, Jr., Erdman JW, Jr. Optimization of a low magnesium, cholesterol-containing diet for the development of atherosclerosis in rabbits. *J. Food Res.* 2:168-178 (2013).

17. King DA, O'Brien WD, Jr. Comparison between maximum radial expansion of ultrasound contrast agents and experimental postexcitation signal results. *J. Acoust. Soc. Am.* 129:114-121 (2011).

18. Herzog CA. Incidence of adverse events associated with use of perflutren contrast agents for echocardiography. *JAMA* 299:2023-2025 (2008).

19. Wei K, Mulvagh SL, Carson L, Davidoff R, Gabriel R, Grimm RA, Wilson S, Fane L, Herzog CA, Zoghbi WA *et al.* The safety of Definity and Optison for ultrasound image enhancement: a retrospective analysis of 78,383 administered contrast doses. *J. Am. Soc. Echocardiogr.* 21:1202-1206 (2008).

20. Dolan MS, Gala SS, Dodla S, Abdelmoneim SS, Xie F, Cloutier D, Bierig M, Mulvagh SL, Porter TR, Labovitz AJ. Safety and efficacy of commercially available ultrasound contrast agents for rest and stress echocardiography a multicenter experience. *J. Am. Coll. Cardiol.* 53:32-38 (2009).

21. Main ML. Ultrasound contrast agent safety: from anecdote to evidence. *JACC Cardiovasc. Imaging* 2:1057-1059 (2009).

22. Abdelmoneim SS, Bernier M, Scott CG, Dhoble A, Ness SAC, Hagen ME, Moir S, McCully RB, Pellikka PA, Mulvagh SL. Safety of contrast agent use during stress echocardiography in patients with elevated right ventricular systolic pressure: a cohort study. *Circ. Cardiovasc. Imaging* 3:240-248 (2010).

23. Khawaja OA, Shaikh KA, Al-Mallah MH. Meta-analysis of adverse cardiovascular events associated with echocardiographic contrast agents. *Am. J. Cardiol.* 106:742-747 (2010).

24. Miller DL, Quddus J. Diagnostic ultrasound activation of contrast agent gas bodies induces capillary rupture in mice. *Proc. Natl. Acad. Sci. USA* 97:10179-10184 (2000).

25. Miller DL. Induction of pulmonary hemorrhage in rats during diagnostic ultrasound. *Ultrasound Med. Biol.* 38:1476-1482 (2012).

26. Miller DL, Dou C, Sorenson D, Liu M. Histological observation of islet hemorrhage induced by diagnostic ultrasound with contrast agent in rat pancreas. *PloS one* 6:e21617 (2011).

27. Miller DL, Li P, Gordon D, Armstrong WF. Histological characterization of microlesions induced by myocardial contrast echocardiography. *Echocardiography* 22:25-34 (2005).

28. Zachary JF, Hartleben SA, Frizzell LA, O'Brien WD, Jr. Arrhythmias in rat hearts exposed to pulsed ultrasound after intravenous injection of a contrast agent. *J. Ultrasound Med.* 21:1347-1356 (2002).

29. Wood SC, Antony S, Brown RP, Chen J, Gordon EA, Hitchins VM, Zhang Q, Liu Y, Maruvada S, Harris GR. Effects of ultrasound and ultrasound contrast agent on vascular tissue. *Cardiovasc. Ultrasound* 10:29 (2012).

30. Bao S, Thrall BD, Miller DL. Transfection of a reporter plasmid into cultured cells by sonoporation in vitro. *Ultrasound Med. Biol.* 23:953-959 (1997).

31. Tachibana K, Uchida T, Ogawa K, Yamashita N, Tamura K. Induction of cell-membrane porosity by ultrasound. *Lancet* 353:1409 (1999).

32. Miller DL, Quddus J. Sonoporation of monolayer cells by diagnostic ultrasound activation of contrast-agent gas bodies. *Ultrasound Med. Biol.* 26:661-667 (2000).

33. Marmottant P, Hilgenfeldt S. Controlled vesicle deformation and lysis by single oscillating bubbles. *Nature* 423:153-156 (2003).

34. Deng CX, Sieling F, Pan H, Cui J. Ultrasound-induced cell membrane porosity. *Ultrasound Med. Biol.* 30:519-526 (2004).

35. Forbes MM, Steinberg RL, O'Brien WD, Jr. Examination of inertial cavitation of Optison in producing sonoporation of chinese hamster ovary cells. *Ultrasound Med. Biol.* 34:2009-2018 (2008).

36. Anfinsen CB. Principles that govern the folding of protein chains. *Science* 181:223-230 (1973).

37. Goldberg AL. Protein degradation and protection against misfolded or damaged proteins. *Nature* 426:895-899 (2003).

38. Macario AJL, Conway de Macario E. Sick chaperones, cellular stress, and disease. *N. Engl. J. Med.* 353:1489-1501 (2005).

39. Lindquist S. The heat-shock response. *Annu. Rev. Biochem.* 55:1151-1191 (1986).

40. Storti RV, Scott MP, Rich A, Pardue ML. Translational control of protein synthesis in response to heat shock in D. melanogaster cells. *Cell* 22:825-834 (1980).

41. Lindquist S. Regulation of protein synthesis during heat shock. *Nature* 293:311-314 (1981).

42. Bienz M, Gurdon JB. The heat-shock response in Xenopus oocytes is controlled at the translational level. *Cell* 29:811-819 (1982).

43. Lindquist S. Translational efficiency of heat-induced messages in Drosophila melanogaster cells. *J. Mol. Biol.* 137:151-158 (1980).

44. Landry J, Bernier D, Chrétien P, Nicole LM, Tanguay RM, Marceau N. Synthesis and degradation of heat shock proteins during development and decay of thermotolerance. *Cancer Res.* 42:2457-2461 (1982).

45. Li GC, Werb Z. Correlation between synthesis of heat shock proteins and development of thermotolerance in Chinese hamster fibroblasts. *Proc. Natl. Acad. Sci. USA* 79:3218-3222 (1982).

46. Subjeck JR, Sciandra JJ, Johnson RJ. Heat shock proteins and thermotolerance; A comparison of induction kinetics. *Br. J. Radiol.* 55:579-584 (1982).

47. Theodorakis NG, Morimoto RI. Posttranscriptional regulation of hsp70 expression in human cells: effects of heat shock, inhibition of protein synthesis, and adenovirus infection on translation and mRNA stability. *Mol. Cell. Biol.* 7:4357-4368 (1987).

48. Li D, Duncan RF. Transient acquired thermotolerance in Drosophila, correlated with rapid degradation of Hsp70 during recovery. *Eur. J. Biochem.* 231:454-465 (1995).

49. Mao RF, Rubio V, Chen H, Bai L, Mansour OC, Shi ZZ. OLA1 protects cells in heat shock by stabilizing HSP70. *Cell Death Dis.* 4:e491 (2013).

50. Gerner C, Vejda S, Gelbmann D, Bayer E, Gotzmann J, Schulte-Hermann R, Mikulits W. Concomitant determination of absolute values of cellular protein amounts, synthesis rates, and turnover rates by quantitative proteome profiling. *Mol. Cell. Proteomics* 1:528-537 (2002).

51. Snoeckx LH, Cornelussen RN, Van Nieuwenhoven FA, Reneman RS, Van Der Vusse GJ. Heat shock proteins and cardiovascular pathophysiology. *Physiol. Rev.* 81:1461-1497 (2001).

52. Xu Q. Role of Heat Shock Proteins in Atherosclerosis. *Arterioscler. Thromb. Vasc. Biol.* 22:1547-1559 (2002).

53. Xu Q, Metzler B, Jahangiri M, Mandal K. Molecular chaperones and heat shock proteins in atherosclerosis. *Am. J. Physiol. Heart Circ. Physiol.* 302:H506-H514 (2012).

54. Currie RW, Karmazyn M, Kloc M, Mailer K. Heat-shock response is associated with enhanced postischemic ventricular recovery. *Circ. Res.* 63:543-549 (1988).

55. Donnelly TJ, Sievers RE, Vissern FL, Welch WJ, Wolfe CL. Heat shock protein induction in rat hearts. A role for improved myocardial salvage after ischemia and reperfusion? *Circulation* 85:769-778 (1992).

56. Hundt W, O'Connell-Rodwell CE, Bednarski MD, Steinbach S, Guccione S. In vitro effect of focused ultrasound or thermal stress on HSP70 expression and cell viability in three tumor cell lines. *Acad. Radiol.* 14:859-870 (2007).

57. Liu H-L, Hsieh H-Y, Lu L-A, Kang C-W, Wu M-F, Lin C-Y. Low-pressure pulsed focused ultrasound with microbubbles promotes an anticancer immunological response. *J. Transl. Med.* 10:221-221 (2012).

58. Kruse DE, Mackanos MA, O'Connell-Rodwell CE, Contag CH, Ferrara KW. Short-duration-focused ultrasound stimulation of Hsp70 expression in vivo. *Phys. Med. Biol.* 53:3641-3660 (2008).

59. Wu F, Wang Z-B, Cao Y-D, Zhou Q, Zhang Y, Xu Z-L, Zhu X-Q. Expression of tumor antigens and heat-shock protein 70 in breast cancer cells after high-intensity focused ultrasound ablation. *Ann. Surg. Oncol.* 14:1237-1242 (2007).

60. Liu G-J, Moriyasu F, Hirokawa T, Rexiati M, Yamada M, Imai Y. Expression of heat shock protein 70 in rabbit liver after contrast-enhanced ultrasound and radiofrequency ablation. *Ultrasound Med. Biol.* 36:78-85 (2010).

61. Locke M, Nussbaum E. Continuous and pulsed ultrasound do not increase heat shock protein 72 content. *Ultrasound Med. Biol.* 27:1413-1419 (2001).

62. Nussbaum EL, Locke M. Heat shock protein expression in rat skeletal muscle after repeated applications of pulsed and continuous ultrasound. *Arch. Phys. Med. Rehabil.* 88:785-790 (2007).

63. Udelsman R, Blake MJ, Stagg CA, Li DG, Putney DJ, Holbrook NJ. Vascular heat shock protein expression in response to stress. Endocrine and autonomic regulation of this age-dependent response. *J. Clin. Invest.* 91:465-473 (1993).

64. Snoeckx LH, Contard F, Samuel JL, Marotte F, Rappaport L. Expression and cellular distribution of heat-shock and nuclear oncogene proteins in rat hearts. *Am. J. Physiol.* 261:H1443-1451 (1991).

65. Gil AG, Silván G, Illera M, Illera JC. The effects of anesthesia on the clinical chemistry of New Zealand White rabbits. *J. Am. Assoc. Lab. Anim. Sci.* 43:25-29 (2004).

66. Gil AG, Silván G, Villa A, Millán P, Martínez-Fernández L, Illera JC. Serum biochemical response to inhalant anesthetics in New Zealand white rabbits. *J. Am. Assoc. Lab. Anim. Sci.* 49:52-56 (2010).

67. Constans J, Conri C. Circulating markers of endothelial function in cardiovascular disease. *Clin. Chim. Acta* 368:33-47 (2006).

68. Spiel AO, Gilbert JC, Jilma B. von Willebrand factor in cardiovascular disease: focus on acute coronary syndromes. *Circulation* 117:1449-1459 (2008).

Figures and Tables

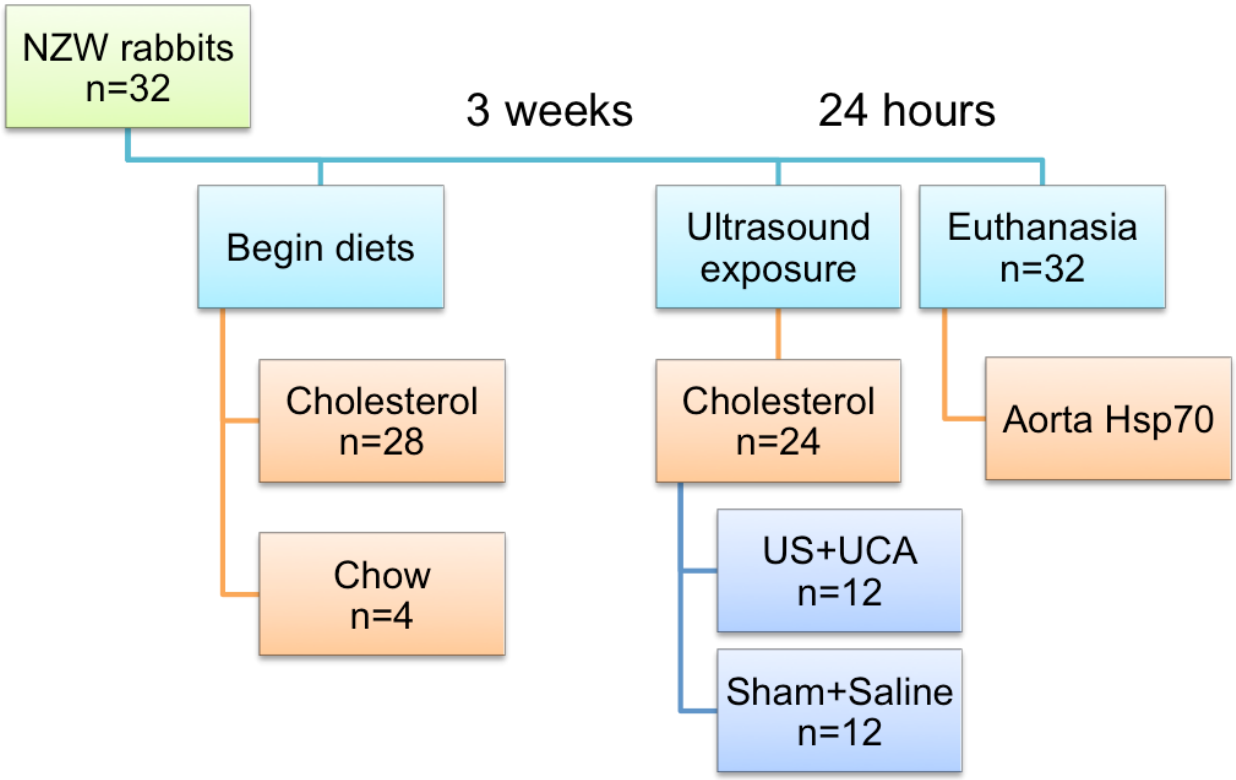

Figure 4.1. Study design with 32 New Zealand White (NZW) rabbits. After 3 weeks on either chow diet or the 1% cholesterol, 10% fat, 0.11% Magnesium diet, rabbits (n=24) underwent ultrasound imaging at 2.1 MPa with intravenous administration of the Definity® UCA, or a sham procedure. Serial saphenous vein blood samples were collected from these animals under restraint. An additional 4 rabbits on cholesterol diet and the 4 on chow served as cage controls. Rabbits were euthanized 24 hours after the ultrasound procedure (day 22), and aorta tissue was collected for analysis. UCA, ultrasound contrast agent.

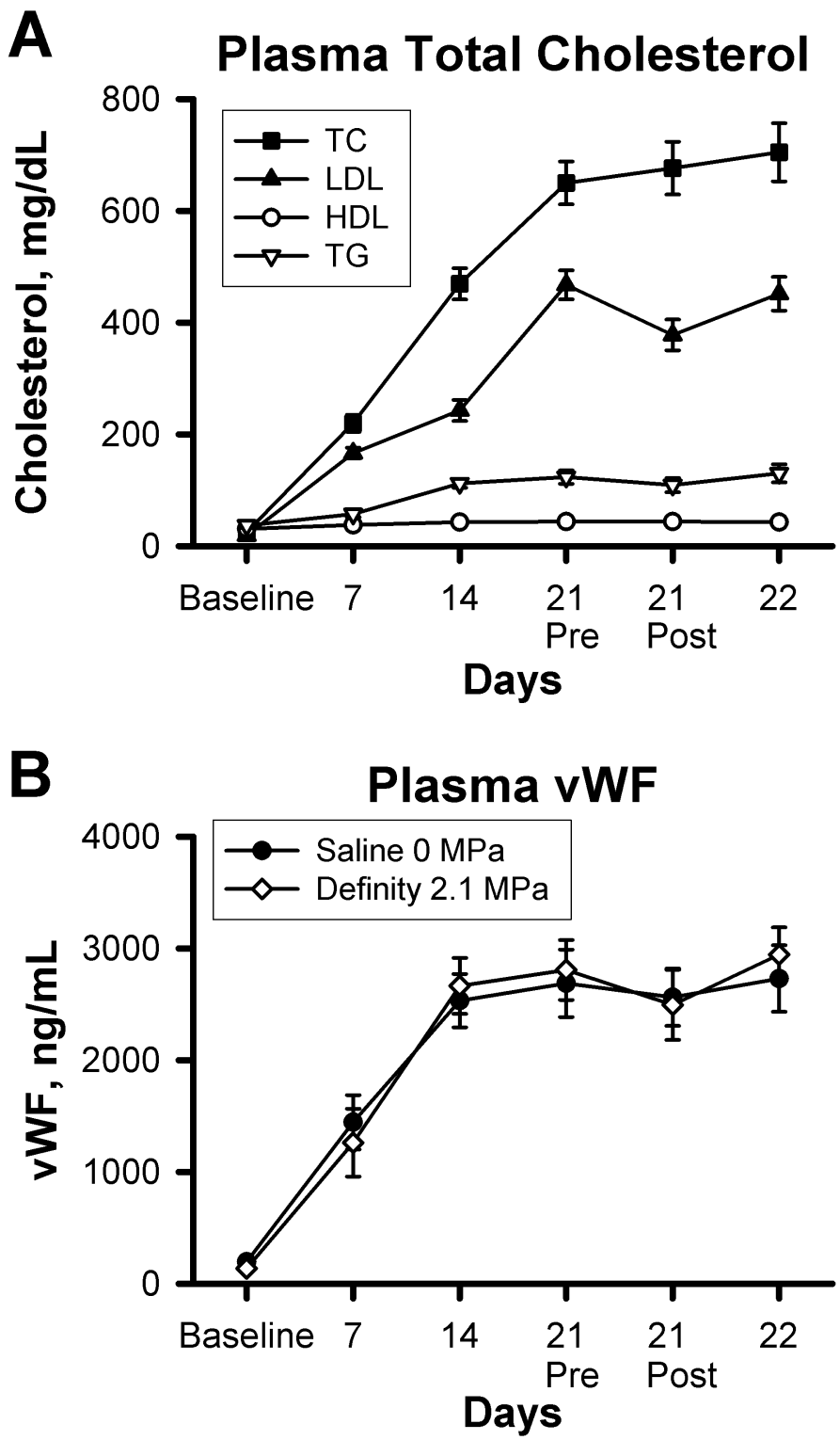

Figure 4.2. Plasma cholesterol and von Willebrand Factor (vWF). A, plasma total cholesterol was measured by enzymatic colorimetric kit. B, vWF was measured by ELISA.

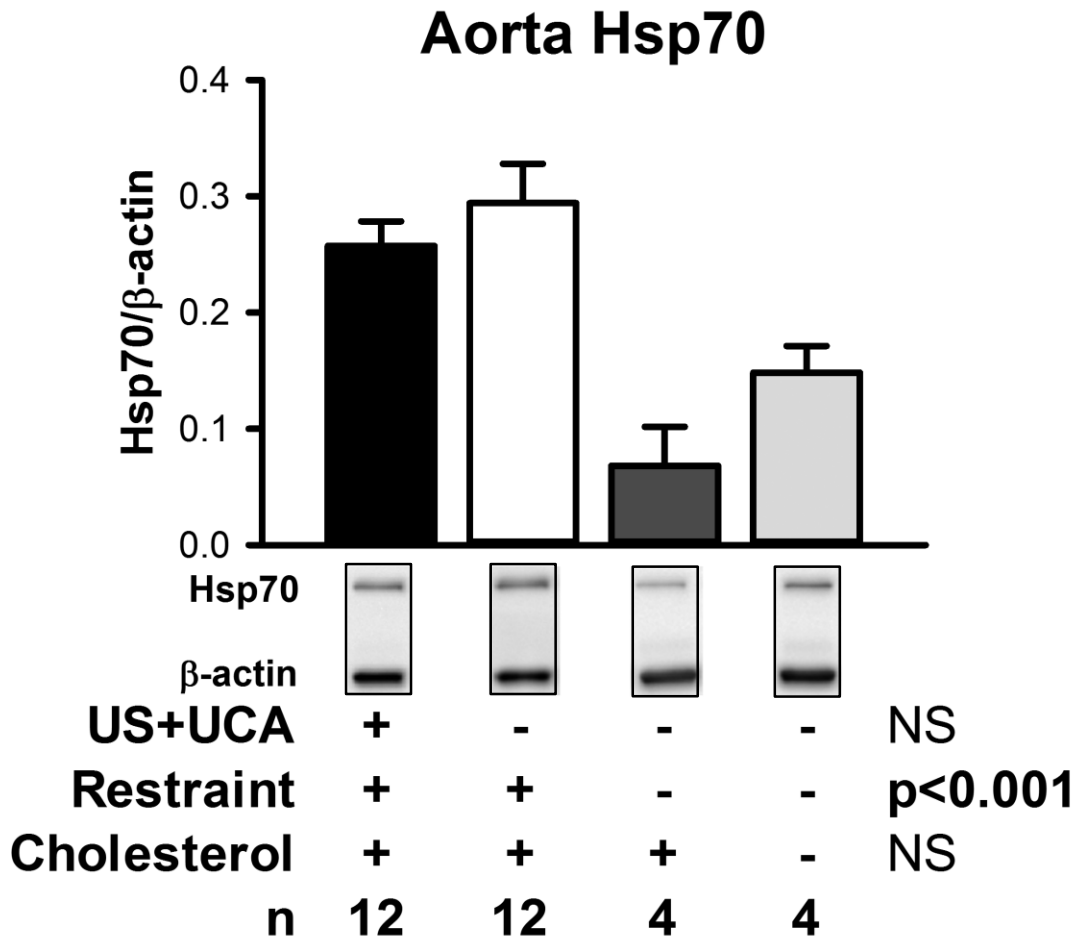

Figure 4.3. Aorta tissue Hsp70 analysis on day 22. Aorta tissue from the site of exposure was carefully dissected from the surrounding tissue and frozen in liquid nitrogen. Tissue lysates were analyzed for Hsp70 by Western blot, with β-actin as a loading control. Western blot lanes shown are representative of the mean of each group, and the lanes are separated to indicate that they are derived from separate blots. Bars are SEM. Labels +/- indicate presence/ absence of the treatment.

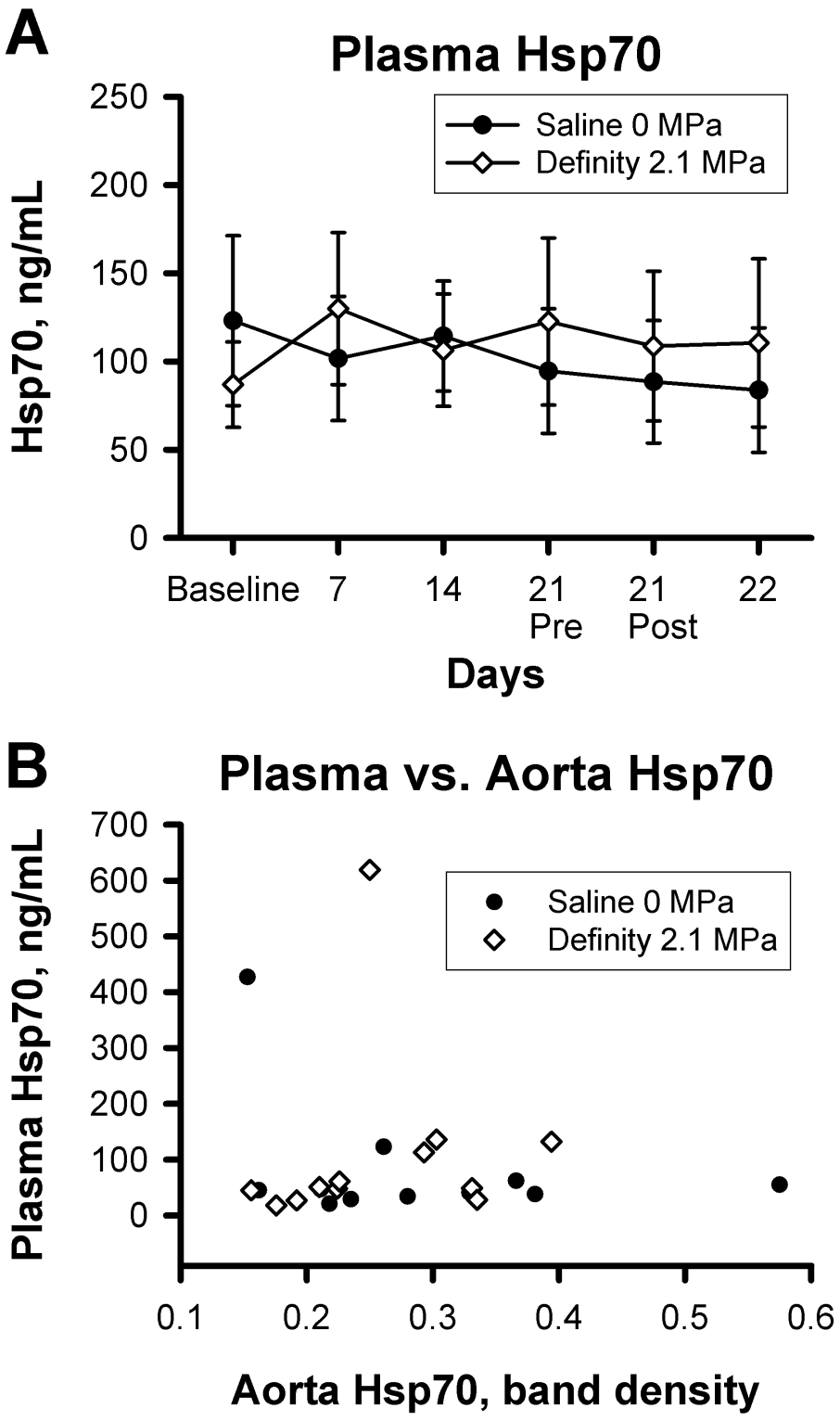

Figure 4.4. Plasma Hsp70. A, Plasma Hsp70 was measured by ELISA. B, no correlation between plasma and tissue Hsp70 levels. Bars are SEM. Hsp70, Heat shock protein 70.

CHAPTER 5: Contrast ultrasound imaging of the aorta does not affect progression of atherosclerosis or cardiovascular biomarkers in ApoE$^{-/-}$ mice

Abstract

Objective – Ultrasound Contrast Agents (UCAs) enhance cardiovascular ultrasound imaging. Adverse biological effects have occurred after administration of UCAs, and more research is needed for a comprehensive understanding of the risks involved. We used the ApoE$^{-/-}$ mouse model of atherosclerosis to characterize the effects of ultrasound and UCAs on atherosclerosis and plasma biomarkers.

Methods – Male ApoE$^{-/-}$ mice (8 weeks old, n=24) were intravenously infused with UCA (2x10^{10} Definity® microbubbles/hr) and exposed to 2.8 MHz center frequency ultrasound (10 Hz pulse repetition frequency, 1.4 µs pulse duration, 2 min exposure duration, two sites) at one of three peak rarefactional pressure amplitudes (0, 1.9 or 3.8 MPa PRPA), and then consumed either a chow or Western diet for 4 weeks (n=4 per group). Blood plasma samples were collected before ultrasound exposure and at 2 and 4 weeks post-exposure, and assayed for total cholesterol and von Willebrand Factor (vWF). A pathologist measured atheroma thickness in formalin-fixed, hematoxylin & eosin-stained transverse aorta sections and scored them for severity of atherosclerosis.

Results – Plasma total cholesterol initially averaged 286 mg/dL in the Western diet group and increased to 861 mg/dL after 4 weeks on the diet ($p<0.0001$). Total cholesterol did not increase significantly in the chow diet group. Plasma vWF increased after two weeks on the Western diet ($p<0.0001$). Atheroma thickness was greater in animals consuming the Western diet than in chow-fed animals ($p<0.05$). Ultrasound had no significant effect on plasma total cholesterol, plasma vWF or atheroma thickness.

Conclusions – Contrast ultrasound did not increase the severity of atherosclerosis or alter cardiovascular biomarkers in the ApoE$^{-/-}$ mouse model.

Introduction

Ultrasound Contrast Agents (UCAs) are used to enhance ultrasound imaging of the cardiovascular system. UCAs are administered intravenously as a solution of micron-sized bubbles, consisting of an inert gas encased in a shell of phospholipid or albumin. When ultrasound is applied to the heart or blood vessels, the ultrasonic waves interact with UCAs in the circulation, causing the bubbles to oscillate or collapse. The interaction of ultrasound with UCAs opacifies the blood, allowing for improved imaging of cardiac structure and function[1], arterial stenosis[2], vascularization of atherosclerotic plaques[3], and other aspects of the cardiovascular system. When used for cardiac left-ventricular opacification, UCAs can enhance the visual quality of ultrasound scans in patients that are difficult to image, and improve diagnostic accuracy[4,5].

While UCAs have clear clinical utility in detection and diagnosis of cardiovascular disease, concerns have been raised over their safety. There have been reports of adverse cardiovascular events after ultrasound with UCA administration in animal models and humans. In experimental studies from our research group and others, UCAs have been shown to induce cardiac arrhythmias[6], hemorrhage[7-9], impair endothelium-dependent vasodilation[10], and alter atheroma thickness and the circulating biomarker von Willebrand Factor[11]. Reports of cardiopulmonary complications and deaths in human clinical patients associated with UCA administration added to these concerns, and patients with pre-existing cardiovascular disease appeared to be at increased risk[12]. As a result, the U.S. Food & Drug Administration (FDA) mandated warning labels for two commercially available UCAs, Definity® (Lantheus Medical Imaging, North Billerica, MA) and Optison™ (GE Healthcare, Princeton, NJ) in 2007.

The reported adverse events highlight the importance of further research in this area. The biological effects of contrast ultrasound may be a function of ultrasound pressure level or UCA concentration, so it is necessary to test for adverse events using a variety of scenarios and experimental models. In this study, we used the ApoE$^{-/-}$ mouse model of atherosclerosis to determine thresholds for arterial damage at several different ultrasound pressure levels, with concomitant UCA administration. We fed groups of mice either a standard chow diet or a high fat, high sugar, cholesterol-containing Western diet to modulate the progression of atherosclerosis after a single

contrast ultrasound exposure. We hypothesized that contrast ultrasound would induce vascular injury and accelerate the progression of atherosclerosis, that this effect would be pressure-dependent, and that the threshold for effects of contrast ultrasound on biomarkers would be lower than FDA limits established for clinical ultrasound imaging.

Materials and Methods

Animals and Experimental Design

The University of Illinois Institutional Animal Care and Use Committee approved all live animal procedures. Male ApoE$^{-/-}$ mice (8 weeks old, fed chow prior to study diets, n=24; Jackson Labs, Bar Harbor, ME) were randomized to experimental groups and exposed to ultrasound at one of three pressure levels with intravenous infusion of UCA as described in *Exposimetry*, with n=8 mice per group. The mice then consumed either a chow diet (7012; Harlan Teklad, Madison, WI) with 3.1 kcal/g, or a Western diet containing 21% milkfat, 34% sucrose, 0.2% cholesterol w/w, and 4.7 kcal/g (TD.10885; Harlan Teklad), for 4 weeks after ultrasound exposure (n=4 per group). Mice were individually housed, fed *ad libitum* with fresh diet provided twice per week, and given *ad libitum* access to water. Serial blood samples were collected at baseline, 2 weeks post-exposure and 4 weeks post-exposure. Blood samples were collected from the submandibular region by puncture with a 5 mm lancet (Goldenrod; MEDIpoint Inc., Mineola, NY) into an EDTA-coated capillary tube (Microvette; Sarstedt AG & Co., Nümbrecht, Germany), centrifuged at 2500 x *g* and 4ºC for 10 minutes, aliquotted and frozen at -70ºC. Mice were euthanized 4 weeks post-exposure and tissues were collected for analysis (**Figure 5.1**).

All mice were anesthetized with isoflurane and euthanized by cervical dislocation. After euthanasia, mice were placed in dorsal recumbency and a ventral midline incision was made to expose the abdominal and thoracic cavities. The aorta was perfused with 0.8 mL 10% neutral-buffered formalin (NBF) through the left ventricle of the heart and allowed to fix for 30 minutes. An additional 0.2 mL NBF was added to the outer surface of the aorta. Next, under magnification, microscissors and fine-point forceps were used to remove the fat surrounding the three aortic arch branches (brachiocephalic, left common carotid, left subclavian). The length of the aorta was removed from its origin at

the left ventricle to a few millimeters distal to its bifurcation into the common iliac arteries. The aorta was freed from surrounding vessels by making cuts at each of the three branches of the arch, the origin of the aorta at the heart, and distal to the aortic bifurcation into the common iliac arteries.

After removal, the entire aorta was sectioned transversely. The first two cuts were made midway between the 1st and 2nd and 2nd and 3rd aortic branches off the arch. The third cut was made 2 mm distal to the second cut. All subsequent sections were made 2.5 mm from the previous section. The average length of aorta removed was 3.5 cm, with 15 sections per aorta. All sections were placed in a single embedding cassette with the distal cut side down in order from the cranial to the caudal end of the aorta, fixed in 10% NBF for 24 hours, and embedded in paraffin.

Exposimetry

Ultrasound exposures were performed with a focused f/2, 19 mm diameter lithium niobate single-element transducer (Valpey Fisher, Hopkinton, MA USA) driven by a high-power pulse source (RAM5000; Ritec, Inc., Warwick, RI USA). Ultrasonic field distribution measurements were performed in 22ºC degassed water according to established procedures[13,14] and yielded a center frequency of 2.8 MHz, fractional bandwidth of 11%, focal length of 26 mm, -6 dB focal beamwidth of 0.98 mm, and -6 dB depth of focus of 11 mm. Weekly calibrations were performed as previously described[11]. A custom transducer holder was machined from aluminum and designed to incorporate both a high-frequency array transducer (MS-400; VisualSonics, Inc., Toronto, Canada) for image guidance and the single-element transducer described above for exposures. The transducers were angled to focus on the same anatomical location at a depth of 14 mm inside the animal.

Male ApoE$^{-/-}$ mice (8 weeks old, n=24) were anesthetized with 5% isoflurane with 2 L/min supplemental O_2 for induction of anesthesia, and then maintained at 2% isoflurane (adjusting the isoflurane level as necessary to keep the animal properly anesthetized) with 2 L/min O_2 via facemask. Heart and respiratory rates were monitored throughout the experiment. The average heart rate was 368 beats per minute and the average respiratory rate was 29 breaths per minute. Hair was removed from the ventral side of the animal with clippers (Wahl, Sterling, IL) followed by a depilatory agent (Veet;

Reckitt Benckiser, Parsippany, NJ). A high frequency ultrasound system (Vevo 2100; VisualSonics, Inc., Toronto, Canada) was used to image the aorta and position the single-element transducer for ultrasound exposures. Once transducers were positioned, mice were intravenously infused with UCA (2.6% Definity® in saline, 1.8 mL/hour, $2x10^{10}$ microbubbles/hour, 10 min. total infusion time) through a lateral tail vein with a 27g x ½" butterfly catheter (Surflo; Terumo, Somerset, NJ) attached to a 1 mL syringe (BD, Franklin Lakes, NJ) and an infusion pump (KD Scientific, Inc., Holliston, MA). When the UCA infusion was started, the aorta was exposed to 2.8-MHz center frequency ultrasound (10 Hz pulse repetition frequency, 1.4 µs pulse duration, 2 min exposure duration) at one of three peak rarefactional pressure amplitudes (0, 1.9 or 3.8 MPa PRPA). The 1.9 MPa PRPA matched Definity®'s 90% collapse threshold[15]. The Mechanical Index (MI) was also determined as part of the routine calibration procedure[16], and yielded 0, 1.1 and 2.3, respectively. The purpose for providing the MI is because it is a regulated quantity[17] of diagnostic ultrasound systems, and its magnitude is available to system operators. Ultrasound exposures were performed at two sites on the aorta: the arch near the branch to the left common carotid artery, and the abdominal region immediately caudal to the diaphragm. After the second exposure, the UCA infusion was stopped and mice were allowed to recover from anesthesia.

Histology

Aorta sections were cut from paraffin blocks at 3 µm thickness, mounted on microscope slides, and stained with hematoxylin and eosin. One microscope slide, with 3 sections of the paraffin block, was created for each animal. A board-certified pathologist blinded to the exposure conditions measured the thickest atheroma in the aorta using an ocular micrometer (Olympus America Inc., Center Valley, PA) and assigned an atherosclerosis score between 0 and 5 using the American Heart Association classification scheme for human atherosclerotic lesions[18]. Score 0 = Absence of atherosclerosis; Score 1 = Presence of isolated foam cells; Score 2 = Lipid accumulation mainly within the foam cells; Score 3 = Lipid accumulation within the foam cells and small pools of extracellular lipid; Score 4 = Intracellular lipid, lipid pools and core of extracellular lipid; and Score 5 = Lipid core and fibrotic layer, or multiple lipid cores and fibrotic layer, or mainly calcified or fibrotic plaque.

Blood Analysis

Plasma total cholesterol was measured using an enzymatic colorimetric kit (Wako Chemicals, Richmond, VA) with samples plated in triplicate. Human control sera (Wako) were included in each assay to evaluate the reproducibility of measurement. Intra-assay precision was defined as the variability among replicates of the same sample within an assay, and inter-assay precision as the variability among replicates of the same sample over multiple assays. Coefficient of Variation (CV) was used as a measure of precision[19] and defined as $\frac{Standard\ Deviation}{Mean} \times 100$. The intra-assay CV for control sera was 3.5%, and the inter-assay CV was 9.2%. The intra-assay CV for mouse plasma samples was 2.3%.

vWF was measured using a sandwich enzyme-linked immunosorbent assay (ELISA) as previously described[20] with the following modifications: to adapt the assay for mouse plasma instead of rabbit plasma, a standard curve from 25-0.39 ng/mL was used instead of 100-3.13 ng/mL, and mouse plasma was diluted 1:25 for analysis instead of 1:100. Samples were plated in duplicate. The same antibodies and reagents were used for mouse and rabbit plasma, as a BLAST search[21] demonstrates 83% sequence alignment between human (accession: CCQ25771.1) and mouse (accession: AAN07781.2) vWF, and 81% between mouse and rabbit (accession: DAA34807.1) vWF. For mouse plasma samples, the intra-assay CV was 3.2%, and the inter-assay CV was 13%.

Statistical Analysis

Statistical analysis was performed in SAS 9.3 (SAS Institute, Inc., Cary, NC) for Windows, and graphs were created in SigmaPlot 12.3 for Windows. Atheroma thickness data were analyzed by analysis of variance (ANOVA) within the general linear mixed models procedure of SAS 9.3. Feed intake, body weights, plasma total cholesterol, and plasma vWF data were analyzed by repeated measures analysis of covariance (ANOCOVA), using baseline values as covariates, also within the general linear mixed models procedure of SAS 9.3. The covariance structure of repeated measures data was assessed graphically and quantitatively, and an appropriate covariance model was fit. Non-parametric atherosclerosis score data were analyzed using a two-sample Wilcoxon

rank sum test with diet as the treatment variable. Each model was first run with all fixed effects and covariates of interest (diet, time point, PRPA, and baseline values) incorporated, and then reduced to eliminate non-significant variables. When a significant result was reported for a fixed variable with more than two categories, multiple comparisons were made using estimate statements based on the least squares means, followed by Bonferroni adjustment for multiplicity. Data met the necessary assumptions of each test. The threshold for statistical significance was set at $p<0.05$.

Results

Contrast ultrasound does not affect feed intake or body weight

Animals on chow diet consumed more feed by weight, but less kilocalories (kcal), than animals on the Western diet (4.1 g/day feed intake for chow animals vs. 3.3 g/day for Western diet animals, $p<0.0005$; 12.8 kcal/day feed intake for chow animals vs. 15.4 kcal/day for Western diet animals, $p<0.005$). Animals on chow diet weighed less than animals on the Western diet (24.6 g final body weight for chow animals vs. 26.5 g for Western diet animals, $p<0.005$). Ultrasound did not significantly affect feed intake or body weight.

Contrast ultrasound does not affect plasma cholesterol or von Willebrand Factor

Total cholesterol initially averaged 283 mg/dL and did not increase significantly in the chow diet group (**Figure 5.2a**). While cholesterol levels in chow-fed animals remained stable, animals in the Western diet groups experienced a rapid and significant elevation to an average of 726 mg/dL after 2 weeks on the diet ($p<0.0001$ by repeated measures ANOCOVA), and levels remained significantly elevated after that, averaging 861 mg/dL after 4 weeks. Ultrasound ($p=0.25$), diet*ultrasound ($p=0.89$), and diet*ultrasound*timepoint ($p=0.37$) were not significant variables in the statistical model, and so were removed.

Plasma vWF initially averaged 112 ng/mL in all animals (**Figure 5.2b**). Consumption of the Western diet for two weeks significantly elevated vWF to an average of 257 ng/mL as compared to 78 ng/mL for animals continuing to consume chow ($p<0.0001$ by repeated measures ANOCOVA). Levels were highly variable at 4 weeks and no significant differences between diets or ultrasound groups were seen.

Contrast ultrasound does not affect aorta atheroma thickness or atherosclerosis score

Atheroma thickness was significantly greater in animals consuming the Western diet than in chow-fed animals, with an average±SEM of 0.031±0.010 mm for chow and 0.073±0.014 mm for Western at 0 MPa, 0.020±0.007 mm for chow and 0.039±0.012 mm for Western at 1.9 MPa, and 0.025±0.014 mm for chow and 0.036±0.010 mm for Western at 3.8 MPa ($p<0.05$ by ANOVA, n=3-4/group, **Figure 5.3b**). Ultrasound ($p=0.11$) and diet*ultrasound ($p=0.40$) were not significant variables in the statistical model, and so were removed. If the diet*ultrasound variable was retained, the ultrasound variable would approach statistical significance within the Western diet group only ($p<0.08$), and there would be a significant difference between Western and chow at 0 PRPA ($p<0.05$), but not 1.9 ($p=0.24$) or 3.8 ($p=0.50$) PRPA. A regression analysis of the atheroma thickness data, within either the Western diet group or the chow diet group, and treating both the atheroma thickness and the ultrasound PRPA as continuous variables, does not identify any significant trends among PRPA groups ($F_{0.05}(1, 9)=2.51$, $r^2=0.22$, $p=0.15$ for Western; $F_{0.05}(1, 9)=0.08$, $r^2=0.009$, $p=0.78$ for chow).

Atherosclerosis score was also significantly greater for Western diet-fed animals than chow-fed animals, with an average±SEM of 2.25±0.0.946 for chow and 3.33±0.882 for Western at 0 MPa, 1.25±0.479 for chow and 2.00±0.408 for Western at 1.9 MPa, and 1.00±0.577 for chow and 2.50±0.866 for Western at 3.8 MPa (one-sided $p<0.05$ by Wilcoxon rank sum test, n=3-4/group, **Figure 5.3c**). Ultrasound was not a significant variable overall ($p=0.45$), within the chow diet group alone ($p=0.62$), or within the Western diet group alone ($p=0.25$) for atherosclerosis score.

Discussion

Concerns over the safety of UCAs began after reports of adverse cardiopulmonary events and deaths following their administration. Based on these reports, the FDA required revised labeling for Definity® and Optison™ in 2007, adding a “black box” label warning of adverse events and requiring a 30 minute monitoring period for all patients injected with UCAs. However, a small number of adverse events were reported during a span of several years in which millions of patients were safely imaged, so the estimated incidence of adverse events was far lower than for many established medical

procedures[22]. The few deaths that did occur were likely due to underlying disease conditions rather than UCAs[23]. A large body of literature has emerged to demonstrate the safety of UCAs[12,24-27], and a recent meta-analysis[28] of over 5 million patients concluded that the use of UCAs in ultrasound imaging is safe and not associated with an increased risk of myocardial infarction or death. After these reports of UCA safety accumulated, the FDA relaxed its warnings on Definity® in October 2011 and Optison™ in August 2012, noting that serious complications are uncommon and removing the 30 minute monitoring period post-UCA injection. The present study adds support for the safety of UCAs and suggests that UCAs can be utilized even in patients with atherosclerosis.

In addition to their growing safety record, UCAs show promise in therapeutic applications. UCAs have been used to enhance gene and drug delivery[29,30], reduce infarct size and improve ventricular remodeling after cardiac ischemia[31], and induce angiogenesis to improve tissue perfusion[32-37]. These innovative functions of UCAs, in conjunction with their safety record, make a strong case for their continued use in the laboratory and clinic.

We selected the ApoE$^{-/-}$ mouse as a model of atherosclerosis for our investigations, a well-established mouse model[38] that recapitulates many aspects of human atherosclerosis[39]. ApoE is an apolipoprotein important for cholesterol metabolism, particularly in rodents[40]. Deletion of ApoE results in impaired hepatic clearance of lipoproteins from the circulation. As a result, lipoproteins accumulate in the blood, reaching nearly 900 mg/dL in this study, and infiltrate arterial tissue to promote atherosclerosis. The ApoE$^{-/-}$ mouse provides several advantages over the cholesterol-fed rabbit model also used by our research group[41,42]. They are easier to handle, and readily consume the atherosclerotic diet. As in our previous study[11], we measured the biomarker von Willebrand Factor (vWF), a protein produced and secreted by vascular endothelial cells. Alterations in plasma vWF levels reflect endothelial dysfunction[43] and predict risk of cardiovascular events[44]. The ApoE$^{-/-}$ mouse, validated assays and histological techniques comprise a sensitive model system to test for biological effects of contrast ultrasound.

Our findings in this study were different than those observed in the cholesterol-fed rabbit model[11]. The lack of concordance between the two studies may be due to methodological and/or physiological differences. First, we are working with a different animal model, and mice may simply respond differently to ultrasound and UCAs than rabbits. The increased heart, respiratory and metabolic rates of mice may decrease the half-life of UCAs. In this study, we did not collect blood samples immediately before and after exposure. We also measured plaque thickness by examining the entire aortic arch and descending aorta, instead of just the specific ultrasound exposure site, which may explain why we did not observe alterations in aorta plaque thickness. Small sample sizes may also have limited our statistical power. Further studies are needed to determine whether differences in results between the two studies are due to differences in experimental methods or animal physiology.

In conclusion, contrast ultrasound did not affect clinically relevant cardiovascular biomarkers or progression of atherosclerosis in ApoE$^{-/-}$ mice. This study represents an important step in understanding the biological effects of UCAs, and adds to a growing body of literature demonstrating their safety in cardiovascular ultrasound imaging. The focus of this research area has begun to shift away from the potential of UCAs to cause cardiovascular harm, and on to improving cardiovascular health and diagnosis, and it has become clear that the benefits of UCAs outweigh the potential risks in almost all current applications.

Acknowledgements

This work was supported by NIH R37EB002641. The authors do not report any conflicts of interest. We acknowledge Emily Hartman, Rami Abuhabsah, Michael Kurowski, Jessica Ang, and Presence Covenant Medical Center for their contributions.

References

1. Senior R, Shah BN. Myocardial contrast echocardiography for simultaneous assessment of function and perfusion in real time: a technique comes of age. *Circulation* 126:1182-1184 (2012).

2. Porter T, Li S, Kilzer K, Deligonul U. Correlation between quantitative angiographic lesion severity and myocardial contrast intensity during a continuous infusion of perfluorocarbon-containing microbubbles. *J. Am. Soc. Echocardiogr.* 11:702-710 (1998).

3. Akkus Z, Hoogi A, Renaud G, van den Oord SCH, Ten Kate GL, Schinkel AFL, Adam D, de Jong N, van der Steen AFW, Bosch JG. New quantification methods for carotid intra-plaque neovascularization using contrast-enhanced ultrasound. *Ultrasound Med. Biol.* 40:25-36 (2014).

4. Kitzman DW, Goldman ME, Gillam LD, Cohen JL, Aurigemma GP, Gottdiener JS. Efficacy and safety of the novel ultrasound contrast agent Perflutren (Definity) in patients with suboptimal baseline left ventricular echocardiographic images. *Am. J. Cardiol.* 86:669-674 (2000).

5. Reilly JP, Tunick PA, Timmermans RJ, Stein B, Rosenzweig BP, Kronzon I. Contrast echocardiography clarifies uninterpretable wall motion in intensive care unit patients. *J. Am. Coll. Cardiol.* 35:485-490 (2000).

6. Zachary JF, Hartleben SA, Frizzell LA, O'Brien WD, Jr. Arrhythmias in rat hearts exposed to pulsed ultrasound after intravenous injection of a contrast agent. *J. Ultrasound Med.* 21:1347-1356 (2002).

7. Miller DL, Quddus J. Diagnostic ultrasound activation of contrast agent gas bodies induces capillary rupture in mice. *Proc. Natl. Acad. Sci. USA* 97:10179-10184 (2000).

8. Miller DL, Dou C, Sorenson D, Liu M. Histological observation of islet hemorrhage induced by diagnostic ultrasound with contrast agent in rat pancreas. *PloS one* 6:e21617 (2011).

9. Miller DL. Induction of pulmonary hemorrhage in rats during diagnostic ultrasound. *Ultrasound Med. Biol.* 38:1476-1482 (2012).

10. Wood SC, Antony S, Brown RP, Chen J, Gordon EA, Hitchins VM, Zhang Q, Liu Y, Maruvada S, Harris GR. Effects of ultrasound and ultrasound contrast agent on vascular tissue. *Cardiovasc. Ultrasound* 10:29 (2012).

11. Smith BW, Simpson DG, Sarwate S, Miller RJ, Blue JP, Jr., Haak A, O'Brien WD, Jr., Erdman JW, Jr. Contrast ultrasound imaging of the aorta alters vascular morphology and circulating von Willebrand Factor in hypercholesterolemic rabbits. *J. Ultrasound Med.* 31:711-720 (2012).

12. Main ML. Ultrasound contrast agent safety: from anecdote to evidence. *JACC Cardiovasc. Imaging* 2:1057-1059 (2009).

13. Raum K, O'Brien WD, Jr. Pulse-echo field distribution measurement technique of high-frequency ultrasound sources. *IEEE Trans. Ultrason. Ferroelectr. Freq. Control* 44:810-815 (1997).

14. Zachary JF, Sempsrott JM, Frizzell LA, Simpson DG, O'Brien WD, Jr. Superthreshold behavior and threshold estimation of ultrasound-induced lung hemorrhage in adult mice and rats. *IEEE Trans. Ultrason. Ferroelectr. Freq. Control* 48:581-592 (2001).

15. King DA, O'Brien WD, Jr. Comparison between maximum radial expansion of ultrasound contrast agents and experimental postexcitation signal results. *J. Acoust. Soc. Am.* 129:114-121 (2011).

16. AIUM/NEMA (American Institute of Ultrasound in Medicine and National Electrical Manufacturers Association). *Standard for real-time display of thermal and mechanical acoustic output indices on diagnostic ultrasound equipment* Rev. 2 (Laurel, MD and Rosslyn, VA, 2004).

17. FDA (US Food and Drug Administration) Center for Devices and Radiological Health. *Information for Manufacturers Seeking Marketing Clearance of Diagnostic Ultrasound Systems and Transducers* (Rockville, MD, 1997).

18. Kumar V, Fausto N, Abbas AK. *Robbins and Cotran Pathologic Basis of Disease*, 7th edn (Saunders, 2005).

19. Reed GF, Lynn F, Meade BD. Use of coefficient of variation in assessing variability of quantitative assays. *Clin. Diagn. Lab. Immunol.* 9:1235-1239 (2002).

20. Smith BW, Strakova J, King JL, Erdman JW, Jr., O'Brien WD, Jr. Validated sandwich ELISA for the quantification of von Willebrand factor in rabbit plasma. *Biomark. Insights* 5:119-127 (2010).

21. Altschul SF, Madden TL, Schäffer AA, Zhang J, Zhang Z, Miller W, Lipman DJ. Gapped BLAST and PSI-BLAST: a new generation of protein database search programs. *Nucleic Acids Res.* 25:3389-3402 (1997).

22. Grayburn PA. Product safety compromises patient safety (an unjustified black box warning on ultrasound contrast agents by the Food and Drug Administration). *Am. J. Cardiol.* 101:892-893 (2008).

23. Main ML, Goldman JH, Grayburn PA. Thinking outside the "box"-the ultrasound contrast controversy. *J. Am. Coll. Cardiol.* 50:2434-2437 (2007).

24. Herzog CA. Incidence of adverse events associated with use of perflutren contrast agents for echocardiography. *JAMA* 299:2023-2025 (2008).

25. Wei K, Mulvagh SL, Carson L, Davidoff R, Gabriel R, Grimm RA, Wilson S, Fane L, Herzog CA, Zoghbi WA *et al.* The safety of Definity and Optison for ultrasound image enhancement: a retrospective analysis of 78,383 administered contrast doses. *J. Am. Soc. Echocardiogr.* 21:1202-1206 (2008).

26. Dolan MS, Gala SS, Dodla S, Abdelmoneim SS, Xie F, Cloutier D, Bierig M, Mulvagh SL, Porter TR, Labovitz AJ. Safety and efficacy of commercially available ultrasound contrast agents for rest and stress echocardiography a multicenter experience. *J. Am. Coll. Cardiol.* 53:32-38 (2009).

27. Abdelmoneim SS, Bernier M, Scott CG, Dhoble A, Ness SAC, Hagen ME, Moir S, McCully RB, Pellikka PA, Mulvagh SL. Safety of contrast agent use during stress echocardiography in patients with elevated right ventricular systolic pressure: a cohort study. *Circ. Cardiovasc. Imaging* 3:240-248 (2010).

28. Khawaja OA, Shaikh KA, Al-Mallah MH. Meta-analysis of adverse cardiovascular events associated with echocardiographic contrast agents. *Am. J. Cardiol.* 106:742-747 (2010).

29. Bekeredjian R, Grayburn PA, Shohet RV. Use of ultrasound contrast agents for gene or drug delivery in cardiovascular medicine. *J. Am. Coll. Cardiol.* 45:329-335 (2005).

30. Villanueva FS. Getting good vibes: the therapeutic power of microbubbles and ultrasound. *JACC Cardiovasc. Imaging* 5:1263-1266 (2012).

31. Dörner J, Struck R, Zimmer S, Peigney C, Duerr GD, Dewald O, Kim S-C, Malan D, Bettinger T, Nickenig G *et al.* Ultrasound-mediated stimulation of microbubbles after acute myocardial infarction and reperfusion ameliorates left-ventricular remodelling in mice via improvement of borderzone vascularization. *PloS one* 8:e56841 (2013).

32. Song J, Qi M, Kaul S, Price RJ. Stimulation of arteriogenesis in skeletal muscle by microbubble destruction with ultrasound. *Circulation* 106:1550-1555 (2002).

33. Chappell JC, Klibanov AL, Price RJ. Ultrasound-microbubble-induced neovascularization in mouse skeletal muscle. *Ultrasound Med. Biol.* 31:1411-1422 (2005).

34. Chappell JC, Song J, Klibanov AL, Price RJ. Ultrasonic microbubble destruction stimulates therapeutic arteriogenesis via the CD18-dependent recruitment of bone marrow-derived cells. *Arterioscler. Thromb. Vasc. Biol.* 28:1117-1122 (2008).

35. Johnson CA, Sarwate S, Miller RJ, O'Brien WD, Jr. A temporal study of ultrasound contrast agent-induced changes in capillary density. *J. Ultrasound Med.* 29:1267-1275 (2010).

36. Johnson CA, Miller RJ, O'Brien WD, Jr. Ultrasound contrast agents affect the angiogenic response. *J. Ultrasound Med.* 30:933-941 (2011).

37. Johnson CA, O'Brien WD, Jr. The angiogenic response is dependent on ultrasound contrast agent concentration. *Vasc. Cell* 4:10 (2012).

38. Getz GS, Reardon CA. Diet and murine atherosclerosis. *Arterioscler. Thromb. Vasc. Biol.* 26:242-249 (2006).

39. Smith JD. Mouse models of atherosclerosis. *Lab. Anim. Sci.* 48:573-579 (1998).

40. Rader DJ, FitzGerald GA. State of the art: atherosclerosis in a limited edition. *Nat. Med.* 4:899-900 (1998).

41. King JL, Miller RJ, Blue JP, O'Brien WD, Erdman JW. Inadequate dietary magnesium intake increases atherosclerotic plaque development in rabbits. *Nutr. Res.* 29:343-349 (2009).

42. Smith BW, King JL, Miller RJ, Blue JP, Jr., Sarwate S, O'Brien WD, Jr., Erdman JW, Jr. Optimization of a low magnesium, cholesterol-containing diet for the development of atherosclerosis in rabbits. *J. Food Res.* 2:168-178 (2013).

43. Constans J, Conri C. Circulating markers of endothelial function in cardiovascular disease. *Clin. Chim. Acta* 368:33-47 (2006).

44. Spiel AO, Gilbert JC, Jilma B. von Willebrand factor in cardiovascular disease: focus on acute coronary syndromes. *Circulation* 117:1449-1459 (2008).

Figures and Tables

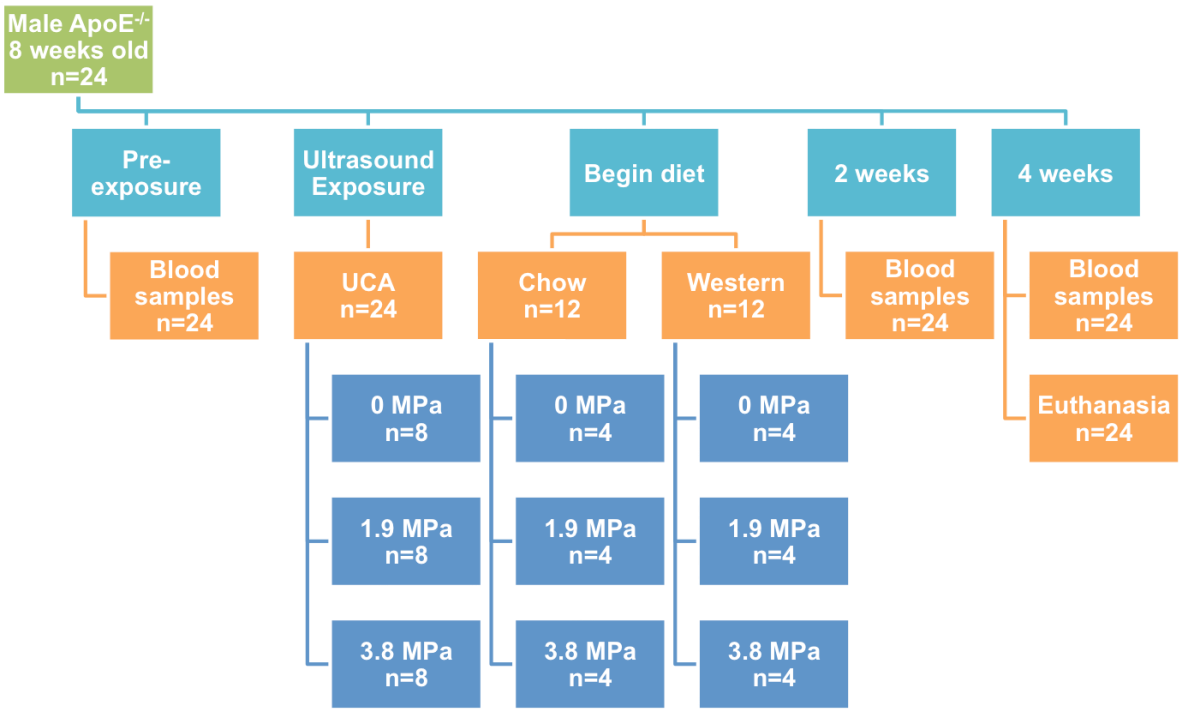

Figure 5.1. Study design. Baseline blood samples were obtained from 24 male ApoE$^{-/-}$ mice. The mice then received contrast agent and were exposed to ultrasound at 0, 1.9, or 3.8 MPa in situ peak rarefactional pressure amplitude (PRPA), with n=8 per group. Half of the mice continued to consume chow diet, and half were switched to the Western diet. Subsequent blood samples were obtained at 2 and 4 weeks. Mice were euthanized at 4 weeks, and aortas were obtained for analysis.

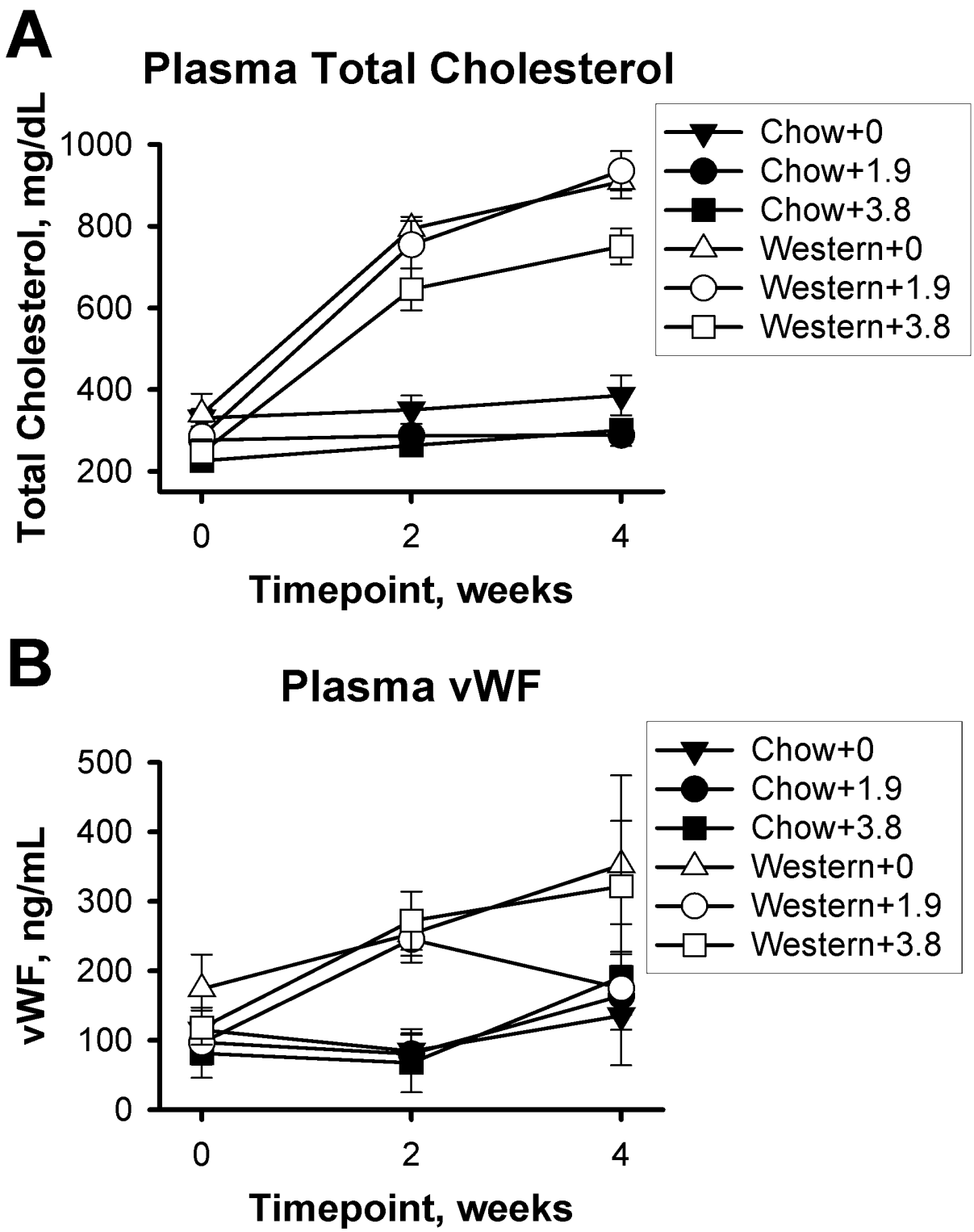

Figure 5.2. Plasma cholesterol (a) and von Willebrand Factor (vWF, b). Plasma total cholesterol was analyzed using an enzymatic colorimetric kit (Wako Chemicals, Richmond, VA). Human control sera (Wako) were included in each assay for quality control. Plasma vWF was determined using an in-house validated sandwich ELISA. Bars are SEM, n=3-4 per group per time point.

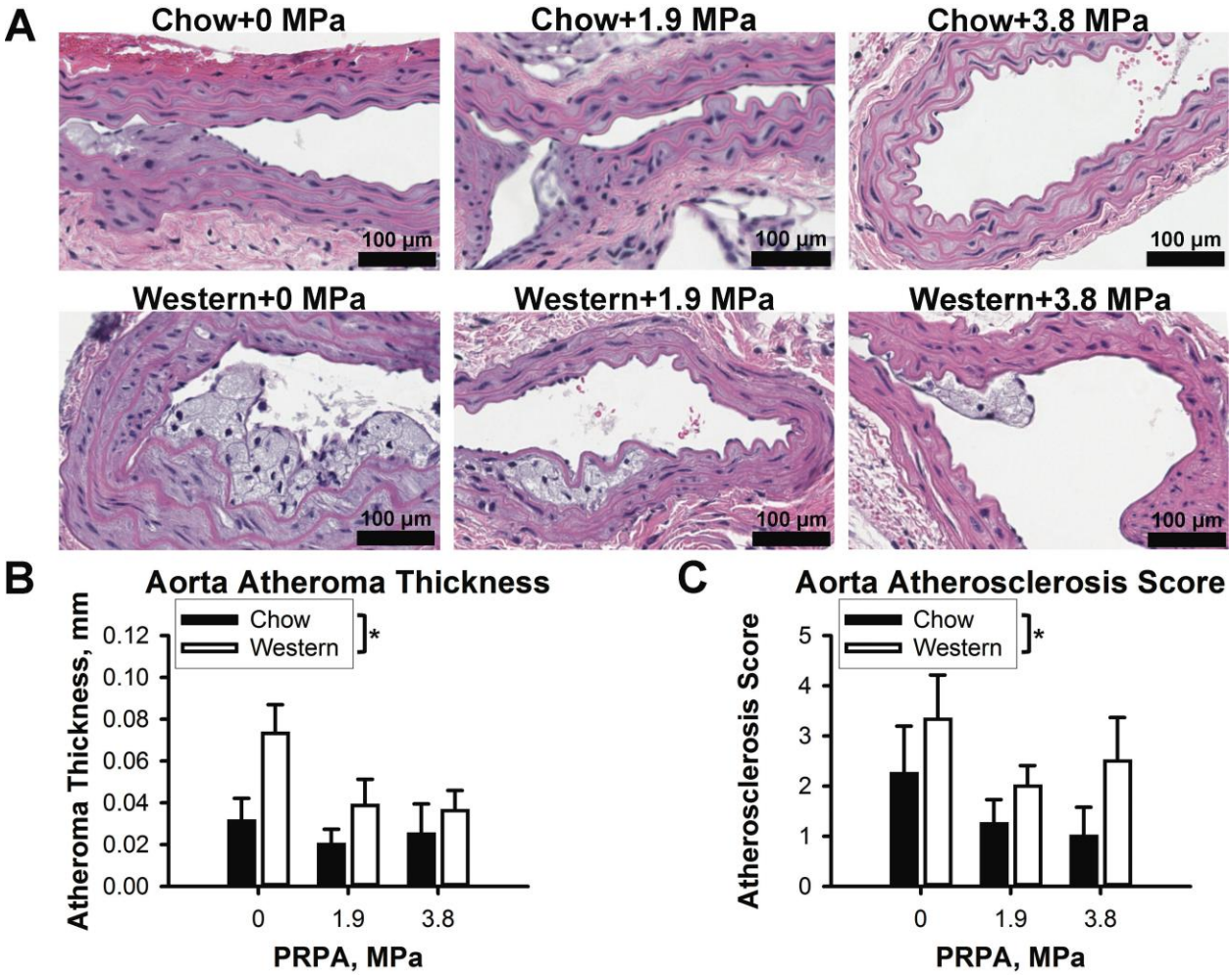

Figure 5.3. Aorta histology. The aortic arch and descending aorta were fixed briefly in situ with 10% neutral buffered formalin (NBF), then carefully excised and fixed in 10% NBF for an additional 24 hours, embedded in paraffin, sectioned, and stained with H&E (a). A pathologist blinded to the exposure conditions measured atheroma thickness with an ocular micrometer (b), and assigned an atherosclerosis score between 0 and 5 using the American Heart Association classification scheme for human atherosclerotic lesions (c). Bars are SEM, n=3-4 per group, *p<0.05. PRPA, in situ peak rarefactional pressure amplitude.

CHAPTER 6: Ultrasound with microbubble contrast agents does not damage skeletal muscle tissue or capillaries in rats

Abstract

This study was designed to evaluate the biological effects of ultrasound and microbubble contrast agents at the tissue-capillary interface, with particular emphasis on the microbubble concentration-dependence of these effects. Eighteen 11-13 week old female Sprague-Dawley rats were divided into 6 groups, with 3 per group. One gracilis muscle per animal was exposed to ultrasound, with the opposite leg serving as a sham control. Animals were euthanized 24 hours post-exposure, and gracilis muscle samples from the site of ultrasound exposure were obtained using a punch biopsy. Formalin-fixed, H&E-stained gracilis muscle sections were evaluated for myofibrillar damage, myocyte necrosis, inflammatory cell infiltrate, hemorrhage, fibrosis, change in fiber size, and presence of centrally located nuclei (which would presumably indicate satellite cell fusion). No adverse biological effects of ultrasound were observed.

Introduction

Ultrasound imaging is ubiquitous in medical practice, and is favored for its low cost, safety and real-time image generation. Ultrasound Contrast Agents (UCAs) are gas-containing microbubbles that were originally developed to improve ultrasound imaging of the heart. In addition to their canonical role in image contrast enhancement, the interaction of ultrasound with UCAs has numerous effects on biological tissue, with capillaries seeming particularly susceptible[1]. One of the more intriguing effects has been an induction of angiogenesis, growth of new capillaries, especially in previously ischemic tissues. The angiogenic effect was first observed in the gracilis muscle of rats[2], and has important implications for the treatment of ischemic conditions like heart attacks, strokes, and peripheral vascular disease. Findings from our research group have extended the initial findings by providing information on vascular endothelial growth factor (VEGF) expression and vascular permeability in the gracilis muscle[3-5]. Although numerous studies have demonstrated capillary damage in animal models after administration of ultrasound with UCAs[1,6,7], recent evidence[5] suggests that the angiogenic effect might be due to an interaction between UCAs and the vascular endothelium, without capillary damage. We used our previously established rat model and its associated methods to investigate ultrasound and contrast agent bioeffects at the gracilis muscle tissue-capillary interface, with a more direct focus on muscle damage. This study evaluated both the UCA concentration-dependence and ultrasound pressure-dependence of acute muscle damage.

Materials and Methods

Animals and Exposimetry

Female Sprague-Dawley rats (n=18, 11-13 weeks old, average body weight of 229 g) were exposed to ultrasound at four concentrations of UCA (0x, 1x, 5x, 10x) and four pressure levels: 0, 0.7, 1.3 and 1.9 MPa (corresponding to Mechanical Indices of 0, 0.7, 1.3 and 1.9, respectively), with n=3 per group (**Table 6.1**). The experimental procedures were performed as previously described[3-5], with minor modifications. Briefly, rats were anesthetized with inhaled isoflurane and placed on a heat pad to maintain body temperature. Hair was then removed from the area of the gracilis muscle with clippers

(Wahl, Sterling, IL) followed by a depilatory agent (Veet; Reckitt Benckiser, Parsippany, NJ) to maximize sound transmission. The tail was cleaned with soap and warm water in preparation for tail vein infusion of UCA. Rats were then secured in dorsal recumbency with a custom-built holder. The site to be exposed was marked, first with a yellow highlighter, and then with a black permanent marker. Mineral oil was then applied to the skin. The bottom of a plastic bucket was removed and covered with plastic wrap (Freeze-tite®; Polyvinyl Films, Inc., Sutton, MA) secured by a rubber band. Degassed water was added to the bucket and heated to 37ºC to avoid vasoconstriction when contacting the animal. The bucket was then lowered until the plastic wrap contacted the skin over the gracilis muscle, and the ultrasound transducer was placed in a custom-built holder and lowered into the bucket.

The UCA solution was then prepared. Definity® (Lantheus Medical Imaging, North Billerica, MA) was agitated in a vial mixer for 45 seconds according to the manufacturer's recommendation. UCA doses were adjusted for the rat as described[5] and mixed with saline in a syringe (BD, Franklin Lakes, NJ) at three different concentrations: 1x (6.7% Definity®, 5×10^8 microbubbles/mL), 5x (17% Definity®, 2×10^9 microbubbles/mL), and 10x (50% Definity®, 5×10^9 microbubbles/mL). Saline alone was infused for control animals. A butterfly catheter (Surflo; Terumo, Somerset, NJ) was inserted into a lateral tail vein, with success verified by aspiration of blood from the vein. First, 0.5 mL UCA solution was manually infused over a 30 second time period to introduce UCA into the circulation. Next, the syringe was placed in an infusion pump (KD Scientific, Inc., Holliston, MA) set to 0.067 mL/min. The UCA infusion and ultrasound exposure were started simultaneously.

Ultrasound exposures were performed using a 1 MHz focused f/3 single-element transducer, with 10 Hz pulse repetition frequency, 10 μs pulse duration, and 5 min exposure duration on each leg. Weekly transducer calibrations were performed in 22ºC degassed water according to established procedures[8,9]. One gracilis muscle per animal was exposed to ultrasound, with the opposite leg serving as a sham control. In order to blind the researcher handling the animals to the exposure conditions during the experiment and subsequent tissue collection, a separate researcher operated the ultrasound equipment and randomly selected the leg to be exposed. The UCA solution

was infused continuously from the beginning of the exposure of the first leg until the exposure of the second leg was completed (15 minutes total).

Animals were euthanized 24 hours post-exposure, and gracilis muscle samples from the site of ultrasound exposure were obtained using a 6 mm punch biopsy. Rats typically removed the black dot marking the exposure site, but the highlighter was visualized using a handheld black light (UVL-23R; UVP, Upland, CA). Biopsy samples were fixed in 10% neutral buffered formalin for 2-6 hours, embedded in paraffin, cut into 3 μm sections, and mounted on slides for evaluation.

Histology

Formalin-fixed, H&E-stained gracilis muscle sections were evaluated for myofibrillar damage, myocyte necrosis, inflammatory cell infiltrate, hemorrhage, fibrosis, change in fiber size, and presence of centrally located nuclei (a marker of satellite cell fusion) by a board-certified pathologist.

Results and Discussion

Ultrasound-mediated destruction of microbubbles has biological effects that range from detrimental to therapeutic. Our objective in this study was to characterize the effects of ultrasound and UCAs on skeletal muscle tissue and capillaries. We performed ultrasound imaging at four different pressure levels, with intravenous administration of the UCA Definity at four different doses. The investigators who originally characterized the pro-angiogenic effect of ultrasound-mediated microbubble destruction[2] reported that 1 MHz ultrasound was effective at rupturing capillaries, while higher frequencies were not. We based our use of a 1 MHz transducer on this information in order to maximize the potential for biological effects. Despite rigorously performed methods, we did not observe histological evidence of damage after the experimental procedure (**Figure 6.1**), supporting our previous hypothesis[5] of a non-destructive ultrasound-UCA-endothelium interaction.

Acknowledgements

This work was supported by NIH R37EB002641. We acknowledge Michael Kurowski and Presence Covenant Medical Center for their contributions.

References

1. Miller DL, Averkiou MA, Brayman AA, Everbach EC, Holland CK, Wible JH, Wu J. Bioeffects considerations for diagnostic ultrasound contrast agents. *J. Ultrasound Med.* 27:611-616 (2008).

2. Song J, Qi M, Kaul S, Price RJ. Stimulation of arteriogenesis in skeletal muscle by microbubble destruction with ultrasound. *Circulation* 106:1550-1555 (2002).

3. Johnson CA, Sarwate S, Miller RJ, O'Brien WD, Jr. A temporal study of ultrasound contrast agent-induced changes in capillary density. *J. Ultrasound Med.* 29:1267-1275 (2010).

4. Johnson CA, Miller RJ, O'Brien WD, Jr. Ultrasound contrast agents affect the angiogenic response. *J. Ultrasound Med.* 30:933-941 (2011).

5. Johnson CA, O'Brien WD, Jr. The angiogenic response is dependent on ultrasound contrast agent concentration. *Vasc. Cell* 4:10 (2012).

6. Villanueva FS. Getting good vibes: the therapeutic power of microbubbles and ultrasound. *JACC Cardiovasc. Imaging* 5:1263-1266 (2012).

7. Chappell JC, Klibanov AL, Price RJ. Ultrasound-microbubble-induced neovascularization in mouse skeletal muscle. *Ultrasound Med. Biol.* 31:1411-1422 (2005).

8. Raum K, O'Brien WD, Jr. Pulse-echo field distribution measurement technique of high-frequency ultrasound sources. *IEEE Trans. Ultrason. Ferroelectr. Freq. Control* 44:810-815 (1997).

9. Zachary JF, Sempsrott JM, Frizzell LA, Simpson DG, O'Brien WD, Jr. Superthreshold behavior and threshold estimation of ultrasound-induced lung hemorrhage in adult mice and rats. *IEEE Trans. Ultrason. Ferroelectr. Freq. Control* 48:581-592 (2001).

Figures and Tables

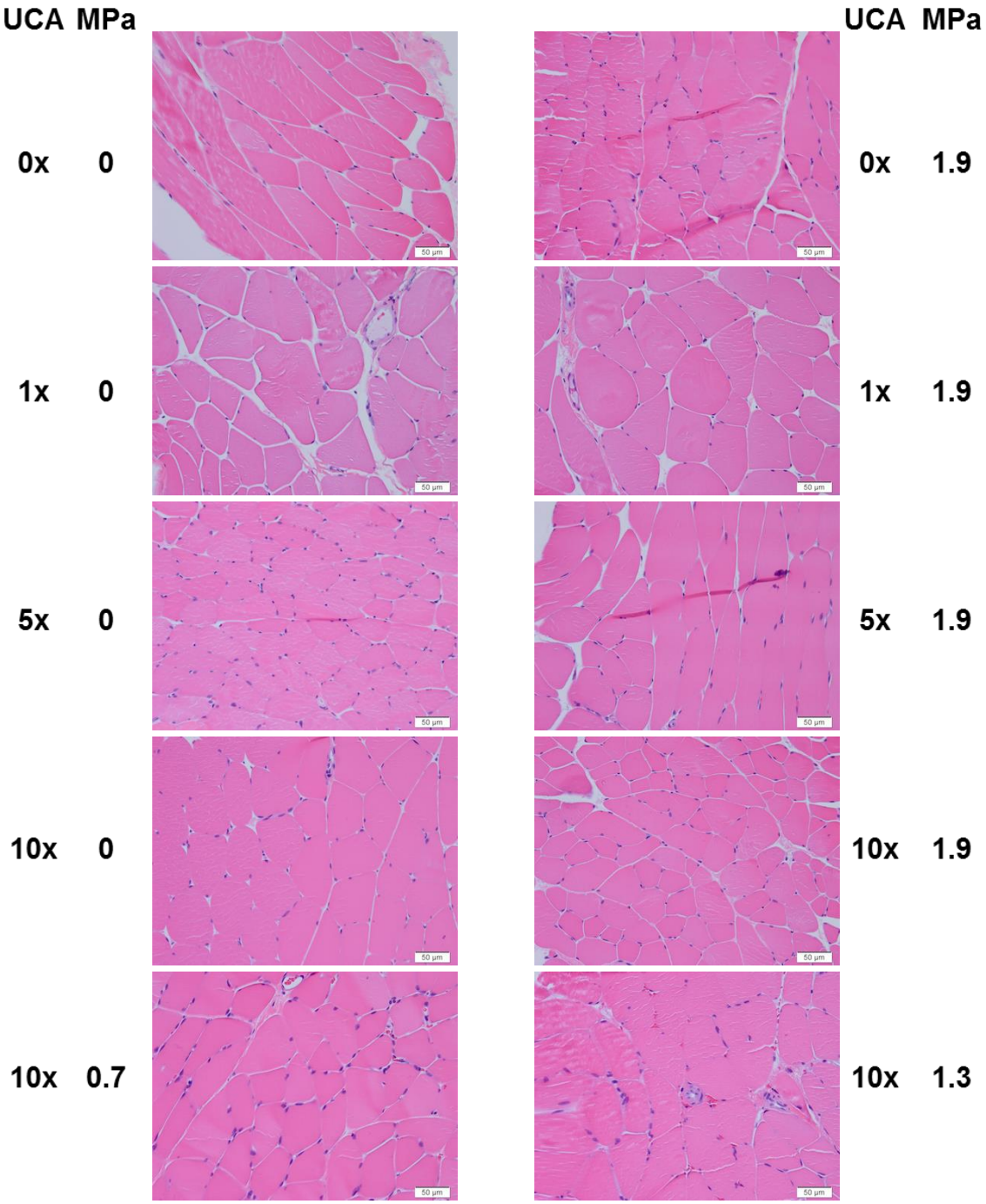

Figure 6.1. Gracilis muscle histology. Gracilis muscle samples were collected by punch biopsy 24 hours after administration of ultrasound and UCA, fixed in 10% neutral buffered formalin for 2-6 hours, paraffin-embedded, cut into 3 µm sections, mounted on slides, and stained with hematoxylin and eosin. Images were captured at 40x magnification and scale bars are 50 µm. Minor tissue folding artifacts that appear in some images are a result of histological processing and do not indicate tissue damage. PRPA, derated peak rarefactional pressure amplitude; UCA, ultrasound contrast agent.

[UCA]	PRPA 0	0.7	1.3	1.9
0	(3)			3
1x	(3)			3
5x	(3)			3
10x	(3)	3	3	3

Table 6.1. Experimental design with 18 female Sprague-Dawley rats. Numbers in parentheses represent samples from sham-exposed gracilis muscles.

CHAPTER 7: Tomatoes and soy germ for reduction of atherosclerosis in ApoE$^{-/-}$ mice

Abstract

Dietary patterns with cardiovascular benefits have been established, but the relative contributions of individual foods and food components, alone or in combination, remain unclear. Male ApoE$^{-/-}$ mice were fed either a purified AIN-93G control diet, a Western diet, or a Western diet with 10% tomato powder, 2% soy germ, or the combination, for four weeks, with ten animals per group. Plasma total cholesterol and triglycerides were measured with enzymatic colorimetric kits, and serum amyloid A (SAA) was measured by ELISA. The remainder of the aorta was also sectioned and stained with H&E. Liver lipids were extracted with chloroform:methanol, and triglycerides, free and esterified cholesterol measured with enzymatic colorimetric kits. Expression of Cyp27a1, Cyp7a1, Abcg5, and Abcg8 in the liver was determined by quantitative polymerase chain reaction. Sections of the aortic root and aorta were cut and stained with H&E to assess extent of atherosclerotic lesions. Western diet animals had greater liver and adipose weights, plasma cholesterol and SAA, liver lipids, and atherosclerosis than AIN-93G animals. Tomato diets further increased plasma cholesterol, but also increased expression of the Abcg5/8 transporters involved in cholesterol efflux. Addition of soy germ alone to the Western diet attenuated Western-diet induced increases in plasma cholesterol, liver lipids and gonadal adipose weight. Tomato and soy germ did not decrease atherosclerosis as measured by H&E-stained sections of the aortic root, aortic arch and descending aorta. The results of this study do not support the use of either tomatoes or soy germ for reduction of atherosclerosis, but suggest beneficial effects of soy germ on lipid metabolism.

Introduction

Cardiovascular Disease (CVD) claims nearly 800,000 lives per year in the United States[1], and remains the leading cause of death despite significant medical advances. A condition known as atherosclerosis drives the development of CVD. Atherosclerosis is a complex pathological process characterized by entrance of cholesterol-containing lipoprotein particles into the arterial wall, with subsequent inflammation and formation of lipid-rich plaques[2]. Atherosclerosis progresses silently throughout life, manifesting itself during adulthood in heart attacks and strokes. Diet has been acknowledged as an important determinant of CVD risk[3]. In epidemiological studies, adherence to a healthy diet rich in fruits, vegetables, nuts and whole grains has been shown to reduce risk of CVD by up to 80%[4] and reduce mortality if CVD is already present[5]. Although the benefits of fruit and vegetable consumption are clear, effective combinations of specific nutritional components remain to be identified. Evidence points to potential cardiovascular benefits of tomatoes[6,7] and soy germ[8,9], but there is a need for controlled animal studies to evaluate their effects on atherosclerosis. We hypothesized that tomatoes and soy germ would decrease atherosclerosis and lipid bioaccumulation in ApoE$^{-/-}$ mice.

Materials and Methods

Experimental Diets

Tomato powder (Drum Dried -20; FutureCeuticals, Momence, IL) and soy germ (SoyLife Complex Regular; Frutarom, Londerzeel, Belgium) were added to a Western diet (TD.10885; Harlan Teklad, Madison, WI). Composition of the experimental diets is given in **Table 7.1**. Diets were balanced for total energy, protein, fat, digestible carbohydrates and fiber. To prevent degradation of the heat-labile carotenoids, diets were pelleted without heat and air-dried overnight. Carotenoids were extracted from diets with hexane and quantified by HPLC using a 150x4.6 mm YMC C30 column (3 µm particle size) with a modified Yeum gradient method[10] as previously described[11].

Animals

The University of Illinois Institutional Animal Care and Use Committee approved all live animal procedures. Male ApoE$^{-/-}$ mice (n=50, **Figure 7.1**) were allowed to acclimate

to the animal facility for ≥2 days, and baseline blood samples were collected from the submandibular region by puncture with a 5 mm lancet (Goldenrod; MEDIpoint Inc., Mineola, NY) into an EDTA-coated capillary tube (Microvette; Sarstedt AG & Co., Nümbrecht, Germany), centrifuged at 2500 x *g* and 4ºC for 10 minutes, aliquotted and frozen at -50ºC. Mice were then randomized to one of five experimental diets: AIN-93G control (AIN), Western diet (WD), Western diet with 2% soy germ (WDSG), Western diet with 10% tomato powder (WDTP), or Western diet with 10% tomato powder and 2% soy germ (WDTPSG), with ten mice per diet, and fed three times per week (35-40 g total, adequate for *ad libitum* intake) for four weeks. Mice were individually housed and given *ad libitum* access to water. Feed intake was measured each time the animals were fed and body weights were measured weekly. After four weeks, mice were fasted overnight (10-14 hours), and blood samples were collected from the submandibular region. Mice were then euthanized with CO_2 and perfused with 20 mL cold PBS. Liver and gonadal adipose were removed, sectioned, frozen by immersion in liquid nitrogen, and stored at -50ºC. A portion of the liver was added to 5 mL RNA preservation solution (RNAlater; QIAGEN, Valencia, CA) for 24 hours at 4ºC, then blotted dry and stored at -50ºC. The heart was excised with 1 mm aorta attached. The bottom half was removed with careful attention to the orientation of the aorta, immersed in OCT inside a 12x12x20 mm tapered cryomold (Electron Microscopy Sciences, Hatfield, PA), frozen in 2-methylbutane surrounded with dry ice, wrapped in parafilm, and stored at -50ºC. The rest of the aorta was dissected into 14-15 pieces, fixed in NBF, sectioned and stained with H&E as previously described (Chapter 5).

Blood Analysis

Total cholesterol and triglycerides were measured using enzymatic colorimetric kits (Wako Chemicals, Richmond, VA) with samples plated in triplicate and human control sera (Wako) included in each assay to evaluate the reproducibility of measurement. Intra-assay and inter-assay coefficients of variation for mouse plasma samples were 2.3% and 2.4% for total cholesterol, and 2.7% and 4.0% for triglycerides. Intra-assay and inter-assay coefficients of variation for control sera were 2.4 and 2.9% for total cholesterol and 1.3% and 3.4% for triglycerides. Serum Amyloid A (SAA) was measured

by ELISA (Life Technologies). The antibodies in the assay react with murine SAA1 and SAA2. Intra-assay and inter-assay precision were 5.2% and 7.7%.

Liver Lipid Analysis

Total lipids were extracted from an average of 0.42g liver using chloroform:methanol and quantified by weight as previously described[12,13]. Lipids were then re-suspended in the cholesterol assay buffer by vortexing and homogenization, and assayed for triglycerides and free/esterified cholesterol with enzymatic colorimetric kits (BioVision, Milpitas, CA).

Gene Expression Analysis

Total RNA was isolated from liver tissue using TRIzol (Life Technologies, Grand Island, NY) and the RNeasy kit (QIAGEN). RNA purity was determined by spectrophotometry at 260 nm, 280 nm, and 230 nm (BioSpectrometer Basic with µcuvette G1.0 1mm; Eppendorf, Hamburg, Germany). RNA integrity was determined by agarose gel electrophoresis, with ethidium bromide (Sigma-Aldrich, St. Louis, MO) used as a fluorescent agent to visualize RNA. An average of 11.0 mg liver tissue yielded 544 ng/µL RNA, with average 260/280 of 1.9 and 260/230 of 2.2. Complementary DNA was synthesized from RNA using the High-Capacity cDNA Reverse Transcription kit (Life Technologies), with reactions performed in a thermal cycler (Eppendorf). Quantitative polymerase chain reaction was carried out in an ABI Prism 7900HT sequence detection system (Applied Biosystems, Foster City, CA) using Taqman probes (Life Technologies; assay IDs: Mm00470430_m1 for Cyp27a1, Mm00484150_m1 for Cyp7a1, Mm00446241_m1 for Abcg5, Mm00445980_m1 for Abcg8, Mm02342430_g1 for Ppia) in duplex, with the reference gene peptidylprolyl isomerase A (Ppia) in a primer-limited formulation, and the QuantiNova probe kit (QIAGEN). Gene expression was normalized to Ppia and the AIN-93G control group using the $\Delta\Delta C_T$ method[14].

Histology

Serial 10 µm cryosections of the aortic root[15] were cut from OCT-embedded samples at -20ºC using a cryostat (Leica Microsystems, Nussloch, Germany) and mounted on charged microscope slides (Superfrost Plus Gold; Fisher Scientific, Pittsburgh, PA). A set of six microscope slides was created for each sample, with six sections per slide.

Sections were allowed to dry and adhere to the slides for 30-60 min, fixed in NBF for 5 min, dipped in water for 1 min, allowed to dry for 60 min, and stored at -20ºC until staining. Slides were then stained with H&E. Images were captured using an Olympus BX51 microscope with DP25 camera. Six serial sections with all three valve leaflets visible were quantified by manually tracing lesion area using the DP2 program (Olympus America Inc., Center Valley, PA). Only foam cell lesions underneath the valve leaflets were included. To quantify the extent of atherosclerotic lesions in the rest of the aorta (from 1 mm distal to the aortic root to the renal bifurcation), lesion area was determined for each of the 14-15 pieces and summed for total lesion area. The arch lesion area was based on sections of the first three pieces.

Statistical Analysis

Statistical analysis was performed in SAS 9.3 (SAS Institute, Inc., Cary, NC) for Windows, and graphs were created in SigmaPlot 12.3 for Windows. Differences among means were determined using analysis of variance (ANOVA) and analysis of covariance (ANOCOVA) in the general linear mixed models procedure, with repeated measures testing for serial measurements. Covariance structures were compared graphically and quantitatively, and an appropriate covariance model was fit. Normality was assessed with the Shapiro-Wilk W test in the univariate procedure. Data that did not meet the necessary assumptions were transformed. Each model was first run with all fixed effects and covariates of interest, and then reduced to eliminate non-significant variables. When a significant result was reported for a fixed variable with more than two categories, specific comparisons were made using estimate statements based on the least squares means, and significance values were adjusted for multiple comparisons with the Tukey-Kramer or Bonferroni methods. Regression analyses were conducted in the regression procedure. Regression models were evaluated for normality (Shapiro-Wilk W), heterogeneity of residual variances (statistically by Spearman rank-order correlation between absolute values of residuals and predicted values, and graphically by plotting residuals vs. predicted values), serial correlation (Durbin-Watson D statistic), and influential observations (Cook's D statistic).

Results

Animals and Diets

The diet pelleting process did not impact carotenoid levels or isomerization (**Figure 7.2**). The pelleted diet appears to have more lycopene than the other diets, but this difference was not statistically significant ($p=0.24$ by ANOVA). A portion of the pellet with slightly more tomato powder may have been used for extraction.

All mice gained weight progressively during the study ($p<0.0001$ by ANOCOVA with baseline body weight as covariate, **Figure 7.3A**). After two weeks, mice in the WDSG, WDTP, and WDTPSG groups were significantly heavier than AIN mice ($p<0.01$ after Bonferroni adjustment). These differences persisted after three and four weeks, with WDTPSG animals also having greater body weights than WD animals ($p<0.05$). Western diet-fed animals had greater liver weight than AIN-93G control animals ($p<0.01$ by ANOVA, **Figure 7.3B**), and no differences were seen among Western diet groups. Animals in the WD ($p<0.05$ by ANOVA), WDTP ($p<0.0001$), and WDTPSG ($p<0.0001$) groups had greater gonadal adipose weights than AIN animals. Animals in the WDSG group experienced an attenuated increase in gonadal adipose tissue, with no significant difference from AIN ($p=0.21$) or WD ($p=0.69$), but significantly less adipose than WDTP and WDTPSG ($p<0.05$).

Animals consumed 3-4 g feed (12-18 kcal) per day (**Figure 7.3C-D**). Animals in Western diet groups consumed significantly more kcal per day than the 12.7 kcal/day average for animals fed AIN-93G (14.3 kcal/day and $p<0.05$ for WD, $p<0.0001$ for WDSG (16.4 kcal/day), WDTP (15.8 kcal/day), and WDTPSG (17.7 kcal/day) by repeated-measures ANOVA; all feed intake p values adjusted with a Tukey test). WDSG ($p<0.05$) and WDTPSG ($p<0.0005$) animals consumed more feed than WD animals, but WDTP animals did not ($p=0.27$). Among the tomato and soy groups, WDTPSG animals consumed more than WDTP ($p<0.05$) but not WDSG ($p=0.35$). Feed intake was greater overall in week 4 than week 1 ($p<0.05$). The diet*timepoint interaction variable was not significant ($p=0.69$), preventing more detailed sub-comparisons.

Blood Analysis

There were no differences in plasma total cholesterol at baseline (p=0.23 by repeated-measures ANOVA; **Figure 7.4A**). After 4 weeks on experimental diets, plasma cholesterol levels increased significantly within all groups (p=0.001 for AIN, p<0.0001 for all Western diet groups by repeated-measures ANOVA), and were significantly higher in all Western-diet groups than AIN-93G (p<0.0001). The WDTP and WDTPSG groups had significantly higher plasma cholesterol than the Western diet group (p<0.0001). The WDSG group did not have significantly higher cholesterol levels than the WD group (p=0.47), despite consuming significantly more feed each day. Total cholesterol and feed intake were correlated in linear regression analysis ($F_{0.05}(1,47)=26.82$, $r^2=0.36$, p<0.0001). Plasma triglycerides did not differ among groups at 0 or 4 weeks, or within groups over time (**Figure 7.4B**).

SAA levels were not different among groups at the beginning of the study (p=0.54 by repeated-measures ANOVA, **Figure 7.4C**). SAA increased within all groups after four weeks compared with initial levels (p<0.0001). At 4 weeks, Western diet groups had significantly higher SAA than the AIN-93G group (p<0.0001), but no differences were seen among the Western diet groups. Data were log-transformed to meet the assumption of normality.

Liver Lipids and Gene Expression

Total liver lipids were greater in Western diet animals than in AIN-93G animals (83.8 vs. 162 mg/g liver, p<0.01 by ANOVA with Tukey-Kramer adjustment for multiple comparisons, **Figure 7.5A**). WDTP (167 mg/g, p<0.001) and WDTPSG (185 mg/g, p<0.001), but not WDSG animals (126 mg/g, p=0.12), also had significantly higher liver lipids than AIN animals. Similarly, liver free cholesterol was elevated in WD (p<0.05 by ANOVA with Tukey-Kramer adjustment for multiple comparisons), WDTP (p<0.01), and WDTPSG (p<0.05) groups, but this increase was attenuated in the WDSG group (p=0.24, **Figure 7.5B**). Liver total and esterified cholesterol were increased in Western diet groups (p<0.05), with no differences among the groups (**Figure 7.5C-D**). No differences were seen among groups in liver triglycerides (p=0.67, **Figure 7.5E**).

Relative Cyp27a1 expression levels were unchanged across experimental groups (p=0.37, **Figure 7.5F**). Cyp7a1 expression levels were affected by diet (p<0.05 for

overall diet effect by ANOVA), with levels reduced by half in the WD and WDTPSG groups, though differences among diets were too small to be statistically significant after adjustment for multiple comparisons. Abcg5 and Abcg8 levels were increased in the WDTP group relative to AIN and WD ($p<0.05$ by ANOVA with Tukey-Kramer adjustment for multiple comparisons), but were unchanged in the other Western diet groups.

Histology

Aortic root lesion areas were 35,500 μm^2 for AIN, 92,400 μm^2 for WD, 98,700 μm^2 for WDSG, 101,000 μm^2 for WDTP, and 129,000 μm^2 for WDTPSG. When normalized to the total inner area of the aortic root, all Western diet groups had significantly greater percent lesion area than AIN, but were not different from each other (3.7% lesion area for AIN, 10.4% and $p<0.05$ for WD, 10.7% and $p<0.005$ for WDSG, 12.5% and $p=0.05$ for WDTP, 13.9% and $p<0.05$ for WDTPSG; by ANOVA with Bonferroni adjustment for multiple comparisons; **Figure 7.6A**). Lesion area in the rest of the aorta was significantly greater than AIN controls in the WDSG ($p<0.01$), WDTP ($p<0.01$), and WDTPSG ($p<0.05$) groups, but not different among Western diet groups (**Figure 7.6B**). Data were log-transformed to meet the assumption of normality. No differences were seen among groups in aortic arch lesion area. Linear regression analyses revealed weak but significant correlations between lesion area in the aortic root and the rest of the aorta ($F_{0.05}(1,32)=11.42$, $r^2=0.26$, $p<0.005$ for raw aortic root values; $F_{0.05}(1,32)=11.00$, $r^2=0.26$, $p<0.005$ for normalized aortic root values), between plasma total cholesterol and aortic root lesion area ($F_{0.05}(1,32)=8.79$, $r^2=0.22$, $p<0.01$ for raw values; $F_{0.05}(1,32)=15.39$, $r^2=0.32$, $p<0.001$ for normalized aortic root values; aortic root lesion area dependent variables were log-transformed to correct heterogeneity of residual variances), and between plasma total cholesterol and aorta lesion area ($F_{0.05}(1,42)=14.98$, $r^2=0.26$, $p<0.001$; the aorta lesion area dependent variable was log-transformed to correct non-normality and heterogeneity of residual variances). Feed intake did not contribute significantly to the normalized aortic root lesion area statistical model ($p=0.13$), nor was it correlated with normalized aortic root lesion area ($F_{0.05}(1,32)=3.37$, $r^2=0.10$, $p=0.08$).

Discussion

This study evaluated the ability of dietary tomato and soy germ to reduce atherosclerosis in ApoE$^{-/-}$ mice. While it would be interesting to study the impact of either tomato powder of soy germ individually, evaluation of both in combination is a particularly novel aspect of this study. Tomatoes were selected based on previous literature suggesting their beneficial cardiovascular effects. Consumption of lycopene, a bioactive carotenoid pigment found in tomatoes, has been shown to improve endothelial function in a randomized controlled trial[16], and an inverse relationship between serum lycopene concentration and arterial stiffness has also been noted[17]. Whole tomatoes contain many other phytochemicals and micronutrients that can benefit cardiovascular health[18], so tomatoes can be provided in the diet as a more practical approach than lycopene supplementation. Additionally, previous work has demonstrated greater health benefit to consuming whole tomatoes instead of lycopene supplements[19]. Although some studies have suggested cardiovascular benefits of tomatoes, most experts agree that the literature is not conclusive and that more research is needed[7,20-22]. Soy germ is a component of whole soybeans that is separated from soy protein isolate during processing in an isoflavone-rich “hypocotyledon” fraction. It was selected as an additional dietary ingredient based on clinical trial data[8,9], as well as prior literature on the hypocholesterolemic effects of other soy products[23,24]. While soy germ has not been previously tested for its effects on atherosclerosis, numerous studies have suggested antiatherosclerotic effects of soy isoflavones[25], including reduced monocyte activation[26,27], and increased excretion of dietary cholesterol[24]. These effects may be dependent on direct activation of ERα by isoflavones[28], and other studies have shown that isoflavones without soy protein reduce atherosclerosis in cholesterol-fed rabbits[29] and ApoE$^{-/-}$ mice[30]. It has also been suggested that the effects of soy isoflavones are mediated through increases in LDLR activity[31]. The amounts of tomato powder and soy germ chosen for this study result in bioaccumulation of tomato and soy bioactive components and metabolites, and correspond to realistically achievable levels of consumption in humans. Tomato powder consumption (10% w/w) by the mice in this study is comparable to 1 cup tomato sauce, ½ cup tomato paste, or 6 cups raw tomatoes per day in humans[32-34]. Soy germ consumption (2% w/w) results in similar

serum isoflavone concentrations to men consuming soy foods or isoflavone supplements[34,35].

All Western diet-fed animals had higher plasma total cholesterol levels than AIN-93G diet animals, which was expected, and helps to serve as a positive control. Cholesterol levels in WDTP and WDTPSG-fed animals were higher still, contrary to our hypothesis, but the WDSG group did not experience this increase despite consuming significantly more feed than WD animals. Similarly, Western diet animals experienced a doubling of total liver lipids and increased gonadal adipose weights, but the WDSG group had attenuated increases. Gonadal adipose is a major adipose depot, comprising about 30% of dissectable adipose in Bl/6 mice[36,37].

The attenuated increases in plasma cholesterol, liver lipid accumulation and adipose weight in WDSG animals led us to hypothesize that soy germ was affecting cholesterol excretion. The primary route of cholesterol disposal from the liver is by secretion into bile, either as bile acids or free cholesterol[38]. We measured gene expression of Cyp7a1 and Cyp27a1, two enzymes involved in bile acid synthesis, and Abcg5/8, which form a heterodimer to efflux cholesterol from the liver into bile. Soy germ did not significantly impact expression of these genes. The regulation of bile acid metabolic enzymes such as CYP7A1 may occur at post-transcriptional levels, including mRNA stability and enzyme activity[39]. There was a modest, yet significant, induction of Abcg5/8 transcription in the WDTP group. This suggests tomato may be able to influence cholesterol efflux, though not enough to overcome the hyperlipidemia of the Western diet-fed ApoE$^{-/-}$ mouse model.

Circulating triglycerides in ApoE$^{-/-}$ mice are only moderately higher than in WT mice[40-42], and in this study, did not increase further in Western diet-fed animals. Why do ApoE$^{-/-}$ mice on Western diet have elevated liver lipids, elevated blood cholesterol (primarily in VLDL and remnants, which typically carry some triglyceride), but not elevated blood triglycerides, as compared to ApoE$^{-/-}$ mice fed the purified AIN-93G control diet? Triglycerides in circulating lipoproteins are removed in extrahepatic tissues by lipoprotein lipase, which is present on capillary endothelial cells[43], and at the liver by hepatic lipase. While ApoE$^{-/-}$ mice have defective hepatic lipoprotein uptake, they do not have defective lipolysis, so the triglycerides may be hydrolyzed to free fatty acids and

taken up by liver and other tissues, producing atherogenic remnant lipoproteins[40,44]. Once these dietary fatty acids reach the liver, they may be used to esterify cholesterol for export in lipoproteins[45]. Contributions to hepatic lipid content, which was elevated in Western-diet fed animals, are made by dietary fat intake, by *de novo* lipogenesis in response to dietary fructose[46], and by re-esterification of adipose-derived circulating free fatty acids.

We chose to measure SAA as a circulating biomarker of systemic inflammation. There are several isoforms of SAA, each with their own characteristics. SAA 1 and 2 are similar isoforms that are responsive to dietary interventions. High fat and cholesterol feeding increase circulating SAA1[47,48], while green and yellow vegetables decrease SAA1/2[49]. SAA1/2 levels are similar in healthy humans and mice[50]. SAA3 is another isoform secreted by macrophages[51] and adipocytes[52] that does not contribute to serum levels of SAA1[52]. SAA3 is a pseudogene in humans but is an actual acute phase protein in mice. Based on this information, SAA1/2 were the most appropriate isoforms to measure. We observed an increase in SAA over time, particularly in Western diet groups. Bacterial infection increases circulating SAA to 350 µg/mL in C57 Bl/6 mice[53], suggesting that the 60-100 µg/mL seen in Western diet animals in this study is indicative of low-grade systemic inflammation. The lack of effect of tomato and soy on SAA suggests the dietary intervention was not able to abrogate mild systemic inflammation in this mouse model.

Consumption of tomato or soy did not reduce atherosclerotic lesion area in the aortic root or the rest of the aorta. The aortic root was the most appropriate region to evaluate for this study, because it is one of the first sites to develop atherosclerotic lesions, and the animals in this study were at an early stage of atherosclerosis[54]. The two gold-standard methods for atherosclerosis assessment are aortic root frozen sections, and *en face* preparations of the aorta[15,55]. The aortic root method generates a tissue cross-section for evaluation of lesion morphology and composition, but does not demonstrate lesion area in the entire aortic tree. The *en face* method allows quantitative determination of aorta surface area lesion coverage, but does not provide information on lesion depth or morphology. The two methods can thus be seen as providing complementary information. The method of measuring lesion area in serial cross-

sections of the aortic arch and descending aorta used in this study addressed limitations of the *en face* method by allowing measurement of lesion cross-sectional area throughout the aorta. Some studies have shown plasma total cholesterol levels to be correlated with *en face* lesion area[42,56], but others have reported that they are not well-correlated[41]. Studies also report that aortic root lesion area is correlated with lesion area in the whole aorta measured by the *en face* method[42,55,57], but this may depend on the stage of atherosclerosis, as lesions appear earliest in the aortic root[54,55]. The weak correlations observed in this study may be due to the early stage of atherosclerosis, when aortic root lesions are most prominent.

In summary, we did not observe a decrease in atherosclerosis in ApoE$^{-/-}$ mice with tomato or soy added to a Western diet. The effects of 2% soy germ alone on cholesterol and lipid metabolism suggest beneficial effects that can be investigated in future work.

Acknowledgements

This work was supported by NIH R37EB002641 to WDO and JWE, and a Beckman Graduate Fellowship to BWS. We acknowledge Lauren Conlon, Vera Huang, Jamie Kelly, Nick Olsen, and Josh Smith for assistance with animal procedures, the University of Illinois Veterinary Diagnostic Lab and Presence Covenant Medical Center for assistance with histology, and the Roy J. Carver Biotechnology Center for assistance with gene expression analysis.

References

1. Go AS, Mozaffarian D, Roger VL, Benjamin EJ, Berry JD, Borden WB, Bravata DM, Dai S, Ford ES, Fox CS *et al.* Heart disease and stroke statistics--2013 update: a report from the American Heart Association. *Circulation* 127:e6-e245 (2013).

2. Libby P, Ridker PM, Hansson GK. Progress and challenges in translating the biology of atherosclerosis. *Nature* 473:317-325 (2011).

3. Mozaffarian D, Appel LJ, Van Horn L. Components of a cardioprotective diet: new insights. *Circulation* 123:2870-2891 (2011).

4. Stampfer MJ, Hu FB, Manson JE, Rimm EB, Willett WC. Primary prevention of coronary heart disease in women through diet and lifestyle. *N. Engl. J. Med.* 343:16-22 (2000).

5. Iestra JA, Kromhout D, van der Schouw YT, Grobbee DE, Boshuizen HC, van Staveren WA. Effect size estimates of lifestyle and dietary changes on all-cause mortality in coronary artery disease patients: a systematic review. *Circulation* 112:924-934 (2005).

6. Willcox JK, Catignani GL, Lazarus S. Tomatoes and cardiovascular health. *Crit. Rev. Food Sci. Nutr.* 43:1-18 (2003).

7. Sesso HD. Carotenoids and cardiovascular disease: what research gaps remain? *Curr. Opin. Lipidol.* 17:11-16 (2006).

8. Clerici C, Setchell KD, Battezzati PM, Pirro M, Giuliano V, Asciutti S, Castellani D, Nardi E, Sabatino G, Orlandi S *et al.* Pasta naturally enriched with isoflavone aglycons from soy germ reduces serum lipids and improves markers of cardiovascular risk. *J. Nutr.* 137:2270-2278 (2007).

9. Clerici C, Nardi E, Battezzati PM, Asciutti S, Castellani D, Corazzi N, Giuliano V, Gizzi S, Perriello G, Di Matteo G *et al.* Novel soy germ pasta improves endothelial function, blood pressure, and oxidative stress in patients with type 2 diabetes. *Diabetes Care* 34:1946-1948 (2011).

10. Yeum KJ, Booth SL, Sadowski JA, Liu C, Tang G, Krinsky NI, Russell RM. Human plasma carotenoid response to the ingestion of controlled diets high in fruits and vegetables. *Am. J. Clin. Nutr.* 64:594-602 (1996).

11. Boileau TW, Clinton SK, Erdman JW, Jr. Tissue lycopene concentrations and isomer patterns are affected by androgen status and dietary lycopene concentration in male F344 rats. *J. Nutr.* 130:1613-1618 (2000).

12. Folch J, Lees M, Sloane Stanley GH. A simple method for the isolation and purification of total lipides from animal tissues. *J. Biol. Chem.* 226:497-509 (1957).

13. Smith BW, Simpson DG, Sarwate S, Miller RJ, Blue JP, Jr., Haak A, O'Brien WD, Jr., Erdman JW, Jr. Contrast ultrasound imaging of the aorta alters vascular morphology and circulating von Willebrand Factor in hypercholesterolemic rabbits. *J. Ultrasound Med.* 31:711-720 (2012).

14. Schmittgen TD, Livak KJ. Analyzing real-time PCR data by the comparative C(T) method. *Nat. Protoc.* 3:1101-1108 (2008).

15. Daugherty A, Whitman SC. in *Methods in Molecular Biology* Vol. 209 *Transgenic Mouse Methods and Protocols* (eds Marten H. Hofker & Jan Deursen) Ch. 16, 293-309 (Humana Press, 2002).

16. Kim JY, Paik JK, Kim OY, Park HW, Lee JH, Jang Y, Lee JH. Effects of lycopene supplementation on oxidative stress and markers of endothelial function in healthy men. *Atherosclerosis* 215:189-195 (2011).

17. Kim OY, Yoe HY, Kim HJ, Park JY, Kim JY, Lee S-H, Lee JH, Lee KP, Jang Y, Lee JH. Independent inverse relationship between serum lycopene concentration and arterial stiffness. *Atherosclerosis* 208:581-586 (2010).

18. Canene-Adams K, Campbell JK, Zaripheh S, Jeffery EH, Erdman JW. The tomato as a functional food. *J. Nutr.* 135:1226-1230 (2005).

19. Canene-Adams K, Lindshield BL, Wang S, Jeffery EH, Clinton SK, Erdman JW, Jr. Combinations of tomato and broccoli enhance antitumor activity in Dunning r3327-h prostate adenocarcinomas. *Cancer Res.* 67:836-843 (2007).

20. Arab L, Steck S. Lycopene and cardiovascular disease. *Am. J. Clin. Nutr.* 71:1691S--1695S; discussion 1696S--1697S (2000).

21. Riccioni G. Carotenoids and cardiovascular disease. *Curr. Atheroscler. Rep.* 11:434-439 (2009).

22. Mordente A, Guantario B, Meucci E, Silvestrini A, Lombardi E, Martorana GE, Giardina B, Böhm V. Lycopene and cardiovascular diseases: an update. *Curr. Med. Chem.* 18:1146-1163 (2011).

23. Erdman JW, Jr. Control of serum lipids with soy protein. *N. Engl. J. Med.* 333:313-315 (1995).

24. Potter SM. Overview of proposed mechanisms for the hypocholesterolemic effect of soy. *J. Nutr.* 125:606S-611S (1995).

25. Nagarajan S. Mechanisms of anti-atherosclerotic functions of soy-based diets. *J. Nutr. Biochem.* 21:255-260 (2010).

26. Nagarajan S, Stewart BW, Badger TM. Soy isoflavones attenuate human monocyte adhesion to endothelial cell-specific CD54 by inhibiting monocyte CD11a. *J. Nutr.* 136:2384-2390 (2006).

27. Babu PVA, Si H, Fu Z, Zhen W, Liu D. Genistein prevents hyperglycemia-induced monocyte adhesion to human aortic endothelial cells through preservation of the cAMP signaling pathway and ameliorates vascular inflammation in obese diabetic mice. *J. Nutr.* 142:724-730 (2012).

28. Adams MR, Golden DL, Register TC, Anthony MS, Hodgin JB, Maeda N, Williams JK. The atheroprotective effect of dietary soy isoflavones in apolipoprotein E-/- mice requires the presence of estrogen receptor-alpha. *Arterioscler. Thromb. Vasc. Biol.* 22:1859-1864 (2002).

29. Yamakoshi J, Piskula MK, Izumi T, Tobe K, Saito M, Kataoka S, Obata A, Kikuchi M. Isoflavone aglycone-rich extract without soy protein attenuates atherosclerosis development in cholesterol-fed rabbits. *J. Nutr.* 130:1887-1893 (2000).

30. Sato M, Sato H, Ogawa A, Nomura R, Takashima S, Bang H-J, Matsuoka H, Imaizumi K. Antiatherogenic effect of isoflavones in ovariectomized apolipoprotein E-deficient mice. *J. Agric. Food Chem.* 55:8967-8971 (2007).

31. Kirk EA, Sutherland P, Wang SA, Chait A, LeBoeuf RC. Dietary isoflavones reduce plasma cholesterol and atherosclerosis in C57BL/6 mice but not LDL receptor-deficient mice. *J. Nutr.* 128:954-959 (1998).

32. Grainger EM, Schwartz SJ, Wang S, Unlu NZ, Boileau TW, Ferketich AK, Monk JP, Gong MC, Bahnson RR, DeGroff VL *et al.* A combination of tomato and soy products for men with recurring prostate cancer and rising prostate specific antigen. *Nutr. Cancer* 60:145-154 (2008).

33. van Breemen RB, Xu X, Viana MA, Chen L, Stacewicz-Sapuntzakis M, Duncan C, Bowen PE, Sharifi R. Liquid chromatography-mass spectrometry of cis- and all-trans-lycopene in human serum and prostate tissue after dietary supplementation with tomato sauce. *J. Agric. Food Chem.* 50:2214-2219 (2002).

34. Zuniga K, Clinton SK, Erdman JW. The interactions of dietary tomato powder and soy germ on prostate carcinogenesis in the TRAMP model. *Cancer Prev. Res.* (2013).

35. Gardner CD, Chatterjee LM, Franke AA. Effects of isoflavone supplements vs. soy foods on blood concentrations of genistein and daidzein in adults. *J. Nutr. Biochem.* 20:227-234 (2009).

36. The Jackson Laboratory. Densitometric survey of 11 inbred strains of mice. *Mouse Phenome Database* (The Jackson Laboratory). MPD 22415, accessed June 24, 2014. http://phenome.jax.org

37. Chesler EJ, Philip VM, Voy BH. Multi-system assessment of 8 inbred founder strains and 54 F1 hybrids of the Collaborative Cross. *Mouse Phenome Database* (The Jackson Laboratory). MPD 43489, accessed June 24, 2014. http://phenome.jax.org

38. Bonamassa B, Moschetta A. Atherosclerosis: lessons from LXR and the intestine. *Trends Endocrinol. Metab.* 24:120-128 (2013).

39. Davis RA, Miyake JH, Hui TY, Spann NJ. Regulation of cholesterol-7alpha-hydroxylase: BAREly missing a SHP. *J. Lipid Res.* 43:533-543 (2002).

40. Zhang SH, Reddick RL, Piedrahita JA, Maeda N. Spontaneous hypercholesterolemia and arterial lesions in mice lacking apolipoprotein E. *Science* 258:468-471 (1992).

41. Zhang SH, Reddick RL, Burkey B, Maeda N. Diet-induced atherosclerosis in mice heterozygous and homozygous for apolipoprotein E gene disruption. *J. Clin. Invest.* 94:937-945 (1994).

42. Veniant MM, Pierotti V, Newland D, Cham CM, Sanan DA, Walzem RL, Young SG. Susceptibility to atherosclerosis in mice expressing exclusively apolipoprotein B48 or apolipoprotein B100. *J. Clin. Invest.* 100:180-188 (1997).

43. Wang H, Eckel RH. Lipoprotein lipase: from gene to obesity. *Am. J. Physiol. Endocrinol. Metab.* 297:E271-E288 (2009).

44. Goldberg IJ, Eckel RH, McPherson R. Triglycerides and heart disease: still a hypothesis? *Arterioscler. Thromb. Vasc. Biol.* 31:1716-1725 (2011).

45. Baum SJ, Kris-Etherton PM, Willett WC, Lichtenstein AH, Rudel LL, Maki KC, Whelan J, Ramsden CE, Block RC. Fatty acids in cardiovascular health and disease: a comprehensive update. *J. Clin. Lipidol.* 6:216-234 (2012).

46. Samuel VT. Fructose induced lipogenesis: from sugar to fat to insulin resistance. *Trends Endocrinol. Metab.* 22:60-65 (2011).

47. Lewis KE, Kirk EA, McDonald TO, Wang S, Wight TN, O'Brien KD, Chait A. Increase in serum amyloid A evoked by dietary cholesterol is associated with increased atherosclerosis in mice. *Circulation* 110:540-545 (2004).

48. Tannock LR, O'Brien KD, Knopp RH, Retzlaff B, Fish B, Wener MH, Kahn SE, Chait A. Cholesterol feeding increases C-reactive protein and serum amyloid A levels in lean insulin-sensitive subjects. *Circulation* 111:3058-3062 (2005).

49. Adams MR, Golden DL, Chen H, Register TC, Gugger ET. A diet rich in green and yellow vegetables inhibits atherosclerosis in mice. *J. Nutr.* 136:1886-1889 (2006).

50. Godenir NL, Jeenah MS, Coetzee GA, Van der Westhuyzen DR, Strachan AF, De Beer FC. Standardisation of the quantitation of serum amyloid A protein (SAA) in human serum. *J. Immunol. Methods* 83:217-225 (1985).

51. Meek RL, Eriksen N, Benditt EP. Murine serum amyloid A3 is a high density apolipoprotein and is secreted by macrophages. *Proc. Natl. Acad. Sci. USA* 89:7949-7952 (1992).

52. Chiba T, Han CY, Vaisar T, Shimokado K, Kargi A, Chen M-H, Wang S, McDonald TO, O'Brien KD, Heinecke JW *et al.* Serum amyloid A3 does not contribute to circulating SAA levels. *J. Lipid Res.* 50:1353-1362 (2009).

53. Amar S, Zhou Q, Shaik-Dasthagirisaheb Y, Leeman S. Diet-induced obesity in mice causes changes in immune responses and bone loss manifested by bacterial challenge. *Proc. Natl. Acad. Sci. USA* 104:20466-20471 (2007).

54. Nakashima Y, Plump A, Raines E, Breslow J, Ross R. ApoE-deficient mice develop lesions of all phases of atherosclerosis throughout the arterial tree. *Arterioscler. Thromb. Vasc. Biol.* 14:133-140 (1994).

55. Meir KS, Leitersdorf E. Atherosclerosis in the apolipoprotein-E-deficient mouse: a decade of progress. *Arterioscler. Thromb. Vasc. Biol.* 24:1006-1014 (2004).

56. Wilund KR, Yu L, Xu F, Hobbs HH, Cohen JC. High-level expression of ABCG5 and ABCG8 attenuates diet-induced hypercholesterolemia and atherosclerosis in Ldlr-/- mice. *J. Lipid Res.* 45:1429-1436 (2004).

57. Tangirala RK, Rubin EM, Palinski W. Quantitation of atherosclerosis in murine models: correlation between lesions in the aortic origin and in the entire aorta, and differences in the extent of lesions between sexes in LDL receptor-deficient and apolipoprotein E-deficient mice. *J. Lipid Res.* 36:2320-2328 (1995).

Figures and Tables

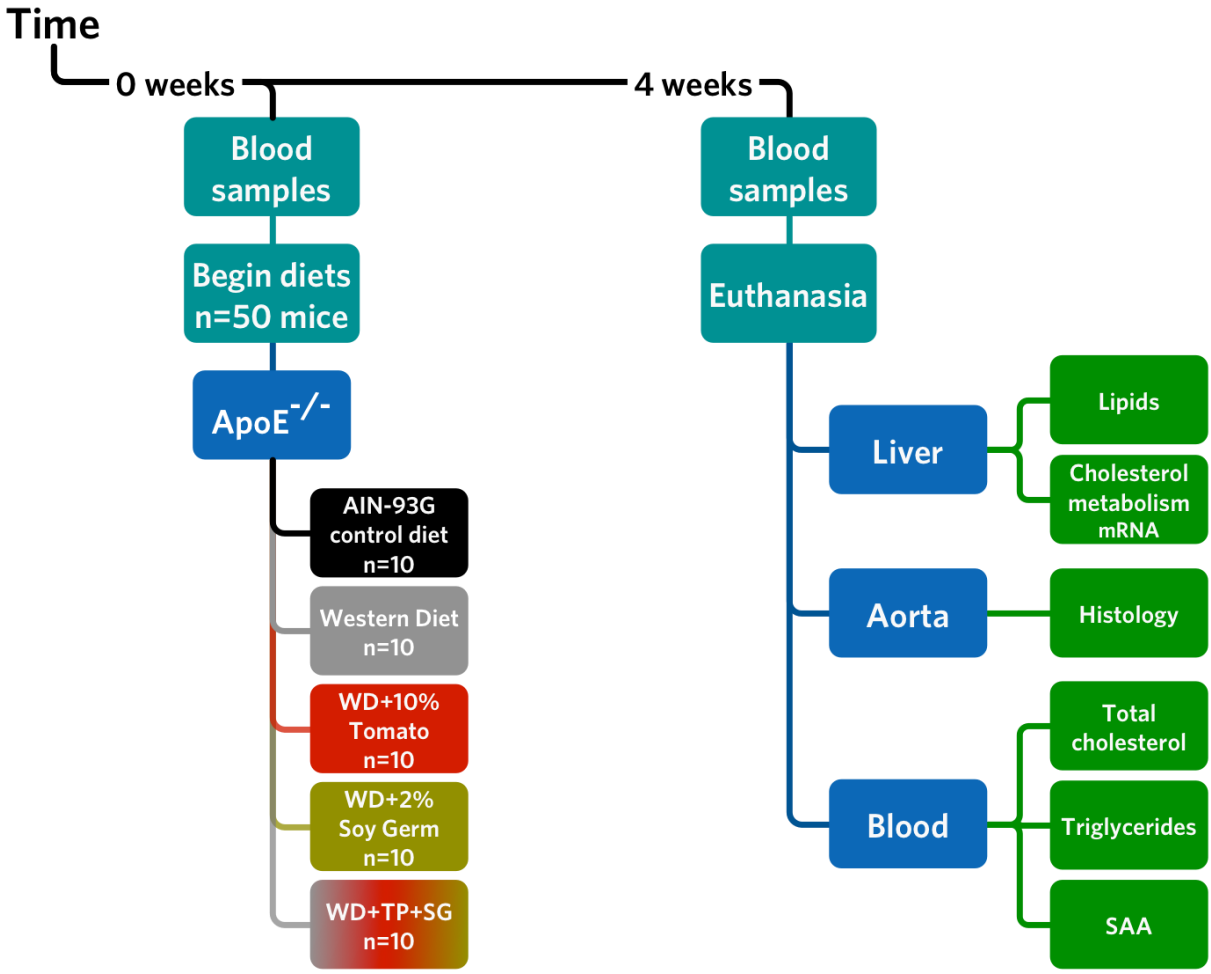

Figure 7.1. Experimental design. Male ApoE-/- mice were fed their respective diets for four weeks, and tissues were then collected and analyzed.

A

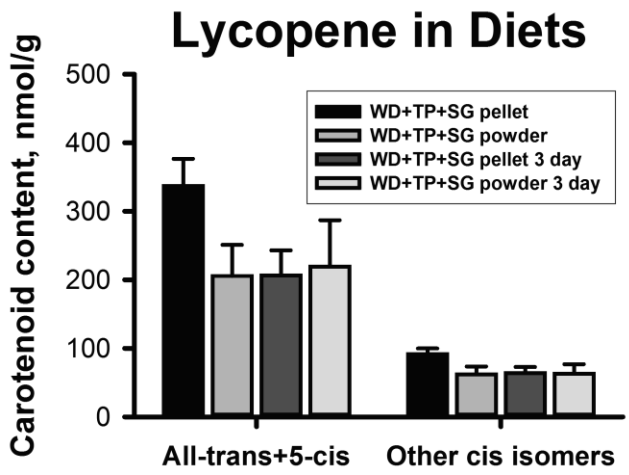

B

Sample	At+5c (%)	Other cis (%)
100% TP	88	12
WD+TP+SG pellet	80	20
WD+TP+SG powder	79	21
WD+TP+SG pellet 3 day	78	22
WD+TP+SG powder 3 day	80	20

Figure 7.2. Lycopene profiles of experimental diets. A, lycopene content was measured by HPLC. B, lycopene isomer profiles in tomato powder and experimental diets. For the "3 day" diet samples, 12 grams of diet were left in a mouse cage in the animal facility with bedding (no water bottle or animal) for 3 days. Powdered diet was left in plastic feed bowls, and pellets were left in the hopper on top. Each bar shows the mean+SEM of triplicate measurements. B, lycopene isomer profiles of experimental diets. WD, Western Diet; TP, Tomato Powder; SG, Soy Germ.

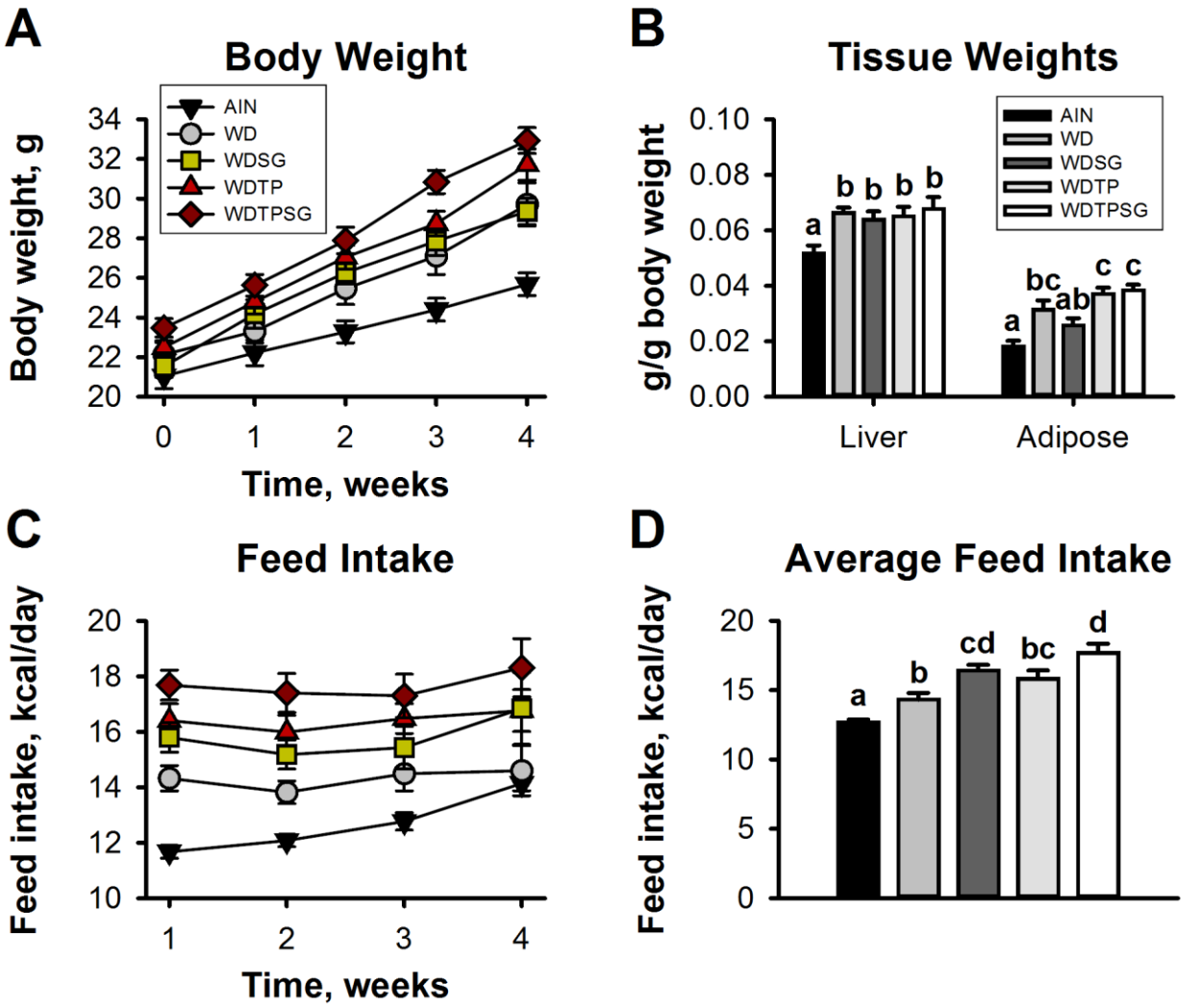

Figure 7.3. Feed intake, body and tissue weights. Feed intake was measured three times per week, body weights measured weekly, and liver and gonadal adipose weights were measured at euthanasia. Means not sharing a letter are significantly different. Errors bars are SEM.

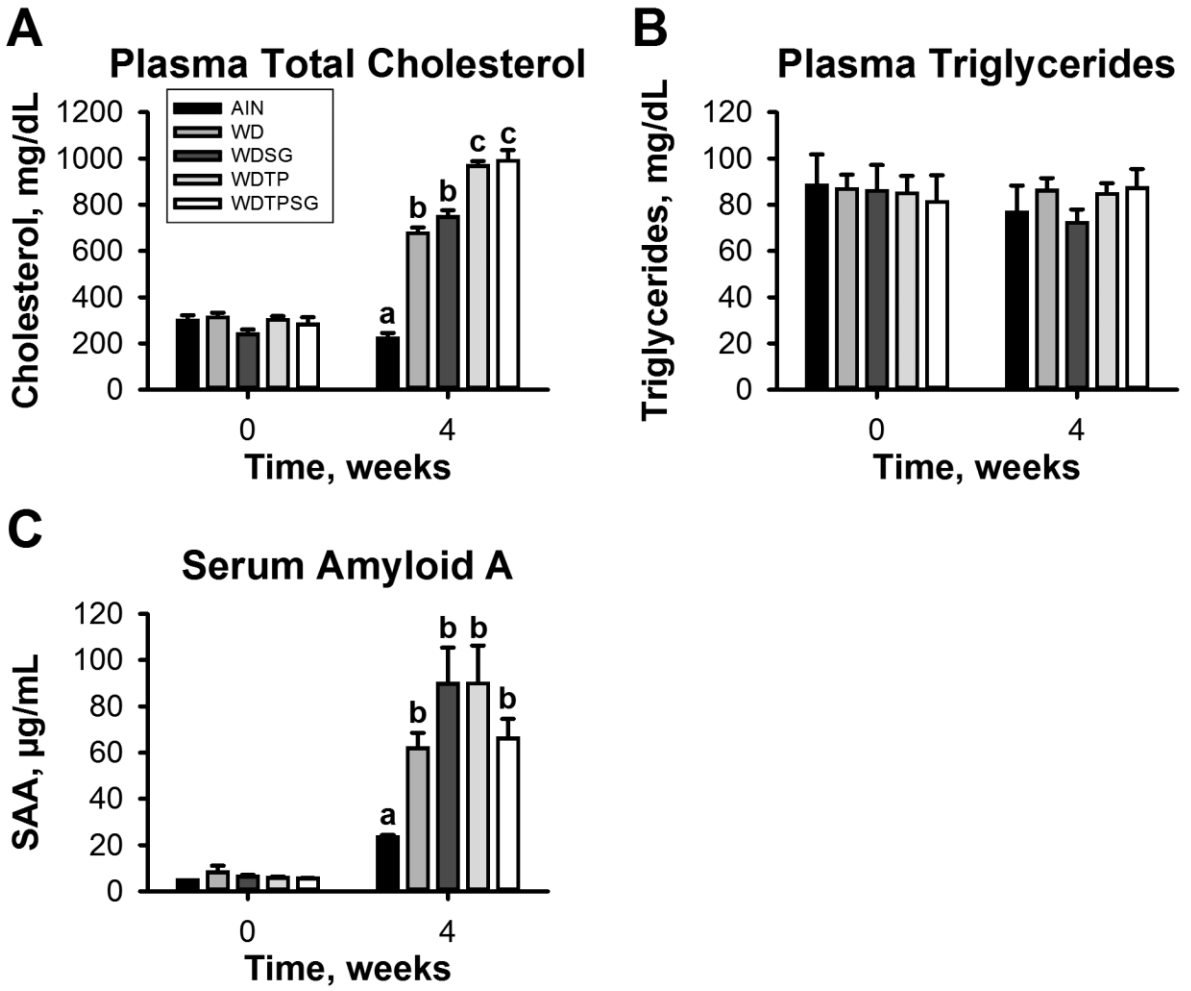

Figure 7.4. Plasma biomarkers. Plasma total cholesterol and triglycerides were measured with enzymatic colorimetric kits, and serum amyloid A was measured by ELISA. Means not sharing a letter are significantly different. Errors bars are SEM.

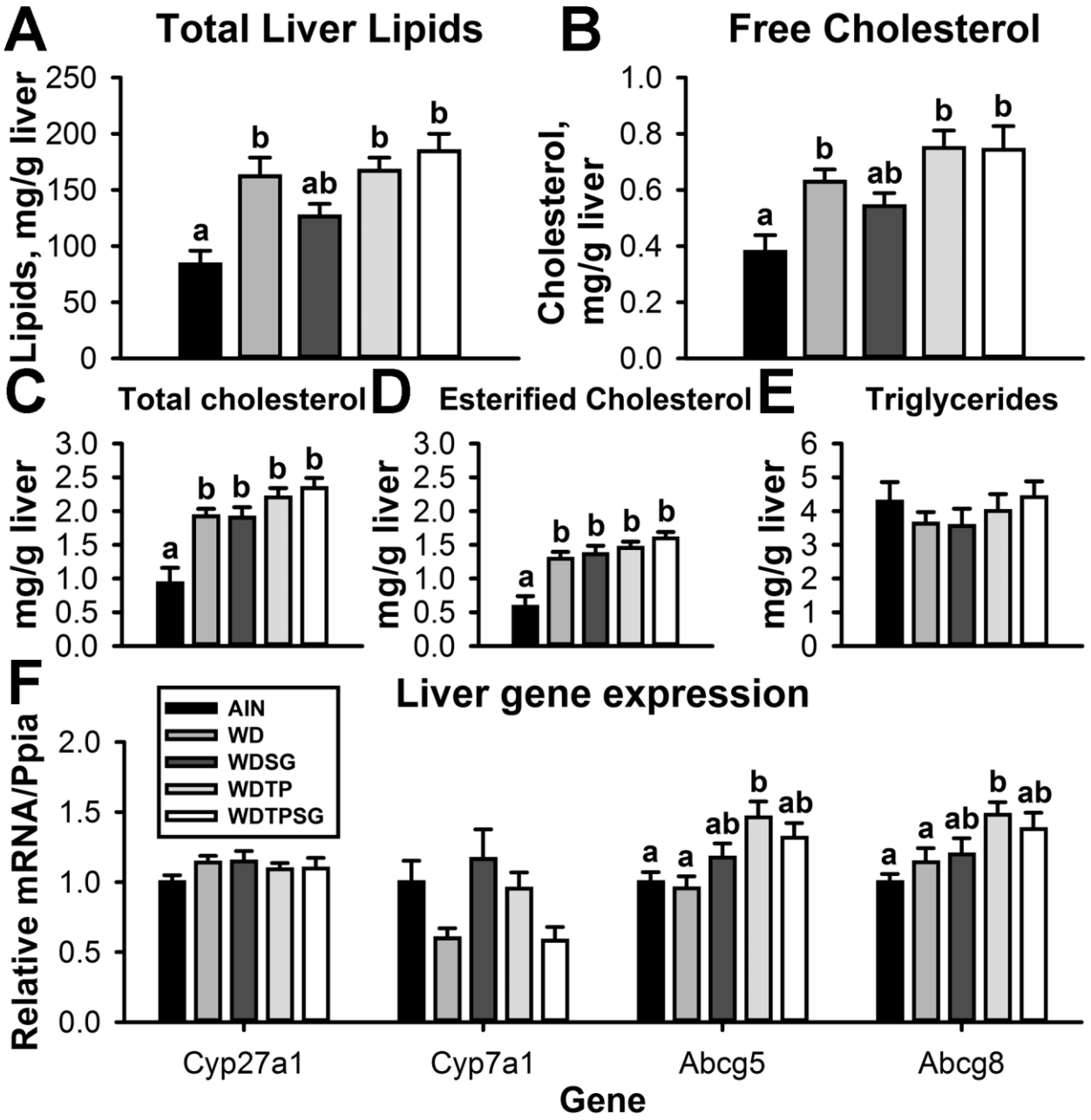

Figure 7.5. Liver lipids and gene expression. A, liver lipids were extracted with chloroform:methanol and total lipids determined by weight. B-E, triglycerides and free/esterified cholesterol were measured in the lipid extracts with enzymatic colorimetric kits. F, gene expression was measured by quantitative real-time polymerase chain reaction and normalized with the $\Delta\Delta C_T$ method. Means not sharing a letter are significantly different. Errors bars are SEM.

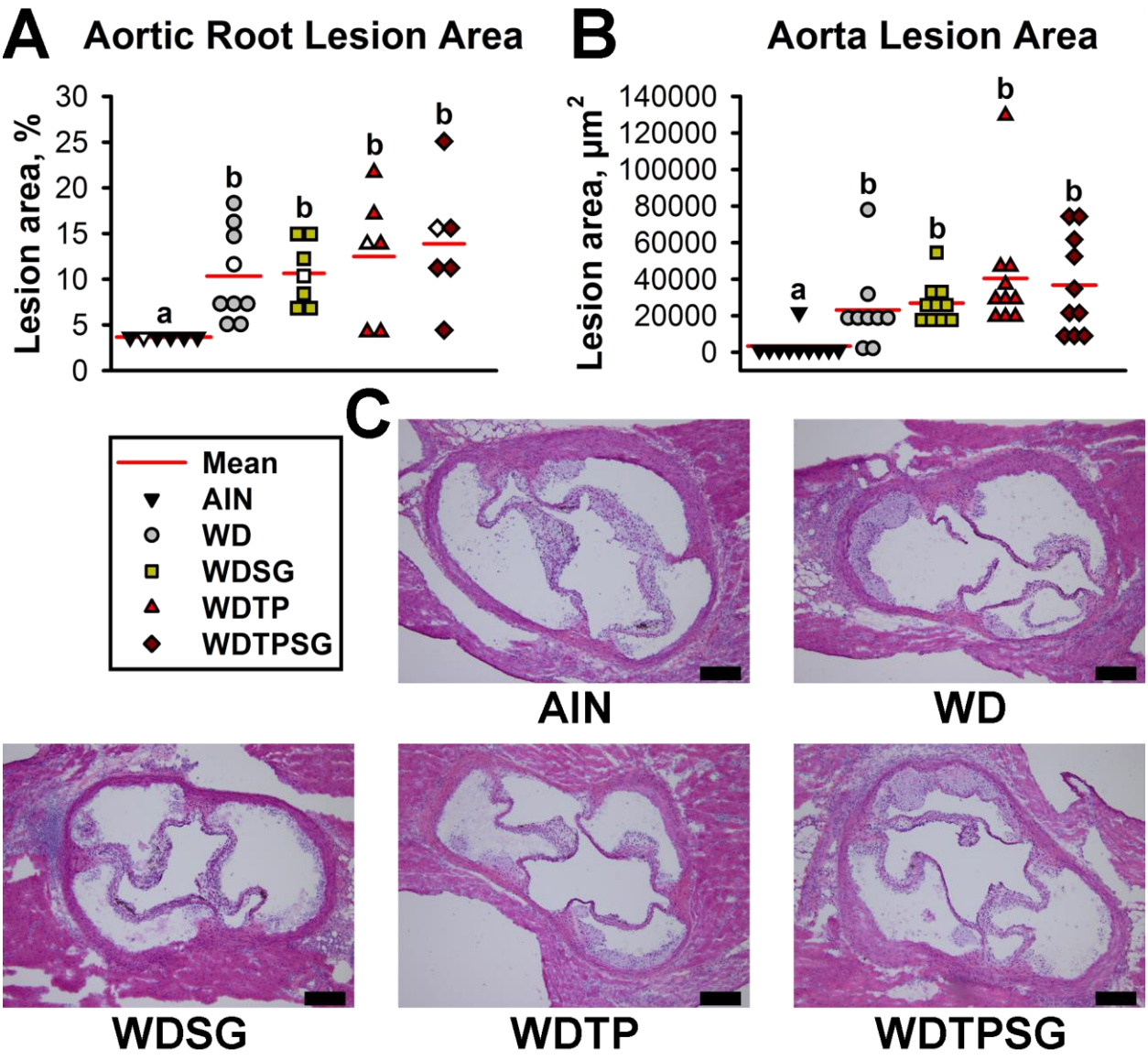

Figure 7.6. Atherosclerosis in the aorta. A, dot density plot of atherosclerotic lesion area in the aortic root. Frozen sections of the aortic root were cut from OCT-embedded tissue samples and stained with H&E. Lesion area was manually traced in six serial sections per animal, normalized to the total inner area of the aortic root, and averaged to provide a value for each animal. Each dot represents the normalized lesion area for one animal, group means are represented by red lines, and means not sharing a letter are significantly different. Symbols with white fill are the representative samples shown in C. B, dot density plot of atherosclerotic lesion area in the aorta. Aortas from the arch to the renal bifurcation were divided into 14-15 pieces, fixed in 10% neutral buffered formalin, and embedded in paraffin. Cross-sections of each piece of the aorta were stained with H&E, and lesion area was manually traced. Each dot represents the total lesion area for one animal. C, Representative H&E stained aortic root sections. Scale bars are 200 µm.

Ingredient (g/kg)	AIN-93G	WD	WDSG	WDTP	WDTPSG
Casein	200	195	184.9	180.6	170.5
L-Cystine	3	3	3	3	3
Corn Starch	397.5	55.46	55.46	43.26	43.26
Maltodextrin	132	60	60	60	60
Sucrose	100	340	340	298.8	298.8
Soybean Oil	70	20	15.2	15.14	10.34
Cellulose	50	50	44.9	22.66	17.58
Mineral Mix	35	43	43	43	43
Vitamin Mix	10	19	19	19	19
Choline Bitartrate	2.5	3	3	3	3
TBHQ	0.014	0.04	0.04	0.04	0.04
Anhydrous Milkfat	0	210	210	210	210
Cholesterol	0	1.5	1.5	1.5	1.5
Tomato Powder	0	0	0	100	100
Soy germ	0	0	20	0	20
Total	**1000**	**1000**	**1000**	**1000**	**1000**
Fat (% w/w)	7.2	23.2	23.2	23.2	23.2
Protein (% w/w)	17.4	17.0	17.0	17.0	17.0
CHO (% w/w)	58.3	44.7	44.7	44.7	44.7
kcal/g	3.68	4.55	4.55	4.55	4.55
Fat (% kcal)	17.6	45.8	45.8	45.8	45.8
Protein (% kcal)	18.9	14.9	14.9	14.9	14.9
CHO (% kcal)	63.4	39.3	39.3	39.3	39.3

Table 7.1. Composition of experimental diets. WD, Western diet; WDSG, Western diet with 2% soy germ; WDTP, Western diet with 10% tomato powder; WDTPSG, Western diet with 10% tomato powder and 2% soy germ.

CHAPTER 8: Summary and future directions

This final chapter will provide an overview of the dissertation, which has described a body of work focused on two areas: the biological effects of ultrasound and ultrasound contrast agents, and nutritional interventions to reduce atherosclerosis. The first chapter provided a survey of the literature on these two topics, beginning with lipoprotein metabolism and atherosclerosis, continuing with sections on cardiovascular risk factors, cardiovascular imaging, and cardiovascular effects of the diet, and concluding with descriptions of animal models and techniques used in atherosclerosis research.

Several chapters of the dissertation (Chapters 3-6) report investigations of the biological effects of ultrasound when used with ultrasound contrast agents to image blood vessels. This contrast ultrasound imaging procedure is clinically useful for cardiovascular disease diagnosis, but the interaction of ultrasound with the circulating contrast agents may affect the arteries being imaged in unique ways that are not well understood. It is important to characterize these biological effects to ensure that contrast ultrasound does not accelerate the deposition of plaque in the arteries being imaged. Contrast ultrasound exposures were performed on rabbits and mice, and histological and biochemical techniques were utilized to assess biological effects. As a step toward evaluation of these biological effects, an assay for measurement of von Willebrand Factor (vWF), a blood biomarker of endothelial function, was developed for rabbit samples (Chapter 2). The ELISA format was chosen for this purpose, as it is quantitative and relatively user-friendly. Although there were no commercially available antibodies directed against rabbit vWF, a pair of anti-human vWF antibodies were selected based on the sequence homology between human and rabbit vWF. The assay was then validated according to expert recommendations. All steps of the assay were carefully evaluated, its repeatability and precision were established. The validation process included demonstrations of Minimum Required Dilution (the dilution of plasma necessary to avoid matrix interference), spike recovery, intra- and inter-assay precision, antibody specificity, sensitivity, and freeze-thaw stability of plasma vWF. This assay was used in Chapter 3, in a study where blood samples were obtained from rabbits before and after ultrasound exposure to evaluate effects of contrast ultrasound on the vascular endothelium. Ultrasound-exposed rabbits had decreased vWF one hour after ultrasound

exposure (independent of contrast agent). This effect could potentially indicate disruption of the endothelium by ultrasound. Plaque thickness was also lower in animals receiving contrast agent with ultrasound than in animals receiving ultrasound alone. This could possibly be a protective effect, whereby contrast agent protects against ultrasound-induced accelerations in plaque deposition. It was interesting that the vWF effect was independent of contrast agent. If contrast agent protects the vascular tissue from ultrasound-induced stress, the effects of contrast ultrasound on vWF would likely be contrast agent-dependent. This work uncovered novel vascular effects of the ultrasound-contrast agent interaction.

Next, another rabbit study was conducted (Chapter 4). The goal of this study was to assess the effect of contrast ultrasound on a new biomarker, Hsp70. Hsp70 is a cellular chaperone induced in times of cellular stress to aid in management of damaged proteins. It was hypothesized that additional stress resulting from the ultrasound procedure would be reflected in elevated Hsp70 protein levels. Groups of rabbits consumed either the cholesterol diet or a chow diet, with some cholesterol-fed rabbits exposed to ultrasound with contrast agent. Hsp70 protein levels were quantified in aorta tissue at the site of ultrasound exposure by Western blot. Neither ultrasound with contrast agent nor cholesterol diet affected Hsp70 levels. However, physical restraint of the animals was also evaluated, and was associated with significantly higher Hsp70.

The cholesterol-fed rabbit model has some benefits but also many drawbacks. The aorta is large and easy to target with ultrasound, and rabbits' blood cholesterol profile is similar to humans. However, rabbits are large, expensive and unwieldy, leading to small sample sizes and requiring a major investment of laboratory personnel and resources, and they develop jaundice and anorexia when fed the cholesterol diet. In light of these concerns, there was interest in switching to a different animal model that would be a more consistent and effective model of atherosclerosis and that would be easier to work with, allowing for increased sample sizes. The ApoE$^{-/-}$ mouse, a well-established and widely used model, addressed these needs. The mice are easy to handle and also maintain their food consumption when fed a high-fat, high-cholesterol, high-sucrose diet known as the Western diet. In addition to the animal model, histological techniques also needed to be improved. In the past, the aorta tissue was frequently damaged during

isolation, making histological evaluation difficult. Methodological improvements were made that allowed isolation of the aorta intact for pathological evaluation. This model was then used to assess the biological effects of contrast ultrasound in Chapter 5. No effects of contrast ultrasound on tissue morphology or circulating biomarkers were seen.

A study was conducted to evaluate ultrasound bioeffects in another context, the gracilis muscle tissue and capillaries of rats (Chapter 6). In this study, 18 female Sprague-Dawley rats were divided among 4 concentrations of ultrasound contrast agent and 4 ultrasound pressure levels. The gracilis muscle was exposed to ultrasound, and contrast agent was infused through the tail vein. One day after ultrasound, animals were euthanized and tissues were collected for analysis. Histological sections of the gracilis muscle were evaluated by a pathologist. The histological measures were designed to identify structural and morphological damage across a spectrum of severity. Although the methods were well-executed, no effects of ultrasound or contrast agent on gracilis muscle damage were seen. There may have been biological effects of the procedure, but they may have been too subtle to capture at the level of gross morphology. Molecular techniques like immunohistochemistry may uncover effects of contrast ultrasound at the cellular level. Another possible explanation for the lack of effect is that there simply were not any adverse effects of the procedure. Our pressure levels were designed to be clinically relevant, but an increased ultrasound pressure level might induce damage.

In summary, we have not been able to demonstrate consistent patterns of adverse events caused by contrast ultrasound imaging. When we began our investigations into the biological effects of contrast ultrasound, concerns were raised after reports of cardiopulmonary complications and deaths in patients who had undergone contrast ultrasound. The FDA responded by mandating warning labels for ultrasound contrast agents, noting the potential for serious complications and requiring a 30 minute monitoring period after contrast ultrasound. Over the next several years, a number of clinical trials were conducted, and a meta-analysis of over 5 million patients showed that the use of ultrasound contrast agents did not increase the risk of adverse events. The few adverse events that were initially noted were probably due to pre-existing vascular disease, and not caused by ultrasound contrast agents. The FDA then relaxed its

warnings, noting that serious complications are uncommon and removing the 30 minute monitoring period post-injection. Although the human clinical literature has produced convincing evidence for the safety of microbubble contrast agents, the preclinical animal literature in this area is weighted heavily toward demonstrating harmful effects of ultrasound and ultrasound contrast agents. This may partly be due to inherent publication bias, whereby negative studies are not published. Our studies showing lack of adverse effects of contrast ultrasound help to harmonize the preclinical and clinical literature. It is possible that the effects of contrast ultrasound manifest as subtle molecular changes. Future studies could utilize immunohistochemistry and other molecular techniques to probe these changes.

Chapter 7 describes a more nutrition-focused project aimed at evaluating dietary tomatoes and soy germ, added alone or in combination to a high fat, high sugar, cholesterol-containing Western diet, for reduction of atherosclerosis in ApoE$^{-/-}$ mice. It is important to note that addition of tomatoes and soy to a Western diet for ApoE$^{-/-}$ mice can be used as a dietary approach to attenuate or slow atherosclerosis. Development of atherosclerosis is inevitable in these mice due to their genetic modification, but the rate of progression of atherosclerosis might be modified. Addition of soy germ alone to the Western diet attenuated Western-diet induced increases in plasma cholesterol, liver lipids and adipose, while addition of tomatoes alone increased expression of the Abcg5/8 transporters involved in cholesterol efflux. Overall, however, tomato and soy did not decrease atherosclerosis as assessed by histopathology. This is probably not due to the amounts of tomato and soy added to the diets, because the dose levels used have been previously shown to result in tissue and blood accumulation of their biologically active components. The lack of effect of the dietary intervention on atherosclerosis is likely due to a combination of factors, with two explanations being most likely. First, the dietary intervention may not have been long enough. We selected an earlier timepoint in light of the relatively modest effect sizes of most dietary interventions, but it may be that differences among groups would become more pronounced over a longer period of time. Second, the extreme phenotype of the Western diet-fed ApoE$^{-/-}$ mouse may have masked any beneficial effects. While soy and its products have established cardiovascular benefits, the cardiovascular effects of

tomatoes are currently unclear. This study does not support the use of either tomatoes or soy germ for reduction of atherosclerosis, but suggests that soy germ may have positive metabolic effects. Future studies could feed the diets for a longer period of time. The addition of tomatoes and soy germ to an AIN-93G diet instead of a Western diet should also be considered. This would lead to a more mild atherosclerotic phenotype that could be more amenable to dietary interventions.